THE UNIVERSITY OF
SYDNEY

A Stochastic Method for Representation, Modelling and Fusion of Excavated Material in Mining

Christopher Innes

A thesis submitted in fulfilment
of the requirements for the degree of
Doctor of Philosophy

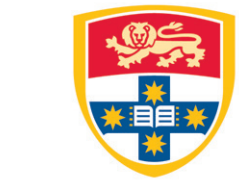

THE UNIVERSITY OF
SYDNEY

Australian Centre for Field Robotics
School of Aerospace, Mechanical and Mechatronic Engineering
University of Sydney

2015

Declaration

I hereby declare that this submission is my own work and that, to the best of my knowledge and belief, it contains no material previously published or written by another person nor material which to a substantial extent has been accepted for the award of any other degree or diploma of the University or other institute of higher learning, except where due acknowledgement has been made in the text.

Christopher Innes

24 May 2015

Abstract

Christopher Innes
University of Sydney

Doctor of Philosophy
2015

A Stochastic Method for Representation, Modelling and Fusion of Excavated Material in Mining

The ability to safely and economically extract raw materials such as iron ore from a greater number of remote, isolated and possibly dangerous locations will become more pressing over the coming decades as easily accessible deposits become depleted. An autonomous mining system has the potential to make the mining process more efficient, predictable and safe under these changing conditions.

One of the key parts of the mining process is the estimation and tracking of bulk material through the mining production chain. Current state-of-the-art tracking and estimation systems use a deterministic representation for bulk material. This is problematic for wide-scale automation of mine processes as there is no measurement of the uncertainty in the estimates provided. A probabilistic representation is critical for autonomous systems to correctly interpret and fuse the available data in order to make the most informed decision given the available information without human intervention.

This thesis investigates whether bulk material properties can be represented probabilistically through a mining production chain to provide statistically consistent estimates of the material at each stage of the production chain. Experiments and methods within this thesis focus on the load-haul-dump cycle.

The development of a representation of bulk material using lumped masses is presented. A method for tracking and estimation of these lumped masses within the

mining production chain using an 'Augmented State Kalman Filter' (ASKF) is developed. The method ensures that the fusion of new information at different stages will provide statistically consistent estimates of the lumped mass.

There is a particular focus on the feasibility and practicality of implementing a solution on a production mine site given the current sensing technology available and how it can be adapted for use within the developed estimation system (with particular focus on remote sensing and volume estimation).

Acknowledgements

I would first and foremost like to thank and acknowledge my supervisor Eric Nettleton. For having faith in me and providing the opportunity to study at the RTCMA. Your insightful input, leadership and support were critical in the production of this thesis. Your continued support and feedback, even after leaving the University, to the development of this thesis and to myself speaks largely to the strength of your character and is something for which I am particularly thankful for.

I would also like to acknowledge my co-supervisor Arman Melkumyan. I have appreciated the dedication and assistance you have provided through the development of this thesis. Your technical knowledge combined with the patience to teach has been pivotal in producing this thesis. I am also grateful for the additional time and feedback you have provided me during the closing stages of my PhD.

A thankyou to the many others at the ACFR / RTCMA who have provided assistance over the duration of my stay. Notably Shrihari Vasudevan for his insights into volume estimation and research methodology. To Hugh Durrant-Whyte for having the vision to develop the RTCMA in the first place. To Sven Schneider and Andres Hernandez for taking the time to assist in my experiments at Marulan and Sven particularly for having someone to talk about F1 with. To Steve Scheding, for providing support and feedback during the closing stages of my PhD.

From the wider University, a thankyou to Thomas Bishop and Jason Lessels from agricultural sciences for providing me the opportunity to tutor. I would also like to thank Jason specifically for our weekly lunches to discuss statistics, life and everything.

To my family for all their support over the years. My parents for providing me the self-belief to strive for more and always providing a loving home to come to. I would like to make a special mention to my Dad who took a week out of his time to help support my final experiments.

Finally my biggest thanks is to my wife Kim, for her unwavering love and support. I would not have been able to do this without you.

For my family.

Contents

List of Figures

List of Tables

Nomenclature

Abbreviations

ACFR	Australian Centre for Field Robotics
ASKF	Augmented State Kalman Filter
BLUE	Best Linear Unbiased Estimator
BRGS	Broyden-Fletcher-Goldfarb-Shanno
CDF	Cumulative Density Function
EKF	Extended Kalman Filter
FEM	Finite Element Modeling
GPS	Global Positioning System
IGM	In-Ground Model
LHD	Load-Haul-Dump
MA	Mathematical Averaging
MAS	Mine Automation System
MCS	Mine Control System
MHT	Multiple Hypothesis Tracking
MPCS	Mine Picture Compilation System
MPS	Mine Planning System
LKF	Linear Kalman Filter
OGM	Out-of-Ground Model
RFID	Radio Frequency Identification
ROM	Run-of-Mine
RTCMA	Rio Tinto Centre for Mine Automation
SLAM	Simultaneous Localisation and Mapping
TIN	Triangulated Irregular Network

Chapter 1

Introduction

The aim of this thesis is to provide a comprehensive method for representing, tracking and fusing information in preserved correlated process chains. Particular focus is placed on open pit mining process chains. By doing this in a systematic and comprehensive manner, significant benefits can be gained over traditional state-of-the-art deterministic methods.

A preserved correlated process chain is a definition given in this thesis to a specific subset of problems which arises when considering process chains and the movement of a quantity of items through this chain. The first notable characteristic of these process chains is the 'preservation' quality. This is where the total amount of an item estimated in the system is preserved (i.e. a 'closed system'). The second property of this specific problem subset is the spatial correlations between the items in the system (and subsets of these items) as they progress through the process chain.

An example of a preserved correlated process chain is the mining cycle. An amount of raw material is removed from the ground, the material is then transported to a processing facility. Once processed the material is then stored until transportation to a client. Over this process the total mass of material in the system remains constant (even though the core product to be transported may be a subset of the total mass removed). The mass that has been removed from the system is also correlated with its original location in the ground. The ability to correctly model these properties

could provide powerful benefits such as real-time probabilistic estimates of material properties at any unique location as well as reconciliation estimates.

The proposed method in this thesis shows that a system providing these benefits is possible. To validate this claim, large and small scale experiments will demonstrate these benefits. The experiments aim to mimic a generic open pit mining process. The method in this thesis is shown to provide a statistically consistently method for representing material at unique locations in a process chain using a probabilistic framework. As part of the large scale experiment, an innovative method for providing volume estimates of bulk material is used to assist in validation.

1.1 Motivation

A fully autonomous mine would provide a solution to many of the problems that the world faces today and in the future.

Developing countries, such as China and India, are driving increased demand for raw materials and refined products such as steel (produced primarily using iron ore and coking coal). Some have predicted presently known world reserves of iron ore to be depleted within 79 years at current production rates [129]. The ability to safely and economically extract raw materials such as iron ore from a greater number of remote, isolated and possibly dangerous locations will become more pressing over the coming decades as easily accessible deposits become depleted. An autonomous mining system has the potential to make the mining process more efficient and safe to handle these changing conditions.

The ability to accurately track and estimate bulk material properties through a production chain in mining would be highly valuable both in autonomous and non-autonomous environments. In the mining industry, having incorrect estimates of ore grade and quantity in transport stockpiles can lead to financial penalties for the mine [85]. Improving the quality of information, by tracking material through the production process, provides mine engineers with a more accurate inventory of their product

and enables better planning strategies to avoid these penalties.

One of the paradigm shifts in modern field robotics which has allowed for significant improvements in performance in unstructured environments has been the transition from a deterministic representation of the world to a stochastic representation. Thrun [118] describes the transition and reasoning in the following: "in recent years the probabilistic approach has become the dominant paradigm in a wide array of robotic problems. Probabilistic algorithms have been at the core of a series of fielded autonomous robots, exhibiting an unprecedented level of performance and robustness in the real world. These recent successes can be attributed to at least two developments: the availability of immense computational resources even on low-end PCs and, more importantly, fundamental progress on the basic algorithmic and theoretical levels".

In the mining industry, state-of-the-art tracking and estimation techniques use a deterministic representation. This is problematic when considering a vision for a robust autonomous mine.

In non-autonomous systems, the human operator fuses their expert knowledge and experience with their level of understanding of the trustworthiness of the data provided by the deterministic system in order to make a decision upon it. This can possibly lead to sub-optimal decisions being made on the basis of this process as the operator can both over and underestimate the true level of uncertainty in the data provided.

There is a need for a system which can appropriately define the uncertainty in the estimates provided to the operator. In an autonomous system, a probabilistic representation is essential for making the most informed decision on the available information.

This need for a probabilistic estimate of bulk material properties is the driving principle for the research of this thesis.

1.2 Thesis Objectives

This thesis aims to fill a gap in knowledge regarding a method for tracking, modelling, estimating and fusion of new information as material moves through a process chain. The methods discussed in this thesis provide numerous benefits to managing these chains more effectively. These include providing a richer representation of the material at different stages while at the same time remaining statistically consistent to ensure appropriate levels of confidence can be achieved. This has great potential in increasing the effectiveness of decision making on the material data at each stage in the process chain.

One of the main goals of this thesis is to provide an understanding of the problems and possible solutions to this problem using an estimation theory framework as the basis with the work targeted for use in a mining environment.

One of the main challenges when attempting to provide a comprehensive solution to the above problem, as will be discussed further in Chapter 2 (specifically Sections 2.3.1 and 2.3.2), is the lack of prior work addressing this problem in mining or indeed other lumped material process chains. One of the objectives and contributions of this thesis is the investigation and identification of the research problems as well as the problems associated with implementing a practical solution within a mining environment.

Methods and experiments are presented which demonstrate potential solutions for some of the fundamental problems in this area. However, given the lack of prior work in this field, trade-offs were made in regards to the depth of investigation into each specific problem to ensure appropriate coverage of all the research problems could be made. This was done to ensure that this thesis can provide a complete picture of the feasibility of a stochastic method for representation, modelling and fusion of excavated material in mining. It also provides a demonstration of not only the benefits of solving each problem in isolation but the net benefit of integrating the tracking, modelling, estimation and the fusion of new information.

1.3 Thesis Contributions

This thesis is primarily concerned with a method for stochastically representing and estimating bulk material properties over a process chain. The contributions of this thesis address many of the different aspects in making this method feasible for implementation in an open pit mining environment.

- A novel approach for representing groupings of logically separated bulk material (referred to as 'lumped masses') as the basis for modelling processes and estimation of bulk material properties. This representation allows for the complexity in the estimation research problem to be reduced to a more manageable size.
- A method for probabilistically modelling the extensive properties of lumped masses as they move through a process chain. An Augmented State Kalman Filter (ASKF) is used as the basis for this method.
- A novel constraint for the ASKF which ensures that spatial correlations between extensive material properties are maintained correctly. This constraint is based on the assumption the process chain is a 'closed system' where the total amount of material in the system is conserved. By maintaining the spatial correlations between extensive properties of lumped masses the fusion of new information on an extensive property of a lumped mass propagates to correlated lumped mass extensive property states.
- A novel method for estimating 2.5D bulk volumes to integrate into a stochastic bulk material estimation system. This method is based on Gaussian processes and is compared to a series of state-of-the-art methods to validate its performance. The advantage of the proposed method over the comparative methods is greater accuracy and precision under sparse data sets while simultaneously providing an estimate of the uncertainty in the bulk volume estimate.
- A novel method for modelling and representation of intensive lumped mass properties as they progress through a process chain. This method includes a

method for averaging intensive properties when combining two lumped masses together. The effectiveness of this representation and modelling method for intensive properties is discussed within the context of the state dependencies between intensive and extensive properties.

- This thesis introduces an algorithm for reconciling intensive lumped mass properties to their source location. This method is based on the constrained ASKF implementation and modelling methods derived in this thesis. The algorithm combines the spatial correlations developed between the extensive properties with the method for combining intensive lumped mass properties together in an iterative methodology.

1.4 Thesis Structure

Chapter 1 provides an overview of the contributions in this thesis. It also introduces the objectives of this thesis and presents the motivations for this research work.

Chapter 2 introduces the fundamentals of open pit mining. This is followed by a review of current mine automation, tracking and estimation systems. The significance of this research within an open architecture Mine Automation System (MAS) is discussed. This is then followed by an introduction to the principles of probability, Bayesian filtering, control theory, machine learning and bulk volume estimation.

Chapter 3 presents the novel 'lumped mass' representation for physically unique groupings of bulk material. This is followed by the method for modelling extensive 'lumped mass' properties through a process chain using an ASKF. The constraint on the ASKF is derived to ensure that the total amount of material in the system remains constant. The methodology is then tested on two real world data sets.

Chapter 4 introduces the stochastic method for bulk volume estimation using Gaussian processes. This includes an introduction to Gaussian process regression. The method for 2.5D bulk volume estimation is derived and compared to current state-of-the-art methods using real world data sets.

Chapter 5 discusses the modelling and representation of intensive material properties using the 'lumped mass' representation. This includes a discussion on the dependence between the extensive and intensive properties. The methodology for representing intensive properties is tested through experimentation. An algorithm for reconciling the intensive properties is developed and then tested through experimentation to prove its validity.

Chapter 6 discusses how all of the contributions of this thesis can be combined together into a single integrated system and some of the potential problems involved in implementing this on an open pit mine site. This chapter also includes possible future areas where further research would benefit an end-to-end tracking and estimation system for an open pit mine.

Chapter 7 provides conclusions and future work considerations specific to each of the contributions presented in this thesis.

Chapter 2

An Introduction to Tracking, Estimation Methods and Mining

2.1 Introduction

This chapter reviews the typical processes involved in open pit mining. A basic understanding of the mining process allows for a greater understanding of the significance of this research work in this field. The review of open pit mining includes current developments in mine automation systems as well as material tracking systems which are currently available. A short introduction to the research work being done at the Rio Tinto Centre for Mine Automation (RTCMA) is also presented. The introduction focuses on how the development of a complete mine automation system (MAS) influences the research work presented in this thesis.

The second part of this chapter reviews the core theory in developing probabilistic estimation, tracking and observation systems. This begins with an introduction to probability and Bayesian theory, which are the foundations of the current state of the art methods in the development of the prior probabilistic systems. This is followed by a discussion of tracking and estimation methods with specific focus on the suitability for use in a mining scenario. Finally there is an introduction to machine learning

techniques. This section discusses the possible applications of machine learning to tracking and estimation. The machine learning section reviews the techniques necessary for deriving models based on spatial data, which is needed for developing the probabilistic bulk volume observation technique. This is followed by a section on volume estimation which covers current volume estimation techniques and systems in industry. Volume estimation in mining is also introduced, this section discusses the shortfalls of current state-of-the-art techniques when considering the implementation into the estimation and tracking framework presented in this thesis.

A note on some definitions used in this thesis:

For this thesis, material properties are separated into two categories, **extensive** and **intensive**.

Extensive properties are defined as properties which are directly correlated to the amount of material in the system. In mining some pertinent examples include mass and volume. Chapter 3 deals with tracking and estimation of **extensive** material properties.

Intensive properties are defined as properties which are invariant to the amount of material present (provided the material is homogeneous). These include properties such as chemical composition, density, hardness etc. In practice there is a dependence when modelling intensive properties on the extensive properties of the material in the system. A further discussion on tracking and estimation of **intensive** material properties is included in Chapter 5.

Additional information on the classical definition of intensive and extensive properties can be found in thermodynamic and material science literature [110].

2.2 An Introduction to Open Pit Mining

One of the key applications of the work in this thesis is open pit mining. The majority of experimental work was designed on the premise of mimicking a subset of processes

which occur on open pit mine sites. The research is designed with the intent of working in collaboration with other research projects with similar autonomous operation themes in the mining domain. For this reason, a generic understanding of the open pit mining process is helpful in understanding the significance of the work, as well as the related work in the field. This section is not intended as a definitive explanation of the factors and processes involved in open pit mining. A more detailed description can be found in reference books such as the 'SME Mining Engineering Handbook' by Darling [32]. This section instead provides the reader, unfamiliar with the theory and practice of open pit mining, a high level view of the processes and factors involved to better understand the contributions described in this thesis.

2.2.1 An Overview

The physical processes involved in moving material through an open pit mine depends on many factors. These include the type of material being excavated, the concentration of the material as well as the ore body geology to name a few. This review will emphasise the movement of material from its location in the ground through to a final stockpile for transportation off the mine site. These processes are the most relevant to this thesis. Figure 2.1 provides a flowchart showing the general process flow involved in the design of an open pit mine.

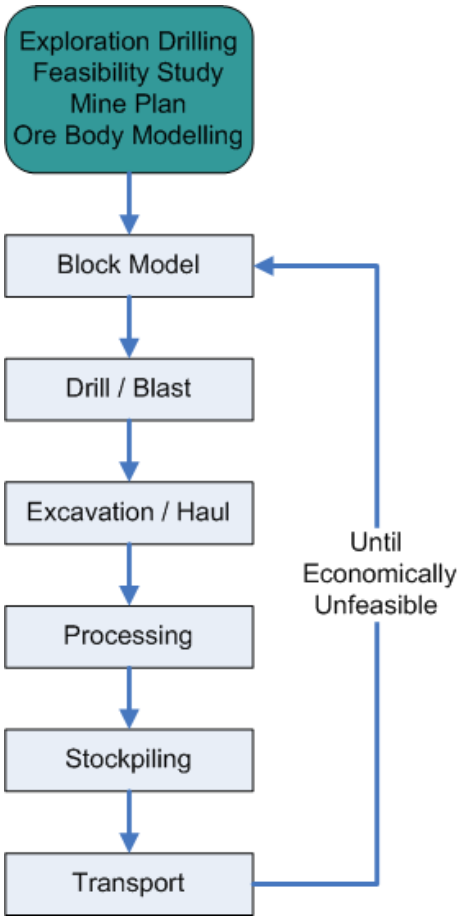

Figure 2.1 – A simplified model of the design and processes in open pit mining.

2.2.2 The Mine Development

One of the first stages in developing an open pit mine is the exploratory drilling phase. The purpose of this phase is to develop a greater understanding of the geology of the ore body. The distance between drill holes is sparse when compared to production drilling during the blast phase of production (see Section 2.2.4). The ore body is modeled once exploration has been completed using the data gained from exploratory drill holes. This is usually through a spatial interpolation techniques such as Kriging [27]. Figure 2.2 gives an example of an exploration drilling pattern over a hypothetical ore body.

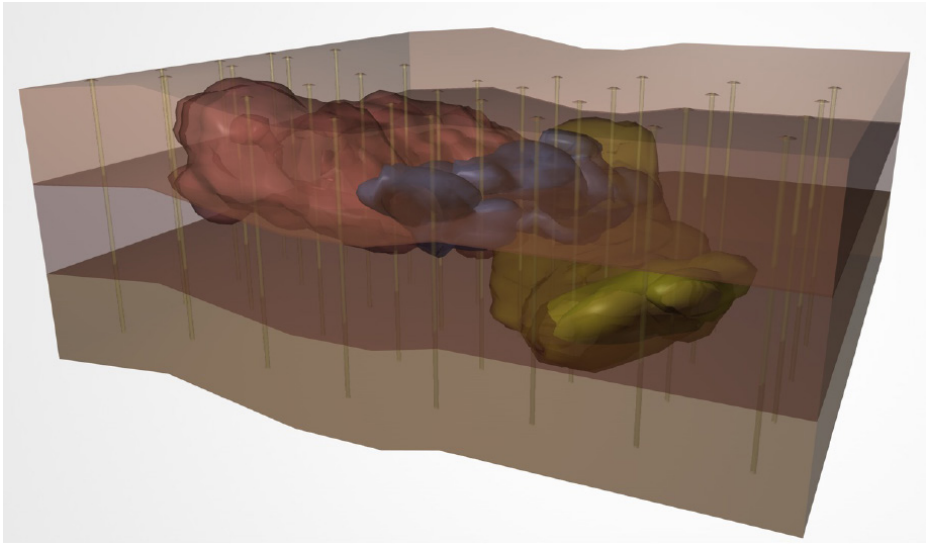

Figure 2.2 – An example of an exploration drilling pattern and hypothetical ore body. The data gathered from the exploration drilling is used to develop a geological model of the ore body.

The results of the exploration drilling combined with the ore body modelling process forms a key part in the decision on whether to create an open pit mine. The results provide valuable geological information such as the stripping ratio (how much waste material must be removed compared to product material) and the spatial geology of the ore body (deep and narrow ore bodies may prove more economical as underground mines). Other key issues affecting whether or not to create an open pit mine include environmental and safety impact when developing the ore body.

All these factors influence the decision whether or not it is economical to create an open pit mine. If the decision is made to create an open pit mine, development of the pit can begin. This often involves the removal of the overburden (waste material located above the ore body) before actual mining of the desired ore can begin. The pit is progressively made deeper with a series of haul truck access roads providing the means to remove material. Open pit mines progress downwards through a series of benches. These benches vary in size depending on the type of equipment used in excavation, the selectivity required in the mining operation as well as the stability of the bench walls, given the geological properties of ore. An example of a series of benches can be see in 2.3.

Figure 2.3 – A series of benches at an iron ore mine in West Australia. The height of the benches vary depending on equipment, stability of bench walls and selectivity required in the mining operation.

2.2.3 Mine Visualisation and Ore Body Estimation

One of the important aspects of mining is having a reliable model of the ore located in ground, thus enabling the effective creation of mining plans. A typical mine will generally have contractual obligations to produce a certain quantity and quality of material at a predefined intervals. Providing incorrect levels of ore grade and quantity to the client can lead to financial penalties for the mine operator [85].

As discussed in Section 2.2.2, prior to visualisation of the material as a block model the ore body is modelled using geostatistic techniques such as Kriging [102]. Kriging is a methodology which can account for directional dependencies of spatially correlated data. This allows inferences to be made on the material properties at different spatial locations. The sampling variations in material properties used in this method can be typically represented as log-normal distributions [65]. This is due to the natural constraint of these physical properties. For example chemical composition of

material(e.g Fe%, Si%) must always be greater that 0%.

The ore body which is being excavated can be visualised through a block model. Some examples of software which provide this functionality are Maptek's Vulcan [74] and Gemsoft's GEMS [46]. It is common for software suites such as these to have optimised mine planning functionality as well.

A block model is a method for discretising the ore body into smaller regions based on a level of homogeneity of the material in that area. Figure 2.4 gives and example of a block model on an iron ore mine site. The material in this example is separated into four blocks.

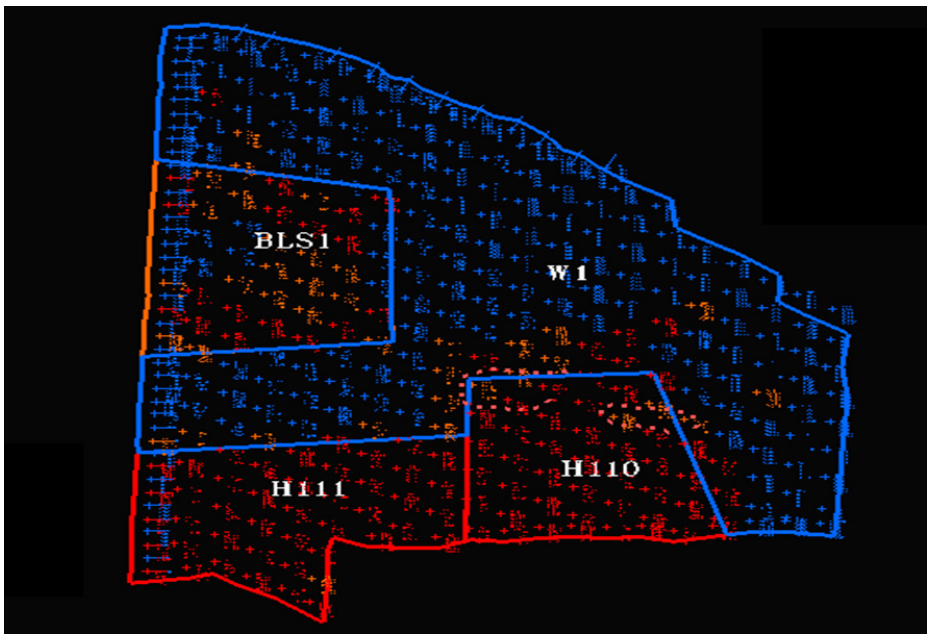

Figure 2.4 – An example iron ore block model. The ore body is divided into geologically similar regions. In this figure, regions denoted with a W are waste blocks, H are high grade blocks and BLS are blending blocks.

One of these sections (W1) is a waste material block and consists of material which is either too low in concentration for the desired output or too high in impurities. Material from this block is excavated (if required) and moved to a waste dump. Two of the other sections are designated as 'High Grade' (H111 and H110) and would be excavated and processed under the assumption that material from these areas

maintains a certain level of quality, in terms of chemical composition, in order to be classified as 'High Grade' material. The remaining block (BLS1) is designated to be used for blending. This is used on mine sites where the grade of material in the block is not at the required level but can be blended in a stockpile with higher grade blocks to create a product which is within the required grade levels.

Mine planners use optimisation software in order to determine what is the best sequence of excavation in order to provide a certain level of output quantity and quality while maximising the current blocks available for mining.

2.2.4 Drill and Blast

Often the materials of interest are located within hard rock formations. This makes it very difficult to excavate unless the material is broken up beforehand. Explosives can be used to break up the hard material. This is achieved by first drilling into the rock. A number of drill holes are created in a predesignated pattern in order to achieve certain blast characteristics. When drilling is complete, the holes are filled with explosives and an exclusion zone is created before the explosive material is detonated. Geologists occasionally take filings from the drill holes to validate geological models.

Figure 2.5 – An example of blast hole drill pattern. The drill holes are filled with explosives and detonated in order to make the excavation of hard material easier.

Figure 2.5 gives an example of blast hole drilling. Once the material is blasted a geologist inspects the area and mark out the block model boundaries. This enables the excavator operator to define the boundaries of their work area. Figure 2.6 gives an example of the boundaries outlined by a geologists tape. The tape has been highlighted green for clarity.

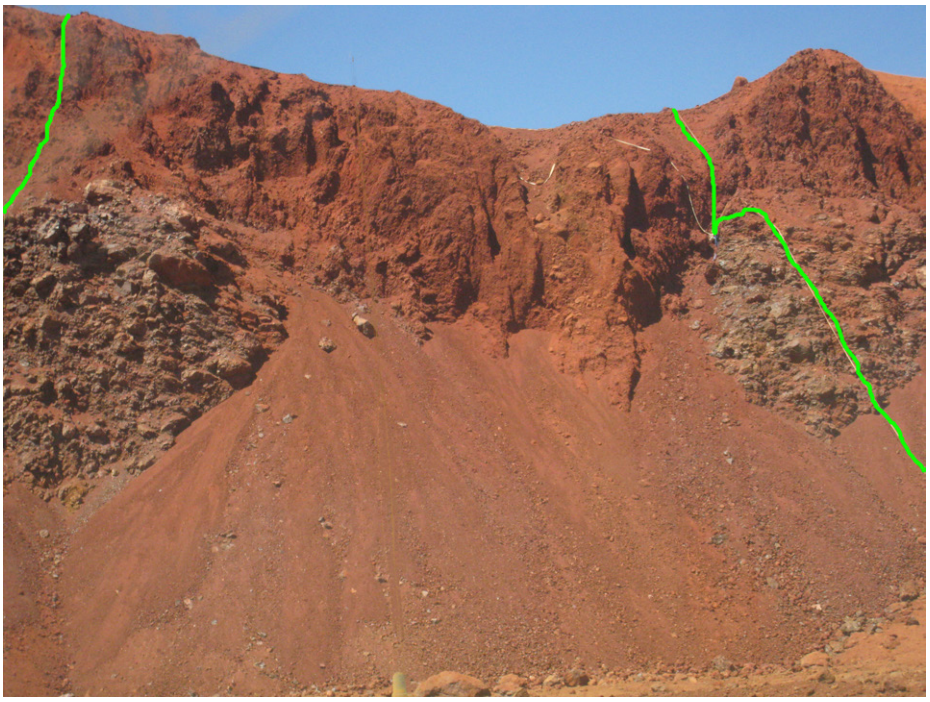

Figure 2.6 – A recently blasted bench with block boundaries highlighted. The grade block boundaries are marked by a geologist after blasting. The tape used to mark the boundaries has been highlighted green for clarity in this picture.

2.2.5 Excavation and Haul

Excavators (or shovels) and haul trucks work in unison to remove the material from a designated grade block. Ideally, an optimum amount of trucks are assigned to each excavator to ensure that the excavator is not waiting for an unloaded haul truck. Conversely the amount of haul trucks is constrained so that the amount of time waiting to be loaded by an excavator is at a minimum. The excavator operator works from a designated grade block as decided by the mine plan. The excavator loads the material onto the haul truck until the haul truck is at capacity. Once this is achieved, the haul truck travels to either a run-of-mine (ROM) stockpile or a processing point to unload the material before returning to the excavator to repeat the process. An example of the loading process can be seen in figure 2.7.

Figure 2.7 – The excavator operator fills the haul truck with material from the grade block tasked for excavation. The haul truck unloads the material at a ROM stockpile or processing point.

2.2.6 Processing

The processing of the material is dependent on the type of material being excavated. It also depends on the product which the mine is seeking to produce. For example, if the mine is required to produce material of a specific grade, any material outside this grade undergoes a process to either increase or decrease the chemical properties to meet the required grade. Certain types of mined material (e.g. iron ore) are frequently put through crushing and screening procedures to reduce the material to a uniform size. Figure 2.8 shows an example of a crush and screening process plant.

Figure 2.8 – Mined material needs to be processed to produce a product with predesignated properties in regards to size and chemical composition. This picture shows a processing plant used to crush and screen iron ore into lumps and fines.

Figure 2.9 gives an example of a possible process chain which may occur on an iron ore site. In this scenario, iron ore is separated into four distinct products. These include low grade lumps and fines and high grade lumps and fines. Lumps is a term used to describe material which is equivalent to a small rocky pebble size. Fines describes material which is significantly smaller and can be considered similar in size to sand and dust. It should be noted that in this example the amount of grade classes is fixed as high and low grade. It is possible to have as many grade classes as desired. This can be beneficial when combining the output of multiple mine sites at a central transport facility. In this example the central transport facility is a port. The different products can then undergo further blending at the port location to reach the desired grade level and provide a reduced number of grade classes to the final customer.

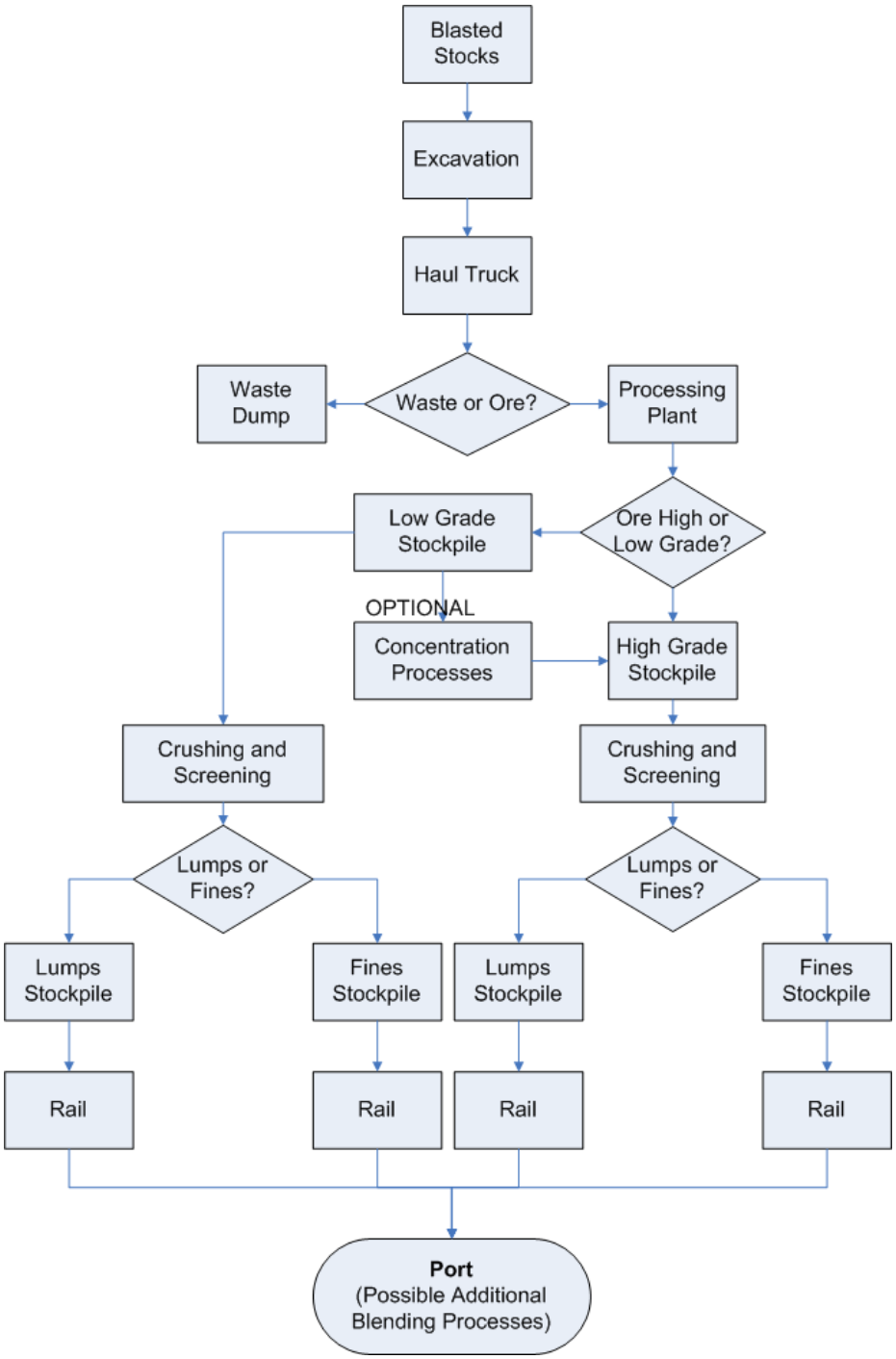

Figure 2.9 – An example iron ore process flow map showing the movement of material from blasted stocks through to railing stockpiles.

2.2.7 Stockpiling

Stockpiles can occur both before and after plant processing occurs. Pre-processing stockpiles can be used when material will never be processed, such as waste product. Stockpiles can also be used to ensure an adequate buffer of input material into other processes, such as crushing. Material can also be stored for later use in blending stockpiles if the pit development does not allow the material to be blended to the required grade immediately.

Stockpile design is an area which is particularly important when trying to obtain a uniform product. Research has been done on which stockpile designs would produce the least amount of variability [104] when being reclaimed for transport.

Final stockpiles are stockpiles where material is kept before being transported off-site to a central transport facility or directly to the customer. It is very important to have an accurate measure of both how much material is in each stockpile as well as the grade level of the material so that the appropriate material can be transported.

Figure 2.10 – A stockpile of iron ore which will be transported by rail to a port facility.

Figure 2.10 provides and example of a stockpile of material. In this instance the material is waiting to be transported by rail to a port facility for shipping. A boom-reclaimer system is used to remove the material from the stockpiles to be placed into

the waiting rail cars.

2.3 A Mine Automation System

The research work in this thesis can be applied without any additional input from other automation systems. However, one of the primary aims of this research is that it will work in synergy with a wide variety of other systems which are being concurrently developed (see Section 2.3.4). As a result, the benefits which can be obtained from using the results of this research work in co-operation with the other proposed systems will be substantial when compared to using the results in isolation.

An understanding of how this research work relates to other work being developed gives a greater understanding of why specific choices were made in the research process.

One of the key applications of this research is mine automation. This section outlines the current state-of-the-art mining automation systems. Examples from other primary industries such as agriculture, forestry and horticulture are also provided. This section includes the systems presently available which track and estimate material through a process chain in these industries. This section provides an overview of sensor systems which are designed for, or can be applied to, the mining environment. Sensor systems play a key role in applying the contributions of this thesis to a real world application.

2.3.1 Current Mine Automation Systems

A prominent trend in mine automation is to automate (or tele-operate) equipment. Examples include a wide range of mining equipment such as excavators [106], Load-Haul-Dump (LHD) vehicles [39], rock breakers [40], haul trucks [3][8] and drills [22]. Mining is an inherently dangerous job so the ability to remove employees from potentially dangerous environments is a great benefit. The possibility for enabling more

flexible and diverse working arrangements will improve the ability to employ and maintain staff [56]. This is particularly an issue in Australia where mine sites are often located in very remote areas [71].

Automation of equipment in uncontrolled environments such as mining is a difficult task. Other industries have made good progress in solving this problem. Practical examples include autonomous cargo handling machinery [41] and autonomous crop management equipment [48]. Automation in even less controlled environments than the prior examples has also made significant advancements, most notably in automating road vehicles [120].

Substantial work has been carried out on methods for optimising specific stages in the mining process and providing decision support systems to aid mine workers, the goal being to achieve greater productivity and efficiency. Robinson [104] for example looks at the variance on different blended stockpile configurations to determine the best configuration for achieving a consistent blend. Giacaman *et al.* [45] describe a forecast modelling system for the loading and transportation of material to a stockpile. This is used to predict the effect of changed equipment carrying capacity. Sensogut and Ozdeniz [109] describe a statistical study of a stockpile using finite element analysis to predict the behavior of a stockpile under specific environmental conditions. Bastos *et al.* [13] describe an improved method for truck dispatching using a stochastic approach when compared to current state-of-the-art deterministic systems. The approach used in this paper is a particularly significant as it is a shift from the standard deterministic approaches in this area of research. A further discussion of tracking and estimation systems similar to the work in this thesis is described in Section 2.3.2.

The component which is lacking from mine automation research is not the automation of equipment or decision support systems, rather what is needed is a complete end-to-end system which enables automation of information processes as well as the flow of information from all systems on a mine site. Current automation and information systems are set up on mine sites and tend to work in isolation from other systems. This leads to a 'silo' effect of information in the system. One of the causes of this is the multitudes of propriety software on mine sites, each with their own data storage and

interface policies. Jansen [53] presents additional contributing factors which impact the ability to track and reconcile material up to the point of mineral processing. In the study by Jansen, he proposes that incorporating "The magnitude and behavior of error in the measurements" of material would be valuable in developing tools to reducing these sources of error.

This is not an exclusive mining problem. Thompson *et al.* [117] discuss similar problems which arise in the horticultural (fishing) industry. One possible solution suggested in this paper is for 'vertical' integration of companies involved in the production chain, with a single database accessible through a common standard. This database would store information about the fish starting at its point of harvest all the way to the consumer.

An ideal mining solution is to have just one automation system for an entire site. By having a singular system which controls all systems on a mine site, information from any system can be accessed freely and common data integrity policies can be implemented. Individual autonomous information systems can make good use of the flow of information from different systems to provide tangible benefits. An example of this is an autonomous blast hole drill gathering information about rock hardness as it drills blast holes. An automated process for relating rock hardness to a geological model could be applied [131]. This model can then be fused with the underlying geological model to improve the accuracy of the model to enable better mine planning.

The aim of the RTCMA [94][1], based at the University of Sydney, is to develop this end-to-end automation system. Part of this system is a common framework in which information can be stored and shared from a variety of different sources, such as commercial automation solutions for different aspects of the mining process. For more information on this system and where the research in this thesis contributes to this system see Section 2.3.4.

2.3.2 Material Tracking Systems

In the field of material tracking, the majority of the research and products available today are based on the tracking of discrete products. Examples of this include the tracking of packages through couriers, parts stored in a warehouse and tracking of luggage through an airport. This is usually done through a combination of Radio Frequency Identification (RFID) tags, Global Positioning Systems (GPS) and barcode scanning [19] [83]. When the material and processes involved become less constrained the range of research and products decrease substantially.

Research in the field of integrated real-time material tracking in mining is limited. The state-of-the-art is represented by commercial products from companies such as QMASTOR [60], Snowden [88, 89, 116] and OreTracker [4] which provide deterministic estimates at different locations in the system. The 'DISPATCH' system from Modular Mining [125] also provides a limited degree of ore tracking during the haul cycle. It has database fields for a material type, which is recorded with the vehicle GPS position. However, the material properties are not estimated online. The current practice in mining is to assume all trucks carry a common constant percentage of their maximum load. This value, termed a 'load factor', is used in the calculation of average mass of material moved by trucks calculated over a long time line. When used in conjunction with estimated total truck movements of a specified time frame (possibly from a dispatch system), it can be used to estimate productivity [61]. The method does not represent the actual material movements in a haul truck on a haul by haul basis. Over a shorter time frame, loads are prone to fluctuations based on operator skill through over or under filling of trucks and excavation of material outside the designated mining area. It also relies on the accuracy of initial in-ground estimates of the material being excavated for estimates of material properties.

One recent development in the field of material tracking in mining combines conventional material tracking theory with the unconstrained mining environment. Metso's SmartTag [127] uses RFID tracking of embedded devices in the ore from blasting through to stockpiles to track groupings of material.

One of the key disadvantage amongst these different options is the lack of a probabilistic representation which allows for fusion from multiple different inputs. As an example, Figure 2.11 shows a few of the possible sensors on a mine site. The information from these sensors is likely be stored in a database. One use for this data is to validate mining factors (e.g. haul truck load factors). This thesis shows that the information from these sensors can be used in real-time to provide consistent probabilistic estimates of material properties at different locations. Alarie and Gamache [10] present a statistic that transportation costs make up 50% of costs in mining. Being able to use more accurate representations of material at different locations could allow for greater optimisation of production vehicles which will mean substantial savings can be achieved.

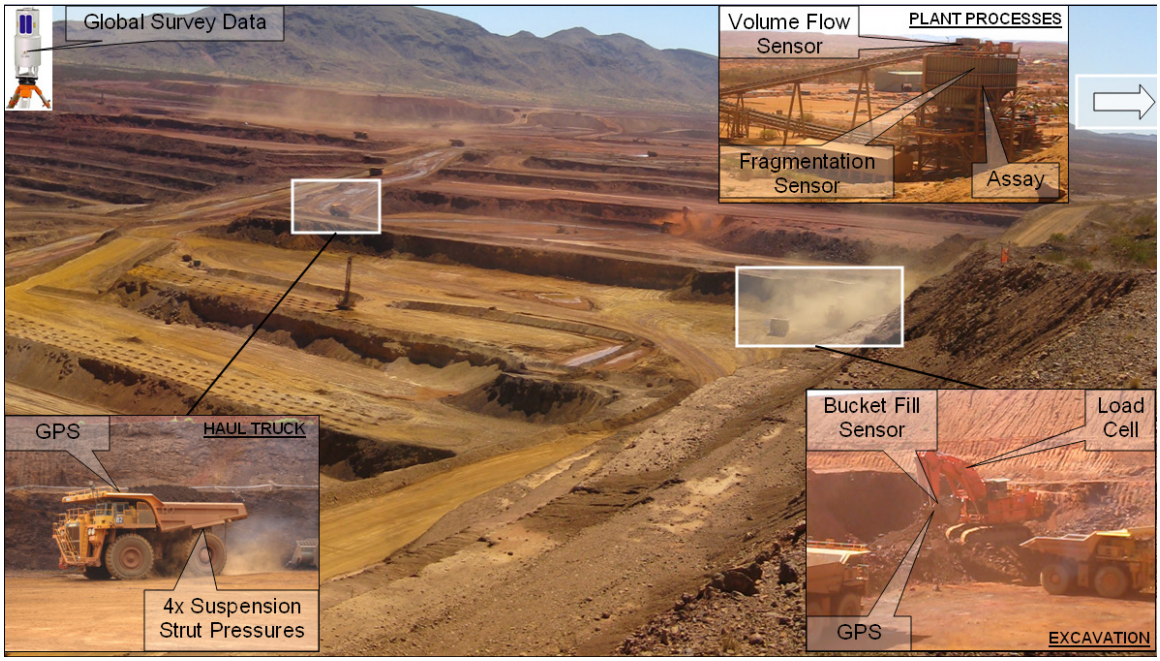

Figure 2.11 – An example of the range of sensors which could be utilised on a mine site. The ability to utilise the information from these sensors in an end-to-end estimation system would be highly valuable.

Another aspect which is missing from current state-of-the-art methods is a statistically correct method for correlating the properties of spatially distributed groups of material. Ideally, when new information is introduced about material at a specific location, that information should be utilised to determine more about material at

previous locations. One example is learning more about the mass of material in a haul truck from a sensor such as the strut pressure sensors on the haul truck shown in Figure 2.11. When this data is fused it should be able to not only provide an improved estimate of the amount of material in the haul truck; but also correlate that new understanding of how much material is in the haul truck to provide an improved estimate of how much material has been removed from the grade block where the material was mined. This thesis provides a systematic method for tracking material and correlating the properties correctly to able to allow these effects.

The current deficiencies in mining systems as stated previously are shared with other industries. The forestry industry has developed multiple tracking techniques to track logs from their source location through to the manufacturer [42]. A large driver for this work has been to certify that the wood is not illegally logged [114]. D'Amours *et al.* [31] describe in their journal article similar problems which also arise in the mining industry. Most notably that 40% of operational costs arise from transportation which stokes a large demand for research and products involved in process chain and truck dispatch optimisation. Commercial tracking systems such as Heleveta's TracElite [2] provide estimates of the material as it passes through predefined nodes in the production chain. There are some properties of the forestry industry which make estimation and tracking of the material comparatively easier than in the mining scenario. For example, the material in logging can be more easily defined as discrete set of logs rather than a large continuous grouping of material. This allows for more conventional tracking techniques such as barcoding and RFID tags to be used.

Another example of a similar primary industry is the agricultural industry. Similar commercial systems (with comparable features to current mining tracking and estimation systems) exist to track agricultural stock movements. These include products such as CropBase [6], Farm Files Crop [7] and Cattleworks [5]. Research work has been done in probabilistic modelling of various farming variables to be used in decision support systems as well which aid in decisions such as optimal stock levels and planting schedules. A review of this research can be found in Janssen's paper [54] which provides a description of state-of-the-art research in this field.

Whilst the work in this thesis is focused on mining, the theory can be translated to other process chain systems. In the agricultural industry, a system which enables a probabilistic representation and maintains the proper spatial correlations between agricultural stock at different stages would provide many benefits. One example would be more effective weed control systems. If at harvest the level of weeds (such as rye grass in a wheat crop) can be sensed by either the harvester or during unloading to silos, this information can be correlated back to the point of harvest. This could be used to develop a probabilistic spatial map of weed density. This information can then be used in more targeted weed control systems. This could lessen the environmental impact from herbicide use, reduce costs and improve yield.

One of the most prominent problems in the food industry is both disease and bio-terrorism [99]. The knowledge that a particular food has been contaminated greatly reduces the consumer confidence in the product. An effective real-time system which can correlate spatially separated material would be able to, upon detection of impurities in a food source, determine which other products have come from the same source. This could enable effective targeted quarantine measures at a rapid pace.

2.3.3 Mine Sensing Equipment

One of the greatest enablers for automation work is the development of sensing systems. Over recent years, the cost of sensor systems has decreased while their capabilities have improved. Gates [44] describes this briefly in his article on the parallels between the robotics and computer industries "Another barrier to the development of robots has been the high cost of hardware, such as sensors that enable a robot to determine the distance to an object as well as motors and servos that allow the robot to manipulate an object with both strength and delicacy. But prices are dropping fast. Laser range finders that are used in robotics to measure distance with precision cost about $10,000 a few years ago; today they can be purchased for about $2,000. And new, more accurate sensors based on ultrawideband radar are available for even less".

This thesis introduces methods for representing material stochastically at different stages in the process chain. A probabilistic representation provides the capability to fuse data from information sources, each source providing individual estimates and corresponding uncertainties, to improve the estimate of the material properties present. This section outlines recent developments in mine sensor technology which could be used as inputs into the probabilistic estimation and tracking system discussed in this thesis.

Remote sensing has seen significant development recently. This has led to the development of safety systems for mine equipment such as haul trucks [90] by companies like Acumine Pty Ltd [72]. 3D terrestrial laser scanners are also now becoming prominent in surveying tasks. This is due to their ability to gather dense amounts of spatial data over long distances at considerable speed. This has allowed for the removal of surveyors from possible dangerous areas of the mine such as bench crests. Several different models of these laser scanners are reviewed by Lichti *et al.* [68] along with possible applications. Vasudevan *et al.* [123] provide an example of how the data gathered from these scanners can be used to create large scale stochastic terrain models for mining by using Gaussian processes. This concept is extended upon in Chapter 4, where a stochastic method for bulk volume estimation is discussed.

Utilising visual sensors to estimate properties, such as volume, in a mining environment is particularly challenging due to the large amounts of dust present on site. Figure 2.12 provides an example of the dust which can occur during mining operations. Sensors such as a millimeter wave radar [20][57] would be useful in this domain due to their ability to penetrate through dust. Being able to reliably estimate a surface using a 3D point cloud is a vital component when estimating volume.

Figure 2.12 – The dust generated through an excavator loading a haul truck. This dust makes it difficult to use sensors such as lasers and cameras to gather surface data.

Remote sensing technology has also has improved in its ability to determine intensive properties of material at different locations in the mining process. An example of this is hyper-spectral cameras [108][79][86] which have been used to determine probabilistic classification of intensive material properties at the bench face.

There has also been considerable commercial development of mining specific sensor systems. Some current working examples include the following; the autonomous estimation of haul truck contents (mass and volume). This has been tested live in research by Duff *et al.* [38] and commercialised by Transcale [121]. MotionMetrics [82] has also developed a system for payload estimation on excavators.

2.3.4 The RTCMA Mine Automation System

The vision of the RTCMA is to create a fully autonomous mine. This has led to the development of the Mine Automation System (MAS). As explained in Section 2.3.1, there is a need for a common system for storing and communicating information on

a mine site. The MAS aims to provide this functionality. Although automation is the primary goal of the system, human operator input is expected to be a valid and required input into the system. As a result, the services provided by MAS include valuable decision support for mine operators even with low levels of automation.

The research work at the RTCMA focuses on representing information in a Bayesian framework. Representing information probabilistically allows for autonomous systems a greater understanding of how trustworthy the data is, thus enabling more informed decisions to be made. It also allows for information from multiple sources to be fused together in a consistent manner. This is explained in greater detail in Section 2.4.2.

The work in this thesis aims to describing the flow of material from the bench as it is excavated, hauled, processed and then stockpiled. The material properties are to be reconciled with in-ground estimates during the process of moving the excavated material from the pit to transport stockpiles. New information is fused from sensors at different stages during this process. The model should be able to, on demand, provide an estimate of the location and grade of all available stock (which is not considered in-ground) on the mine. The intent of this work is to aid in the development of a common operating picture of a mine site, this common operating picture can then be used by other systems to assist in automation or optimisation work.

The key goals of the research work for this thesis to aid in the development of this common operating picture can be described as follows:

- **Provide a probabilistic inventory of all available stock**: This is to be limited to material which is not considered in-ground. For the purposes of this thesis, broken stocks currently being excavated are included in this system. The system ideally will extend through to the final stockpiles for transportation. The system should provide information on important material properties at each location.
- **Fusion of new information**: This requirement drives the need for a common way of representing the quality of estimates of material over multiple stages in the mining processes.

- **Conservation of material**: A method is needed to ensure that the total material in the system remains consistent and all flows of material are accounted for.
- **Reconciliation with geological model**: In order to reconcile probabilistic estimates in the out-of-ground model with the in-ground-model, a statistically consistent way of correlating new fused information during the mining process to the materials point of excavation is required.

The contributions discussed in Chapters 3 - 5 aim to provide a method for fulfilling these stated goals.

2.4 An Introduction to Bayesian Estimation and Volume Estimation

Probability theory is a key component in the work presented in this thesis. The following section describes theories which build upon the basics of probability theory. This includes sections on Bayesian filtering, machine learning and estimation theory techniques.

A section discussing current state-of-the-art volume estimation techniques is presented and a method using a probabilistic representation is compared to these techniques.

2.4.1 Probability Theory

Over the past 20 years, the use of probabilistic representations in robotics has led to many important developments [119]. One example is a robust technique for mapping and localisation known as Simultaneous Localisation and Mapping (SLAM) [36].

A deterministic representation works under the assumption that all inputs into the system are known and singular in value. An example is determining the speed of

a standard road vehicle. The speedometer in the vehicle may read 80 Km/h. This estimate of the speed is based on the assumption of pre-known singular values for tyre circumference and engine / transmission ratios.

In reality, a variety of factors influence the accuracy of the assumption of a fixed tyre circumference and engine / transmission ratio. These include tyre wear, engine / transmission wear as well as tyre temperature and tyre pressure.

Being able to handle the inherent uncertainty of the inputs into a system is one of the prime advantages of using a probabilistic representation. A probabilistic representation operates under the assumption that each input into the system is affected by some level of 'randomness'. To represent this 'randomness' (which can also be referred to as uncertainty) a valid probability distribution is formed over all possible values which each input can take. This can be a discrete number of states (e.g the probability of heads or tails when flipping a coin has two states), a continuous function of possible values or a combination of the two.

There are three probability theorems which must be followed in order to form valid probability distributions [15].

Theorem 2.4.1 (1. Nonnegativity)**.** $P(A) \geq 0$*, for every event A.*

Theorem 2.4.2 (2. Additivity)**.** $P(A \cup B) = P(A) + P(B)$*, if events A and B are mutually exclusive of each other. Following from this, if a sample space has an infinite number of mutually exclusive elements* $(E_1, E_2, \dots)$*. The following will also be true.* $P(E_1 \cup E_2 \cup \dots) = P(E_1) + P(E_1) + \dots$

Theorem 2.4.3 (3. Normalisation)**.** $P(S) = 1$*, the probability of the entire sample space S will be equal to 1.*

Further information on applying probability representations relevant to the work in this thesis is discussed in Section 2.4.2.

2.4.2 Bayesian Filtering

Bayesian theory was originally developed by Thomas Bayes and came to light in his posthumous essay published in 1763 [14]. The significance, popularisation and application of this discovery to statistical inference is credited to Pierre-Simon de Laplace [9]. Bayesian theory forms the basis for various control theory methods which utilise a probabilistic representation. This work was pioneered by both Wiener [126] and Kolmogorov [64]. This pioneering work led to the development of the still widely used Kalman Filter in 1960 [58][59][78]. Bayesian filtering since this development has broadened extensively from the conventional closed form linear estimation solutions to a general approach to solving control problems [50].

The core principle when using Bayesian statistics is the assumption of a prior probabilistic model of a random variable during modelling. When new evidence is introduced about this particular variable, 'Bayes theorem' is used in determining the level of belief between the prior model and the new evidence. The resulting distribution formed is known as the 'posterior'. Bayes theorem is summarised in Theorem 2.4.4.

Theorem 2.4.4 (Bayes Theorem)**.** $P(x|z) = \frac{P(z|x)P(x)}{P(z)}$*, x is the random variable of interest and z is independent observational evidence of this variable.*

Bayes theorem $P(x|z)$ could be thought of as the result of the prior model being conditioned with the observational evidence z. $P(z|x)$ is often thought of as the 'sensor model'. Where a model must be formed to describe how the observation evidence 'z' relates to the random variable of interest x. As an example, consider a radar station estimating the cartesian co-ordinates (x,y,z) of a target. The sensor available to the station may provide only a range and a bearing to the target from the radar station. Thus a model needs to be created in order to condition the observational evidence 'z' (range-bearing data) on the prior model 'x' (x,y,z co-ordinates).

Fundamentally, Bayes theorem allows for the fusion of observational evidence with the prior model. This is provided that both the prior model and observational evidence are valid probability distributions. The application of Bayes theorem can be

demonstrated using the example shown in Figure 2.13. In this scenario the variable of interest is the mass of the material in the haul truck. A prior model of the amount of material expected to be in the haul truck is shown in Figure 2.13 (b). One possible method for building this prior model is through empirical observational evidence of the mass by measuring a statistically significant amount of prior loads. There are multiple methods for developing the prior model, ideally the appropriate model is validated in experimental cases where a ground truth value is available.

In this example the prior model of mass in the haul truck is assumed to be Gaussian distributed. Now suppose observational evidence from a sensor is provided which gives another probabilistic model of the mass of material in the haul truck. This could be from a load scale such as the one shown in Figure 2.14 (a). It also could come from other sensors such as suspension strut pressures or possibly a volume estimation system with a density model. The important factor is that the probabilistic distribution model for the observational evidence is valid. Figure 2.14 (b) shows a possible observational evidence model along with the prior model of the mass of material in the truck. Again, in this scenario the observational model is assumed to be Gaussian distributed. The Gaussian assumption is not a requirement for Bayes theorem, the distribution can be of any shape provided it is a valid probability distribution.

(a) A truck being loaded by an excavator.

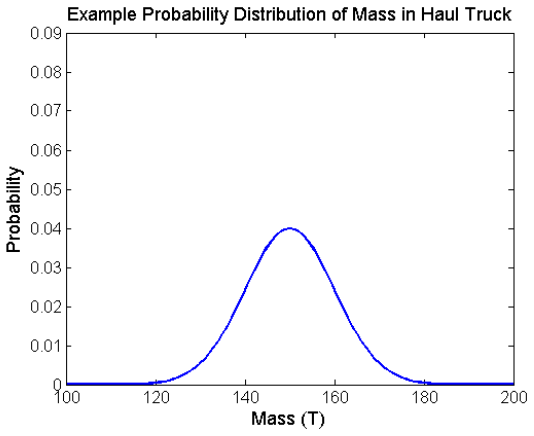

(b) A prior model of the material located in the truck.

Figure 2.13 – An example showing the mathematical representation of the prior model of material located in the haul truck.

(a) A truck located on a set of scales which observe mass.

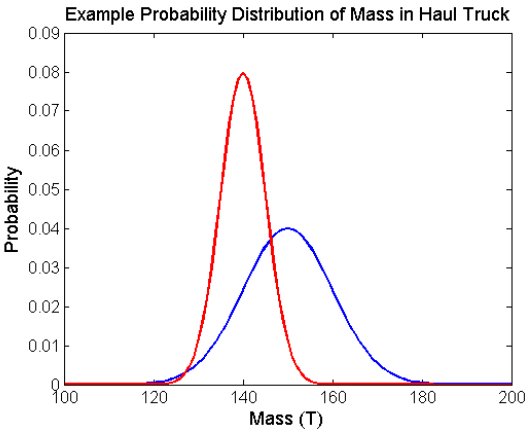

(b) A model for the mass in the truck as provided by the scales is shown in addition to the prior model. The red line illustrates the observational model where as the blue line is the prior model.

Figure 2.14 – An example showing the prior model and observational model estimates of the mass of material in the haul truck.

Figure 2.15 gives the result of fusing the prior model and the observational evidence using Bayes theorem 2.4.4. One of the important features to note is that the fused model is influenced more by the observational evidence. This is expected as the observational probability distribution had a lower uncertainty. In other words it can be considered to be more 'believable'. Another feature is that the fused model has a smaller uncertainty than either the prior model or the observational model. This is always the case when using Bayes theorem. As a result regardless of the quality of the observational evidence, in regards to accuracy and precision, an improvement on the prior model is possible. This is dependent however on being able to correctly model the probabilistic distribution of the observational evidence.

2.4.3 Estimation and Control Theory

Control theory enables the user to estimate the behavior and outcomes from a specific set of actions in a dynamic system. Estimation theory deals with the measurement of parameters and systems with random components. Estimation theory can allow

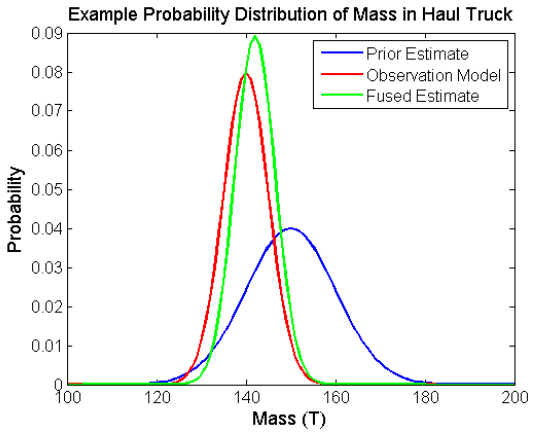

Figure 2.15 – An example showing the fused estimate using Bayes rule. The green line is the fused model. The red line is the observational model of mass of material in the haul truck. The blue line is the prior model on the mass of material located in the truck.

machinery to estimate position, pose, speed as well as many other characteristics. These are some of the reasons it is integrated with control theory to assist in guidance, target tracking and autonomous operations [124].

From the review of material tracking systems in Section 2.3.2 it was evident that there is a lack of systems that take a similiar approach to tracking material through a process chain. This section reviews some of the fundamental estimation and control theory techniques and the applications of these techniques. This gives an overview of the benefits and drawbacks of particular methods in light of being applied to a material tracking scenario.

The Linear Kalman Filter

The Linear Kalman Filter (LKF) is often chosen due to its Best Linear Unbiased Estimator (BLUE) property. It provides the optimal solution in regards to estimation accuracy for any series of operations in which the processes and observations are linear (Gaussian distributed). A brief history of the creation of the Kalman filter was covered in Section 2.4.2. Due to the popularity of the Kalman filter there are many books available describing how the Kalman filter operates and how it is derived [21][12][47][49]. There are several other benefits for using a standard LKF, besides

the BLUE principle. The LKF is capable of being very efficient due to the fact it assumes all noise and processes as Gaussian. A Gaussian distribution requires two variables to define a distribution (mean and variance). Due to this fact, it is efficient in memory storage when the state vector (x) is large. The covariance matrix (P) remains only x^2 in size.

One of the main drawbacks of the LKF is that it can only handle linear systems. This is important when considering estimation of non-linear states. One mine automation example is determining the position of an autonomous LHD vehicle described in a paper by Scheding *et al.* [107]. Being able to consistently estimate the position of the vehicle is shown to be a non-linear process given the effects of wheel slippage. The non-linearity is a factor of the terrain, weather, tyre wear, mass and velocity. The paper by Scheding *et al.* uses an extended Kalman filter (EKF) to model the wheel slip in relation to the position of the LHD.

The LKF traditionally has a fixed state vector. The state vector is a list of the properties in the system which are being estimated. In mining as well as other industries, the material being moved through the process chain is constantly changing in regards to size and location. A state vector which is able to increase and decrease in size to cater for the material as it moves the process chain would be beneficial. It would allow for a more memory efficient means of representing the state space. Additionally it does not require prior knowledge of the exact states which are to be estimated. For these reasons a standard LKF is likely to be a poor choice for representing all the material in single state space.

The Extended Kalman Filter

The EKF is a version of the Kalman filter which can handle non-linear processes and observations. The negative aspect of using the EKF is that it is sub-optimal in regards to accuracy and maintaining statistical consistency, (except in cases where both the processes and observations are linear in which case the EKF is identical to the LKF). The consistency of the states estimated is not guaranteed. The EKF

functions by 'linearising' the non-linear observation and processes, the quality of this linearisation largely decides the quality of the estimate provided by the filter. There is a strong case to argue that a number of processes in the mining cycle have significant non-linearities to influence the consistency of the estimated property values from the filter. One example is blasting and estimating the fragmentation of rock post blast [37]. Hodouin *et al.* [51] describe in their paper several cases of non-linearity which occur during mineral processing ranging from comminution to mineral separation. There are other sections of the mining process which can be considered approximately linear. These mainly involve the standard load-haul-dump cycle (This assumption is validated in Section 3.6.3). The difficulty in implementing an EKF is that it requires an accurate system model in order for the linearisation to be reasonable. In complex systems where systems models are difficult to derive this becomes problematic.

The Particle Filter

A common theme of the previous two methods of estimation is the requirement that each property is Gaussian distributed. This assumption makes it difficult to handle systems with complex non-linear processes. There are a wide variety of Monte Carlo methods which can be applied which overcome these problems. One of the most notable methods is particle filters (also known as bootstrapping, sequential Monte Carlo filters). Particle filters operate by partitioning the state space into a finite set of particles. A probability measure is applied over the set of particles such that areas of high probability are populated by a greater number of particles. Each particle has its own probability mass. A state equation is then applied to project the particles further in time. Observations update each particle's probability mass. Chen [26] provides a great resource for learning about the methods involved in developing a particle filter. Arulampalan *et al.* [11] also provide a tutorial on how to start developing particle filters. The main advantage of using a particle filter is that it is not constrained to the Gaussian distribution. It can handle cases where there is multi-modal distributions and far greater complexity in the probability distributions. The optimality of the solution in regards to representing the true underlying distribution can also be con-

trolled by the number of particles, such that when the number of particles approaches infinity the solution resembles the Bayesian distribution from which the particles are drawn.

The prior stated benefits are useful in the material tracking scenario. Tracking certain properties of material, especially intensive material properties could benefit from the richer representation available in Monte Carlo methods such as particle filtering. An example of this would be the concentration of chemical properties iron ore. The properties of iron, silica, alumina and phosphorous is likely to form a multi-modal distribution when combined from two separate groupings of material with two different chemical property profiles. The particle filter could provide the means to model this combination more accurately than a method which assume a Gaussian distribution for all state variables. This particular problem is discussed in further detail in Chapter 5.

Particle filters however do present several practical problems. The first one is the computational complexity of the filter. Daum [34] illustrates in his paper titled "Curse of Dimensionality and Particle Filters" that as the dimension of the state vector increases the computational complexity increases significantly. In a material tracking scenario, there is likely to be as many states as there is unique locations of material. To maintain a single correlated framework for all material has the potential to become too computationally expensive. As well as computationally expensive, the particle filter is also one of the more difficult filters to maintain and develop. After several iterations of the particle filter, it is likely the majority of particle's probability mass will reduce to near zero. This is known as the degeneracy problem, which is often overcome by increasing the number of particles in the filter, which in turn increases the computational complexity. There is also the need to resample the particles around the particles of high probability mass to ensure that the complexity of the distribution is adequately defined. A central problem with implementing a system such as this on a mine site is that the system may eventually be distributed across a wireless network. A particle filter is significantly less memory efficient than a LKF or EKF, given that the memory required to store the data is directly proportional to the

amount of particles used in estimation. A summary of non-linear filters was by done by Daum [33] and is a useful reference for a more comprehensive comparison between the different non-linear filter types.

A Comparison of Filtering Methods

The preceding section focuses on an overview of three commonly utilised filtering methods. For each filtering method there are multiple subtle versions which alter the behavior of each techniques to fit a specific role. The attributes required of the filter are discussed further in both Chapter 3 and Chapter 5. In brief, the filter needs to achieve the goals stated in Section 2.3.4.

The challenge in developing a filter to fulfill these requirements is that mining is quite a complex process. This is due to the amount of mining processes and the variations in these processes from mine site to mine site, even in the same mineral group. This makes creating a generic filter with process models for each process practically unfeasible in regards to this thesis. For this reason the processes were limited to mass transfer processes such as the load-haul-dump cycle in this thesis. This was due to the fact that proxies for this process chain can be developed cost-effectively and the process and material can be controlled relatively easily.

In the 'ideal world' of unlimited processing speed, unlimited bandwidth and extensive research and development time an ideal solution to the representation problem would be to use a pure discrete Bayesian filter. A pure discrete Bayesian filter can be considered similar to a particle filter, except the particles are not randomly sampled but evenly distributed over the variables of interest. The number of particles tends towards positive infinity. Effectively, this produces the most accurate discrete representation of the underlying probabilistic distribution being modeled. In real world applications pragmatic choices must be made. Particle filters allow for the most robust method for representing the underlying distribution comparative to the LKF and EKF given the particle filters ability to represent non-gaussian multi-modal distributions more accurately. The trade off, again like a pure Bayesian filter is both

memory, processing time and greater development complexity. In cases where the underlying distribution is approximately Gaussian, the LKF / EKF perform almost as effectively with considerably less operational and development overheads. Given this information, it is highly important to have a good understanding of the underlying distribution in question. In Section 3.6.3, an analysis of the experimental data set (containing mass only) used in this thesis is performed. An analysis of a set of truck scales is also done. In both cases the result is the underlying distribution can be thought of as approximately Gaussian.

Given this result, a particle filter for representation of extensive material properties in this experimental scenario would be excessive. Therefore a LKF/EKF solution provides a good point of origin in developing a filtering system to track the extensive material properties over the system processes.

The Augmented State Kalman Filter

One of the prominent trends in the previously mentioned material tracking systems (Section 2.3.2) is the inability to track spatial correlations between material properties as it progresses through a process chain. This problem can be considered quite similar to a robotics problem which has been encountered. Smith *et al.* [113] [112] describe the creation of a map which correlates uncertain spatial relationships. Specifically the paper claims the following "The map contains the estimates of relationships among objects in the map, and their uncertainties, given all the available information. The procedures provide a general solution to the problem of estimating uncertain relative spatial relationships". Since the publication of the paper by Smith *et al.*, the solution has become to be known as an Augmented State Kalman Filter (ASKF). Given the stated contribution, the ASKF provides an excellent foundation for tracking material. Though the ASKF forms the foundation for the filtering method described in this thesis, the ASKF in its original form does not solve all the necessary requirements. These are namely that in essence the 'map' in mining requires the addition as well as subtraction of features, it also requires the ability to conserve mass in the system.

One of the other techniques used in robotics which has similarities to the ASKF is what is known as Simultaneous Localisation and Mapping (SLAM) which is described in tutorials such as those by Dissanayake *et al.* [36]. The purpose of the SLAM algorithm is for an autonomous vehicle to map the features of an environment. As the vehicle moves over the environment, the features which are mapped are then used to localise the vehicle. There has been work in the field to optimise this process to run over large areas and with computational efficiency. An example is the implementation by Montemerelo *et al.* [87] known as FastSLAM, which uses a combination particle and EKF filter.

The techniques for ore tracking used in this thesis are closely related to target tracking and autonomous vehicle localisation. In particular, the augmented state estimation method developed here can be likened to the Simultaneous Localisation and Mapping (SLAM) problem. However, instead of dynamically changing the state vector to add features to a map, we dynamically change the state vector to add or remove lumped masses of excavated material. The augmented state representation is also used to constrain estimates to conserve mass throughout the system. The point of excavation can also be considered similar to the vehicle in SLAM which is to be localised.

Constrained Kalman Filtering

One of the difficulties in developing a filter for practical use is incorporating real-word constraints and ensuring consistency. Constrained Kalman filters have been developed to ensure that physical real world constraints are incorporated into a Kalman filter framework. Massicotte *et al.* [76] provide an example of how a positivity constraint can be introduced to a state variable. Another example is in Simon and Chia's paper [111], which describes a method for state equality constraints being integrated into the Kalman filter. Rao *et al.* [98] show a method for horizon constrained filtering which can be used to solve nonlinear constraints, though at the expense of the BLUE property of the Kalman Filter. One of the requirements of the material tracking problem is to ensure that the amount of material in the system remains consistent. An example would be an estimate of the material removed from a grade block and the

estimate of the amount of material in a haul truck. This is what is referred to in this thesis as the conservation of mass principle. The total mass estimated to be removed by the haul truck from the grade block should always be consistent. Such that if there is 300T estimated to be removed from the grade block, that material should be allocated to specific subsequent locations in the mining process, including mass which has become unrecoverable throughout the mining process (such as through losses).

Developing this constraint is discussed in Chapter 3.

2.4.4 Machine Learning

The problems addressed by machine learning can be broadly classified into two main fields, regression and classification. Regression is the act of developing a function to best represent a set of data over a designated domain. Classification can be thought of as associating a particular set (or subset) of data with a class. Mjolsness and DeCoste [84] describe machine learning as "the study of computer algorithms capable of learning to improve their performance of a task on the basis of their own previous experience". This describes how fundamentally machine learning techniques allow for data to drive model development. This is where machine learning differs from control theory approaches. Conventional control theory relies largely on the developer to input into the system an amount of application specific knowledge. One example of this are the system models used in Kalman filters to transition between time states. A machine learning approach still requires knowledge of the system, but in a more generic way.

There are many approaches to machine learning. Some examples include neural networks, graphical models, mixture models, principle component analysis, support vector machines and kernel machines. There are several books available which can give an introduction to machine learning techniques [105][17][92]. The area in which this thesis is particularly focused is on Gaussian processes (A kernel machine method). This is used for probabilistic volume estimation in Chapter 4.

The similarities between the Kalman filter and the machine learning technique of

Gaussian processes is highlighted in Reece and Roberts paper [101]. The techniques for fusing additional data follows the same mathematical process. The paper by Ko and Fox [63] gives an example of how Gaussian processes can be integrated into particle filters and Kalman filters to improve prediction and observational models compared to the standard parametric models. This however comes at a cost of additional computational complexity. The decision in this thesis not to use Gaussian processes to model the system processes and observations (volume estimation in the large scaled experimentation will use Gaussian processes) is again one of pragmatism. Given there is currently no probabilistic system available to track material the first step is to trial the simplest solution possible. A simple solution has the benefit of being quicker to develop and easier to understand and therefore maintain. Once the performance of the simplest solution is evaluated, if the accuracy is outside the targeted levels a re-evaluation may be necessary. Gaussian process regression is also typically a computationally expensive task which could inhibit real-time operation. This is discussed further in Section 4.8.

One of the contributions of this thesis is a system for probabilistic volume estimation where Gaussian process regression is used to model a 2.5D surface and a triple integration is performed to estimate the volume and uncertainty.

The decision to use Gaussian processes is based on the need to represent volume probabilistically. Gaussian processes allow for a continuous probabilistic representation over a set of variables, which is important when considering developing a probabilistic volume estimation method to integrate into a similarly probabilistic tracking system. Gaussian processes are able to appropriately assign uncertainty over areas where data is not available. By correctly correlating the spatial relationships between data points, Gaussian processes are the best linear unbiased estimator of the underlying probabilistic representation [62]. This makes Gaussian processes a powerful tool to be used for interpolating over sparse data points.

When considering volume estimation, the ability to have a multi-resolution representation allows for a flexible manner in which speed and accuracy can be made as a trade off when numerically integrating or representing a volume of material. Gaussian

processes are a non-parametric technique, which places a lot of emphasis on allowing the data to drive the probabilistic representation. A series of hyper-parameters used in the covariance function change the general behavior of the function chosen. The hyper-parameters can be optimised by such methods as maximising the marginal likelihood of the output function (given a set of training data) conditioned on the hyper-parameters. The textbook by Rasmussen and Williams [100] is an excellent source for further learning in Gaussian processes.

Gaussian processes (though using a different name and methodology) have been effectively used in the mining domain for some time. Kriging [77] is a common technique which is used in geostatistics to correlate spatial data and generate interpolated geological models. One difference between conventional Kriging and Gaussian processes is that in Kriging a variogram is designed to represent the uncertainty in spatially separated data points. Gaussian processes use covariance functions (with a set of hyper-parameters) which effectively generate the variogram intrinsically from the given training data. There has been prior work in the field of terrain modelling using Gaussian processes such as the paper by Plagemann *et al.* [97] on developing a predictive terrain model using Gaussian processes to enhance path planning for a legged robot. An example in the mining domain is shown in the paper on modelling large scale mine geometry using Gaussian processes by Vasudevan *et al.* [122].

A more in-depth discussion on the mechanics and algorithms involved in performing Gaussian process regression can be found in Chapter 4.

2.4.5 Volume Estimation

Estimating the volume of a region or of a discrete item has become increasingly valuable across a range of industries. In mining, there is a trend towards greater estimation of volume at different sections in the mining process. One possible explanation for this is the benefits provided by greater process control, planning and reconciliation which can be achieved by improving the quality of information is becoming more renown. One of the areas in which current volume estimation techniques

are lacking is in regards to providing an adequate encapsulation of the quality of the volume estimate. The quality of the estimate is important when considering how to integrate the volume estimate with prior knowledge of the volume of the material at a particular location. This thesis is particularly focused on the 2.5D problem of estimating a volume of material located on the ground in which the surface is observed by a sensor system. The techniques can also be applied to estimation of non 2.5D problems provided certain constraints are met.

One of the requirements, of the approach in this thesis, for estimating the volume of a large irregular surface is obtaining a 3D point cloud of the surface by a sensor system. Example sensor systems include laser, radar and camera. Typical methods for estimating volume require interpolation between the data set points in order to map the surface. The volume is estimated from the interpolated surface to the ground plane. The primary problem with the current range of methods is that there is no way of accurately estimating the surface when data on the surface is missing (such as a physical occlusion) or the distance between points is sparse. This has increasingly led to hard engineered solutions where dense 3D point clouds of the surface are gathered in order to ensure accuracy. The downside of this solution is that the sensors are typically expensive and the process is more time intensive as it requires observations with no occlusions.

Gaussian processes provide a framework for surface modelling which overcome these problems. Gaussian processes provide a method for incorporating uncertainty in sensor observations. This enables less accurate sensors to be utilised, as well as providing a statistically sound method for inference on the surface model by adequately encapsulating the spatial correlations in the data. These spatial correlations are learned during the estimation process. The functional representation the surface model provided by the Gaussian process method allows for volume to be estimated by an integration of the function over a designated area. This integration can be done either intrinsically or a set of inference points can be gathered and integral approximations can be made on these points.

This thesis provides a method for volume estimation using Gaussian processes to

model the surface of the data. Experiments are performed to validate the performance of this method against other state-of-the-art methods. The experiments provide a comparison of covariance functions used in the Gaussian process model to determine their effect on the volume estimation process. This method is used to estimate material in a stockpile bin (a proxy for a grade block). This method of volume estimation is used as an input into the material tracking and estimation system which is discussed in Chapter 3.

To gain an understanding of how this method differs from current state-of-the-art techniques, an overview of other techniques follows. Volume estimation techniques have been implemented in a variety of different industries to suit the needs of each particular situation. One example is approximating the volume as simple shapes [95] (spheres, cubes, prisms etc), which can be used in quality assurance measures in the food industry. In the medical industry, the marching cubes and voxel representation [70] (and the latter marching tetrahedrons) are popular to visualise and estimate volumes of body components from imaging systems such as MRI (Magnetic Resonance Imaging).

In the mining industry, estimating irregular 3D volumes and the geostatistical properties has been discussed and implemented by systems such as LYNX [52][28] to estimate the volume and geological properties of ore bodies.

This thesis addresses the problem of estimating volume from a 2.5 D surface data and its corresponding uncertainty. There have been many techniques designed to address this problem as it is a common requirement in surveying tasks. One of the most common volume estimation techniques used is a triangulated surface projected against a plane [130]. Triangle polygons are often generated using a Delaunay triangles algorithm [35][67]. The triangles are tesselated in such a way that no triangle overlaps with another. This forms a continuous surface known as the Triangulated Irregular Network (TIN). Once the triangle tessellation is complete, the volume of a sectional plane can be generated by adding the volumes of each triangular prism together. An example of this process for a mining application can be seen in the paper by Kudowor *et al.* [66].

Another method commonly used is elevation maps (also known as height maps). An elevation map is effectively a series of (x,y) points arranged in a grid format with corresponding elevation (z) values. From the elevation map, volume can be calculated in several ways. This can be either through a cell based method in which trapezoidal prisms are formed over the gridded data or through a mathematical integration method such as trapezoidal, Simpson and averaging. Recently Bewley *et al.* [16] describe a real-time volume estimation system for a dragline which uses a height map as the basis for its volume estimation. In this example, averaging is done to create the height for each cell in the grid; the volume is then calculated using the area of the grid multiplied by the averaged height grid for that particular cell.

The inaccuracy of using linear interpolators (such as TINs) is a well reported problem in surface estimation. Chen and Lin [25] discuss using a cubic spline in order to more accurately represent the surface and avoiding the "sharp edges" prevalent in linear methods such as trapezoidal and triangular prisms. Using irregular intervals while integrating has been proposed as one method for improving accuracy [23]. Easa [43] discusses a similar solution to Chen and Lin, but instead using a Hermite polynomial with allowance for intervals which are unequal during integration. Yanalak [128] provides a comparison of the current state-of-the-art volume estimation techniques over three separate volume cases along with a method for calculating volumes using rectangular prisms.

As discussed in Section 2.3.2, a method for measuring the uncertainty of an estimate is necessary when trying to incorporate this information into a wider probabilistic system as it allows for effective fusion of information. Therefore, the representation provided by Gaussian processes is ideal for incorporating into such a system. Swales [115] uses an approach similar to this in his paper on volume estimation of beach fronts to estimate erosion. This is done using Kriging and the average of three numerical integration methods to determine the volume estimate. The method in this thesis differs in its approach to that used of Swales beyond the methodology differences between Gaussian processes and Kriging. The uncertainty estimated in the method by Swales is calculated by averaging the estimated error at each inferred point times the

total area. The derivation using Gaussian processes in this thesis (see Section 4.3.3) requires the inclusion of the covariance between inferred points when calculating the uncertainty, this requires a 4D integral compared to a 2D integral.

Chapter 4 discusses how Gaussian processes can be used in the volume estimation process to provide accurate estimates of volume along with the associated uncertainty in the volume estimates.

Chapter 3

Modelling Extensive Material Properties

3.1 Introduction

Tracking of discrete products through a process chain has received a significant amount of research (see Section 2.3.2). The current state-of-the-art methods typically involve tracking products in inventory systems (with assumed known properties) through discrete identifying marks such as bar codes, RFID tags and serial codes.

The process chains in primary industries such as mining and agriculture have several factors which make these prior techniques in tracking systems less ideal. The nature of bulk materials from these particular primary industries makes it difficult to place identifying markers on each piece of material given the size and amount of material.

In open pit mining, the commercial tracking systems (as well as reconciliation systems) described in Section 2.3.2 are not end-to-end. The estimation of material properties over the processes which are tracked is also not done probabilistically.

One of the problems with current state-of-the-art tracking and estimation systems is the discrepancies between the input of one system compared to the output of an earlier system. To make reconciliation possible, this discrepancy is often accounted

for by the use of 'factors'. The paper by Morley [88] describes briefly the process of reconciliation with factors as well as some of the negative aspects in using this approach. An example of a common factor used is the relative grade received at the plant compared to the expected grade given the geological model. For example this factor could be 105%, meaning that the ore processed at the plant is 5% higher on average then the expected grade from the geological model.

One of the difficulties in using reconciliation on mine sites is being able to use the data effectively to improve operational performance. The large length and time scales over which the data is collected and reported means the data is often used reactively. The large length factors also make it difficult to isolate which mine processes are causing a bias in the results. This can mask operational problems within the system. As an example, the reconciliation factor over a set of processes for a material property may be 100%. This would suggest the mine plan is performing as expected. However, another possibility is that one process may be operating at 110% while another at 90%, but given the large length scale this is averaged to 100% for a given reconciliation factor and would suggest that there is no operational issues.

A probabilistic end-to-end estimation and tracking system would provide the capabilities for improving not only reconciliation in mining, but also substantial benefits for control and planning in an autonomous mine.

In order to achieve this, a new probabilistic representation for material properties at each stage in the mining process is necessary. As discussed in Section 2.4.2, a probabilistic representation allows for consistent fusion of information from a variety of sources of different quality. One of the benefits of using a Bayesian approach is that provided the observational model is correct, any additional information always decreases the uncertainty of the prior estimate. This allows for utilisation of noisy sensors such haul truck strut pressure monitors to be able to be actively used in mine operations to improve the performance of the estimation system.

Estimating the material properties at each location in the mining process, while maintaining the spatial correlations between the estimated material and its prior source locations, enables the capability to reconcile over the shortest of length scales

in the mine process chain. For example, observing the amount of material in the excavator bucket would enable using this information to update the estimated amount of material removed from the grade block from which it was excavated.

In an autonomous system, a real-time inventory of material at each location on a mine site would have significant operational benefits. It firstly provides feedback to planning systems in a format which enables for effective mine plan decision making. For example, if the estimate of the grade of material in the stockpile is below the required grade, it could prompt an alteration of a mine plan to mine more high grade material. It would also benefit in the control and planning of autonomous equipment. The estimate of mass in a haul truck would be useful in determining an accurate dynamic model enabling better control and path planning.

This chapter introduces a system for probabilistic estimation using a Bayesian framework. In addition to this, it is shown that integration of both the tracking and probabilistic estimation systems provides several substantial benefits. These benefits include more effective use of information sources, real-time reconciliation and the ability to ensure that all flows of mass in the system are accounted for (ensuring a conservation of mass). This is validated through small and large scale experiments which simulate a process chain of an open pit mine.

The method used in this chapter is a constrained augmented state Kalman filter. A brief review of this technique and similar Bayesian methods is found in Section 2.4.3.

3.2 Problem Formulation

3.2.1 The Lumped Mass Model

One of the problems in tracking of bulk material is managing the scale at which the material properties are represented as a single entity (with a single mean and variance on each property). When dealing with extensive properties one solution is to set the scale at the same resolution as the information sources. An example of this solution

would be to represent material in a haul truck as one entity given that sensors, such as haul truck strut pressure monitors, typically measure that total mass of material in the haul truck. A similar scenario can be applied to material in an excavator bucket. An entire stockpile volume can be estimated by acquiring 3D point cloud data of the stockpile surface to estimate the bulk volume.

One of the issues involved in this process is that different sensing systems provide different levels of resolution on the various material properties. Therefore additional processing and modelling may be required when integrating sensor data of different resolutions. This is needed to maintain a system where all material properties at a particular unique logical location can be defined by a single mean and variance.

The 'lumped mass model' is a term used in this thesis to describe the method for representing and discretising the excavated material into manageable components based on a unique logical location. This is done to reduce the complexity of the estimation problem into smaller manageable parts. The lumped mass model implies that material is estimated based on its separation from other lumps of material. A unique logical location describes a grouping of material which provides a useful resource for mine operations and observation of the material properties. For example, the material in a haul truck is a unique logical location. Grouping the material stored at this location is logical both for observing the properties as well as for using the information about the material properties at this location to aid in the planning and control of the vehicle.

At any point of time the system is estimating as many lumped masses as there are logically separated groupings of material. The properties of a lumped mass can be represented as a probabilistic vector $P(X_n)$. An example of X_n can be seen in Equation 3.1 using properties which may be of interest in iron ore mining.

$$X_n = [M, V, Fe, SiO_2, Al_2O_3, Fragmentation]^T \tag{3.1}$$

Where n represents the location identifier for the lump (e.g. excavator bucket, haul truck, stockpile), M is mass, V is volume, Fe is iron%, SiO_2 is silicon dioxide%,

Al_2O_3 is aluminium oxide% and $Fragmentation =$ is ore fragmentation level.

A probabilistic estimate exists for each of the listed material properties defined in the vector X_n.

3.2.2 Comparing Mass, Volume and Bulk Volume

Mass and volume represent the two extensive properties of lumped material which can measure the quantity of the material present.

The majority of volume estimation techniques on large scales measure bulk volume. Bulk volume is the volume of area the material occupies including the gap spaces between the material. Volume can be extrapolated from this by determination of the bulk factor (see Equation 3.2).

$$B_f = \frac{V_b}{V_t} \tag{3.2}$$

Where B_f is the bulk factor, V_b is bulk volume and V_t is volume.

Depending on the consistency of the material and the configuration in the space which it is occupying, the bulk factor can vary significantly. These variations may be small in certain scenarios. An example is excavating a fine soft, homogeneous and dry material. The nature of material such as this minimises the gap between the material. Conversely, material such as blasted stocks on a mine site often fragment the material into a wide spread of sizes. This can lead to variations in the bulk density on a load-by-load basis given the configuration of the material in both the excavator bucket and haul truck.

One of the requirements for integrating both probabilistic estimation and tracking using the method described in this thesis is placing a modelling constraint on one of the extensive material properties. The precise reasoning for this is explained in Section 3.5. The ideal choice is the property which has the most accurate representation of the amount of material present at each location.

Mass and volume (not bulk volume) essentially fulfill the same purpose of describing the amount of material present at a location. In the experiments used in this thesis the observations of mass are considerably more accurate then the observations of volume resulting in much greater accuracy in estimates. Mass is therefore used as the constrained property. Volume can still be included as a property which is tracked and estimated in the lumped mass model.

3.3 The Kalman Filter

A brief introduction to the properties of the LKF and why it is an attractive choice for probabilistic estimation was discussed in Section 2.4.3. This section briefly outlines the mathematical processes involved in the discrete LKF.

The LKF equations can be separated into two steps known as the 'prediction' step and the 'update' step. The prediction step outlines how to project forward in time each of the different state vector values. It is also used to project forward in time the covariance matrix describing how the different state vector elements are correlated to each other.

The prediction equation for the state vector is as follows:

$$x_{k+1} = Fx_k + Bu_k \tag{3.3}$$

x_{k+1} is the predicted state estimate at the time interval $k+1$. x_k is the prior state estimate before prediction at time interval k. F is known as the state-transition matrix and describes how states in vector x_k changes between the time intervals k and $k+1$. u_k is a linear additive input to the state estimate. The matrix B describes how the input u_k relates to the state estimate over the time period between k and $k+1$.

The prediction equation for the covariance matrix is described in Equation 3.4.

$$P_{k+1} = FP_kF' + GQ_kG' \tag{3.4}$$

P_{k+1} is the predicted covariance matrix associated with the state estimate x_{k+1} at the time interval $k+1$. P_k is the prior covariance matrix at time interval k. F is the state transition matrix from Equation 3.3. Q_k and G denote respectively system noise and a projection matrix of that noise onto the estimated system states.

Equations 3.3 - 3.4 combine to form the prediction step. The update step occurs when independent observational data which can either directly or indirectly provide information on one of the systems states. The update process can be broken down into 5 main equations. Equations 3.5 - 3.9 describe the update process.

$$v_{k+1} = z_{k+1} - Hx_{k+1} \tag{3.5}$$

v_{k+1} is referred to as the innovation. The innovation is the residual between the observed data to the predicted states in x_{k+1}. z_{k+1} is a vector containing the observational data. H is the observational model (or sensor model) matrix which describes how the observational data relates to each element in the state vector.

$$S_{k+1} = HP_{k+1}H' + R \tag{3.6}$$

S_{k+1} is the innovation covariance. R is the sensor noise matrix.

$$W_{k+1} = P_{k+1}H(S_{k+1})^{-1} \tag{3.7}$$

W_{k+1} is known as the Kalman weighting (or Kalman gain). The Kalman weight defines how much weighting is given to the observational data given the priori data.

$$x^+_{k+1} = x^-_{k+1} + W_{k+1}v \tag{3.8}$$

x^+_{k+1} is the posterior state estimate. This is the resultant state estimate vector after the observational data has been included. The $-$ and $+$ define prior and post observational update respectively.

$$P^+_{k+1} = P^-_{k+1} - W_{k+1} S_{k+1} W'_{k+1} \tag{3.9}$$

P^+_{k+1} is the posterior covariance estimate.

From Equations 3.3 - 3.9 it is important to note that the LKF is a recursive estimation tool. The only data which is required to be stored is the current estimate of both the state vector (x_k) and covariance matrix (P_k). This efficiency is one of the reasons why the Kalman filter is a very popular choice in a wide range of computationally and memory sensitive applications.

LKF Summary:

The LKF can be broken down into a *prediction* and *update* step. The equations required to complete each step are as follows:

Prediction:

$$x_{k+1} = Fx_k + Bu_k$$

$$P_{k+1} = FP_kF' + GQ_kG'$$

Update:

$$v_{k+1} = z_{k+1} - Hx_{k+1}$$

$$S_{k+1} = HP_{k+1}H' + R$$

$$W_{k+1} = P_{k+1}H(S_{k+1})^{-1}$$

$$x^{+}_{k+1} = x^{-}_{k+1} + W_{k+1}v$$

$$P^{+}_{k+1} = P^{-}_{k+1} - W_{k+1}S_{k+1}W'_{k+1}$$

3.4 Probabilistic Estimation

Bulk material tracking and estimation systems in mining can be improved by taking a Bayesian (see Section 2.4.2) approach for representing data. This allows for appropriate encapsulation of prior knowledge based on modelling and information sources to be effectively weighed when fusing additional data from new information sources.

3.4.1 A Non-tracking Method

One approach to probabilistic modelling is to model each lumped mass with an individual LKF. This would begin with an initialisation of the lumped mass properties based on a theoretical model. The lumped mass properties can then be updated whenever new information is available. This would fulfill the goal of obtaining a probabilistic estimate of the material at each location. An example of this applied to a mining scenario can be seen in Figure 3.1. The 'Out of Ground Model Interface' would be a communications layer which would be capable of retrieving information about material properties from the Kalman filter estimate in regards to a specific lump location when required. The lumps estimated would be generated from one end of the system to the other.

It should be noted that the non-tracking methodology can be applied to a variety of Bayesian filter types. The Kalman filter can be directly substituted for a particle filter for example. Given that dimensionality is less of issue under these conditions

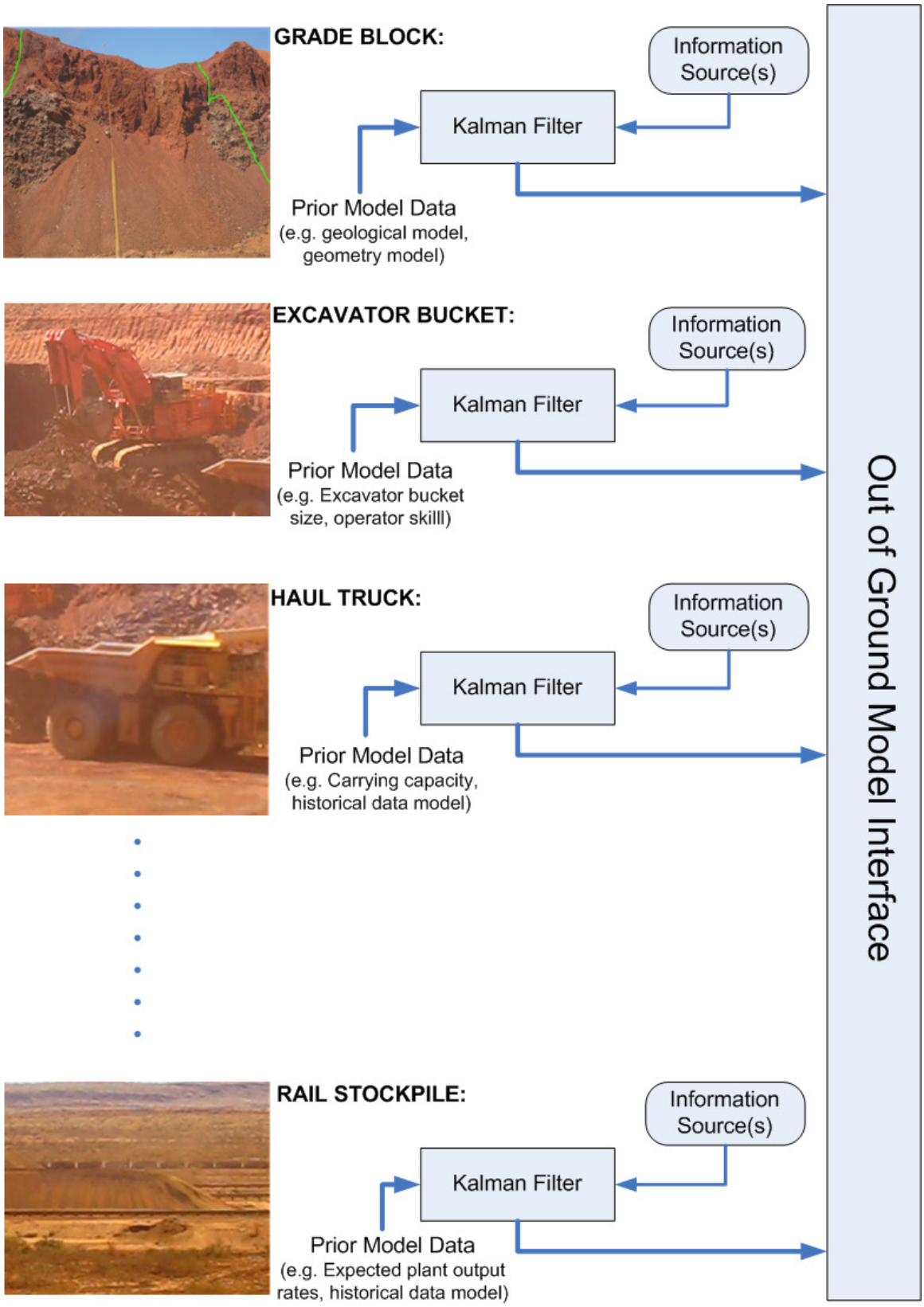

Figure 3.1 – A series of LKFs could be used to estimate lumped masses at different locations. This method however, does not take into account the spatial correlations between extensive lumped mass properties.

(compared to a single framework containing all lumps) this may form a more accurate estimation system for a variety of material properties (particularly intensive).

3.4.2 The Importance of Spatial Correlations in Bulk Material Process Chains

Efficient Utilisation of Information Sources

The primary drawback from the non-tracking system described in Section 3.4.1 is that it does not take into account the spatial correlations which exist between lumped masses.

As an example from Figure 3.1 it is clear to see that additional independent information about the mass of material in the excavator bucket should increase the understanding of how much material has been removed from the grade block. Furthermore, additional information from information sources at the haul truck about the mass of material removed should further increase this understanding of material removed from the grade block.

The non-tracking system does not incorporate this spatial correlation and therefore does not make the most efficient use of the information sources available. A system which could incorporate the spatial correlations consistently when fusing additional information about specific properties of a lumped mass has the potential to reduce the uncertainty of these material property estimates over correlated states.

The Conservation of Mass

One of the issues in current bulk material tracking and estimation methods, as well as with the prior estimation only method, is that there is no statistically consistent method for ensuring a 'conservation of mass'. The principle behind the conservation of mass is that in a closed system the total mass should remain consistent.

Applying this principle to a open pit mining operation, one would expect that the total mass of material removed from the ground should be equivalent to the total mass located in all the lumped masses located on the mine site. This is assuming we temporarily disregard that an open pit mine is an open system, given that mass is removed from the system by train or port to the customer and all material is stored on the mine. The principle can be reduced to smaller frames of reference such as between the excavator and the grade block. In this example system, it is expected the total mass in the excavator bucket is equivalent to the change in mass removed from the grade block.

If the end-to-end estimation system is to be accurate it needs to ensure that there is no 'creation' or conversely 'destruction' of mass between the different processing stages. By maintaining a link to all spatially correlated lumped masses by tracking the material through each stage in the process chain, a method for constraining the total mass present in the system can be developed.

Reconciliation

Reconciliation is an important part of the mining process. It provides validation of both geological and mining models and can be used to improve operational performance. One of the difficulties in applying reconciliation currently is the significant delay between actual production and reconciliation of the product. Another problem is the lack of certainty in the quality of data used during the reconciliation process.

Using a tracking and estimation system which takes advantage of the spatial relationships between the material at different locations creates the opportunity to perform reconciliation in real time.

3.5 A Constrained Augmented State Kalman Filter

One way of accounting for the spatial correlations between lumped masses is to use a single state vector which contains all of the lumped masses to be estimated in the

system. One of the problems which needs to be addressed is that the total number of lumped masses in the system is is likely to be dynamic. An example from mining is that when material is excavated, divided and stockpiled the amount of lumped masses both increases and decreases as the material is divided and grouped together respectively. As a result, a conventional LKF with a fixed length state vector cannot efficiently store the lumped masses to be estimated. The Augmented State Kalman Filter (ASKF) solves this problem with the capability of 'augmenting' new states into the state vector. A brief introduction to the ASKF was presented in Section 2.4.3. Equation 3.10 describes how each of the lumped masses sit inside the Kalman filter state vector.

$$x_k = [X_1, X_2, ..., X_{j-1}, X_j]^T \tag{3.10}$$

x_k is the Kalman filter state vector. The vector $X_i \in x_k$, where $i = [1, 2, ..., j-1, j]$, represents a collection of all lumped masses which are to be estimated in the system. X_i can contain a set of states such as those showed in Equation 3.1.

The factor which still needs to be accounted for in the tracking and estimation is the real-world constraint that the system must conserve mass. A discussion of constraint based Kalman filtering was discussed in Section 2.4.3. Some of the drawbacks of constraints in Kalman filters discussed were that they can add additional computational complexity or remove the BLUE property of the Kalman filter. The proposed method in this thesis preserves the BLUE property of the LKF. This is done by taking advantage of the characteristics of both the ASKF as well as the properties of bulk material process chains. By ensuring that a specific set of system models are applied, a consistent set of spatial relationships between extensive material properties over different lumps can be maintained.

3.5.1 Initialising Lumped Masses into the ASKF

The ability to 'augment' new states into the ASKF is what differentiates it from a standard LKF. Initialising a lumped mass into the system is a relatively straightfor-

ward task. Equations 3.22 and 3.23 detail how to first augment a new lumped mass (X_n) into the state vector (x_k).

$$x_{k|X_n} = \begin{bmatrix} x_k \\ X_n \end{bmatrix} \tag{3.11}$$

where $x_{k|X_n}$ is the Kalman filter state vector, once the new lumped mass has been augmented in, X_n is a vector containing the states of interest to be estimated in each lumped mass (See Equation 3.1).

$$P_{k|X_n} = \begin{bmatrix} P_k & 0 \\ 0 & \sigma^2_{X_n} \end{bmatrix} \tag{3.12}$$

where $P_{k|X_n}$ is the new covariance matrix which includes the initialised covariance values associated with the new lumped mass ($\sigma^2_{X_n}$).

The creation of a new lumped mass in a bulk material process chain is the result of removing material from a previous larger lumped mass. Thus whenever a new lump is initialised into the filter it has a spatial correlation with the prior lumped mass in which it was sourced from. The following equations dictate how to generate the spatial correlation in the ASKF when initialising.

$$x^{\#}_{k+1} = Ax_{k|X_n} \tag{3.13}$$

$x^{\#}_{k+1}$ is the ASKF state vector, the # superscript defines that that this is the post augmentation and initialisation of the new lumped mass X_n. A is defined as a design matrix used to initialise the new lumped mass state correlations to previous states in the ASKF state vector.

$$P^{\#}_{k+1} = AP_{k|X_n}A^T \tag{3.14}$$

$P^{\#}_{k+1}$ is the ASKF covariance matrix post augmentation and initialisation.

An Example Lumped Mass Initialisation

Take a very simple example of a system with one existing lumped mass. For this example the existing lumped mass is a stockpile of bulk material. The stockpile has an excavator remove a portion of material thus generating a new lumped mass in the system which needs to be augmented and initialised. For simplicity the only property estimated is mass (X_n = [m]).

Prior to excavation:

$$x_k = [m_{stockpile}] \tag{3.15}$$

$$P_k = \left[\sigma^2_{stockpile}\right] \tag{3.16}$$

Equations 3.15 and 3.16 represent the ASKF state and covariance matrixes respectively prior to any material being excavated. The next step is the initialisation once a new lump has been generated by removing material from the stockpile and placing it into the excavator.

Material is loaded into excavator:

$$x_{k|X_{excavator}} = \begin{bmatrix} m_{stockpile} \\ m_{excavator} \end{bmatrix} \tag{3.17}$$

$$P_{k|X_{excavator}} = \begin{bmatrix} P_k & 0 \\ 0 & \sigma^2_{excavator} \end{bmatrix} \tag{3.18}$$

The operations performed in Equations 3.17 and 3.18 is that which was described in Equations 3.22 and 3.23.

The next step in the initialisation process is to perform the modelling to generate the spatial correlations between the new lumped mass excavator state and the

prior lumped mass stockpile state. This also updates the state vector estimate of the stockpile lumped mass to take into account the removed material.

The design matrix A describing how the material in the excavator is correlated to the material in the stockpile is described in Equation 3.19.

$$A = \begin{bmatrix} 1 & -1 \\ 0 & 1 \end{bmatrix}, \tag{3.19}$$

Given the design matrix A, equations 3.13 and 3.14 are performed to generate the post initialisation state vector ($x^{\#}_{k+1}$) and covariance matrix ($P^{\#}_{k+1}$).

Post initialisation result:

$$x^{\#}_{k+1} = \begin{bmatrix} m_{stockpile} - m_{excavator} \\ m_{excavator} \end{bmatrix} \tag{3.20}$$

$$P^{\#}_{k+1} = \begin{bmatrix} \sigma^2_{stockpile} + \sigma^2_{excavator} & -\sigma^2_{excavator} \\ -\sigma^2_{excavator} & \sigma^2_{excavator} \end{bmatrix} \tag{3.21}$$

As seen from the results in Equations 3.26 and 3.29 the system behaves intuitively. The mass in the stockpile is reduced by the mass in the excavator. The stockpile variance is increased by the variance associated with the mass of material in the excavator bucket. The cross correlation terms show that the spatial correlation between the two lumped masses is equivalent to the variance of the mass in the excavator bucket.

3.5.2 Combining Lumped Masses in the ASKF

Combining lumped masses occurs when separated lumps are joined together through some external transfer process. The process for combining these lumps is shown

mathematically below for the extensive properties ω_1 and ω_2.

$$x_k = \begin{bmatrix} \omega_1 \\ \omega_2 \end{bmatrix} \tag{3.22}$$

where x_k is the Kalman filter state vector with two extensive material states ω_1 and ω_2.

$$P_k = \begin{bmatrix} \sigma^2_{\omega_1} & 0 \\ 0 & \sigma^2_{\omega_2} \end{bmatrix} \tag{3.23}$$

P_k contains two spatially uncorrelated lumped masses.

Now using the Kalman filter state and covariance prediction formulas (See Equation 3.3 and 3.4, where we assume there is no linear input ($u(k)$) or process noise $Q(k)$. The state transition matrix F to combine the vector state ω_1 into the vector state ω_2 can be given as:

$$F = \begin{bmatrix} 0 & 0 \\ 1 & 1 \end{bmatrix}, \tag{3.24}$$

alternatively if ω_2 is being combined into ω_1 the state transition matrix F can be given as:

$$F = \begin{bmatrix} 1 & 1 \\ 0 & 0 \end{bmatrix}, \tag{3.25}$$

The only remaining step is to remove the empty lumped mass state from the state vector and covariance matrix.

3.5.3 Removing Lumped Masses from the ASKF

Removing a lumped mass should be performed when a system process removes all lumped material from a unique location and it is combined with another lump(or initialised into a new lump at a new location). Mathematically, this process involves removing the rows and columns associated with the lumped mass in the covariance matrix(P_k) and state matrix(x_k).

One of the difficulties in removing a lumped mass from the ASKF is determining when a prior lump has been depleted to effectively zero mass or volume. For material stored in excavator buckets and haul trucks which by their nature remove material when performing certain operations makes it easier to remove these states. For other states such as stockpiles and grade blocks it is a more difficult operation.

An Example Combining and Removal of a Lumped Mass

Following on from the prior example of initialisation of a lumped mass (Equations 3.15 - 3.29), the excavator unloads the material into a haul truck. This example assumes that all the material in the excavator bucket is removed and added to the haul truck.

Prior to haul truck loading:

$$x_k = \begin{bmatrix} m_{stockpile} - m_{excavator} \\ m_{excavator} \end{bmatrix} \tag{3.26}$$

$$P_k = \begin{bmatrix} \sigma^2_{stockpile} + \sigma^2_{excavator} & -\sigma^2_{excavator} \\ -\sigma^2_{excavator} & \sigma^2_{excavator} \end{bmatrix} \tag{3.27}$$

The next step is to initialise the haul truck lumped mass then combine the excavator lumped mass with it. This example assumes that the haul truck has no material currently loaded.

Initialise haul truck:

$$x_k = \begin{bmatrix} m_{stockpile} - m_{excavator} \\ m_{excavator} \\ 0 \end{bmatrix} \tag{3.28}$$

$$P_k = \begin{bmatrix} \sigma^2_{stockpile} + \sigma^2_{excavator} & -\sigma^2_{excavator} & 0 \\ -\sigma^2_{excavator} & \sigma^2_{excavator} & 0 \\ 0 & 0 & 0 \end{bmatrix} \tag{3.29}$$

Transfer excavator lump to haul truck:

$$F = \begin{bmatrix} 1 & 0 & 0 \\ 0 & 0 & 0 \\ 0 & 1 & 1 \end{bmatrix}, \tag{3.30}$$

Then using Equations 3.3 and 3.4 the resultant state vector and covariance matrix can be given as

$$x_{k+1} = \begin{bmatrix} m_{stockpile} - m_{excavator} \\ 0 \\ m_{excavator} \end{bmatrix} \tag{3.31}$$

$$P_{k+1} = \begin{bmatrix} \sigma^2_{stockpile} + \sigma^2_{excavator} & 0 & -\sigma^2_{excavator} \\ 0 & 0 & 0 \\ -\sigma^2_{excavator} & 0 & \sigma^2_{excavator} \end{bmatrix} \tag{3.32}$$

As can be seen in Equations 3.31 and 3.32 the material in the excavator bucket, along with the spatial correlations to the stockpile have been transferred to the haul truck. The excavator lumped mass can now be removed from the state filter if desired by removing both the row in the state vector containing the excavator lumped mass properties as well as in the row and column in the covariance matrix.

In this example this is done by removing the second row from the state vector and the second row and column from the covariance matrix. One can verify whether it is possible to remove a lumped mass by analyzing both the state vector and covariance matrix rows and columns. If all the cell values are equal to 0, removing the lump should not have an impact on the consistency of the filter.

For completeness, the final result from this operation can be seen in Equations 3.33 and 3.34. This is the same as what can be seen in Equations 3.26 and 3.29 which is to be expected given the only process which occurred was a transfer of all the material from the excavator to the haul truck.

$$x_k = \begin{bmatrix} m_{stockpile} - m_{excavator} \\ m_{excavator} \end{bmatrix} \tag{3.33}$$

$$P_k = \begin{bmatrix} \sigma^2_{stockpile} + \sigma^2_{excavator} & -\sigma^2_{excavator} \\ -\sigma^2_{excavator} & \sigma^2_{excavator} \end{bmatrix} \tag{3.34}$$

3.5.4 A Modelling Constraint

One of the trends in the prior models for initialising, combining and removing lumped mass is the tendency to use the set of numbers $-1, 0, 1$. The interactions between different lumped mass extensive properties during movement of the lumped masses through a process chain can be defined into 3 categories. These categories are full negative correlation, no correlation and full positive correlation. This modelling constraint is done to ensure the conservation of mass over all of the lumped masses in the system. Equations 3.35 - 3.39 show the reasoning for this constraint using the extensive material properties ω_1 and ω_2.

Two lumps prior to applying model:

$$x_k = \begin{bmatrix} \omega_1 \\ \omega_2 \end{bmatrix} \tag{3.35}$$

$$P_k = \begin{bmatrix} \sigma^2_{\omega_1} & 0 \\ 0 & \sigma^2_{\omega_2} \end{bmatrix} \tag{3.36}$$

Equations 3.35 and 3.36 describe two lumped masses with a yet to be defined spatial relationship.

Equation 3.37 describes a generic state transition matrix F used in standard linear Kalman filtering to describe the relationship between these two lumped masses.

$$F = \begin{bmatrix} i & j \\ k & l \end{bmatrix} \tag{3.37}$$

Now using the Kalman filter state and covariance prediction formulas (See Equation 3.3 and 3.4), where we assume there is no linear input ($u(k)$) or process noise $Q(k)$. The result becomes the following:

$$x_{k+1} = \begin{bmatrix} i\omega_1 + j\omega_2 \\ k\omega_1 + l\omega_2 \end{bmatrix} \tag{3.38}$$

$$P_{k+1} = \begin{bmatrix} i^2\sigma^2_{\omega_1} + j^2\sigma^2_{\omega_2} & lj\sigma^2_{\omega_2} + ik\sigma^2_{\omega_1} \\ lj\sigma^2_{\omega_2} + ik\sigma^2_{\omega_1} & l^2\sigma^2_{\omega_2} + k^2\sigma^2_{\omega_1} \end{bmatrix} \tag{3.39}$$

In order to constrain the problem to ensure that no mass is created or destroyed the significance of square component of i, j, k, l must be eliminated from the diagonal terms in Equation 3.39. This can be achieved by setting the values of i, j, k, l to the subset of real numbers $-1, 0, 1$.

3.5.5 Mass Loss

One of the assumptions used in all prior examples is that process noise (Q_k) is equal to zero. This assumes no noise is present in the system models. The system models that are needed for conservation of mass assume that mass transfer between lumped masses is the entirety of the mass. As can be seen from Figure 3.2 where an excavator is loading a haul truck with bulk material, this is not the case. The loss of material either over time or during the transfer process must be included in the previously described system. By not including losses in the system it risks becoming inconsistent if these losses are significant.

Figure 3.2 – Portions of bulk material can be 'lost' as lumped masses move through a mining process chain. This material needs to be accounted for to ensure consistency in the estimates given a conservation of mass constraint.

These losses can be accounted for using the existing initialising and combining method

which have been described previously. A new loss lumped mass can be created to represent the material that has separated from the excavator bucket in Figure 3.2.

An Example with Mass Loss

This example shows how to incorporate the losses as shown in Figure 3.2 into the ASKF representation. The process used is described in Section 3.5.1. The initial representation is as follows:

Prior to applying loss model:

$$x_k = \begin{bmatrix} m_{stockpile} - m_{excavator} \\ m_{excavator} \end{bmatrix} \tag{3.40}$$

$$P_k = \begin{bmatrix} \sigma^2_{stockpile} + \sigma^2_{excavator} & -\sigma^2_{excavator} \\ -\sigma^2_{excavator} & \sigma^2_{excavator} \end{bmatrix} \tag{3.41}$$

A loss lumped mass is then initialised which estimates how much material is lost from the excavator during the transfer process.

Initialise loss model:

$$x_{k|X_{loss}} = \begin{bmatrix} m_{stockpile} - m_{excavator} \\ m_{excavator} \\ m_{loss} \end{bmatrix} \tag{3.42}$$

$$P_{k|X_{loss}} = \begin{bmatrix} \sigma^2_{stockpile} + \sigma^2_{excavator} & -\sigma^2_{excavator} & 0 \\ -\sigma^2_{excavator} & \sigma^2_{excavator} & 0 \\ 0 & 0 & \sigma^2_{loss} \end{bmatrix} \tag{3.43}$$

Once the loss lumped mass is initialised it is then applied to the excavator bucket.

Apply loss design matrix to excavator bucket:

$$A = \begin{bmatrix} 1 & 0 & 0 \\ 0 & 1 & -1 \\ 0 & 0 & 1 \end{bmatrix}, \tag{3.44}$$

$$x_{k+1}^{\#} = \begin{bmatrix} m_{stockpile} - m_{excavator} \\ m_{excavator} - m_{loss} \\ m_{loss} \end{bmatrix} \tag{3.45}$$

$$P_{k+1}^{\#} = \begin{bmatrix} \sigma_{stockpile}^2 + \sigma_{excavator}^2 & -\sigma_{excavator}^2 & 0 \\ -\sigma_{excavator}^2 & \sigma_{excavator}^2 + \sigma_{loss}^2 & -\sigma_{loss}^2 \\ 0 & -\sigma_{loss}^2 & \sigma_{loss}^2 \end{bmatrix} \tag{3.46}$$

To complete the process, a haul truck lumped is intialised and then combined with the excavator lumped mass. It is assumed, as in previous examples, that the haul truck has no material currently inside. This follows the process described in Section 3.5.2.

Initialise haul truck lumped mass:

$$x_k = \begin{bmatrix} m_{stockpile} - m_{excavator} \\ m_{excavator} - m_{loss} \\ m_{loss} \\ 0 \end{bmatrix} \tag{3.47}$$

$$P_k = \begin{bmatrix} \sigma_{stockpile}^2 + \sigma_{excavator}^2 & -\sigma_{excavator}^2 & 0 & 0 \\ -\sigma_{excavator}^2 & \sigma_{excavator}^2 + \sigma_{loss}^2 & -\sigma_{loss}^2 & 0 \\ 0 & -\sigma_{loss}^2 & \sigma_{loss}^2 & 0 \\ 0 & 0 & 0 & 0 \end{bmatrix} \tag{3.48}$$

Apply state transition matrix:

$$F = \begin{bmatrix} 1 & 0 & 0 & 0 \\ 0 & 0 & 0 & 0 \\ 0 & 0 & 1 & 0 \\ 0 & 1 & 0 & 1 \end{bmatrix}, \tag{3.49}$$

Result:

$$x_{k+1} = \begin{bmatrix} m_{stockpile} - m_{excavator} \\ 0 \\ m_{loss} \\ m_{excavator} - m_{loss} \end{bmatrix} \tag{3.50}$$

$$P_{k+1} = \begin{bmatrix} \sigma^2_{stockpile} + \sigma^2_{excavator} & 0 & 0 & -\sigma^2_{excavator} \\ 0 & 0 & 0 & 0 \\ 0 & 0 & \sigma^2_{loss} & -\sigma^2_{loss} \\ -\sigma^2_{excavator} & 0 & -\sigma^2_{loss} & \sigma^2_{excavator} + \sigma^2_{loss} \end{bmatrix} \tag{3.51}$$

The excavator lumped mass can then be removed from the ASKF. As can be seen in Equation 3.51, the loss state is correlated to the material now in the haul truck. Thus if one was able to observe for instance that no material was lost with absolute certainty (i.e. zero mean zero variance on the observation of mass lost) then the state vector and covariance matrix would appear as the following:

Posterior state vector and covariance matrix after zero loss observation:

$$x_{k+1} = \begin{bmatrix} m_{stockpile} - m_{excavator} \\ 0 \\ 0 \\ m_{excavator} \end{bmatrix} \tag{3.52}$$

$$P_{k+1} = \begin{bmatrix} \sigma^2_{stockpile} + \sigma^2_{excavator} & 0 & 0 & -\sigma^2_{excavator} \\ 0 & 0 & 0 & 0 \\ 0 & 0 & 0 & 0 \\ -\sigma^2_{excavator} & 0 & 0 & \sigma^2_{excavator} \end{bmatrix} \tag{3.53}$$

By removing the loss lumped mass from Equation 3.52 and 3.53 the same result is obtained as in Equations 3.33 and 3.34 which is the scenario in which no losses were accounted for.

There are many ways in which the loss lumped mass can be modeled. In the scenario shown in Figure 3.2, the process which is likely to occur is that the loss lumped mass is combined with the grade block lumped mass. This usually occurs when a front end loader pushes the material back into the grade block at the end of an excavation.

This could be modeled by creating two lumped mass loss states. One would contain a short lived excavator loss lumped mass which is generated each time the excavator loads and transfers material to the haul truck. This excavator loss lumped mass, after possibly being observed could then be combined into another lumped mass which would stockpile all of the excavator loss lumped masses. At the point in time when the material is pushed back into the grade block, this loss stockpile lumped mass is then combined into the grade block lumped mass.

Losses throughout the process chain can be modeled by using a similar methodology.

3.5.6 Discussion

The constrained ASKF allows for the proper spatial correlations between lumped masses which ensure conservation of mass in the system to be maintained. This approach leaves the core filtering algorithms are unchanged, thus the ASKF retains the BLUE property.

The performance of this integrated tracking and estimation system is ultimately a function of both the performance characteristics of the information sources provided (and how well these are probabilistically modeled) as well as the accuracy of the system modelling. It is also important that both the information sources and system models can be approximated as Gaussian distributions or, in the case of non-linear processes, in an EKF style representation - linearised with an appropriate level of accuracy.

One of the practical difficulties in implementing a system such as this in both an autonomous and manual environment is deciding when and how to initialise, remove and combine new lumped masses. This is discussed further in Chapter 6 with specific focus on implementing a system described in this chapter in a mining scenario.

3.6 Experiments

To verify the constrained ASKF method two scales of experiments are performed. The experiments are designed to simulate mining processes. The processes involved are the removal of material from a stockpile (a proxy for a grade block) by an excavator. The material is then unloaded into a haul truck which then unloads the material at a stockpile (a proxy for a ROM stockpile). This set of processes was chosen for several reasons. One is that the processes which occur are reasonably simple to model accurately. The set of processes are generic enough to be applied across a wide range of mining, horticulture and agriculture scenarios in that material is removed in portions from a start location and subsequently divided and recombined in stages at a final location. Finally, in a mining context, the set of processes listed is considerably cheaper to simulate comparatively to processes which refine and alter the intensive properties of the bulk material.

One of the difficulties in validating spatial systems is finding an accurate measure of ground truth. This problem increases in difficulty as the amount of material increases in size (e.g. measuring the mass of a large stockpile of material). As systems become larger, the amount of control over system processes also diminishes comparatively to

smaller scale systems. For this reason, a small scale experiment was designed. This experiment allows for complete control over the system dynamics. Most importantly it allows for the extensive properties of the material to be observed by highly accurate information sources at each lumped mass location. This can be then used as ground truth in validating the system. This experiment validates conceptually the method for estimation and tracking developed in this chapter.

A second experiment is of a larger scale. It is designed to mimic conditions which are more realistic of a mining scenario. The system dynamics are less controlled. As an example, on this scale compared to the small scale, it is not possible to control the mass transfer process to occur with 100% accuracy. Most significantly, the extensive material properties at each lumped mass location can not be fully observed. This makes it harder to validate the system compared to the small scale experiment. The observational sources are less precise then what is available for the smaller scale experiment. In addition to these factors, the material and environmental conditions are considerably less controlled which has an impact on properties such as bulk density calculation. The large scale aims to show that the constrained ASKF tracking and estimation method developed in this chapter is able to provide consistent estimates, even when the scale of material and equipment increases in size as well as less control of the system dynamics.

Figure 3.3 gives an overview of the two different experiment scales and the processes. The mining scale is included as a reference to show how the experiments aim to simulate the processes which occur on a mine site. As a point of reference in terms of scale, the small scale experiment utilises approximately 3L of material total. The large scale experiment uses approximately 10T of material in total.

3.6.1 Method for Validation

For the system to be validated, the estimate provided by the system for the extensive lumped mass property should be consistent with the ground truth value. This consistency can be verified using a statistically significant number of sample points.

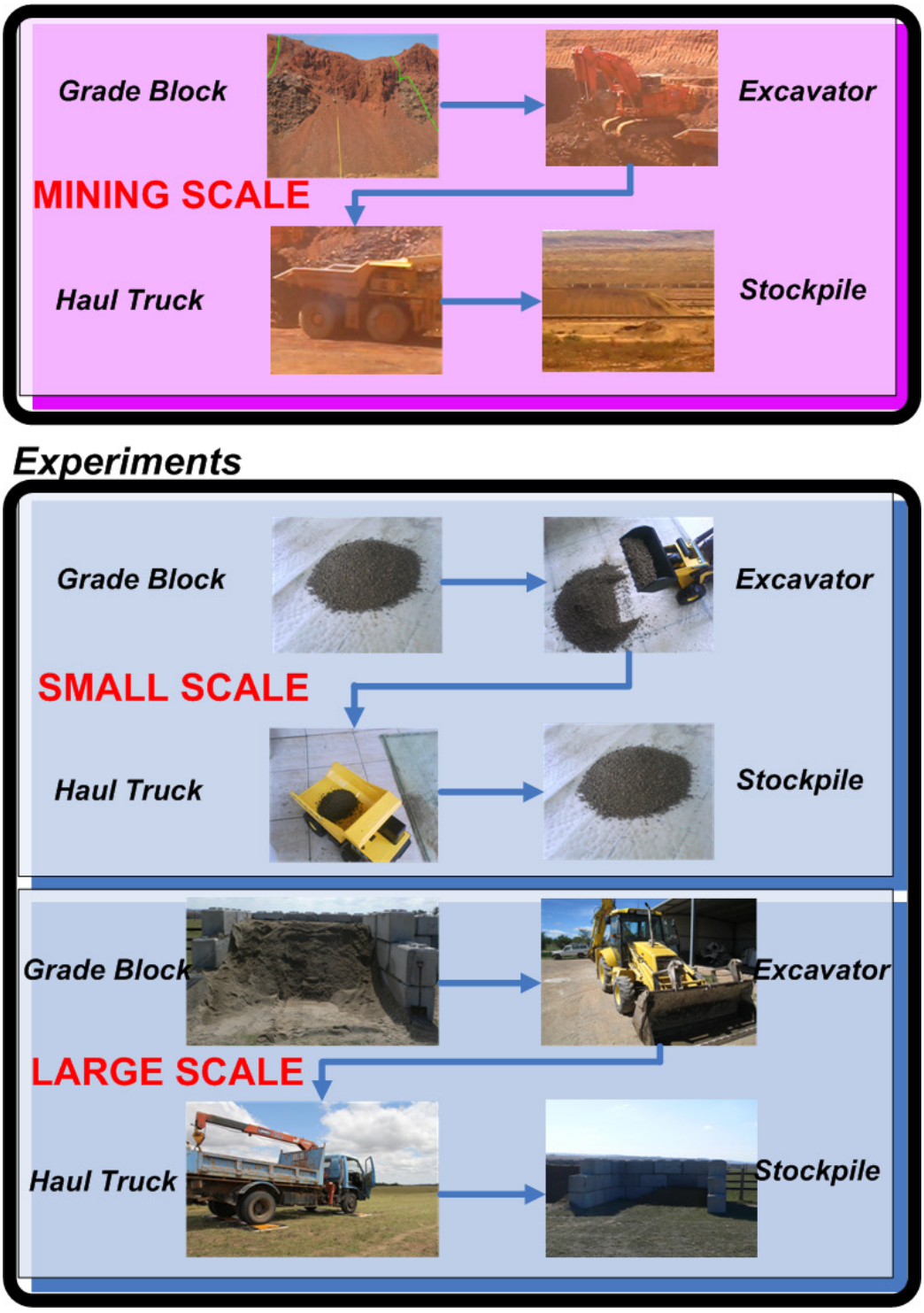

Figure 3.3 – A comparison of the mining scale process chain to the process chains of the experiments performed in this thesis. In the experiments in this thesis the small scale and large scale use approximately 3L and 10T of material respectively.

The ground truth in both scales of experiments is the mass sensor observations. In both experiments, this sensor is a more precise and accurate sensor compared to the bulk volume sensor estimates.

The bulk volume sensor estimates are used as information sources into the system to provide information about the mass at each location. A sensor model is applied to convert the bulk volume estimate to a mass. This model is based on the ability to accurately estimate the bulk factor and the density of the material. For this reason, a beach sand blend is used in both experiments as the material is consistent in size. The sensor model applied is as follows

$$m = V * d \tag{3.54}$$

where m is mass, V is the bulk volume estimated from the information source and d is the bulk density.

The observation noise is calculated by

$$\sigma_m^2 = \sigma_V^2 * d + \sigma_d^2 * V \tag{3.55}$$

where σ_d^2 contains the noise associated with the estimate of the bulk density.

A summary of the goals and assumptions for both the small and large scale experiments:

The central aim of both the small and large scale experiments within this chapter is to validate a method for tracking, estimation and fusion of lumped masses as they progress through a process chain; the experiments are designed to mimic the processes within a mining scenario. The method is described through Equations 3.22 -> 3.53. The method described is a generic approach which provides a method to initialise, transfer, combine and fuse new information about lumped masses as they move through a process chain.

The hypotheses of the method developed in this chapter is:

- Mass is conserved in the system (i.e. over time through application of the above method, no mass is added or removed from the system).
- Estimates of mass at each point in the process chain will remain consistent within 2 standard deviations as the method is applied over time.
- Fusion of new sensor information over time improves the quality of spatially correlated estimates while not invalidating the above two results.

The assumptions of this method are:

- The sensor information will be (through an observation model) represented as approximately Gaussian.
- Lumped masses at any time can be approximately represented as a Gaussian.
- Processes within the chain can be approximately represented as Gaussian. *This includes models for estimating material lost while transferring lumps between locations, initialisation of lumps into the system through external actuations (e.g. loading material from a stockpile using an excavator, material losses, initial stockpile values)*

The intention of the experiments is not to show a complete solution to all the problems involved in the application of the method to a real-world scenario. This aspect is discussed further in Chapter 6 of this thesis. The intent is to prove the underlying method for initialising, transferring, combining and fusing new information about lumped masses as they move through a process chain is valid.

Experimental data (as opposed to simulated date) was used to validate this method as it is essential to validate the assumptions made by the method would be reasonable within a mine like context.

3.6.2 Small Scale

Method

The small scale experiment involves first measuring the initial grade block using a digital kitchen scales ($\pm 1g$ precision) and a measuring cylinder with 5ml gradients. These two sensors can be seen in Figure 3.4.

Figure 3.4 – Information sources used in the small scale experiment. The digital scales are used as the ground truth. The volume estimates are used in conjunction with an estimate of bulk density to provide a mass sensor model.

Each excavator bucket is measured in the measuring cylinder, where it is also weighed. The material is then unloaded into the haul truck. A small portion of material is left in the measuring cylinder which is used to simulate losses. This loss is measured and weighed. The loss data is later used to form a model on how much material is lost over each excavated load. The material left in the measuring cylinder is then placed back into the initial grade block.

Once three excavator loads have been placed into the haul truck, the material is placed into the measuring cylinder where it is measured and then weighed. This material is then unloaded into the final stockpile. A small amount of material is again left in the cylinder to simulate the losses between the excavator and final stockpile. This material after being weighed and measured (again to be used in a loss model) is placed into a separate container which represents material which is lost and likely not to be recovered.

In summary, there are up to seven lumped masses in the system at any one point in time. These include:

- Grade Block
- Excavator Bucket
- Excavator Loss
- Haul Truck
- Haul Truck Loss
- Haul Truck Loss Stockpile
- Final Stockpile

The amount of material initialised in the excavator bucket by the system is based on the average of all of the loads used in the small scale experiment as measured by the scales and measuring cylinder. This data is also used to initialise the uncertainty on the excavator bucket estimate.

The operation of the constrained ASKF over the small scale experiment can be seen in the flowchart in Figure 3.5. Only the excavator bucket and haul truck are observed during the running of the experiment. This is to simulate a similar scenario which is likely to occur on a mine site.

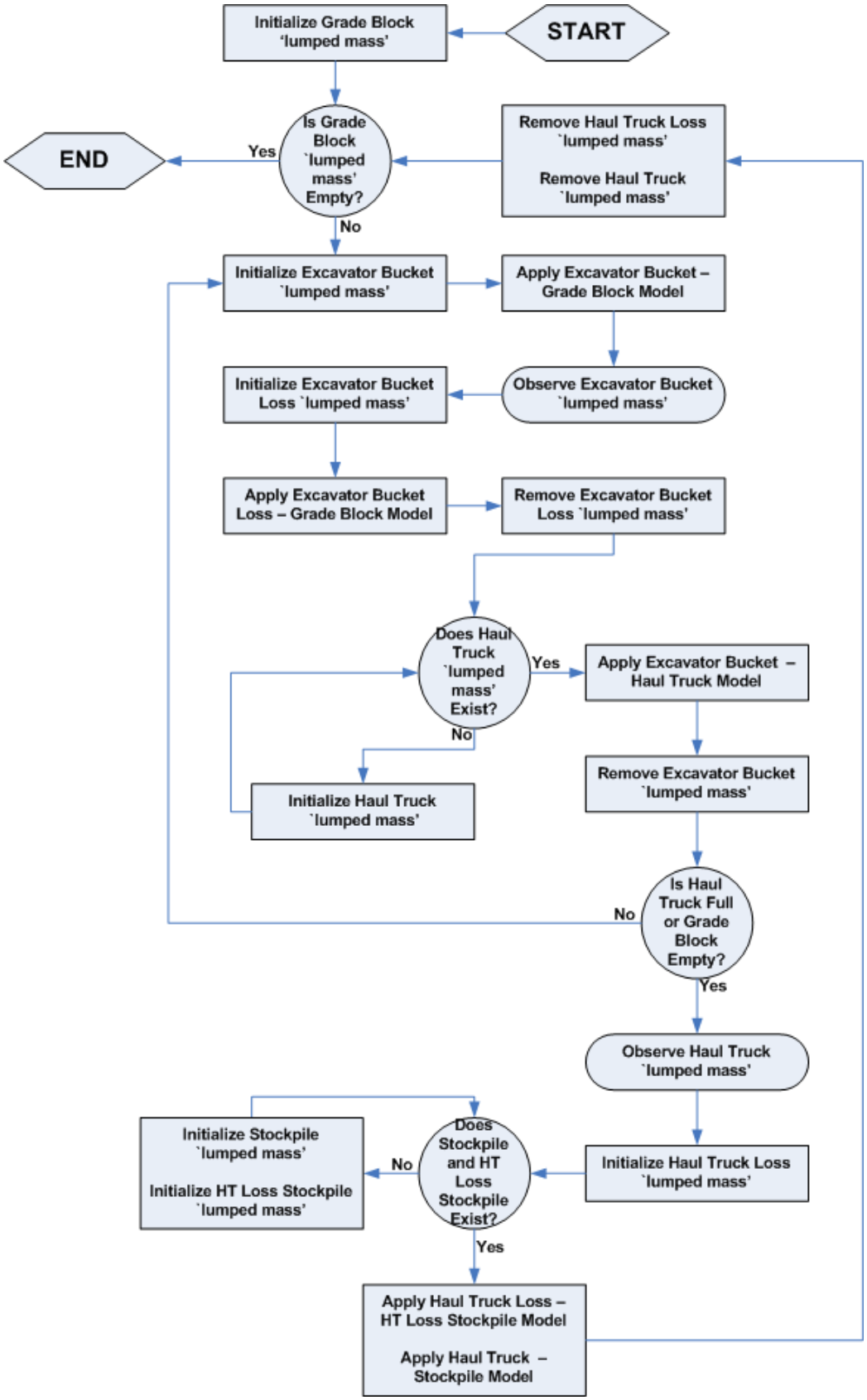

Figure 3.5 – This flowchart describes how the small scale experiment operates within the constrained ASKF framework along with the methodology.

Results

Figure 3.6 shows the residual between the system estimate of mass in the excavator bucket with the ground truth value. It also includes 2σ confidence boundaries from the system estimate. One of the aims of this experiment is to prove that the estimates provided by the system are statistically consistent. In Figure 3.6 95.45% of the residual values should remain within the 2σ confidence boundaries (red lines) in order for the system estimates to be consistent with the ground truth values. As seen in the graph, 3 out of the 43 samples or 93.02% remains within the 2σ confidence boundaries.

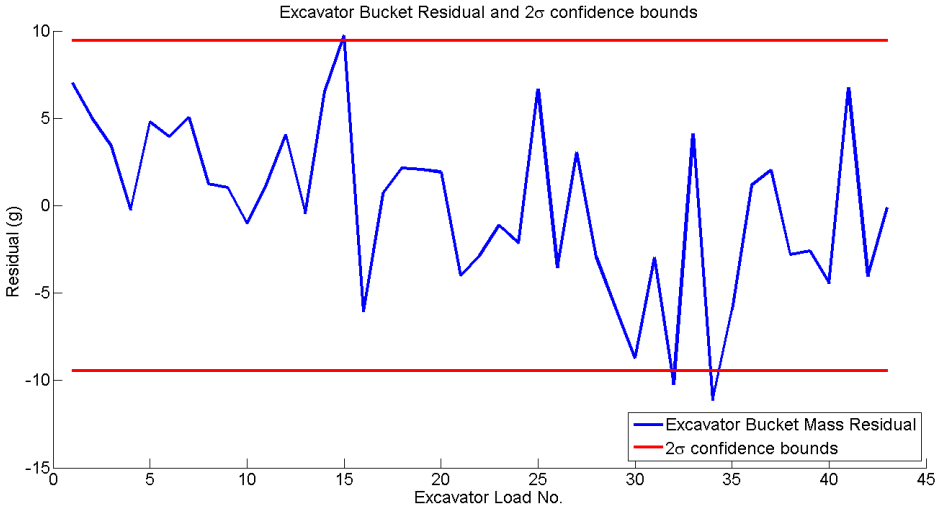

Figure 3.6 – A comparison between the ground truth estimates and the system estimates at the **excavator bucket** lumped mass location. The residual values should ideally be Gaussian distributed with a mean error of 0 and be consistent with the 2σ confidence boundaries estimated from the ASKF system.

Figure 3.7 shows the same variables as Figure 3.6 except the location has changed from excavator bucket to haul truck. In this case 13 out of 15 or 86.6% of the samples are within the 2σ confidence boundaries.

Table 3.5 provides the averaged estimate over the entire experiment of each of the lumped mass locations. This excludes the short lived 'loss' lumped masses which are not observed and are combined into stockpiles which are included in the averaged estimates. In a scenario where both the system models and information sources can

Figure 3.7 – A comparison between the ground truth estimates and the system estimates at the **haul truck** lumped mass location. The residual values should ideally be Gaussian distributed with a mean error of 0 and be consistent with the 2σ confidence boundaries estimated from the ASKF system.

be perfectly modeled as Gaussian distributions and given enough sample points the mean estimate is expected to be 0 (with the error being Gaussian distributed). As can be seen form Table 3.5, the excavator and haul truck states (the locations with the highest amount of samples) have close to 0 mean error with mean errors of 0.01g and 1.4g respectively.

Lumped Mass Location	**Mean Residual**	**Mean 2σ**	**Number of Units**
Grade Block	-12.5 g	86.5 g	1
Excavator Bucket	0.01 g	9.4 g	43
Haul Truck	1.4 g	22.1 g	15
Stockpile	-25 g	221.4 g	1
Haul Truck Loss Stockpile	28.8 g	204.2 g	1

Table 3.1 – A summary of the mean residuals and mean 2σ estimates at each of the lumped mass locations in the small scale experiment.

To test the conservation of mass principle, a comparison between the amount of material in the system at initialisation to the amount of material once the experiment has finished is made. In this experiment the stockpile is initialised with with a mass of $13815g$. The estimated mass at the different lumped mass locations can be seen

in Table 3.2. Summing the values $17.4853g + 12417.7632g + 1379.7515g$ obtains the value of $13815g$. This illustrates that the conservation of mass principle is maintained when using the constrained ASKF.

Lumped Mass Location	**Mass**
Grade Bock	17.4853 g
Stockpile	12417.7632 g
Haul Truck Loss Stockpile	1379.7515 g

Table 3.2 – The estimated mass of the lumped masses in the system at the end of the small scale experiment.

Figure 3.8 provides a graphical representation of the covariance matrix over the small experiment processes. In this figure the haul truck lumped mass states have not been cleared once the trucks have unloaded at the final stockpile. This is to done in this example for two reasons. First, it gives an example of the correlations which develop over time between lumped masses in the process chain (from the grade block to the haul truck to the final stockpile). Secondly, in the experiment only one haul truck is used, by keeping multiple haul truck states in the covariance matrix it provides a representation which is closer to what occurs on a real mine site where multiple haul trucks service one excavator. Zeroed lumped mass locations (excavator, excavator loss, haul truck loss) are also included to give perspective on how some of the additional process states would influence the size of the covariance matrix.

One of the important factors to note is that the covariance matrix is sparse. This is attractive computationally as it allows for the matrix inversion when calculating the Kalman weighting (see Equation 3.7) to take less computational time. This is important given that this is the most computationally expensive operation in the filter.

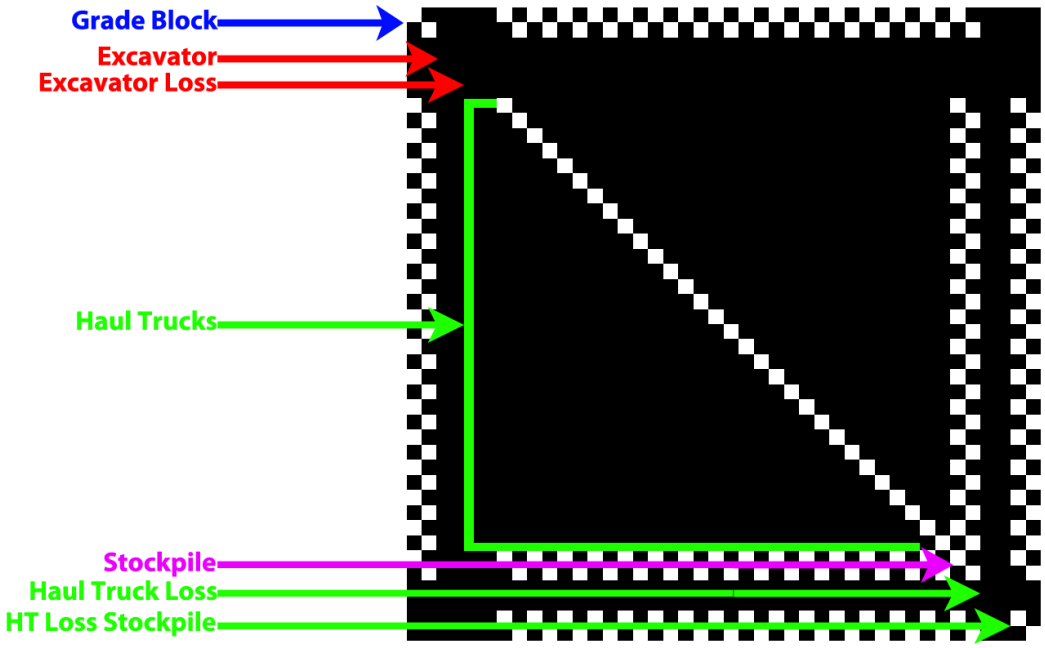

Figure 3.8 – A graphical representation of the covariance matrix (P). The white squares indicate a non-zero value, black indicates a zero value. This is not a consistent system, the lumped mass states of the haul trucks are not zeroed and removed in order to illustrate how the spatial correlations are transferred through the system over time. It also creates a scenario where the amount of lumped masses more closely resembles an actual open pit mine. Each lumped mass consists of mass and volume state.

3.6.3 Large Scale

A Comparison with the Small Scale Experiment

The large scale experiment has the disadvantage of being harder to control and measure all of the processes and lumped masses in the system. This makes it more difficult to verify and model compared to the small scale experiment. The advantage of this experiment is that it provides a more realistic scenario in which the system developed in this thesis aims to be practically utilised.

One of the significant differences between the two experiments is the ability to accurately estimate the density of the material. The small scale experiment was performed in a controlled environment. The material was kept dry, there is also no wind to erode the material away. In contrast, the large scale experiment is performed without any

controls to the weather. The lack of control of the moisture content increases the uncertainty in estimating the density of the material. Areas close to the surface are likely to be less dense since the sun dries the material out, while the material deeper from the surface contains more water and therefore is more dense, this makes the density of the material inconsistent over the entire volume of material. The scale of the experiment performed in this thesis required several days to complete. This leads to the material in stockpiles 'settling' as well as taking on moisture when left overnight. This again increases the uncertainty in estimating the density as the material has a tendency to compact. This causes the density to decrease during this time. These are some of the factors which make modelling the system on the large scale a much more challenging task.

Another point of difference is that it is not possible to explicitly measure the mass of both the grade block and final stockpile. This poses a validation problem compared to the small scale experiment where the material at these locations could have their masses measured directly. To overcome this, the initial grade block ground truth is inferred from the mass scales (see Appendix A.2.3) used to estimate the amount of material in the haul truck. This sensor is used as the ground truth in the large scale experiment due to its accuracy and precision. The amount of material initialised into the grade block is the sum of the mass estimated for each haul truck over the duration of the experiment. Given that a method to observe and model the losses between the grade block, excavator and haul truck was not included as part of this experiment this makes it impossible to include the losses in the initialisation of the grade block. The true mass in the grade block (M_{Grade_Block}) is therefore defined as:

$$M_{Grade\_Block} = \sum M_{Haul\_Trucks} + \sum M_{Losses} \tag{3.56}$$

where M_{Losses} is the material lost between the processes grade block, excavator and haul truck. $\sum M_{Haul\_Trucks}$ is the value which is assumed to be ground truth in this experiment. As a result of this, the large scale experiment does not include loss lumped masses between these states. A similar scenario occurs when inferring

the ground truth for the final stockpile. In this experiment there is no method for observing and estimating the losses between the haul truck and final stockpile. The final stockpile ground truth is inferred as $\sum M_{Haul\_Trucks}$, thus the losses between the haul truck and stockpile are also not included in the estimation and tracking process.

Method

The process followed in the large scale experiment is broadly the same as the small scale experiment. Material is loaded from the grade block, by the excavator where it is then unloaded into a haul truck. When the haul truck is full (after 3 loads) the truck then unloads at the stockpile. Each excavator bucket mass is measured as it enters the haul truck. The haul truck while being loaded is positioned on top of the mass scales. This can be seen in Figure 3.9.

Figure 3.9 – The haul truck waits on a set of truck scales as material from each excavator load is placed into the haul truck. The mass of each excavator load is estimated by subtracting the prior observation of the truck mass from the scales with the estimate of truck mass after the material has unloaded.

The bulk volume of material in the excavator bucket is estimated using a Gaussian process method which is described in Chapter 4. This is done by scanning the grade

block face before and after each excavation, the difference in volume is calculated to be the volume in the excavator bucket. The data for this method is obtained using a Riegl VZ-1000 3D surveying laser (See Appendix A.2.1. 320 uniformly sampled data points are used in the volume estimation process, in this instance a exponential covariance function is used. The results from volume experiments which use a subset of large scale data show that the exponential covariance function is the best placed to encapsulate the uncertainty in the estimate, the uncertainty estimated does have a tendency to be conservative. The Gaussian process method is essential in this process as it provides the ability to encapsulate the uncertainty in the volume estimate. The output from this method is a single mean and variance. This can then be easily integrated into the constrained ASKF representation.

This is then used as an observational source on the mass of material in each bucket (see Section 3.6.1 in the constrained ASKF, the mass observations provided by the scales is used as the ground truth. The process flow of the constrained ASKF can be seen in Figure 3.10.

The Gaussian Assumption

One of the assumptions when using a LKF approach to estimation and tracking is that both the system processes and information sources are Gaussian distributed. This section shows how these assumptions were validated.

When modelling any system, it is often convenient to simplify the problem to make it mathematically, computationally and conceptually more feasible. This simplification can possibly involve the choice of how to represent the probability distributions for the process models, process noise and observation error of the system. One of the most common simplification is to represent these distributions as Gaussian (also known as normal) distributions. The underlying true representation of the different variables we seek to model is often 'unknown'. They are typically approximated through established dynamic laws (e.g. Newton's Laws, Fluid Dynamics etc), empirical methods or a combination of both. In the case of this thesis, the system model properties are

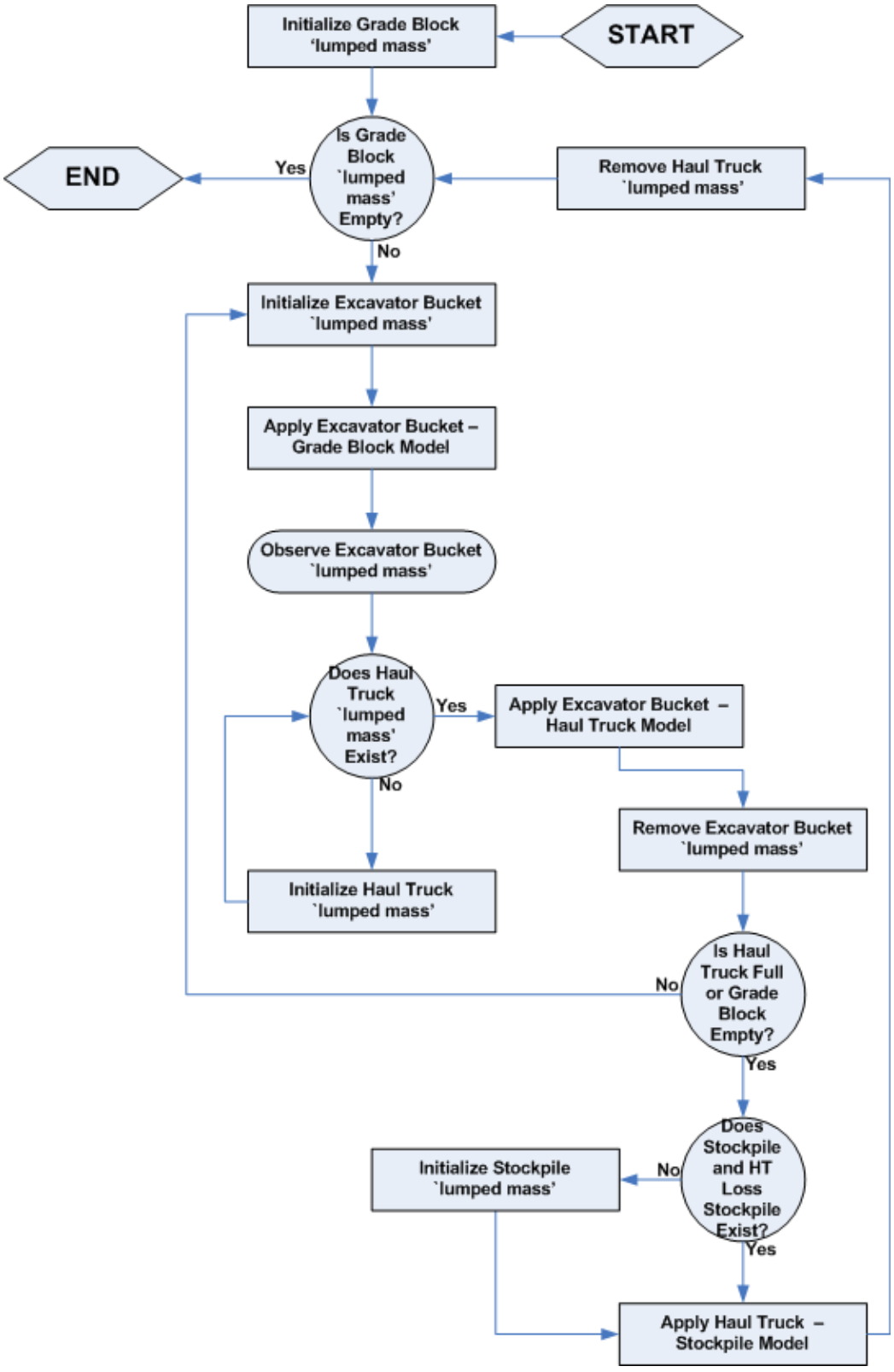

Figure 3.10 – A flowchart showing how the large scale experiment operates within the constrained ASKF framework. This flowchart also shows the methodology of the experiment.

approximated by experimental evidence (empirical).

When making the Gaussian assumption, the underlying probability distribution should be already close to or be able to be transformed close to a Gaussian distribution. There are many different tests and methods which can be used to determine whether or not a set of sampled points comes from a Gaussian distribution. These tests can also provide numerical estimates on how 'close' a distribution is to a Gaussian distribution. These include qualitative graphing methods such as histograms, Quantile-Quantile plots (Q-Q plots) and Gaussian probability plots. There is also quantitative testing methods which include the Kolg-Smirnov test [75], Lilliefors test [69], Pearson's Chi squared test [96], Jarque-Bera test [55] and D'Agostino-Pearson's test [30].

Ideally these tests would be able to show that the distribution of interest has a statistically significant chance of coming from a Gaussian distribution thus validating one of the assumptions of the LKF. Table 3.3 provides a list of Gaussian distribution test algorithms with experimental data from the large scale experiment used in this thesis (data used can be found in Appendix A.1 in Table A.1). The data is of the observed mass inside the excavator bucket. Table 3.3 lists the five example quantitative methods cited previously. The null hypothesis used was that the experimental empirical data has a 95% chance to be from a Gaussian distribution with the parameters derived from the experimental data. For this reason, the Kolg-Smirnov (one-sample) test is not a valid method as the critical values it calculates are incorrect. The critical values are essential in calculating the appropriate confidence intervals on the data. Lilliefor's test performs essentially the same algorithm as Kolg-Smirnov, but with the critical values calculated using Monte Carlo simulation to obtain a more accurate estimate of the critical values for data with smaller sample sizes and from which the comparative Gaussian distribution parameters derived from experimental data.

Not all of the tests in Table 3.3 agree. There are several possible explanations for this. One reason is that the sample size is low (approximately 120 samples) and thus there is a lower probability of obtaining a representative distribution. Another reason is that the underlying distribution may only be borderline Gaussian distributed. This can be seen in Table 3.3 where the probability values for all the test values are $<$

Table 3.3 – Quantitative Gaussian goodness of fit test results for excavator load data set

Method	Significance Level	Probability	Null Hypothesis Satisfied?
Kolg-Smirnov Test	0.05	< 0.001	No
Lilliefor's Test	0.05	0.0268	No
Pearson's Chi Squared(χ^2) Test	0.05	0.0978	Yes
Jarque-Bera Test	0.05	0.0733	Yes
D'Agostino-Pearson's Test	0.05	0.0825	Yes

0.1, given a significance level of 0.05, the test methods provide evidence that the distribution is borderline Gaussian distributed.

Figure 3.11 shows a histogram of the excavator loads over the large scale experiment. From this graph the data appears approximately Gaussian with a slight positive skew of the data at the mean. This can be further seen in Figure 3.12 where the predicted mean of the Gaussian distribution is slightly biased to the right of the mode.

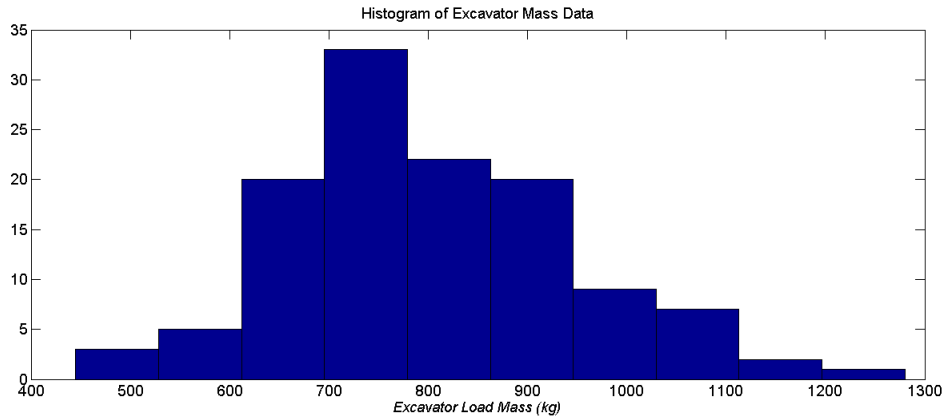

Figure 3.11 – Histogram of excavator load mass data. From this graph, the data appears to take on a shape similar to that of a Gaussian distribution.

The assumption that the observational model of the mass sensor (see Appendix A.2.3) used in the large scale experiment is also Gaussian distributed is validated in the same way. The data set is derived from weighing the haul truck with no loaded mass multiple times.

Table 3.4 shows the results of the different Gaussian tests using this data set. All of the numerical goodness of fit tests agree that the data is likely to come from a Gaussian

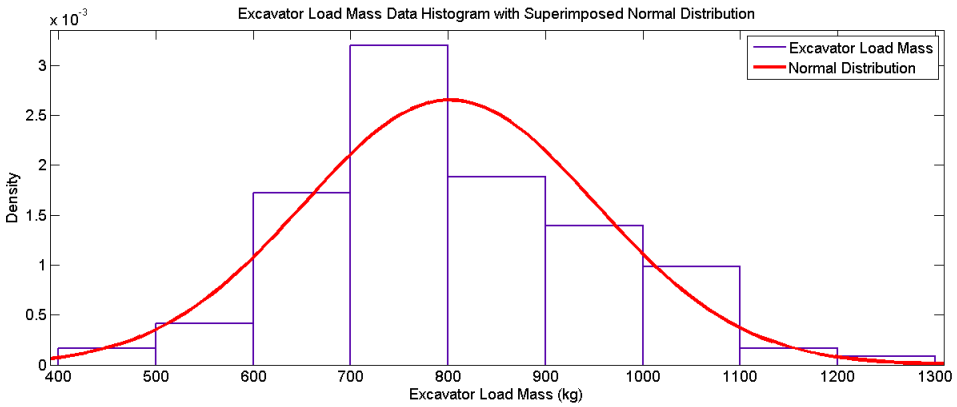

Figure 3.12 – Histogram of excavator load mass data with superimposed Gaussian distribution. The Gaussian distribution is calculated from the data set used to generate the histogram.

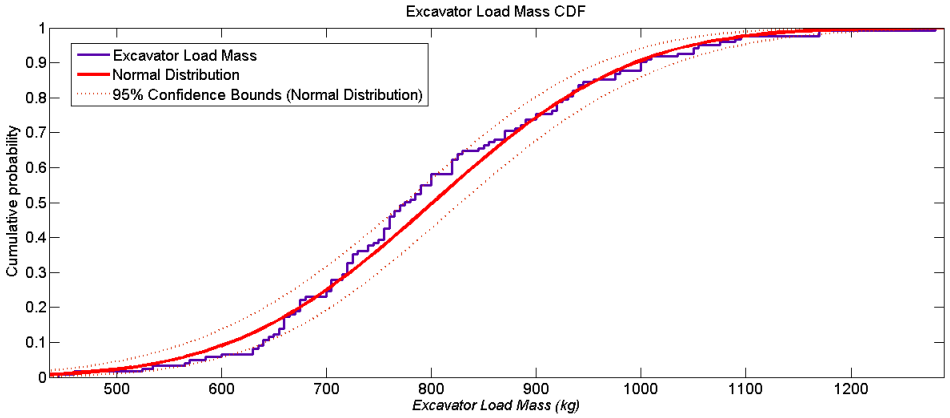

Figure 3.13 – Cumulative density function of excavator load mass data with comparative Gaussian distribution cumulative density function.

distribution. The probability levels show a reasonable level of confidence in these results comparative to the excavator load model. The histogram with superimposed Gaussian distribution generated from the data set seen in Figure 3.14 also shows that representing the underlying distribution as a Gaussian distribution is a reasonable assumption. Similar to the prior analysis using the excavator mass data, there is a tendency for outliers with a positive skew from the mean. The cumulative density function comparison shown in Figure 3.15 illustrates that despite the outlier values, approximating the distribution as a Gaussian distributed appears to be reasonable assumption.

Table 3.4 – Quantitative Gaussian goodness of fit test results for unloaded haul truck data set

Method	Significance Level	Probability	Null Hypothesis Satisfied?
Lilliefor's Test	0.05	0.0697	Yes
Pearson's Chi Squared(χ^2) Test	0.05	0.2831	Yes
Jarque-Bera Test	0.05	0.1173	Yes
D'Agostino-Pearson's Test	0.05	0.1827	Yes

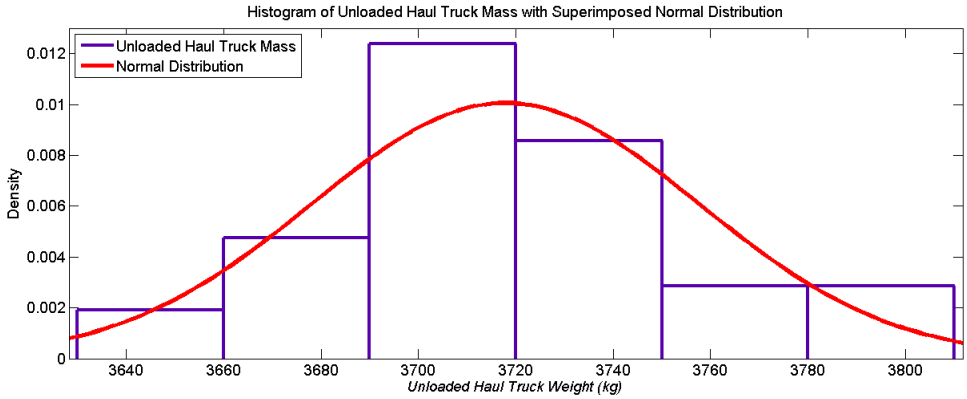

Figure 3.14 – The histogram of unloaded haul truck data with superimposed Gaussian distribution suggests that the sensor has a Gaussian error.

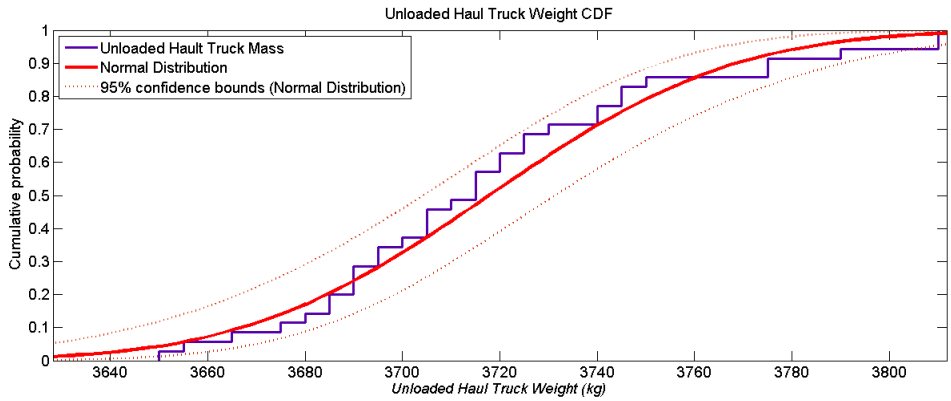

Figure 3.15 – Cumulative density function of unloaded haul truck data with comparative Gaussian distribution.

For completeness, the bulk volume sensor Gaussian assumption is briefly validated through the histogram shown in Figure 3.16. A Gaussian assumption for the underlying data set reasonably encapsulates the underlying distribution. There is a substantial amount of skewing though which does occur around the mean which is

not entirely encapsulated by the Gaussian distribution. The data used in this graph is derived from the large scale experiment described in Section 4.7 using the residual values (as a % of total volume) from the Gaussian process method with exponential covariance function with 320 samples over all of the experiments.

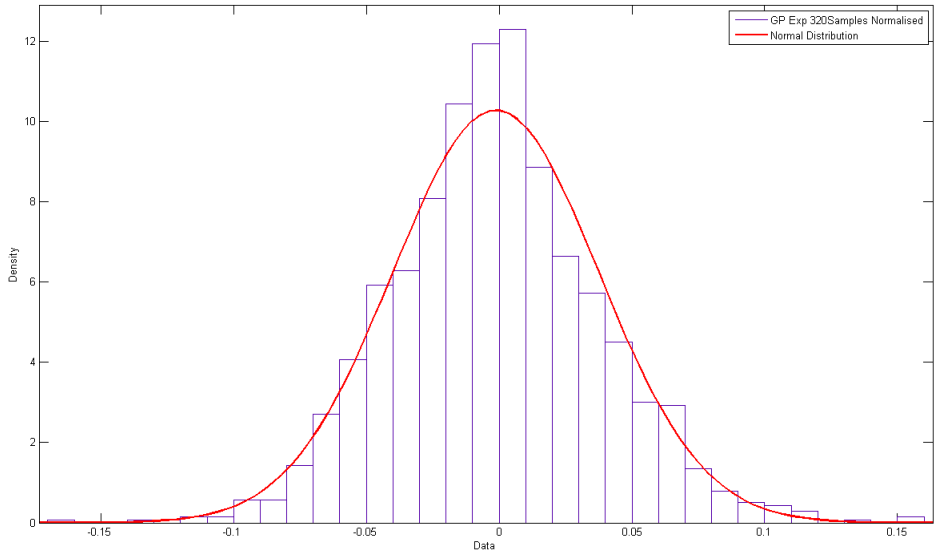

Figure 3.16 – The histogram of residual error of the volume information source with superimposed Gaussian distribution shows that the Gaussian approximation is a reasonable approximation. There appears to be slight biases in the distribution, such as near the mean, overall the Gaussian distribution encapsulates the data well.

The prior statistical analysis of the excavation process and mass / bulk volume information sources is performed to validate the Gaussian assumption which is used in the tracking and estimation process in the ASKF. Each of the data sets could not be exactly described by a Gaussian distribution, however the Gaussian distribution in all cases was able to represent the overall probability mass of the underlying distribution with a reasonable level of accuracy.

Results

Figure 3.17 shows the residual at the excavator lumped mass location along with 2σ confidence boundaries. Over the 105 samples, it is expected that there be approximately 5 values outside of the confidence bounds shown. From the graph, 4 samples are outside the bounds. This shows that the mean and uncertainty estimated by the ASKF is consistent with the ground truth values. The discrepancies in numbers can be explained by factors such as small sample size as well as the fact that the process models and information sources can not be exactly approximated as Gaussian distributions.

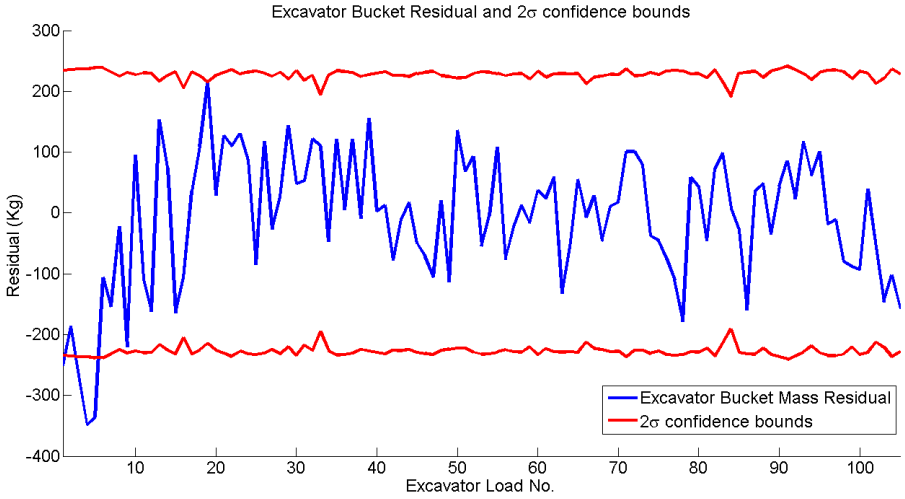

Figure 3.17 – A comparison between the ground truth estimates and the system estimates at the **excavator bucket** lumped mass location in the **large scale** experiment. The residual values should ideally be Gaussian distributed with a mean error of 0 and be consistent with the 2σ confidence boundaries estimated from the system.

Figure 3.18 shows the residual at the haul truck lumped mass location along with 2σ confidence boundaries. Over the 35 samples, it should be expected that there be approximately 2 values outside of the confidence bounds. From Figure 3.18 it can be seen that 3 samples are outside the bounds.

The mean estimates at each of the lumped mass locations is summarised in Table 3.5. The grade block and stockpile having the same mean residual values is a consequence

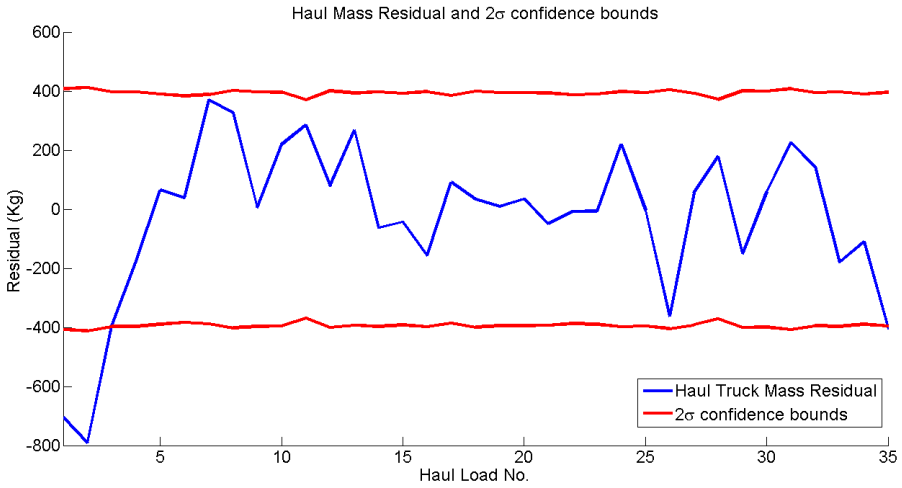

Figure 3.18 – A comparison between the ground truth estimates and the system estimates at the **haul truck** lumped mass location in the **large scale** experiment. The residual values should ideally be Gaussian distributed with a mean error of 0 and be consistent with the 2σ confidence boundaries estimated from the system.

of the ground truth being inferred from the same source as explained at the beginning of Section 3.6.3. At the excavator bucket and haul truck locations the mean residuals have errors of -8.605 Kg and -25.815 Kg respectively. Given an average excavator and haul truck load of 769.2381 Kg and 2307.7143 Kg the mean residual as a % of the average load can be given for both as -1.1%. This small error can again be reasonably explained through small sample size and inaccuracies in the Gaussian approximation.

Lumped Mass Location	**Mean Residual**	**Mean 2σ**	**Number of Units**
Grade Block	903.5258 Kg	2336.7 Kg	1
Excavator Bucket	-8.605 Kg	227.77 Kg	105
Haul Truck	-25.815 Kg	394.6577 Kg	35
Stockpile	-903.5258 Kg	2336.7 Kg	1

Table 3.5 – Summary of mean residual results from the large scale experiment.

The initial grade block had a mass of $80770Kg$. This was calculated from summing all the mass observations of full haul trucks ($\sum M_{Haul\_Trucks}$). Table 3.6 shows the final estimates of the mass of the different lumped masses still present at the end of the experiment. The sum of these lumped masses is $903.5258 + 79866.4742 = 80770$. This shows that like the small scale experiment, mass is conserved during the tracking

and estimation process in the large scale experiment.

Lumped Mass Location	Mass
Grade Bock	903.5258 Kg
Stockpile	79866.4742 Kg

Table 3.6 – The estimated mass of the lumped masses in the system at the end of the large scale experiment.

One of the claimed benefits of using the system described in this chapter is that it is possible to fuse additional information regardless of the quality of the information provided the information source can be accurately modeled as a Gaussian distribution. Figure 3.19 shows a comparison of the residuals and 2σ confidence boundaries at the excavator bucket lumped mass for an ASKF system which fuses in additional information (from a bulk volume sensor) and one which fuses no additional information and provides predictions based on system models. As can be seen from Figure 3.19, fusing additional information is able to reduce the uncertainty on the estimate while at the same time still remaining consistent.

Another of the claimed benefits of the ASKF approach was that it would be able to utilise the fused information to improve the estimates of spatially correlated lumped masses. Table 3.7 provides a comparison of the mean uncertainty in the mass estimates at each of the lumped mass locations between the prediction only and the fusion approach. A shown in Table 3.7, the system with fusion lowers the uncertainty in the spatially correlated lumped masses. This is evident through the information source, bulk volume estimates of excavator loads, lowers the uncertainty of the estimate at the grade block.

Lumped Mass Location	Prediction Only Mean 2σ	Fusion Mean 2σ
Grade Block	2679.7 Kg	2336.7 Kg
Excavator Bucket	261.4039 Kg	227.77 Kg
Haul Truck	452.7648 Kg	394.6577 Kg
Stockpile	2679.7 Kg	2336.7 Kg

Table 3.7 – A comparison of uncertainty estimates across lumped masses between prediction only and with fusion of information sources

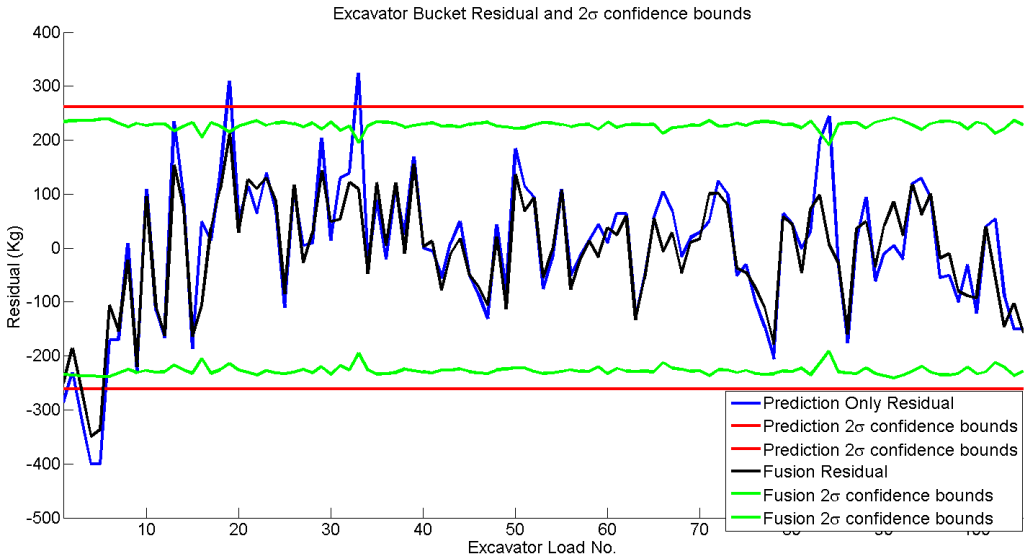

Figure 3.19 – A comparison of the residual at the excavator bucket and ground truth at the excavator bucket between an ASKF system which does not fuse any additional information to one which fuses information from a bulk volume information source. The system with fusion is able to provide a consistent estimate (within 2σ of the estimated uncertainty by the ASKF) with overall less uncertainty then the non-fusion system.

3.7 Discussion

In both small scale and large scale experiments the amount of material estimated at each lumped mass location is consistent within the predicted error. The most convincing results (given the sample size) can be seen in Figures 3.6 and 3.17 of the excavator bucket in both the small and large scale experiments. One of the main differences between the two figures is the predicted 2σ confidence bounds of the estimates provided by the ASKF. The small scale experiments are approximately straight where as the in the large scale experiment the confidence boundaries vary considerably. This is a result of two factors. First in the small scale experiment, the volume observation is a measuring cylinder. The predicted observational error of the bulk volume is assumed as a constant value. The other factor is the uncertainty in the estimate of the bulk density. This uncertainty was calculated by estimating over the data set where the bulk density is calculated at each lump location where a mass and volume observation was taken. This uncertainty is then used in the sensor model

for mass from bulk volume estimates in the ASKF (see Section 3.6.1). A comparison of the bulk volumes and the estimated error is seen in Table 3.8

Experiment	Mean Bulk Density	σ	σ as %
Small	1442.1 Kg/m^3	19.5 Kg/m^3	1.4 %
Large	1437.1 Kg/m^3	324.3 Kg/m^3	22.6 %

Table 3.8 – A comparison in bulk density variation between the small and large scale experiments.

The uncertainty in the bulk density of the small scale experiment is quite small (1.4%). The uncertainty of the bulk volume observation is approximated as a constant value of 1.5% (1σ error of 4mL, average load 265mL). The result of this combination of values in the small scale experiment is that the majority of the uncertainty in the sensor model for mass is encapsulated by the bulk volume estimate uncertainty. The opposite scenario is true for the large scale experiment, the bulk density uncertainty plays the most significant part in calculating the uncertainty of the mass observation. Additionally the uncertainty estimated on the bulk volume estimate is not constant in the large scale experiment.

Some of the additional uncertainty in the large scale experiment can be explained through the method of estimating the bulk density uncertainty. The observation sensors in the large scale experiment are less precise comparatively to the small scale sensors. The mass sensor 1σ operating precision for the large scale experiment was calculated as 1%, this was calculated using the unloaded haul truck (see Section 3.6.3 for more information). From Table 4.10 in Chapter 4 the precision of the bulk volume estimation method is approximately 6% (320 samples, exponential covariance function). The precision of the small scale experiment bulk volume observation estimates comparatively is estimated as 1.5%. The large variance in bulk density ($20\% at 1\sigma$) in the large scale experiment can not be solely explained through the error in precision in the sensors used to estimate the bulk density. Some of the possible reasons for a variable bulk density in the large scale method was explained at the beginning in this section in the comparison between the small and large scale experiments.

One goal of the large scale experiment was to take a less controlled approach to learn

how difficult it would be to implement the ASKF into a more realistic scenario. A variable bulk density is one of the issues which becomes more prominent in a less controlled environment. Using a simplistic method of modelling bulk density (e.g a single gaussian distribution over the entire process) and then applying that in the mass sensor model could be improved. A method for more accurately measuring the bulk density could utilise additional sensors such as ones which estimate the water moisture content of each excavator load. This research is outside the scope of this thesis. The method used in this thesis however, as can be seen in Figure 3.19, was still an improvement compared to no information fusion at all.

3.8 Summary

This section outlined an method for integrated tracking and estimation of extensive properties of a lumped mass. The aim was to create a system which provides a consistent estimate of the extensive material properties at each of the lumped mass locations. The other claims which were made about the constrained ASKF approach was that it would be able to ensure conservation of mass and more effective use of information sources in the system by tracking the spatial correlations between lumped masses. This improved use of information sources would provide the benefit of real-time reconciliation.

The ASKF is constrained by limiting the system models available to a specific subset. This is done to ensure that mass is conserved in the system as well as information to be shared between spatially correlated states correctly during fusion.

Two experiments were performed to validate these claims and test the constraints. The small scale experiment provides the ability control and measure all variables in the system. This allows for an environment which was ideal for proving the modelling constraints using the ASKF are valid. In particular, the unplanned mass transfers in the system (losses) can be modeled and observed. The results show that the estimates provided by the ASKF system in this experiment are consistent with the

error estimated by the system. It was also shown that the conservation of mass is upheld in the system.

The large scale experiment provided a scenario which was closer to the processes and conditions which occur in the real-world. The system models are more difficult to estimate and observing the properties of the lumped masses at different locations is more challenging. The volume estimation techniques proposed in Chapter 4 were used as part of the sensor model for estimating mass. It was shown that fusing this additional information it was able to decrease the uncertainty over the spatially correlated lumped masses in the system. The estimates in the large scale experiment were also shown to be consistent with ground truth values, conservation of mass was also ensured.

This section provides a system to probabilistically estimate and track extensive lumped mass properties. The models presented are applicable only in the case of extensive material properties. Incorporating intensive material properties into the ASKF system requires a different approach. An approach to incorporating intensive material properties is presented in Chapter 5. Some of the more practical considerations in implementing this system on a mine site are discussed in Chapter 6.

Chapter 4

Bulk Material Volume Estimation

4.1 Introduction

As discussed in Section 2.4.5, information to be fused into the tracking and estimation system described in Chapter 3 needs be represented probabilistically. A review of the current state-of-the-art in volume estimation techniques in Section 2.4.5 shows that there is no current system which will intrinsically provide a volume estimate and corresponding uncertainty for 2.5D data set. As a result of this, a method for estimation of volume in 2.5D surfaces is developed to allow for validation of the tracking and estimation system in the large scale experiment presented in this thesis.

A surface scan can be produced from a variety of sensors (radar, camera, laser). The choice of sensor is dependent on the operating conditions. In the mining domain a millimeter wave radar given its dust penetration properties is an excellent choice for surface mapping. In less dusty conditions, laser systems (particularly 3D survey grade lasers) can be very accurate over large distances. Camera systems have the benefit of being generally the cheapest of the sensors. The disadvantages of camera systems however, is that they are typically short range compared to lasers and radars and are restricted by factors such as dust.

In this thesis, the source of the surface scan is a laser. The laser sensors used are a

Riegl LMS-Z620 3D survey laser and a Riegl VZ1000 3D survey laser, data sheets for each sensor can be found in Appendixes A.2.2 and A.2.1 respectively.

There are several areas in which volume estimation can be performed in the mining cycle. One example is surveying before and after a pit during excavation. Doing so allows for an estimate of the volume of material removed during a particular operation. Other examples include stockpiles, excavator buckets and haul trucks. As described in Chapter 3, fusion of additional information on a material property at one location enables that information to be reconciled with spatially correlated lumped masses. This consequently enables greater accuracy in the estimates of the material in the system.

This chapter provides a method for volume estimation which utilises a Gaussian process surface representation to provide an encapsulation of the uncertainty in the surface estimate. Due to the functional representation of both the mean and covariance provided by the Gaussian process surface model, these functions can be integrated to provide a volume estimate with corresponding uncertainty.

Chapter 4 includes an introduction to the basic concepts involved in Gaussian Processes. Gaussian processes are a data-driven machine learning technique, where the training data is required for generating the underlying model. It is strongly recommended that the reader refers to the referenced literature [100] for a more in-depth understanding of how Gaussian Processes are used to generate data-driven models.

4.2 Problem Definition

Given a set of 2.5D data points (with cartesian co-ordinates), the problem can be defined through the following set of requirements:

- Provide means to estimate the volume of material in a given region (S).
- A method for encapsulating the uncertainty in the volume estimate over the region (S).

- Flexibility to accurately estimate the volume and corresponding uncertainty given varying levels of scale, surface formations and sparseness of data over an estimation region S.

4.3 Gaussian Process Method

4.3.1 Introduction

Rasmussen and Williams [100] define a Gaussian process as "a collection of random variables, any finite number of which have a joint Gaussian distribution". One way of interpreting Gaussian processes is known as the 'function-space view' . This is whereby the Gaussian process can be considered as a distribution over functions. Gaussian processes are non-parametric, this means that there is no specific basis function with a set of parameters defining how inputs relate to output values. Gaussian processes are characterised by a mean function ($m(x)$) and a covariance function ($k(x, x')$).

The mean and covariance function are defined as

$$m\left(x\right) = \mathbb{E}\left[f\left(x\right)\right] \tag{4.1}$$

and

$$k\left[x, x'\right] = \mathbb{E}\left[\left(f\left(x\right) - m\left(x\right)\right)\left(f\left(x'\right) - m\left(x'\right)\right)\right] \tag{4.2}$$

Where x is a location on the Gaussian processes (x can be multidimensional which is the case in surface mapping application in this thesis).

Gaussian process regression is a data driven modelling technique. In order to generate the regression model a set of 'training' data is used. The training data consists of a set of sample input variables with a corresponding set of outputs. The training set $\mathcal{D}$ of n observations can be defined as:

$$\mathcal{D} = \{(x_i, y_i) \mid i = 1, \ldots, n\} \tag{4.3}$$

In the training set $\mathcal{D}$, x is the input vector, whereas y is a scalar output vector. It should be noted that the input vector can be of dimension D. The notation for the training set can be simplified to the form:

$$\mathcal{D} = (X, y) \tag{4.4}$$

In this instance X is defined as an aggregate of the D dimensional input vectors. For the purposes of this thesis X is arranged to be of size $n \times D$, y will be arranged as a vector of size n.

One of the requirements of the volume estimation technique is for it to be flexible enough to work on a variety of surface formations. One way of allowing for this is by letting the data drive the model development. For this reason the mean function is set to zero ($m(x) = 0$). The co-ordinate system is manipulated such that the arithmetic average of the data points is equal to zero to facilitate this mean function. This mean function with this manipulated co-ordinate system effectively assumes no prior knowledge on the set of training data. This mean function and co-ordinate configuration allows the model to be driven by the covariance function and the training data.

The training data set $\mathcal{D}$ in the surface mapping scenario, containing n observations, consists of a two dimensional input vector X, where $X = (x, y)$. The output vector y will contain the corresponding z (height) values of the data points.

As described previously in Equation 4.2, the x value corresponds to a location and can be multi-dimensional. The end-result, for surface mapping, is that the Gaussian process can be given a location (an (x,y) co-ordinate) as an input and then the output of the Gaussian process $f(x)$ equates to the z co-ordinate of the input point. Therefore the surface can be considered to be represented by a function rather than a set resolution of data points.

To incorporate the training data a prior joint distribution is formed between the training data points (y and X from Equation 4.4) and a predetermined set of test (also known as inference) points (X_*). This process can be seen in Equation 4.5. f_* corresponds to the output of the Gaussian process at the test points.

$$\begin{bmatrix} \mathbf{y} \\ \mathbf{f}_* \end{bmatrix} \sim N\left(0, \begin{bmatrix} K(X,X) & K(X,X_*) \\ K(X_*,X) & K(X_*,X_*) \end{bmatrix}\right) \tag{4.5}$$

$K(X,X)$ corresponds to the covariance between the training set, $K(X,X_*)$ is equivalent to the covariance between the training set and the test points and so forth. In a process which is theoretically the same as Bayes rule (see Section 2.4.1), the prior distribution is conditioned on the training data in order to generate the posterior distribution. From this posterior distribution, the mean output f_* as well as the covariance function $cov(f_*)$ can be obtained.

The result of conditioning the prior distribution on the training data is as follows:

$$\mathbb{E}(\mathbf{f}_*) = K(X_*,X)\left[K(X,X)\right]^{-1}\mathbf{y} \tag{4.6}$$

$$cov(\mathbf{f}_*) = K(X_*,X_*) - K(X_*,X)\left[K(X,X)\right]^{-1}K(X,X_*) \tag{4.7}$$

Therefore given a covariance function K, training data set $\mathcal{D}$ and set of test points X_* a set of outputs $\mathbb{E}f(x)$ and $cov(f(x))$ can be generated. The prior joint distribution (described in Equation 4.5) is applicable only in scenarios where the training data points are noiseless. In surface mapping, the techniques to gather the 3D point clouds contains some level of sensor noise. A method for incorporating this sensor noise must be introduced. This can be done by altering the prior distribution model to the following:

$$\begin{bmatrix} \mathbf{y} \\ \mathbf{f}_* \end{bmatrix} \sim N\left(0, \begin{bmatrix} K(X,X)+\sigma_n^2 I & K(X,X_*) \\ K(X_*,X) & K(X_*,X_*) \end{bmatrix}\right) \tag{4.8}$$

The posterior mean and covariance function, conditioned on the training data, can be expressed through the following equations:

$$E(\mathbf{f}_*) = K(X_*,X)\left[K(X,X)+\sigma_n^2 I\right]^{-1}\mathbf{y} \tag{4.9}$$

$$cov(\mathbf{f}_*) = K(X_*,X_*) - K(X_*,X)\left[K(X,X)+\sigma_n^2 I\right]^{-1}K(X,X_*) \tag{4.10}$$

This allows for an additional parameter σ_n^2 to be utilised to account for the error (noise) associated with the observed data points.

4.3.2 Choice of Covariance Function

As described in Section 4.3.1, the covariance function (K) performs a critical role in Gaussian process regression. The covariance function controls how the data points are spatially correlated to each other (similar to a variogram in Kriging). Therefore, choosing the appropriate covariance function for the data is important. The ideal choice of covariance is the one which both encapsulates the uncertainty in the surface map consistently as well as providing an accurate and non biased estimate of the surface. These factors are important when considering the integration of the mean and covariance functions in order to determine the volume and corresponding uncertainty.

Squared Exponential

One of the most popular covariance functions is the squared exponential function. The squared exponential function for surface mapping can be written as such:

$$k_{SE}(x, x') = \sigma_f^2 \exp\left[-\frac{1}{2}(x - x')^T M (x - x')\right] \tag{4.11}$$

where

$$M = \begin{bmatrix} \ell_x & 0 \\ 0 & \ell_y \end{bmatrix}^{-2} \tag{4.12}$$

From the covariance function equation several features can be highlighted which give an insight into how the function correlates data. This covariance function, given its exponential term is infinitely differentiable. This results in the output curves being very smooth. The $x - x'$ component defines the squared exponential function as stationary, thus it is invariant to translation. An example (reproduced using data from Rasmussen and Williams [100]) of the squared exponential function can be seen in Figure 4.1. The plus symbols represent training points, the thick line is the mean function output from the Gaussian process. The shaded area represents the 2σ boundaries on the distribution of functions along the mean function.

Matern

The Matern series of covariance functions have many useful properties. The Matern series of covariance functions can be represented by the following equation:

$$k_{Matern}(r) = \frac{2^{1-v}}{\Gamma(v)} \left(\frac{\sqrt{2v}r}{\ell}\right)^v K_v \left(\frac{\sqrt{2v}r}{\ell}\right) \tag{4.13}$$

Where K_v is a modified Bessel function. $\Gamma(v)$ is a Gamma function. r is notation for representing the isotropic function $(x - x')$. This covariance function is stationary and takes the absolute Euclidean distance to points when calculating correlations. The parameters v and ℓ are always positive and define the behavior of the covariance function.

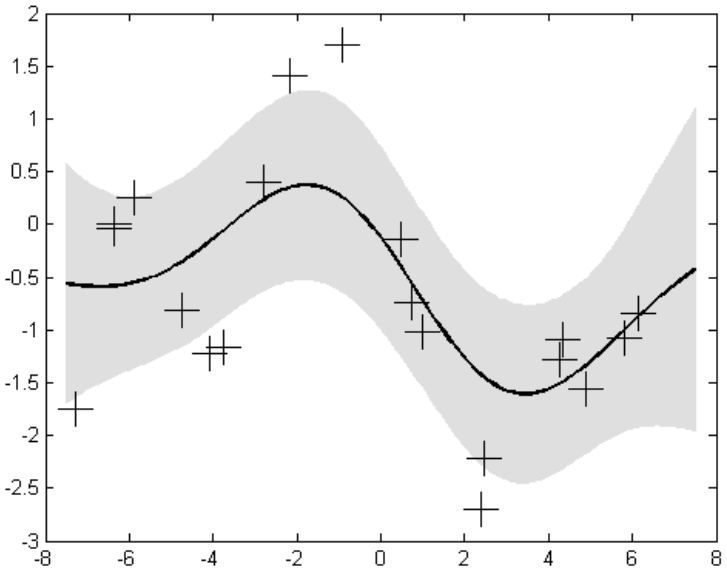

Figure 4.1 – An example Gaussian process regression using the squared exponential covariance function in 1D. Hyper-parameters are set to $\ell = 3, \sigma_f^2 = 1.2, \sigma_n^2 = 1$

Some of the most useful applications of the Matern covariance function occur when $v = p + \frac{1}{2}$. In this scenario, Equation 4.13 is simplified significantly. Of particular interest are the scenarios in which $p = 3$ and $p = 5$. These are commonly referred to in literature as the Matern $\frac{3}{2}$ and Matern $\frac{5}{2}$ covariance functions [81]. The Matern $\frac{3}{2}$ covariance function, when $v = \frac{3}{2}$, is simplified to:

$$k_{Matern3}(r) = \sigma_f^2 \left(1 + \frac{\sqrt{3}r}{\ell}\right) \exp\left(-\frac{\sqrt{3}r}{\ell}\right) \tag{4.14}$$

The Matern $\frac{5}{2}$ covariance function, when $v = \frac{5}{2}$, is simplified to the following:

$$k_{Matern5}(r) = \sigma_f^2 \left(1 + \frac{\sqrt{5}r}{\ell} + \frac{5r^2}{3\ell^2}\right) \exp\left(-\frac{\sqrt{5}r}{\ell}\right) \tag{4.15}$$

The goal of the Gaussian process in this thesis is to map the terrain surface. Therefore the isotropic nature of Equation 4.14 and Equation 4.15 is inadequate to learn the terrain changes which are dimensionally dependent. This can be remedied by altering

the covariance functions to be anisotropic. The resulting Matern $\frac{3}{2}$ covariance function becomes:

$$k_{Matern3}(x-x') = \sigma_f^2 \left(1+\sqrt{3(x-x')^T M (x-x')}\right)\cdots \exp\left(-\sqrt{3(x-x')^T M (x-x')}\right) \tag{4.16}$$

The Matern $\frac{5}{2}$ covariance function becomes:

$$k_{Matern5}(x-x') = \sigma_f^2 \left(1+\sqrt{5(x-x')^T M (x-x')}+\frac{5\left((x-x')^T M(x-x')\right)}{3}\right)\cdots \exp\left(-\sqrt{5(x-x')^T M (x-x')}\right) \tag{4.17}$$

where in both Equation 4.16 and Equation 4.17

$$M = \begin{bmatrix} \ell_x & 0 \\ 0 & \ell_y \end{bmatrix}^{-2} \tag{4.18}$$

The Matern covariance functions in Equation 4.16 and Equation 4.17 are anisotropic like the squared exponential covariance function given in Equation 4.11.

The Matern series of covariance functions are useful for controlling the level of smoothness of the output function. The Matern covariance functions are $v-1$ times differentiable, as $v \to 0$ the output mean function becomes progressively less smooth. When $v \to \infty$ the output mean function becomes very smooth, in fact as $v \to \infty$ the Matern covariance function becomes identical to the squared exponential function.

Exponential

The exponential covariance function is a special case of the Matern covariance function where $p = 0$, therefore $v = frac12$. The anisotropic exponential covariance function for the surface mapping scenario is given by the following:

$$k_{Exp}(x - x') = \sigma_f^2 \exp\left(-\sqrt{(x - x')^T M (x - x')}\right) \tag{4.19}$$

where

$$M = \begin{bmatrix} \ell_x & 0 \\ 0 & \ell_y \end{bmatrix}^{-2} \tag{4.20}$$

The exponential is unique from the previous covariance functions in that it is not differentiable. It does not produce the same level of 'averaging' which is a feature of the covariance functions described previously. Therefore it is well suited for scenarios in which the surface geometry changes rapidly with sharp edges. However, in scenarios where the surface is generally smooth and with no complex sharp features the lack of averaging of the data in the exponential function is less likely to encapsulate the uncertainty correctly. This results in a large increase in the spread of possible function in areas of sparse data. Conversely, the squared exponential and Matern $\frac{3}{2}$ and Matern $\frac{5}{2}$ covariance functions, to varying degrees, have the opposite problem when estimating sharp complex features where the surface features are likely to be smoothed and the corresponding uncertainty being overly confident.

A 2D Comparison of the Covariance Functions

How the choice of covariance function alters both the output mean and covariance function is illustrated in Figures 4.3-4.6. The true model with sampled points can be found in Figure 4.2.

The squared exponential covariance function (Figure 4.3) has the most obvious smoothing effect. The squared exponential can be thought of to work like an averaging function. This averaging effect (in practice a consequence of a long length scale (ℓ)) is the reason the squared exponential output covariance function has a near constant distribution of functions over the surface. The squared exponential covariance function does not deal well with the sharp line change. The Matern $\frac{5}{2}$ covariance

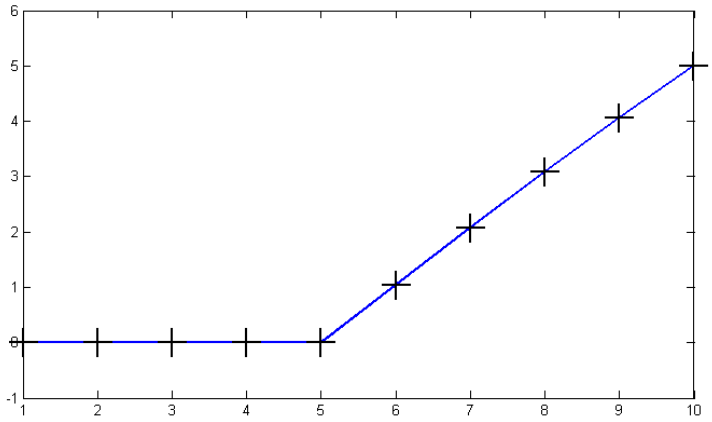

Figure 4.2 – The true line to be modeled by each covariance function with 10 uniformly sampled points.

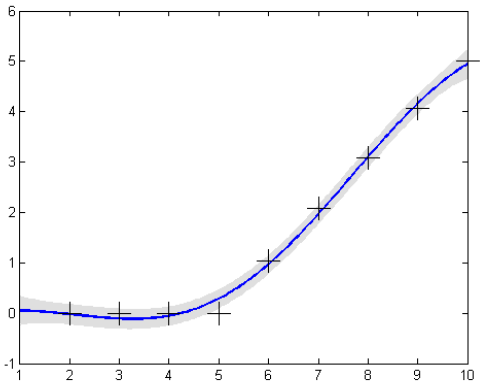

Figure 4.3 – The **squared exponential** estimate of the sampled points from Figure 4.2.

function (Figure 4.4) provides a representation which is less smooth than the squared exponential and thus can better represent the sharper edges in the true distribution, though like the squared exponentional does over smooth the change in direction. The Matern $\frac{3}{2}$ covariance function (Figure 4.5) shows reduction in the level of smoothing as $v \to 0$. The output covariance function is also noticeably different with a decrease in covariance around the sample points. This is due to the reduced averaging effect present in the Matern $\frac{3}{2}$ compared with higher level Matern covariance functions and the squared exponential covariance function. This is a result of a smaller length scale (ℓ), which causes an increased emphasis on passing through the sampled data points.

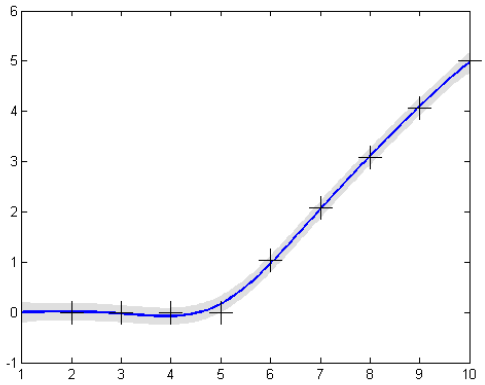

Figure 4.4 – The **Matern** $\frac{5}{2}$ estimate of the sampled points from Figure 4.2.

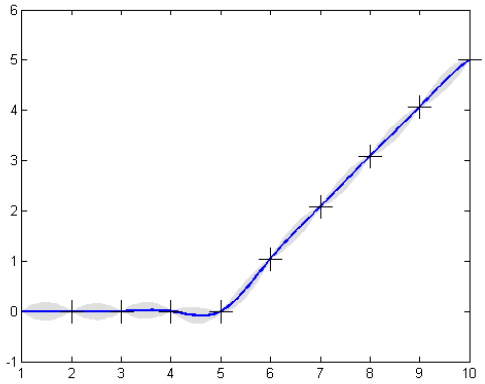

Figure 4.5 – The **Matern** $\frac{3}{2}$ estimate of the sampled points from Figure 4.2.

Figure 4.6 shows how the exponential covariance function, the output mean function is very responsive to sharp edges. The output covariance function also shows how the spread of functions once moved away from the sample data increases significantly when compared to the other covariance functions.

Hyper-parameters and Learning

One of the interesting aspects about Gaussian processes which has not yet been reviewed is the set of hyper-parameters which determine the behavior of each covariance function. In the squared exponential Equation 4.11 three hyper-parameters are listed, σ_f^2 is the signal variance and M contains the two length scale hyper-parameters ℓ_x

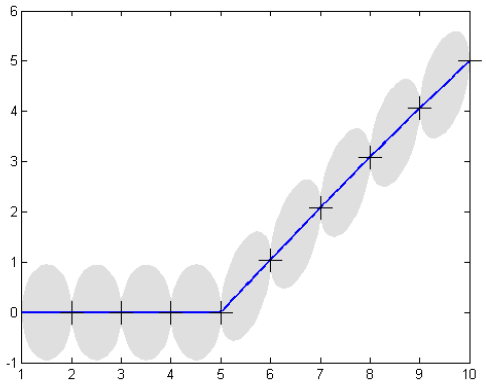

Figure 4.6 – The **exponential** estimate of the sampled points from Figure 4.2.

and ℓ_y which govern how quickly the sample functions vary in both the x and y directions. This thesis represents the hyper-parameter set as θ. In the squared exponential covariance function, $\theta = \left[\ell_x, \ell_y, \sigma_f^2, \sigma_n^2\right]$ where the additional term σ_n^2 describes the signal noise component which is found in Equation 4.8.

The 'learning' which is performed in Gaussian processes is the optimisation of the hyper-parameter terms to find the distribution of functions which best satisfies the output of the training data set (y) given the input data from the training set (X). One possible method for this optimisation process is to maximise the log of the marginal likelihood with respect to θ. This can be performed through the following equation.

$$\log p\left(y|X,\theta\right) = -\frac{1}{2}y^T K_y^{-1} y - \frac{1}{2}\log|K_y| - \frac{N}{2}\log 2\pi \tag{4.21}$$

From this equation, $K_y = K(X,X) + \sigma_n^2 I$ is the covariance associated between the training data X and output y with the inclusion of the sensor noise. Equation 4.21 can be separated into three components. The first term is concerned with finding the best fit of the data with the hyper-parameters. The second term performs 'Occam's Razor' to penalise over-fitting. The final term is a normalisation constant. Optimisation of Equation 4.21 is not a trivial process as the function is non-convex. There is a variety of the optimisers currently available to deal with solving non-convex problems. The text by Nocedal and Wright [93] provides an excellent resource on a range of

optimisation tools which can be applied to solve this problem.

The work in this thesis uses a gradient-based method with a Broyden-Fletcher-Goldfarb-Shanno (BRGS) hessian update for optimising Equation 4.21. This method is classified as quasi-Newton by Nocedal and Wright [93]. It uses a hill climb approach, therefore each hyper-parameter is optimised in sequence. This gradient method ensures that the local maximum is quickly obtained. The negative of this approach is that there is no guarantee that the local maximum is the global maximum. This problem can be reduced by choosing a reasonable set of starting parameters given the training data. Melkumyan and Ramos [80] discuss one solution to this problem by using multiple start points. The main problem with this approach is increased computational requirements. Figure 4.7 shows the result of optimising the parameters shown in Figure 4.1 using the BRGS method. The optimisation is not over fitted with the mean estimate not passing through every data point. The mean function improves on the non-optimised hyper-parameters by accounting for the sinusoidal like fluctuations in the data points. The non-optimised parameters, given the large length scale is unable to properly represent this underlying feature of the training data.

For the surface mapping work in this thesis the hyper-parameters are optimised using 5 separate starting points. The hyper-parameters with the greatest log marginal likelihood are chosen as the parameters to be used in the Gaussian process.

Discussion

Choosing the correct covariance function to model a 2.5D surface depends partially on having prior knowledge on how the surface changes over the region of interest. As described and hypothesized previously, surfaces with rapid sharp changing features should be more suitably modeled by the Matern $\frac{3}{2}$ or exponential covariance functions. These covariances functions are more likely given their formulation to be better at encapsulating the uncertainty in the surface model. Alternatively, smooth consistent surfaces modeled by the Matern $\frac{5}{2}$ and squared exponential covariance functions should be superior at encapsulating the uncertainty in the surface model under these

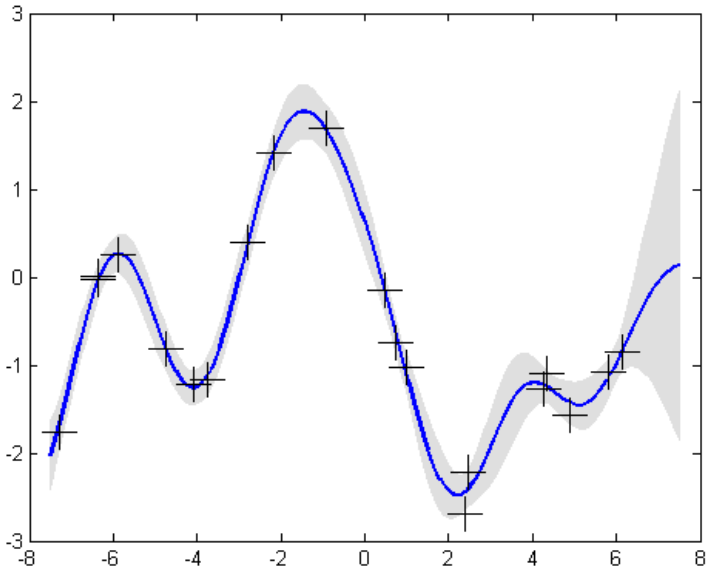

Figure 4.7 – This is the result of optimising the hyper-parameters from Figure 4.1. The squared exponential covariance function hyper-parameters are optimised from $[\ell = 3, \sigma_f^2 = 1.2, \sigma_n^2 = 1]$ to $[\ell = 1.37, \sigma_f^2 = 1.55, \sigma_n^2 = 0.14]$.

conditions.

Figure 4.8(a) shows an example of a 2.5D data set. 64 sampled points are used as training data (Figure 4.8(b)).

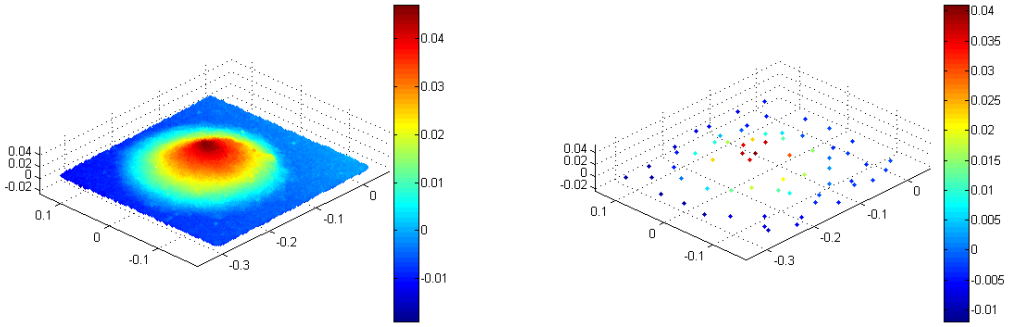

(a) A plot of the raw sensor output (20% of points taken).

(b) 64 samples taken from raw senor output.

Figure 4.8 – This figure provides an example of how much data is able to be gathered by the sensor used in this experiment. From this data set 64 samples are taken.

Figure 4.9 shows how each covariance function described in this thesis estimates the surface shown in Figure 4.8(a) along with a corresponding uncertainty given the training data from Figure 4.8(b). Figure 4.9 shows how each of the described covariance functions performs in a simple 2.5D scenario. Specifically, the squared exponential covariance function produces a highly smoothed surface with a consistent uncertainty over the entire surface. The exponential on the other hand provides a less averaged surface with the uncertainty increasing rapidly when the mean function moves away from the training data.

4.3.3 Theoretical Volume Derivation

The prior sections in this chapter have described how to develop a Gaussian process regression model to generate a functional representation of a 2.5D surface which includes a function for representing the uncertainty in this model. The following is a derivation of how to calculate the probabilistic volume estimate given this representation.

The Gaussian process Equations 4.9 - 4.10 for mean and variance can be expressed in terms of a single point x_* as shown below:

$$E\left[f_*\left(x_*\right)\right] = K\left(x_*, X\right)\left[K\left(X, X\right) + \sigma_n^2 I\right]^{-1}\mathbf{y} \tag{4.22}$$

$$var\left[f_*\left(x_*\right)\right] = K\left(x_*, x_*\right) - K\left(x_*, X\right)\left[K\left(X, X\right) + \sigma_n^2 I\right]^{-1}K\left(X, x_*\right) \tag{4.23}$$

From Equations 4.9 - 4.10 the volume can be expressed as:

$$V = \int_S f_*\left(u\right) du \tag{4.24}$$

where S is a region over which the volume is to be estimated, given this, the following

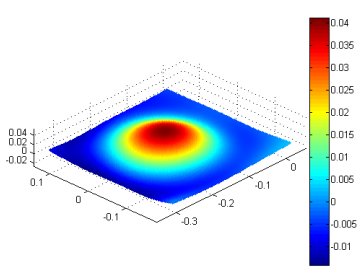

(a) Squared exponential mean surface estimate

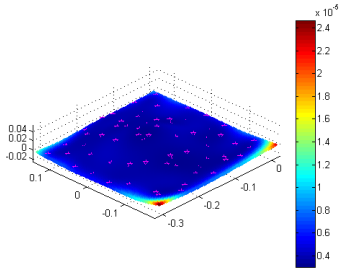

(b) Squared exponential variance function

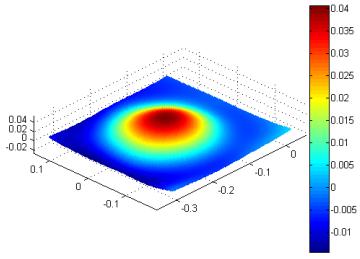

(c) Matern $\frac{5}{2}$ mean surface estimate

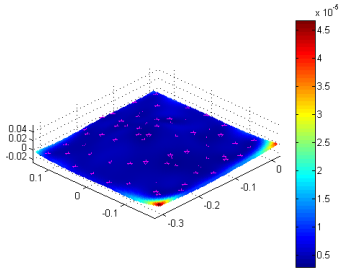

(d) Matern $\frac{5}{2}$ variance function

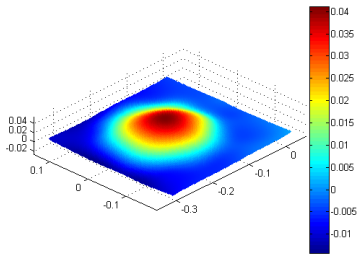

(e) Matern $\frac{3}{2}$ mean surface estimate

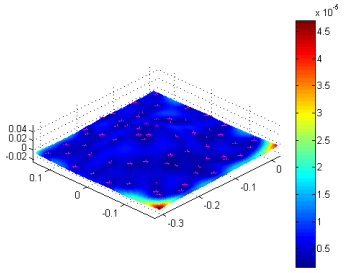

(f) Matern $\frac{3}{2}$ variance function

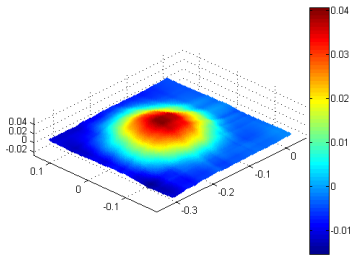

(g) Exponential mean surface estimate

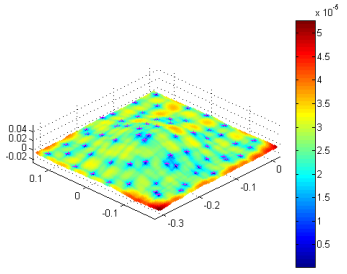

(h) Exponential variance function

Figure 4.9 – An overview of how the different covariance functions influence the mean surface as well as the corresponding uncertainty in this estimate.

statistics hold:

$$E[V] = \int_S E[f_*(u)]\,du = \left(\int_S K(u,X)\,du\right)\left[K(X,X)+\sigma_n^2 I\right]^{-1}\mathbf{y} \tag{4.25}$$

$$\begin{aligned}
var[V] &= E\left[(V-E(V))^2\right] = E\left[\left(\int_S f_*(u)\,du - \int_S E[f_*(u)]\,du\right)^2\right] \\
&= E\left[\left(\int_S (f_*(u)-E[f_*(u)])\,du\right)^2\right] \\
&= E\left[\left(\int_S (f_*(u)-E[f_*(u)])\,du\right)\left(\int_S (f_*(w)-E[f_*(w)])\,dw\right)\right] \\
&= E\left[\int_S\int_S (f_*(u)-E[f_*(u)])\,(f_*(w)-E[f_*(w)])\,dudw\right] \\
&= \int_S\int_S E\left[(f_*(u)-E[f_*(u)])\,(f_*(w)-E[f_*(w)])\right]dudw \\
&= \int_S\int_S cov\,(f_*(u),f_*(w))\,dudw
\end{aligned} \tag{4.26}$$

Therefore to summarise, the mean and variance of the estimate over a region S can be expressed in the following forms:

$$E[V] = \left(\int_S K(u,X)\,du\right)\left[K(X,X)+\sigma_n^2 I\right]^{-1}\mathbf{y} \tag{4.27}$$

$$var[V] = \int_S\int_S cov\,(f_*(u),f_*(w))\,dudw \tag{4.28}$$

where $K(x,x')$ is the covariance function of the GP representing the function $f(x)$ and $cov\,(f_*(u),f_*(w))$ is defined in Equation (4.10).

4.3.4 Numerical Volume Integral Approximation

One of the most computationally efficient ways of calculating the integrals for mean volume and variance (Equations 4.27 and 4.28) would be to develop a closed form solution of the mean and variance integrals. This is a non-trivial task and is out

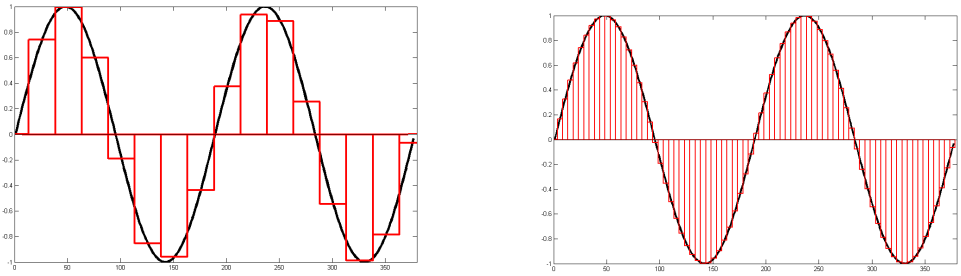

(a) Small amount of integral points **(b)** Large amount of integral points

Figure 4.10 – Accuracy and precision of the rectangular integration method depends largely on the number of integral points used.

of the scope of this thesis. This thesis instead focuses on providing the proof that it is possible to provide probabilistic volume estimates which could then be used to validate a probabilistic tracking and estimation system. The optimisation of this technique for practical application is left as future work. A simple solution is to use the generic approach of numerical approximations of the integral.

Mean Volume

The mean volume can be calculated as a 2D integral over the Gaussian process mean function. There are multiple numerical integration methods to calculate this integral. Some examples include the rectangular, trapezoidal and Simpson methods which have all been well documented in literature [24].

In this thesis, the rectangular method is used. The rectangular method has the advantage of being computationally inexpensive for a comparable number of integration points compared to other numerical integration approximation methods. The limitation of using the rectangular method is that the accuracy of the method is highly correlated to the number of integral points. A comparison of the accuracy of this method over a sine wave using different amounts of integral points is shown in Figure 4.10.

Using the rectangular approximation method the equation for calculating volume becomes:

$$V = \frac{1}{N}\sum_{i=1}^{N} f_*\left(x_i\right) \times \int_S dxdy \tag{4.29}$$

where N is the total number of integral points. $f_*\left(x_i\right)$ is the mean function output from a Gaussian process given an inference location defined by x_i. $\int_S dxdy$ is in this thesis a rectangular region over which the volume is to be integrated.

Variance

The variance over the volume integration as seen in (4.28) is a 4D integral over the covariance function. It can be calculated using the rectangular method as follows:

$$var\left[V\right] = \frac{1}{N^2}\sum_{i=1}^{N}\sum_{j=1}^{N} K_{Post}(X_i, X_j) \times \left(\int_S dxdy\right)^2 \tag{4.30}$$

where $K_{Post}(X_i, X_j)$ is the posterior covariance calculated in (4.10).

4.4 Current Techniques

The effectiveness of the Gaussian process technique for volume estimation is compared against a selection of current state-of-the-art volume estimation techniques. The state-of-the-art techniques were chosen to broadly represent the different types volume estimation techniques used in practice. As such each technique has a fundamentally different method for estimating volume. The example data set in Figure 4.11 is used to show how each of the different state-of-the-art techniques represent volume.

4.4.1 Triangular Prisms

The triangular prisms method requires generating a TIN (further information on TINs can be found in Section 2.4.5) over the sampled data points. From this TIN,

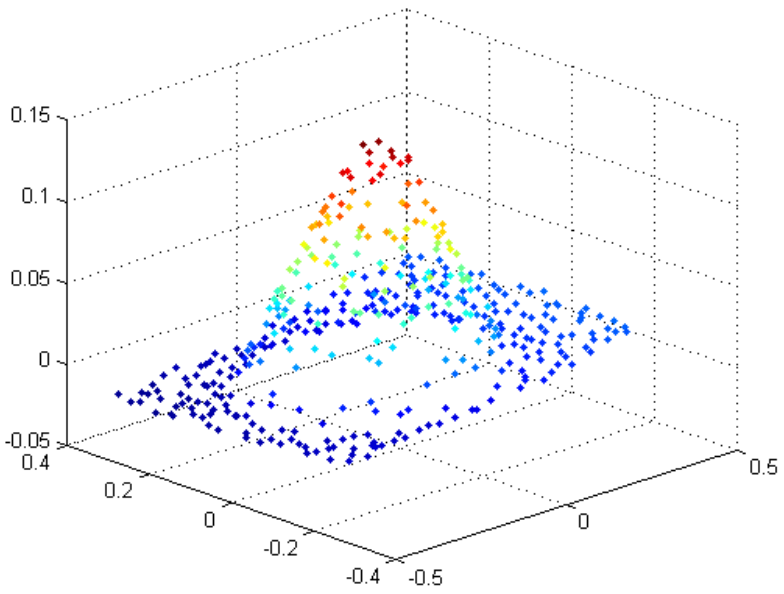

Figure 4.11 – This is a sampled set of 2.5D data which is used by each of the state-of-the-art methods to show how each method calculates the volume.

triangular prisms are formed to a surface plane in which volume is calculated from. The TIN in this thesis is generated using Delaunay triangulation. Figure 4.12 gives the result of using the sample data in Figure 4.11 to create the TIN with Delaunay triangulation.

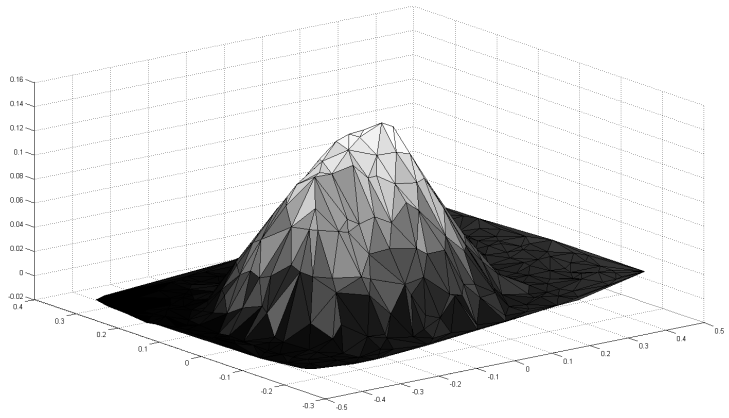

Figure 4.12 – The Delaunay triangles create the TIN, the volume is calculated by triangular prisms to a surface plane.

4.4.2 Rectangular Averaging Grid

The rectangular grid method is one of the simplest methods for calculating volume. The region of interest is divided into a finite set of rectangular cells. The height of the rectangular cells is determined by the average height of the sample data points within the cell bounds. An example of how a surface is represented using this method can be seen in Figure 4.13.

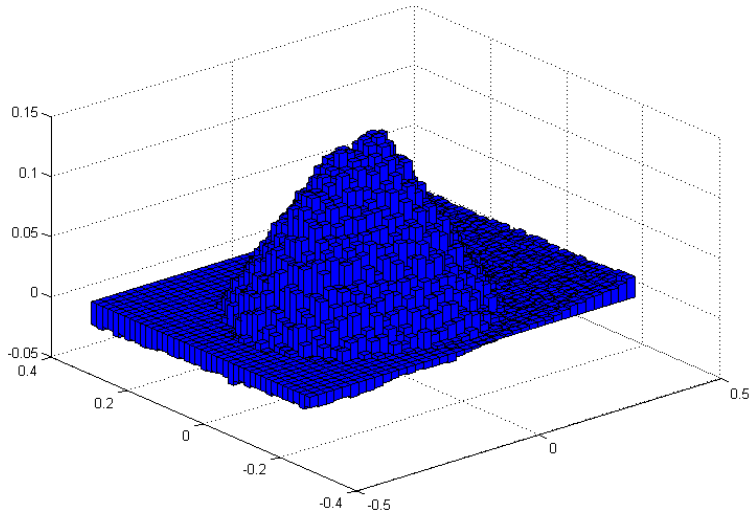

Figure 4.13 – The volume is calculated by summing all the rectangular prisms to a surface plane.

4.4.3 Cubic Spline Interpolation and Integration using Simpson's Method

Cubic spline interpolation is performed using a piecewise 3rd order polynomial function which is used to create smooth surfaces over the input data points. As described in Section 2.4.5, the cubic spline interpolation method is one of the most accurate methods currently available for surface mapping. The volume is calculated from this surface map using Simpson's method for numerical approximation. An example of the style of surface produced by the cubic spline method can be seen in Figure 4.14.

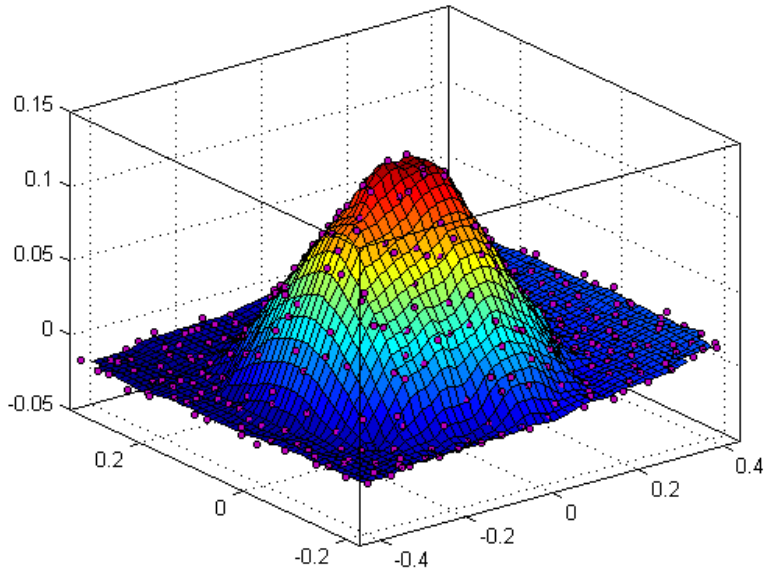

Figure 4.14 – A surface map generated using cubic spline interpolation, the volume is calculated using Simpson's rule for integration.

4.5 Experiments

There are two sets of experiments over which the volume estimation methods are tested. One experiment is a tightly controlled small scale experiment for which a more easily verifiable ground truth can be obtained.

A large scale experiment, for which the exact volume is not verifiable to the same degree as the small scale experiment, is used to investigate how the results of the small scale translate to a larger scale experiment. The larger scale experiment also provides surfaces with more varied formations than what is used in the small scale experiment.

A note on terminology:

The two metrics for comparing each of volume estimation methods in this thesis are **accuracy** and **precision**.

Accuracy is defined as how close the estimated volume is to the true volume.

Precision is defined as a measure of how repeatable a method is.

Accuracy and precision can be thought of in a Gaussian framework simply as the mean residual value and variance of the residual estimates.

4.6 Small Scale Experiment

The small scale experiment aims to simulate a stockpile of material. A total of 10 different stockpiles ranging from 1000mL to 10000mL are constructed to test the volume estimation methods. The stockpiles are scanned by a Rigel VZ-1000 survey laser (see Appendix A.2.1 for data sheet) on a elevated platform to give full perspective over the stockpile. The apparatus and experiment setup is shown in Figure 4.15.

One of the most difficult aspects of volume estimation of bulk material is obtaining a reliable ground truth. Bulk volume is dependent on many factors such as material size and variation, water content and forces applied to the grouping of bulk material. The experiments in this thesis use beach sand blend which mitigates (but does not eliminate) some of these factors, notably material size and variation.

To provide a ground truth estimate of the bulk volume the high saturation of accurate 3d points which the VZ-1000 provides (for an example showing 20% of the points see Figure 4.17a) is used. By using a fast linear interpolater (in this case Delaunay triangulation which overcomes any minor occurrences of laser shadow) over all the data points we can obtain a highly accurate estimate of the surface and consequently a highly accurate estimate of the volume. The principle behind this decision is similar to that of increasing the amount of integral points during numerical integration with

(a) 1000ml measuring cylinder used to add more material for each experiment

(b) Experiment configuration with the Riegl VZ-1000 laser

Figure 4.15 – Small scale volume estimation experiment setup, the survey laser is placed at height in order to reduce the chance of laser shadow on the surface.

the rectangular method as shown in Figure 4.10. As the amount of integral points increases the closer the method comes to approximating the true function.

One common application for bulk volume estimation, is comparing the volume before and after a set of excavation work. The difference between the two volume estimates is used to estimate how much material has been excavated over a particular time frame. In the small scale experiment, a scan of the ground surface before material is added is performed. The bulk volume estimate used to compare each of the techniques is

the difference between the bulk volume estimated from this original scan compared to the bulk volume estimate once the varied amounts of material have been added. In all these cases a consistent reference plane is used as well as a common co-ordinate frame (each scan is geo-registered to a common reference system). The base ground surface before material is added can be seen in Figure 4.16.

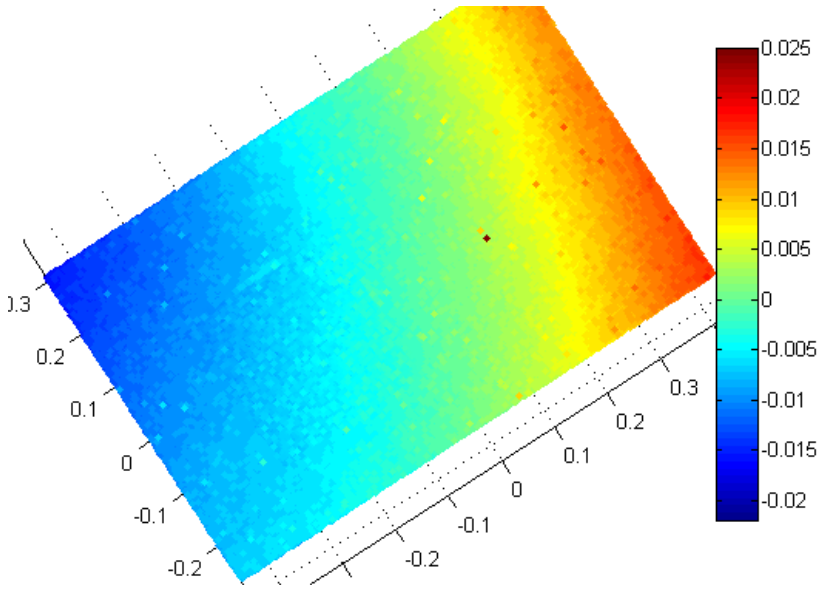

Figure 4.16 – The raw scan data of the ground surface before material is added in the small scale experiment. The volume of this surface is calculated and subtracted from each of the volume estimates which contain material.

4.6.1 Discussion

Given the availability of sensors such as the Riegl VZ-1000 and Riegl LMS-Z620 which provide high density accurate point clouds of the surface, there is a question as to why anything more complex than a simple linear interpolation volume estimation technique (such as a TIN) is necessary.

Although the highly dense point cloud which these sensors can generate have many positive properties, they also have several substantial negative aspects. Currently, obtaining the data is time intensive. The sensor also needs to be within close proximity to the surface to achieve the dense accurate point cloud representation used in the

experiments in this thesis. Another drawback is that it requires significant storage capacity to store the data from these dense point clouds. Consequently, transferring the data over network infrastructure (especially wireless networks) becomes cumbersome. Thirdly, high accuracy / precision instruments are generally expensive which leads to less availability and implementation into robust environments.

To simulate using cheaper sensors which obtain less data (or the same sensor used from a significantly greater distance), three scenarios were developed which use different levels of sampled points from the original point cloud obtained by the sensor. These include a low resolution in which 64 samples are used, a medium resolution with 256 samples and a high resolution with 1024 samples. A visual example showing how each of the different volume estimation methods represent the volume under these different resolutions can be seen in Figures 4.17, 4.18 and 4.19.

Each of the different volume estimation techniques are compared using these three different data set sizes. This provides an insight into how well each of the methods handles sparse data sets. To test the accuracy and precision of each method under these conditions, 100 sets of sampled points from the original complete point cloud (obtained from the sensor) are taken for each of the different resolutions over all of the different volume sizes. The sampling method splits the region into a rectangular grid with each rectangle of uniform size, a random data point is then taken from each rectangle. Each volume method uses the same set of sampled data on each iteration. As stated previously, the ground truth is obtained by using the complete data set and using the triangular prism method with Delaunay triangulation to estimate the volume.

4.6.2 64 Sample Scenario

Figure 4.20 shows two graphs comparing both the accuracy and precision of the Gaussian process method (using each of the covariance functions described in this thesis) and the current state-of-the-art methods in the 64 sample scenario. Figure 4.21 represents the accuracy and precision in this scenario as a percentage of the true

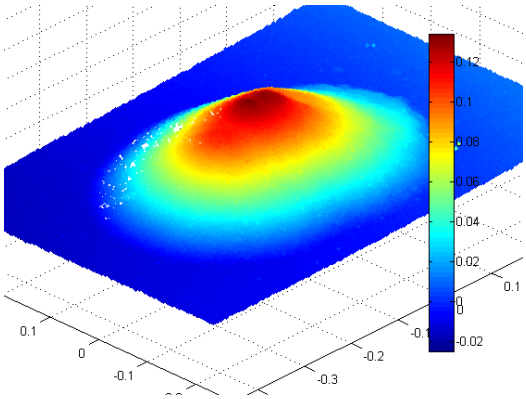

(a) A plot of the raw sensor output (20% of points taken).

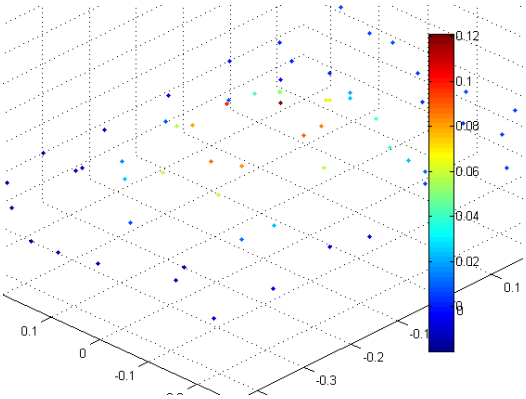

(b) 64 samples taken from raw sensor output.

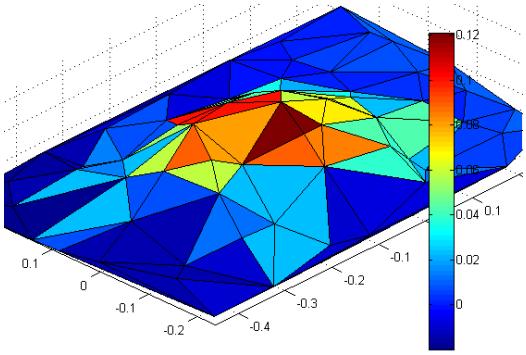

(c) Delaunay triangulated surface from sampled points.

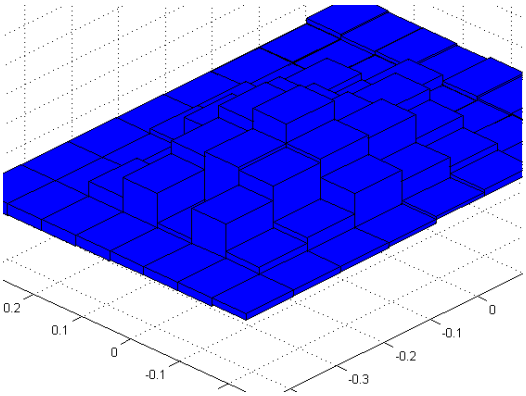

(d) Rectangular grid method from sampled points.

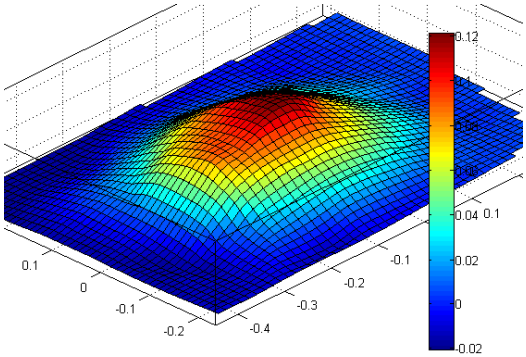

(e) Cubic Spline model from sampled points.

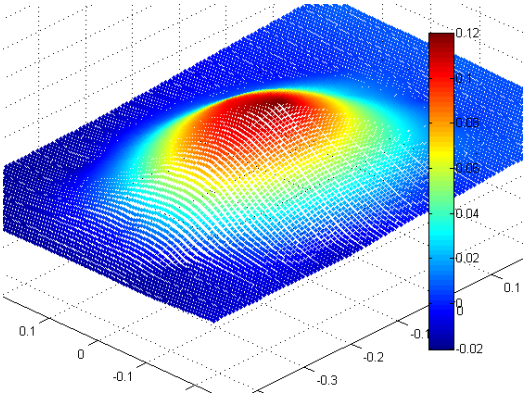

(f) Gaussian process model using squared exponential covariance function.

Figure 4.17 – This shows how each of the different methods estimate approximately 10000mL of volume using **64** samples.

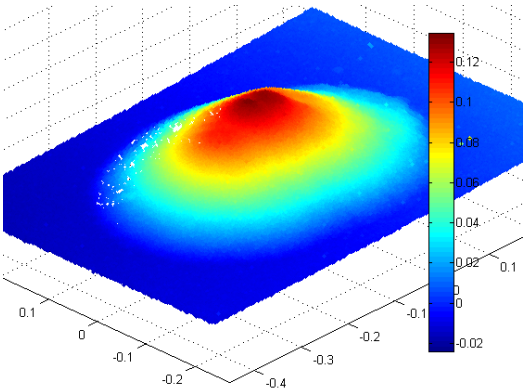

(a) A plot of the raw sensor output (20% of points taken).

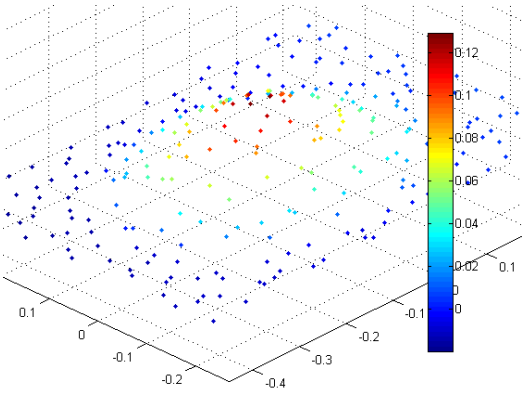

(b) 256 samples taken from raw senor output.

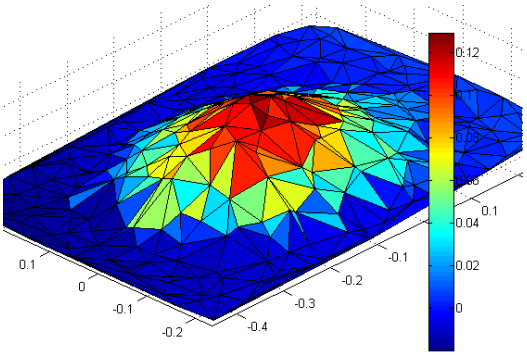

(c) Delaunay triangulated surface from sampled points.

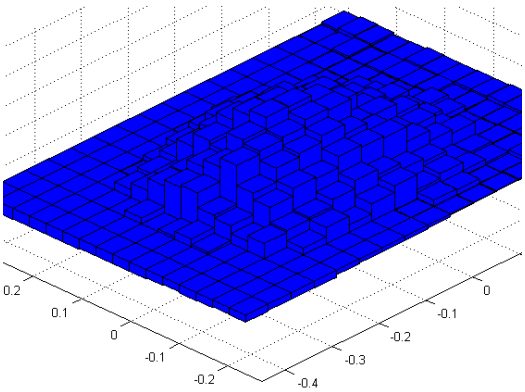

(d) Rectangular grid method from sampled points.

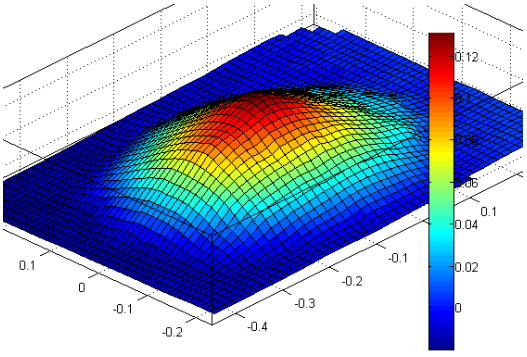

(e) Cubic Spline model from sampled points.

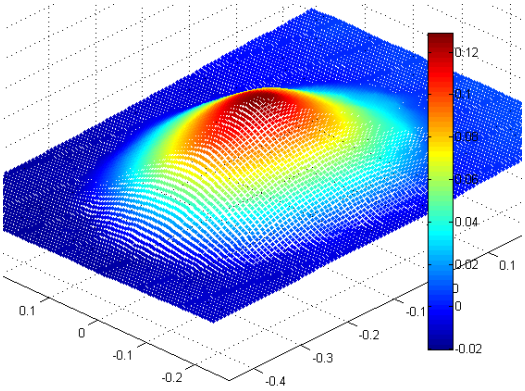

(f) Gaussian process model using squared exponential covariance function.

Figure 4.18 – This shows how each of the different methods estimate approximately 10000mL of volume using **256** samples.

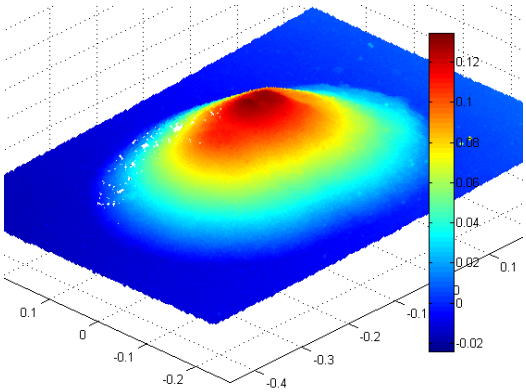

(a) A plot of the raw sensor output (20% of points taken).

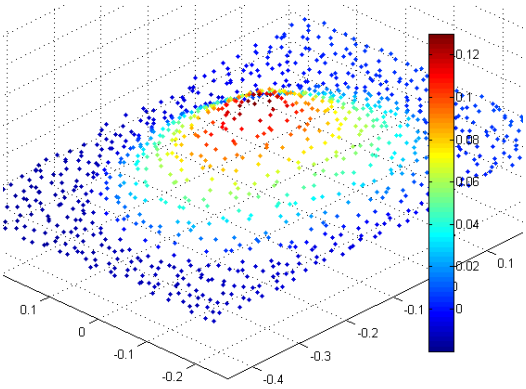

(b) 1024 samples taken from raw senor output.

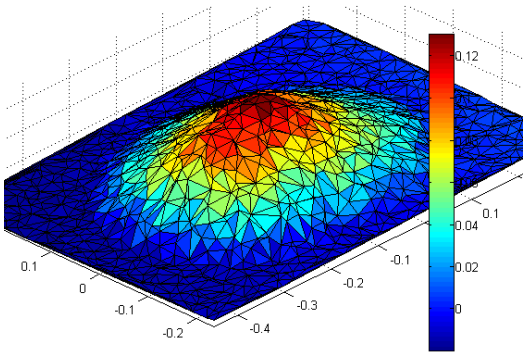

(c) Delaunay triangulated surface from sampled points.

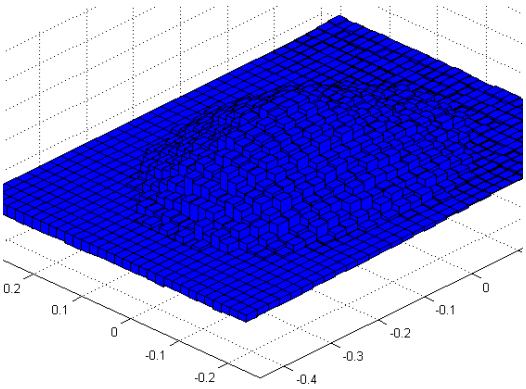

(d) Rectangular grid method from sampled points.

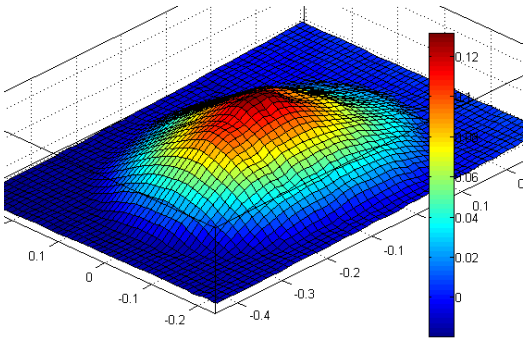

(e) Cubic Spline model from sampled points.

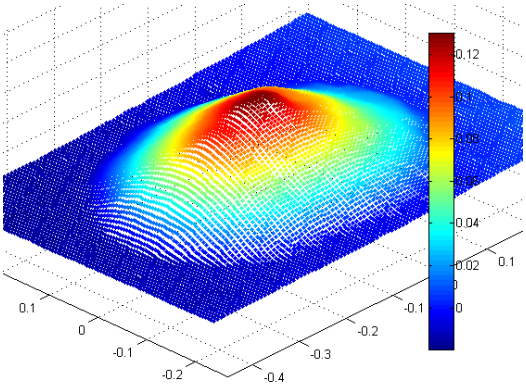

(f) Gaussian process model using squared exponential covariance function.

Figure 4.19 – This shows how each of the different methods estimate approximately 10000mL of volume using **1024** samples.

volume. The 2σ boundaries in Figure 4.20 are calculated from the collection of 100 volume estimates. In comparison, the 2σ boundaries in Figure 4.22 shows the mean 2σ uncertainty level computed by each of the Gaussian process methods over the 100 iterations for each volume experiment.

From Figure 4.21, all of the Gaussian process methods produce very similar results in this scenario. From the current state-of-the-art methods the rectangular grid method provides a good level of accuracy compared to the other state-of-the-art methods, however it is the least precise of all the methods. This is expected for this specific method given it is highly dependent on the sampled points in determining the volume.

The number of intervals used in the cubic spline method for integration was one hundred in each direction. This is the same amount of integral points which the Gaussian process method uses to estimate the mean volume and corresponding uncertainty.

From Figure 4.21 it can be noted that both the triangular prism and cubic spline method overestimate the volume in the majority of the volume experiments. One explanation for this is that given the low number of sample points, these methods do not accurately interpolate the edge of the stockpiled material between to the ground. This can be further seen in Figures 4.17, 4.18, 4.19 which give a visual representation of how the volume estimation techniques function under the different sampling sizes.

Figure 4.22 shows the mean volume output as well as the mean 2σ uncertainty level provided by each of the Gaussian process methods over the 100 iterations for each volume experiment. The exponential covariance function deviates the most from the other covariance functions. Given that the surfaces been estimated in the small scale volume experiments are all reasonably smooth, the exponential covariance function tends to overestimate the uncertainty between training points as can be seen in Figure 4.22.

Table 4.1 provides a measure of how well the uncertainty estimates provided by the Gaussian process methods are in comparison to the ground truth values. Each of the 100 iterations of each of the Gaussian process methods over all the volumes are tested to see if the predicted volume $\pm 1\sigma$ of the estimated uncertainty encapsulates

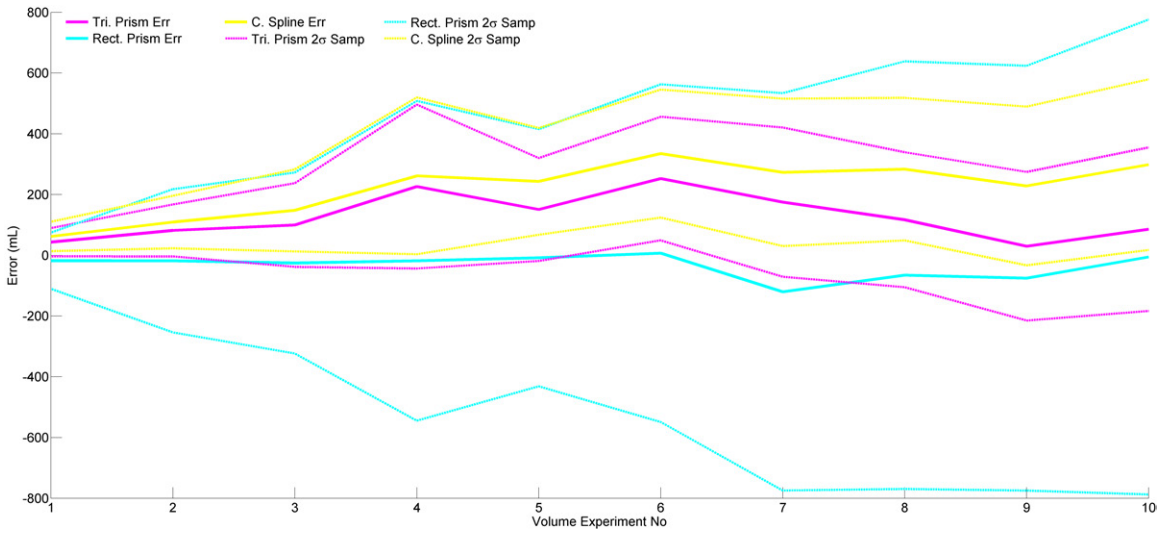

(a) State-of-the-art methods.

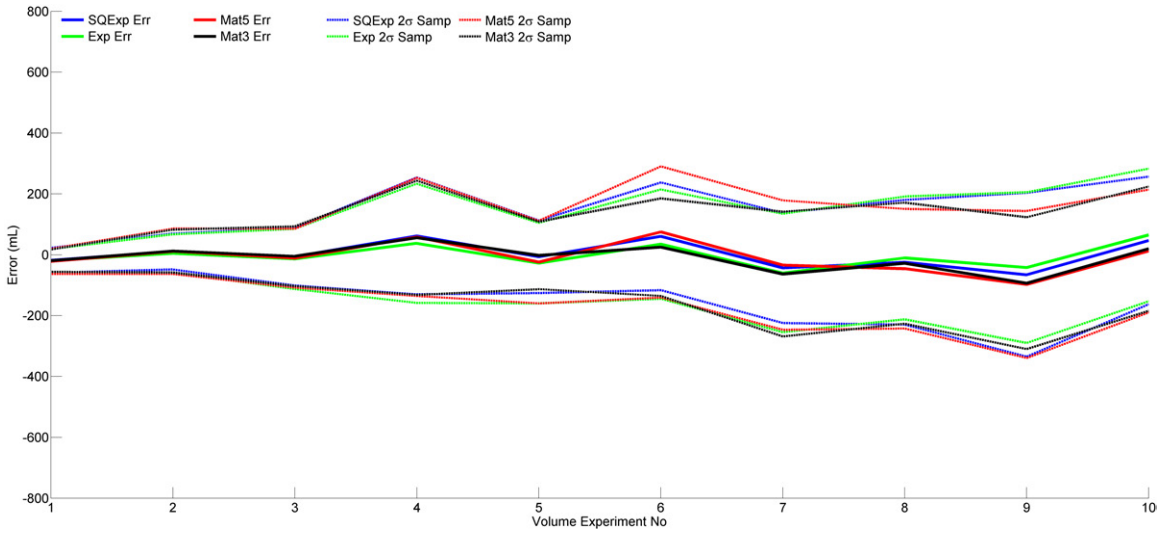

(b) Gaussian process methods.

Figure 4.20 – The mean volume error and a 2σ distribution of mean volume error over the ten different volumes used in this experiment using **64** samples.

the ground truth volume.

If the estimated uncertainty is correct, over 100 iterations it should be expected that $\approx 68.2\%$ of the results encapsulate the ground truth value. From Table 4.1, excluding the exponential covariance function, each of the Gaussian process methods provide (on average) a slightly conservative estimate of the uncertainty over the small scale experiment. The exponential covariance function, possibly due to the surface

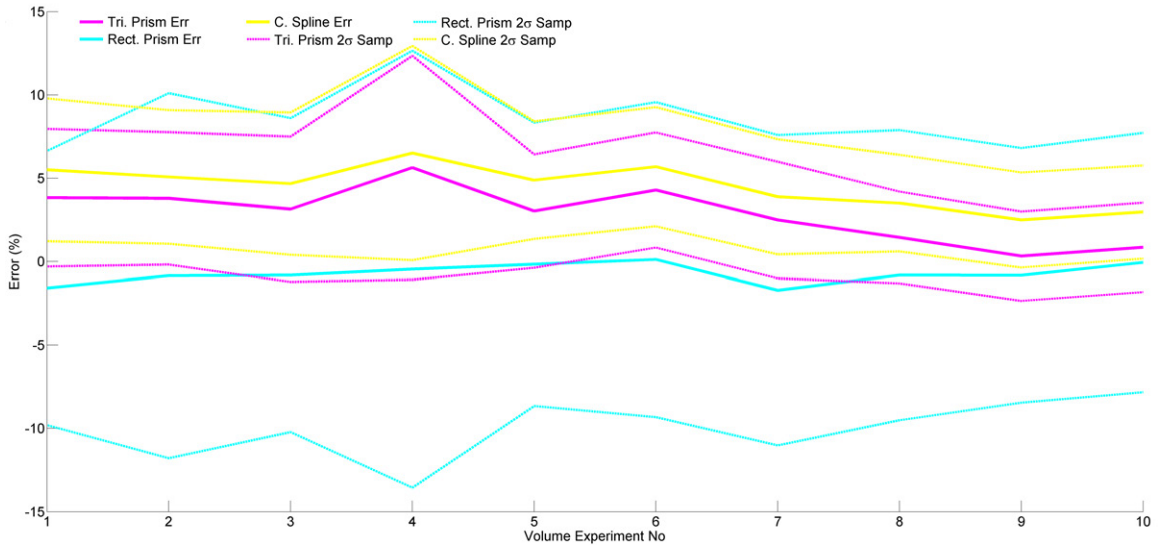

(a) State-of-the-art methods.

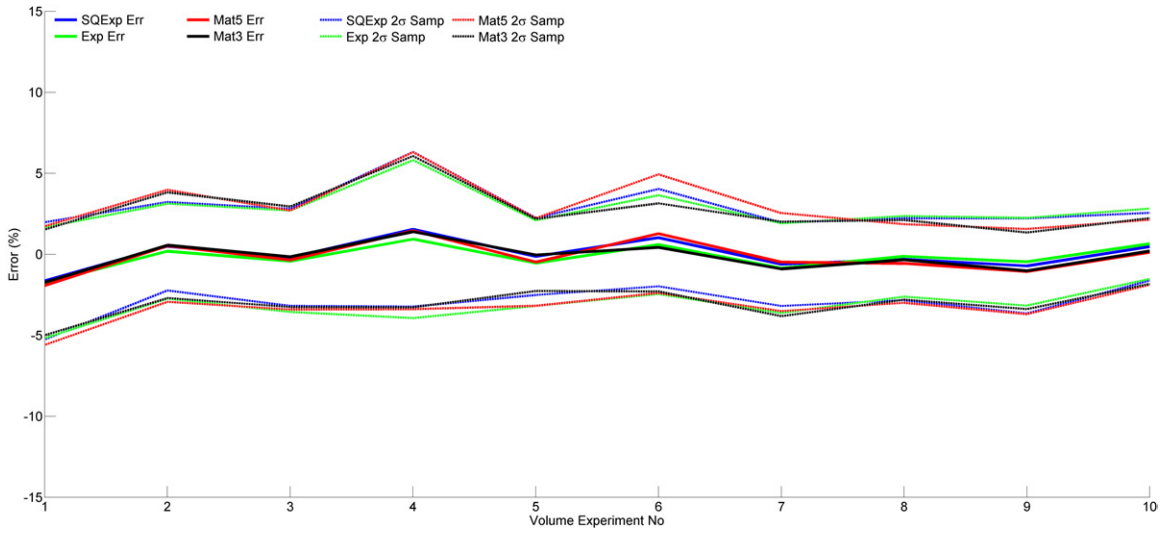

(b) Gaussian process methods.

Figure 4.21 – This figure shows a normalised error of the values in Figure 4.20 with respect to the true volume using **64** samples.

being modeled being relatively smooth and continuous as well as the sparsity of the data, does not encapsulate the uncertainty in the surface model as well as the other covariance functions.

A summary is provided in Table 4.2 which compares the performance of the different methods using only 64 sample points.

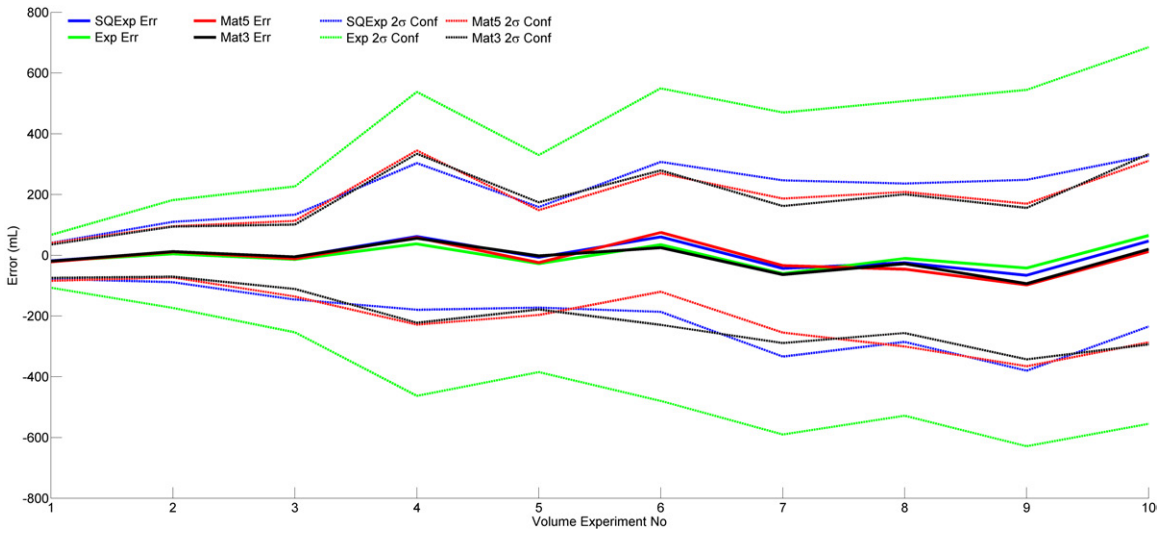

Figure 4.22 – Mean volume error of Gaussian process methods with the corresponding mean 2σ uncertainty estimated by the Gaussian process methods using **64** samples.

Volume Number	1	2	3	4	5	6	7	8	9	10	Mean
GP Squared Exp	70	90	80	73	85	70	85	78	76	78	78.5
GP Matern 5	67	69	80	76	74	60	69	79	60	89	72.3
GP Matern 3	64	74	66	82	86	90	65	75	59	850	74.6
GP Exp	88	100	99	99	99	100	98	100	99	98	98

Table 4.1 – Number of estimates which are within 1σ of ground truth using a sample size of 64 over 100 different combinations of samples per volume.

4.6.3 256 Sample Scenario

Figures 4.23 - 4.25 describe how each of the different methods perform when the amount of samples is increased to 256.

In this scenario, all of the methods have increased in both accuracy and precision. This is not unexpected given that when more data is available, a more accurate surface map should be generated. The cubic spline and triangulation methods improved in accuracy the greatest and have converged to a level of accuracy which is similar to that of the Gaussian process methods.

One of the interesting volume estimation results is from volume experiment number 1. In this scenario all of the methods perform poorly (relative to the performance over the other volume experiments using 256 samples). From Table 4.3 it can be seen

Method	Normalised Mean Error	Normalised 2σ Sampling Error	1σ Consistency (GP methods only)
Triangular Prism	2.88 %	3.76 %	-
Rectangular Grid	- 0.71 %	9.30 %	-
Cubic Spline	4.52 %	3.81 %	-
GP Sq. Exp.	- 0.0074%	2.96 %	78.5 %
GP Matern $\frac{5}{2}$	- 0.15%	3.15 %	72.3 %
GP Matern $\frac{3}{2}$	- 0.16 %	2.90 %	74.6 %
GP Exp.	- 0.18%	3.02 %	98 %

Table 4.2 – Summary of all methods over 64 Samples and all ten volumes.

Volume Number	1	2	3	4	5	6	7	8	9	10	Mean
GP Squared Exp	14	97	89	39	86	77	93	94	84	80	75.3
GP Matern 5	14	92	87	39	86	77	91	93	73	75	72.7
GP Matern 3	14	91	79	40	83	76	88	91	67	74	70.3
GP Exp	17	100	85	77	95	97	97	100	86	99	85.3

Table 4.3 – Number of estimates which are within 1σ of the ground truth using a sample size of 256 over 100 different combinations of samples.

that all the Gaussian process methods understate the uncertainty. The similar trend lines of the error values of the different methods provide evidence to the possibility that there is a slight bias in the sampling of the points which are used to estimate the surface and volume. This result suggests that the sampling method used in this thesis is not necessarily the best solution for surface and volume estimation. The sampling method could possibly be improved by sampling more points around complex features. An example of this would be the apexes at the top of a stockpile or between the ground and the stockpile. In these areas the general surface trend changes rapidly, more points would allow for these features to be represented more accurately.

This method of sampling is commonly used in manual surveying. While overall less points are sampled in manual surveying, the points sampled are all of generally high value in representing the surface features.

Developing an improved sampling method for surface estimation from raw sensor data

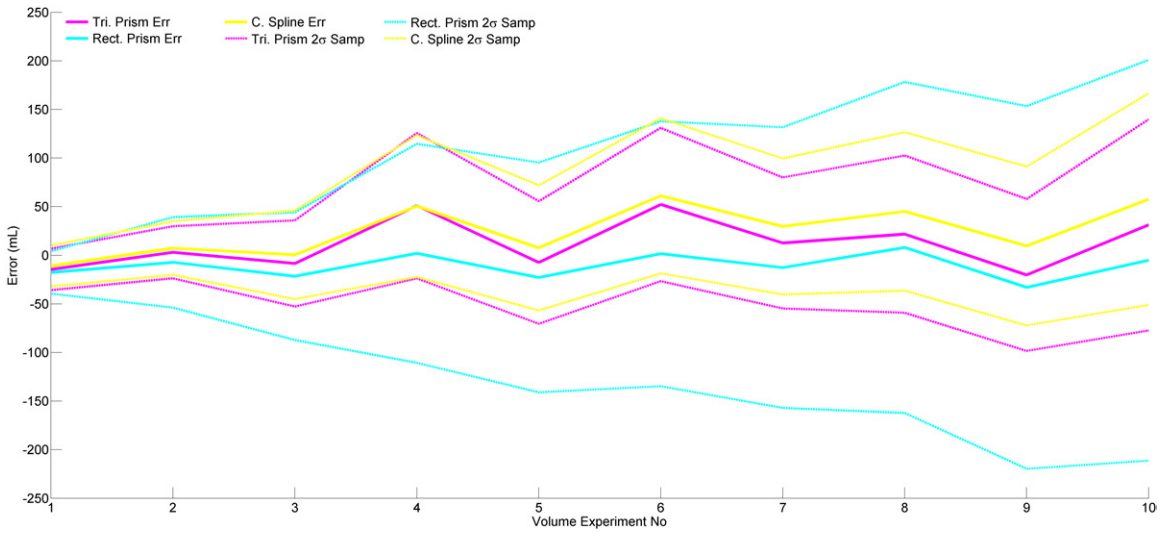

(a) State-of-the-art methods

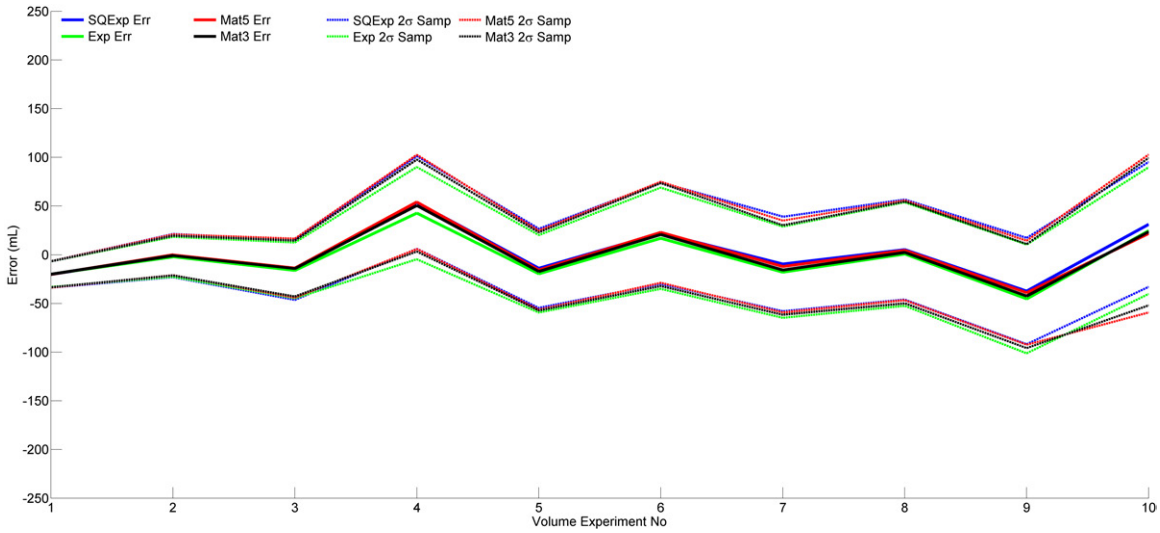

(b) Gaussian process method

Figure 4.23 – Mean volume error and 2σ distribution of mean volume error over the ten different volumes using **256** sample points.

would likely be able to increase the accuracy and precision of all the methods tested in this thesis. The actual development of this sampling method is not within the scope of this thesis.

Table 4.4 provides a summary of the performance of the different techniques using 256 samples.

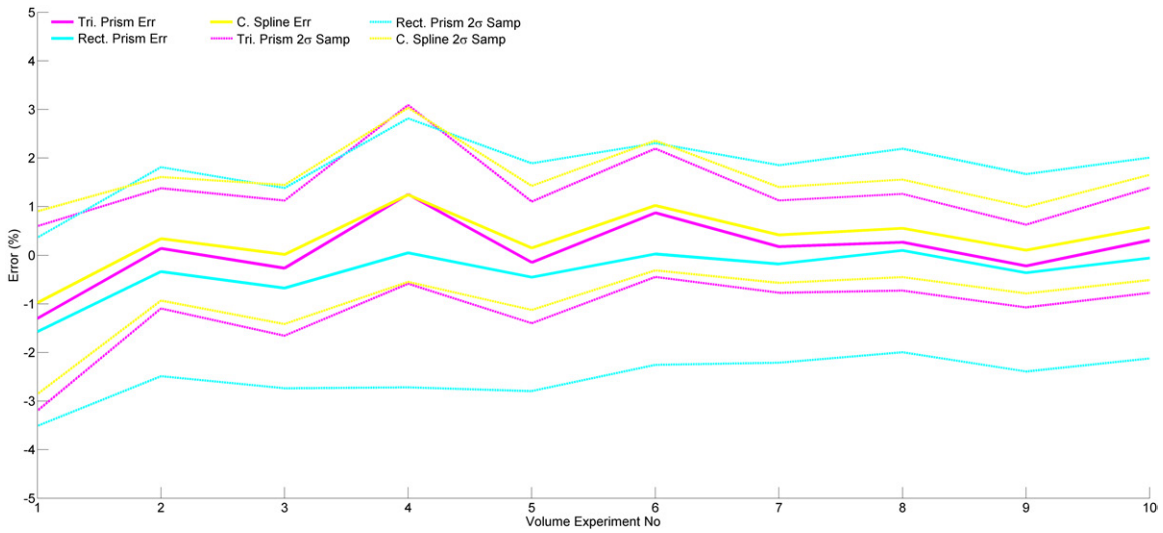

(a) State-of-the-art methods

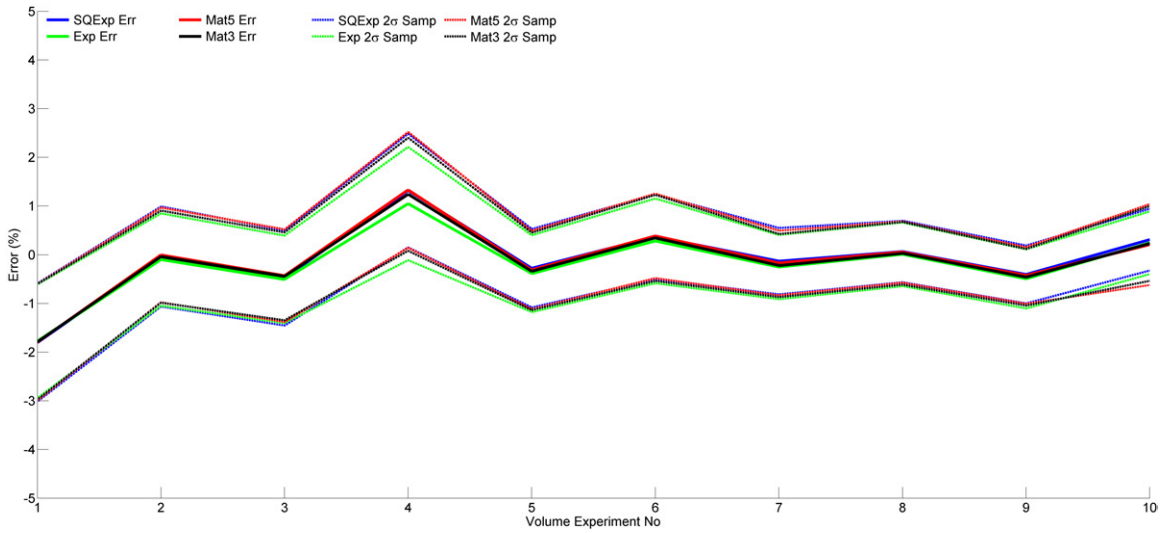

(b) Gaussian process method

Figure 4.24 – This figure shows a normalised error of the values in Figure 4.23 with respect to the true volume using **256** samples.

4.6.4 1024 Sample Scenario

In the 1024 sample scenario, all of the tested methods have converged to very similar levels of accuracy and precision (Figures 4.26 - 4.28.

The uncertainty estimated by the Gaussian process methods has also become more accurate compared to the 64 and 256 sample scenarios. This can be seen in Table 4.5

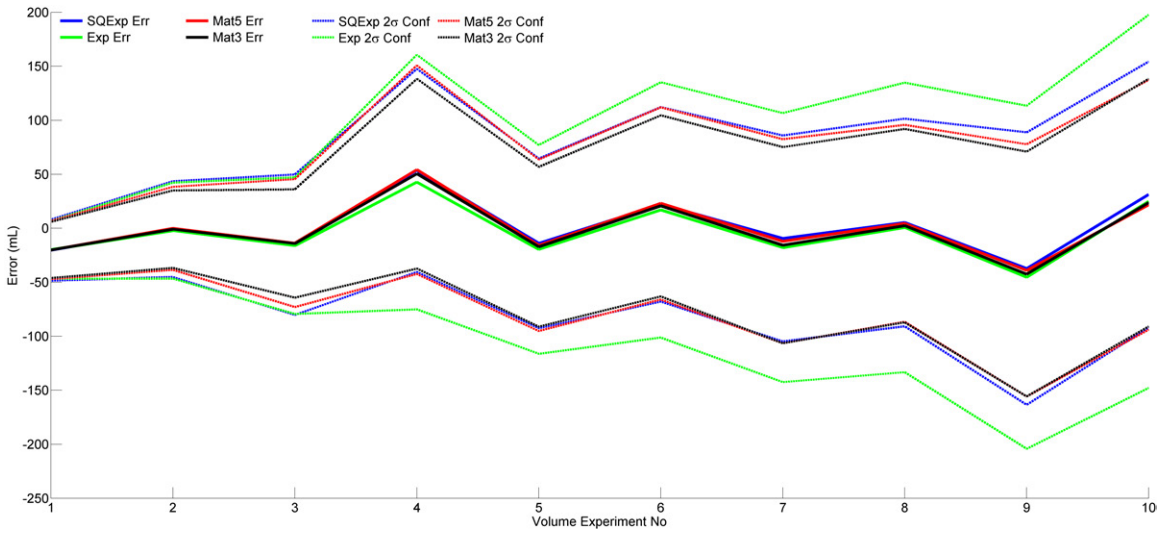

Figure 4.25 – Mean volume error of Gaussian process methods with the corresponding mean 2σ uncertainty estimated by the Gaussian process methods using 256 samples.

Method	Normalised Mean Error	Normalised 2σ Sampling Error	1σ Consistency (GP methods only)
Triangular Prism	0.11 %	1.28 %	-
Rectangular Grid	- 0.35 %	2.18 %	-
Cubic Spline	0.34 %	1.29 %	-
GP Sq Exp.	- 0.11%	0.86 %	75.3 %
GP Matern $\frac{5}{2}$	- 0.12%	0.87 %	72.7 %
GP Matern $\frac{3}{2}$	- 0.14 %	0.85 %	70.3 %
GP Exp.	- 0.19%	0.84 %	85.3 %

Table 4.4 – Summary of all methods over 256 Samples and all ten volumes

where the uncertainty estimated is now much closer to the expected value of $\approx 68.2\%$. One of the other significant changes in results is the improvement of the exponential covariance function in estimating the uncertainty of the volume. These improvements can be attributed to the increase in sample size. This improves the accuracy of the learning process to determine the most accurate hyper-parameters for the given data set. This is particularly true for parameters such as sensor noise.

Disregarding the result from volume experiment number 1 (which follows on from the same trend as the 256 sample experiment), each of the covariance functions are overall still conservative on estimating the uncertainty. This result can be seen in

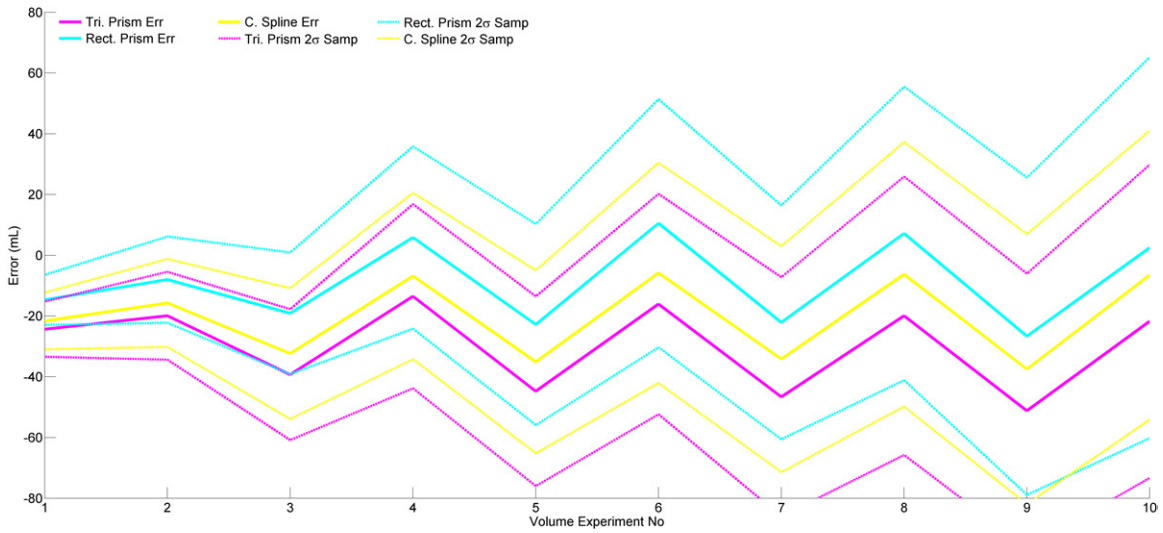

(a) State-of-the-art methods

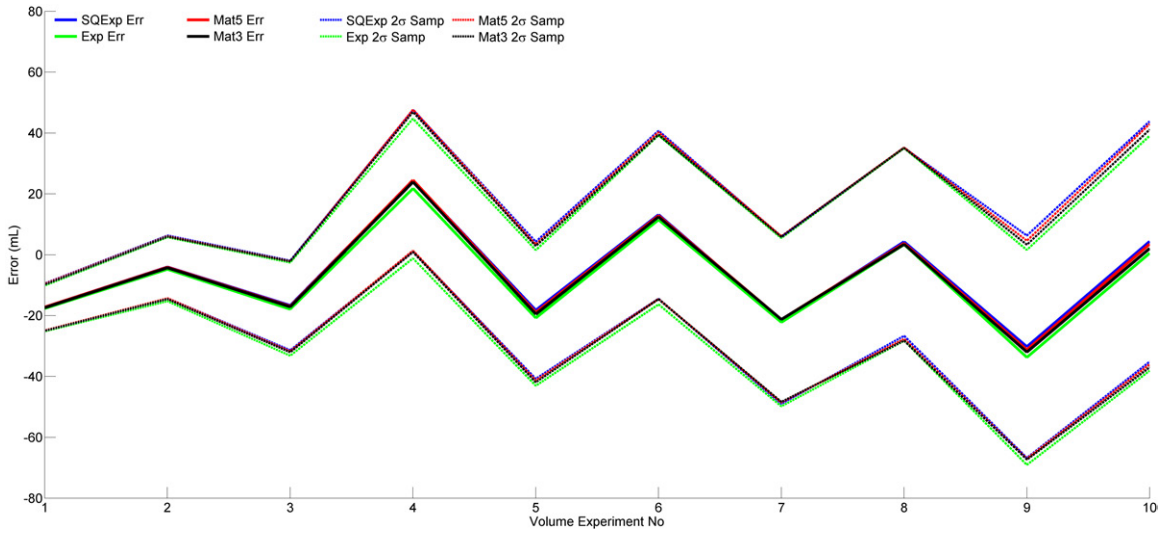

(b) Gaussian process method

Figure 4.26 – Mean volume error and 2σ distribution of mean volume error over the ten different volumes using **1024** samples.

Table 4.5.

Table 4.6 provides a summary of all the different methods using a sample size of 1024.

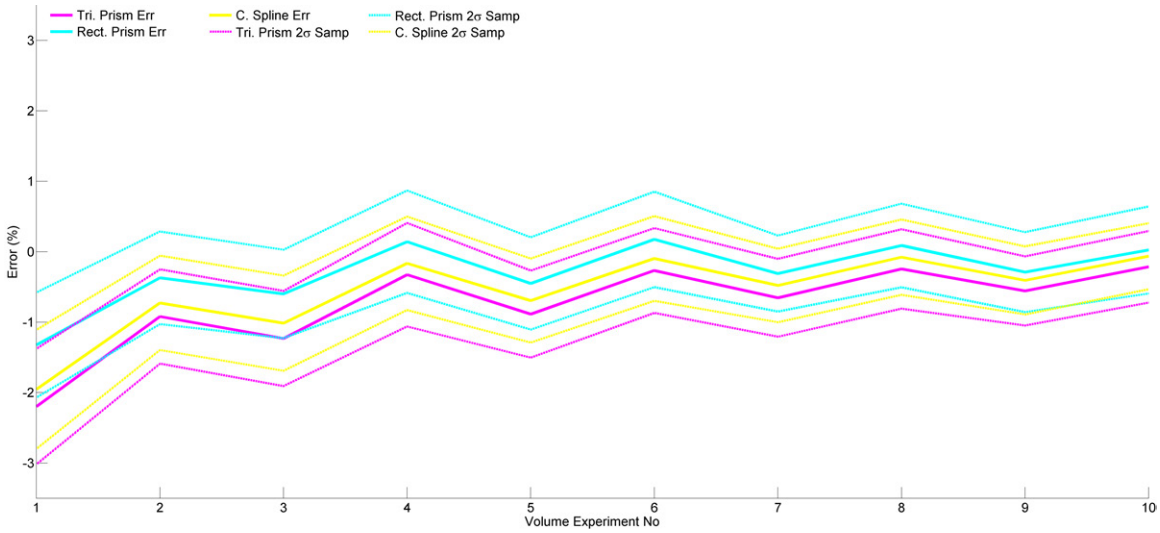

(a) State-of-the-art methods

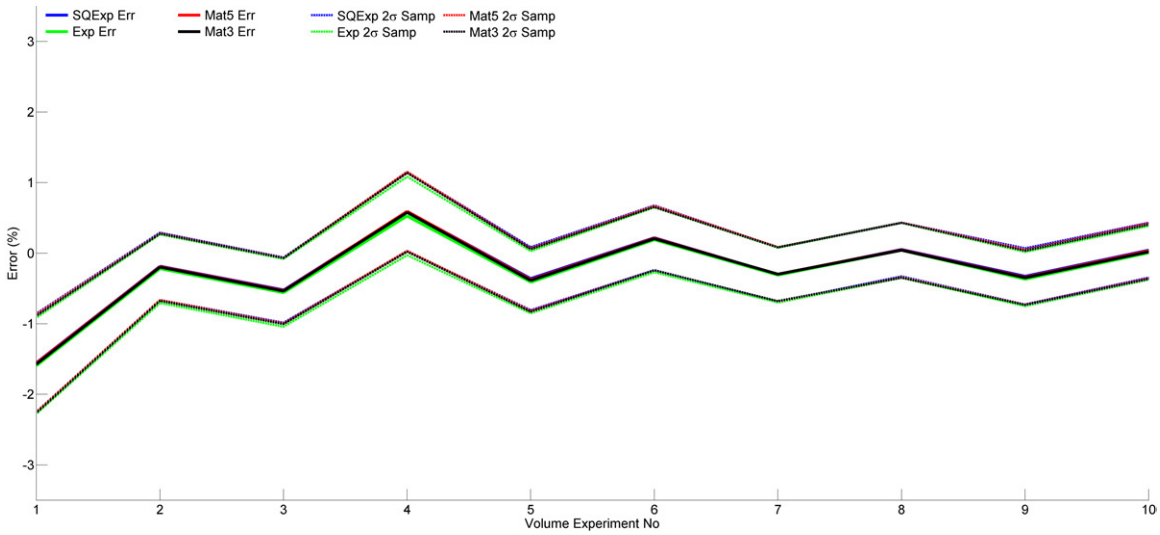

(b) Gaussian process method

Figure 4.27 – This figure shows a normalised error of the values in Figure 4.26 with respect to the true volume using **1024** samples.

4.7 Large Scale Experiment

In order to test how the Gaussian process volume estimation method compares in an environment which more closely represents an open pit mine, another series of experiments is performed.

These tests form part of the experiment which was used in the large scale experiments

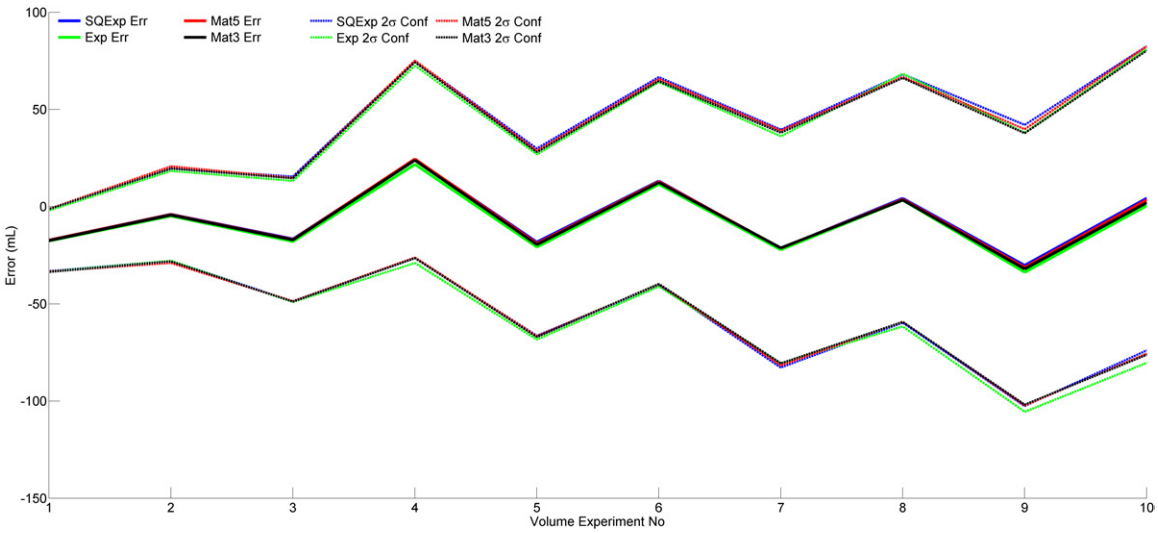

Figure 4.28 – Mean volume error of Gaussian process methods with mean 2σ uncertainty estimated of the volume estimate in the **1024** sample experiment.

Volume No.	1	2	3	4	5	6	7	8	9	10	Mean
GP Sq Exp	1	96	50	55	68	84	76	94	62	96	68.2
GP Mat 5	1	95	49	56	64	84	76	94	59	96	67.4
GP Mat 3	1	96	46	56	64	85	74	93	54	97	66.6
GP Exp	0	94	39	63	61	85	70	93	53	97	65.6

Table 4.5 – Number of estimates which are within 1σ of the true volume using a sample size of 1024 over 100 different combinations of samples.

Method	Normalised Mean Error	Normalised 2σ Sampling Error	1σ Consistency (GP methods only)
Triangular Prism	-0.75 %	0.62 %	-
Rectangular Grid	- 0.29 %	0.64 %	-
Cubic Spline	-0.57 %	0.60 %	-
GP Sq Exp.	- 0.24%	0.46 %	68.2 %
GP Matern $\frac{5}{2}$	- 0.24%	0.46 %	67.4 %
GP Matern $\frac{3}{2}$	- 0.25 %	0.46 %	66.6 %
GP Exp.	- 0.27%	0.46 %	65.6 %

Table 4.6 – Summary of all methods over 1024 Samples and all ten volumes.

in Chapter 3 to provide proof that probabilistic tracking of extensive bulk material properties is possible.

In this larger scale experiment, material is removed sequentially from a 'simulated' grade block using a front end loader. An example of this grade block and the volume to be estimated can be seen in Figure 4.29.

Figure 4.29 – An example of the volume to be estimated in the larger scale experiment. This scenario aims to simulate the removal of material from a grade block in an open pit mine.

The volume estimated is the amount of material removed from the grade block before and after each excavator load. This volume is used as an estimate for the amount of material in the excavator bucket.

As part of the preprocessing of the original data sets for each volume, GPS co-ordinates are used to provide a rectangular boundary over the grade block to include only the material in the grade block and not the fixed walls in which the material is stored.

Like the small scale experiment, three different resolutions are used to gauge the accuracy and precision of each method. In this scenario, the resolutions are set at 96, 320 and 1124 samples. The ground truth is calculated using the same method as the small scale experiment, all of the data points are used to form the surface using Delaunay triangulation, then using triangular prisms to determine the volume.

An example of the different stages of excavation and the corresponding representation

from each volume estimation technique can be seen in Figures 4.30 - 4.32. In these examples 320 sample points are used.

4.7.1 96 Sample Scenario

Figures 4.33 - 4.35 show how each method performs as material is removed from the grade block over time.

In this scenario, the squared exponential, Matern $\frac{5}{2}$ and Matern $\frac{3}{2}$ methods produce similar levels of accuracy (as can be seen in Figures 4.33 and 4.34). The exponential covariance function deviates from the other Gaussian process methods on several of the volume experiments. This could be attributed to the way in which the exponential covariance function handles sparse data sets. It typically produces a model which is much sharper between sample points. Comparatively, the other covariance functions smooth (average) the model significantly more over the sparse data (producing, relatively, more similar results).

The state-of-the-art-methods provide both slightly lower accuracy and precision than the Gaussian process methods. The one exception is the rectangular grid method. This method is as accurate as the Gaussian process methods but considerably less precise.

From Table 4.7 there is a considerable difference to that of the similar scenario in the small scale example (the 64 sample case). The expected value for each entry of the table is approximately 68.2%.

Table 4.7 shows that each of the covariance function is very conservative in the estimates given of the uncertainty. The least conservative of the four options is the exponential covariance function. This is the opposite result to which occurred in the small scale experiment.

The relative level of uncertainty estimated by each of the Gaussian process methods can be seen more clearly in Figure 4.35. The uncertainty estimated by each of the covariance functions appears to be correlated to the amount of averaging each of the

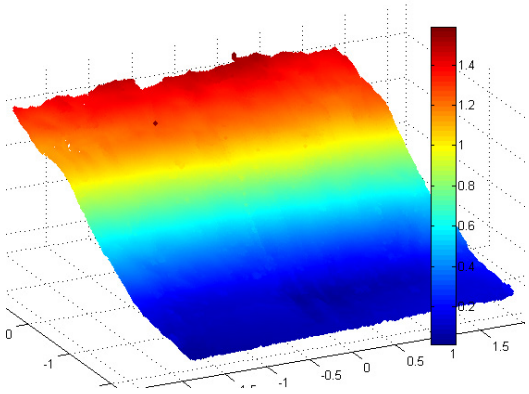

(a) A plot of the raw sensor output.

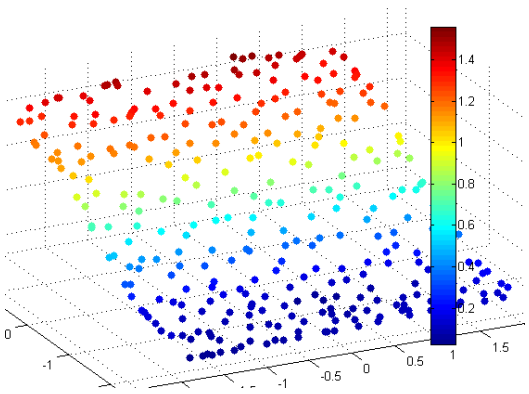

(b) 320 samples taken from raw sensor output.

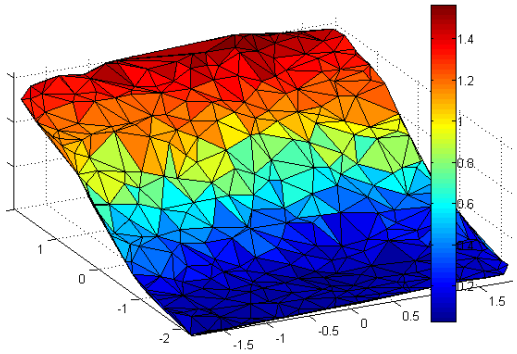

(c) Delaunay triangulated surface from sampled points.

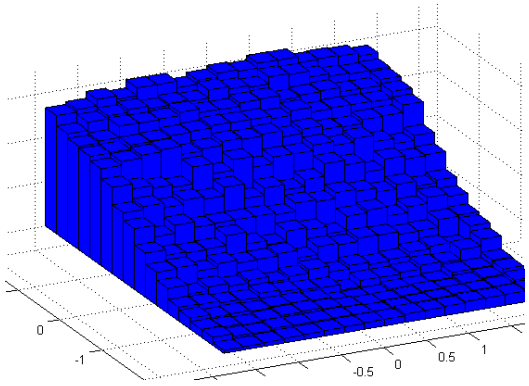

(d) Rectangular grid method from sampled points.

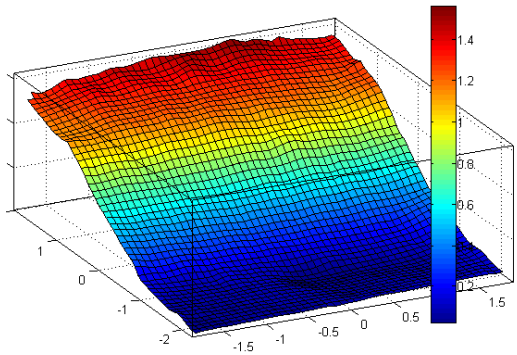

(e) Cubic Spline model from sampled points.

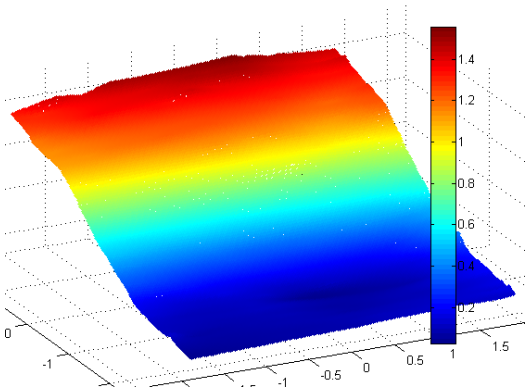

(f) Gaussian process model using exponential covariance function.

Figure 4.30 – An example of how each volume estimation method represents the simulated **grade block prior to excavation** on the large scale experiment. 320 samples are used in each of the volume estimation methods.

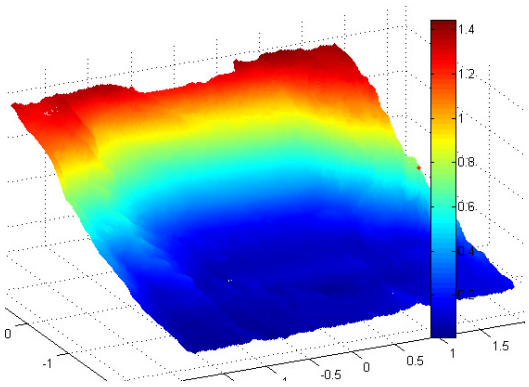

(a) A plot of the raw sensor output.

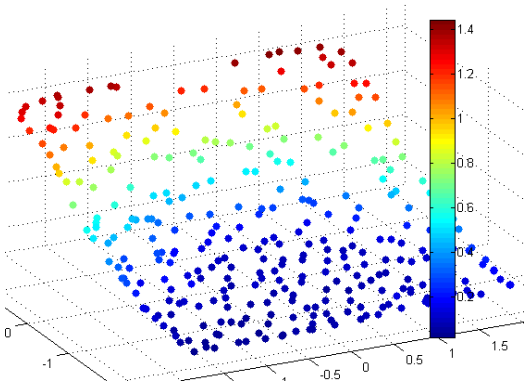

(b) 320 samples taken from raw sensor output.

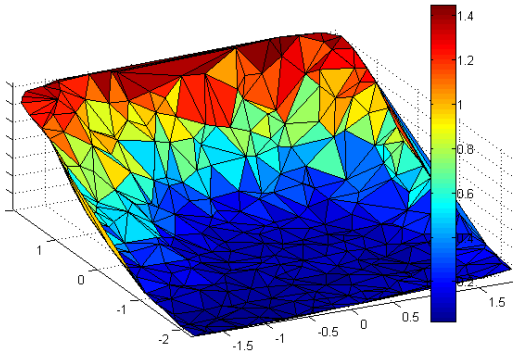

(c) Delaunay triangulated surface from sampled points.

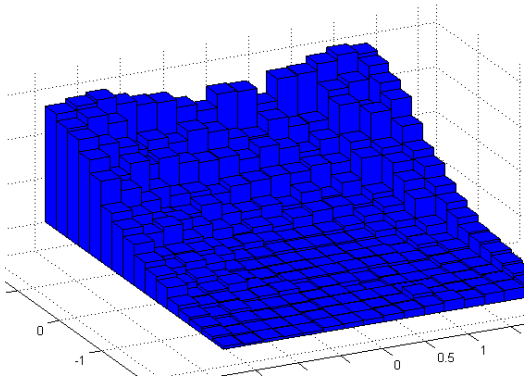

(d) Rectangular grid method from sampled points.

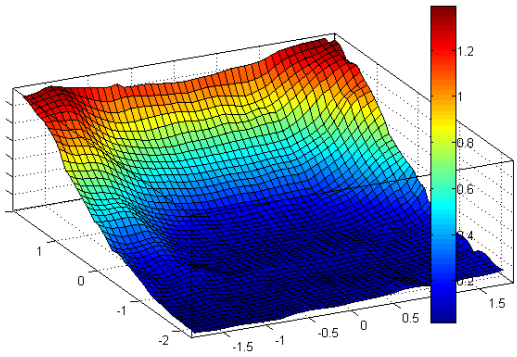

(e) Cubic Spline model from sampled points.

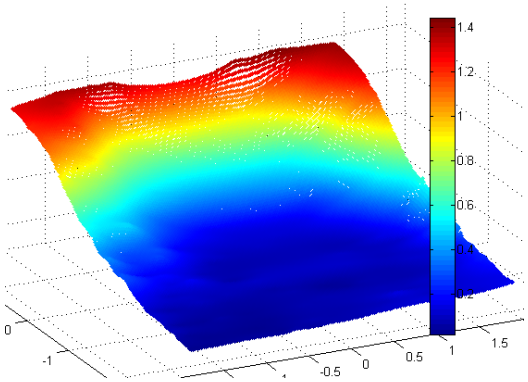

(f) Gaussian process model using exponential covariance function.

Figure 4.31 – An example of how each volume estimation method represents the simulated **grade block after six excavator loads** on the large scale experiment. 320 samples are used in each of the volume estimation methods.

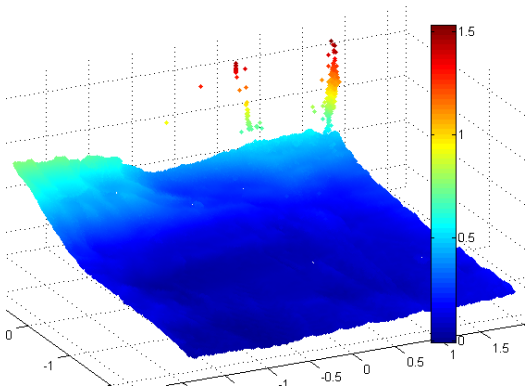

(a) A plot of the raw sensor output.

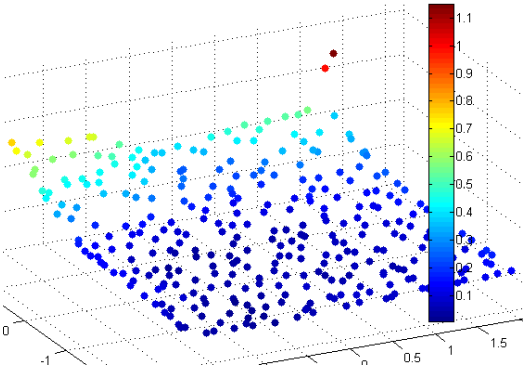

(b) 320 samples taken from raw senor output.

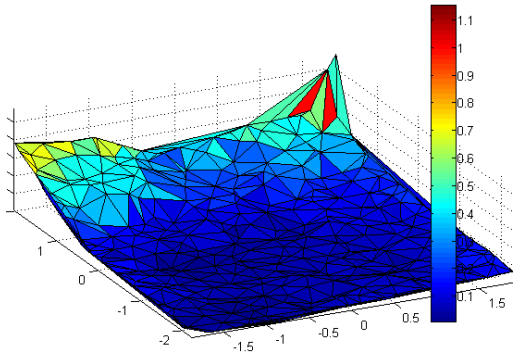

(c) Delaunay triangulated surface from sampled points.

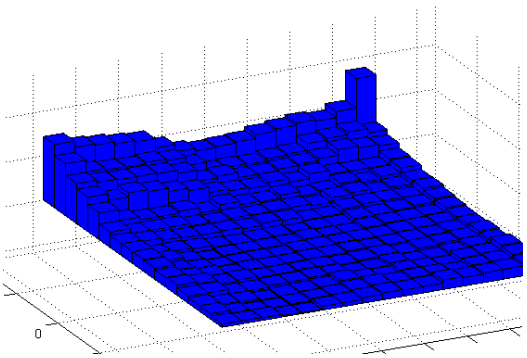

(d) Rectangular grid method from sampled points.

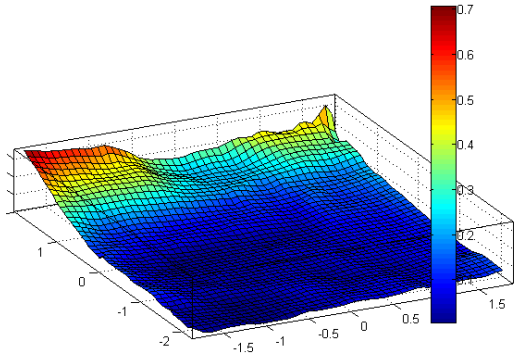

(e) Cubic Spline model from sampled points.

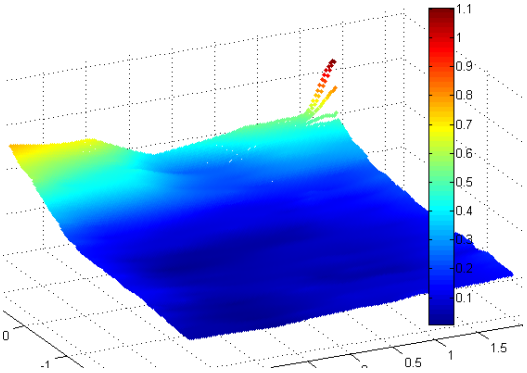

(f) Gaussian process model using exponential covariance function.

Figure 4.32 – An example of how each volume estimation method represents the simulated **grade block after thirteen excavator loads** on the large scale experiment. 320 samples are used in each of the volume estimation methods.

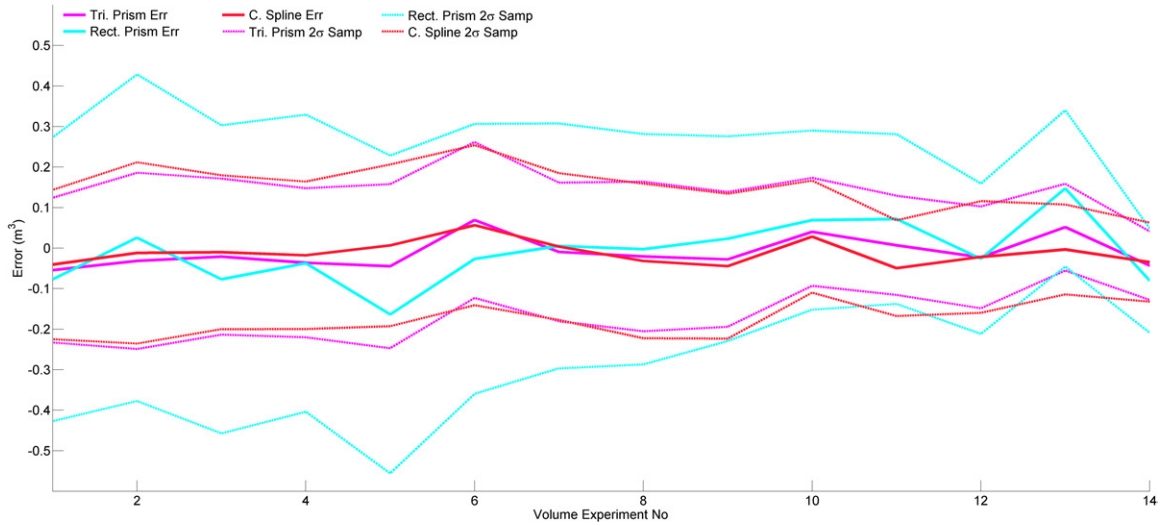

(a) State-of-the-art methods

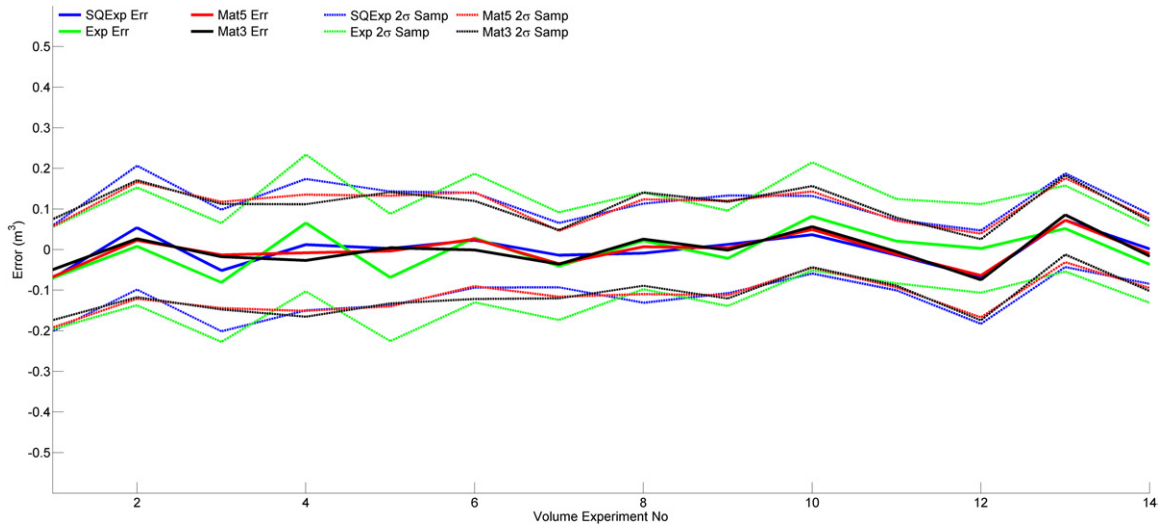

(b) Gaussian process method

Figure 4.33 – Mean volume error and 2σ distribution of mean volume error over the fifteen different volumes in the large scale experiment using **96** samples.

covariance functions performs. This can be seen in Figure 4.35 whereby the variance estimated in order of least to most conservative is exponential, Matern $\frac{3}{2}$, Matern $\frac{5}{2}$ then squared exponential. This is the same order as the number of times each covariance function is differentiable from lowest to highest.

The outcome of this experiment shows that the choice of covariance function (even quite similar covariance functions) does have an impact upon the estimation perfor-

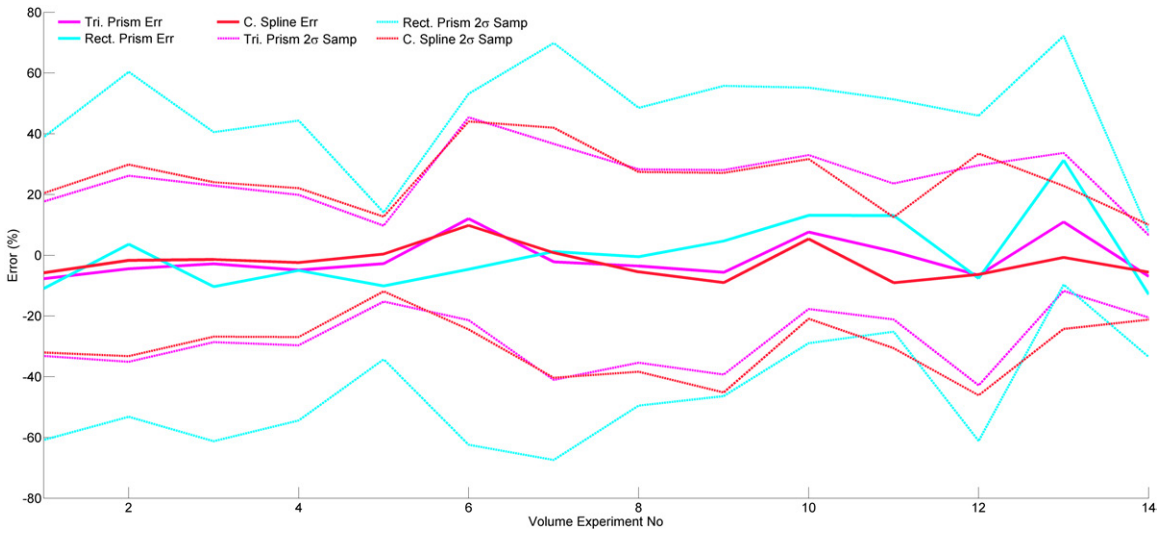

(a) State-of-the-art methods

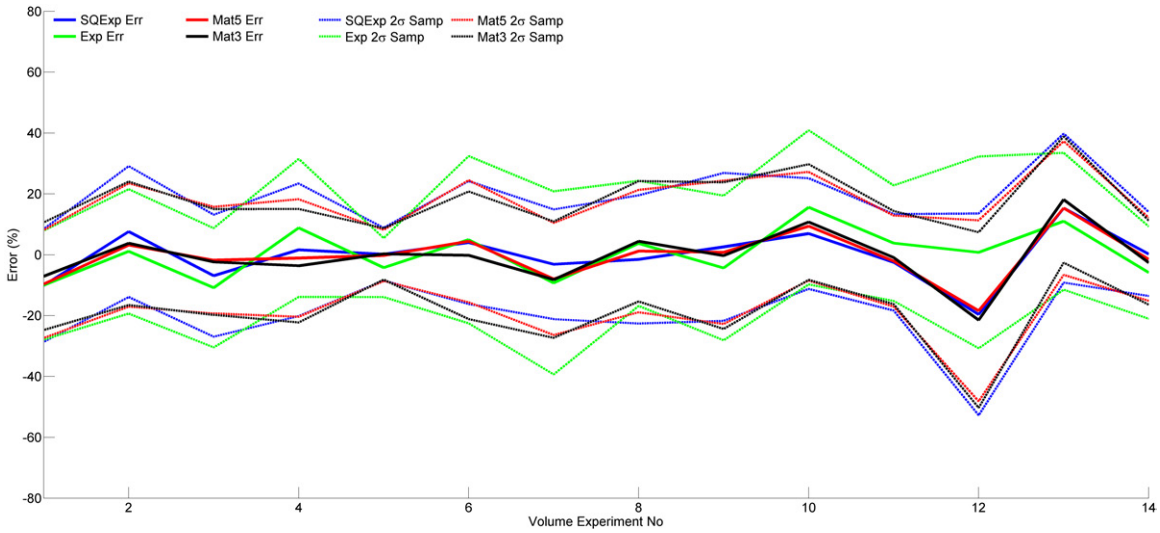

(b) Gaussian process method

Figure 4.34 – This figure shows a normalised error of the values in Figure 4.33 with respect to the true volume using **96** samples.

mance. Based on the previous results, the best method for estimating the uncertainty under these types of surface conditions in the large scale experiment is the exponential covariance function.

This matches the prior hypothesis in Section 4.3.2 that the exponential covariance function would perform better at representing surfaces with more complex fast changing features. In the small scale example the more smoother covariance functions were

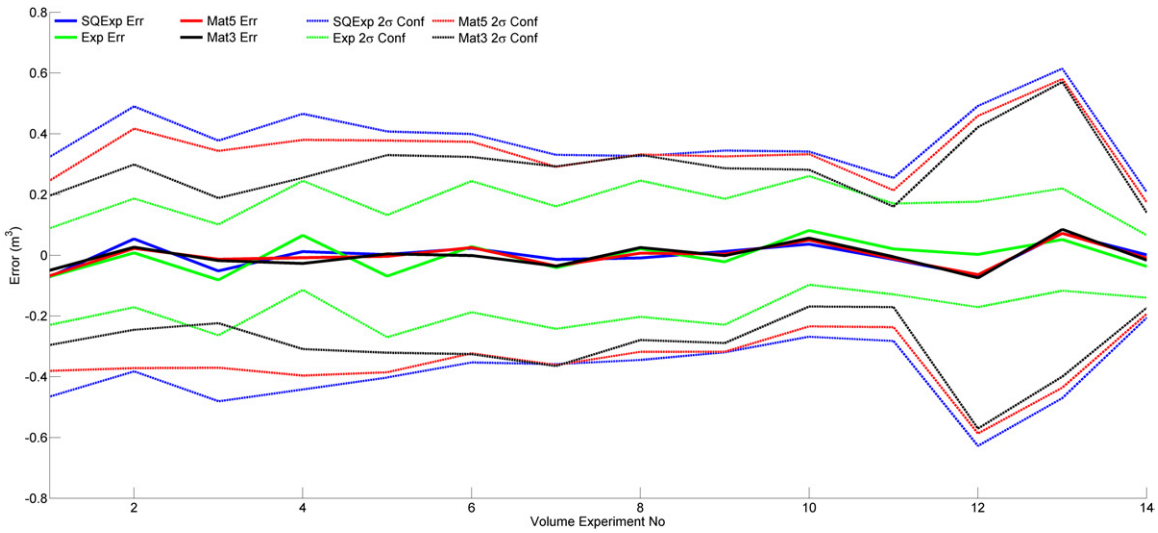

Figure 4.35 – Mean volume error of Gaussian process methods with mean 2σ uncertainty estimated of the volume estimate in the **96** sample large scale experiment.

better at estimating the uncertainty in the smooth stockpile volume scenarios.

Volume No.	**1**	**2**	**3**	**4**	**5**	**6**	**7**
GP Sq Exp	100	100	100	100	100	100	99
GP Mat 5	100	100	100	100	100	100	99
GP Mat 3	100	100	100	100	100	100	99
GP Exp	89	98	90	92	95	98	100

Volume No.	**8**	**9**	**10**	**11**	**12**	**13**	**14**	**Mean**
GP Sq Exp	99	100	100	100	100	100	100	99.86
GP Mat 5	99	100	100	100	100	100	100	99.86
GP Mat 3	99	100	100	100	100	100	100	99.86
GP Exp	100	100	97	99	100	99	89	96.14

Table 4.7 – Number of estimates which are within 1σ of the true volume using a sample size of 96 over 100 different combinations of samples.

A summary of the results for all the methods in the 96 sample case can be seen in Table 4.8.

4.7.2 320 Sample Scenario

The results in the 320 sample case for the large scale experiment can be seen in Figures 4.36 - 4.38. The accuracy and precision of all methods increased compared to the 96

Method	Normalised Mean Error	Normalised 2σ Sampling Error	1σ Consistency (GP methods only)
Triangular Prism	-1.12 %	26.93 %	-
Rectangular Grid	0.36 %	46.64 %	-
Cubic Spline	-2.21 %	27.95 %	-
GP Sq Exp.	- 0.38%	19.97 %	99.86 %
GP Matern $\frac{5}{2}$	- 0.59%	18.82 %	99.86 %
GP Matern $\frac{3}{2}$	- 0.67 %	18.87 %	99.86 %
GP Exp.	- 0.37%	21.83 %	96.14 %

Table 4.8 – Summary of all methods over 96 Samples and all fifteen volumes

sample scenario. The Gaussian process methods still outperform the state-of-the-art methods as can be seen in the summary in Table 4.10.

Increasing the amount of sample points leads to a clear differentiation between the uncertainty estimated by each of the Gaussian process methods. This can be seen in Figure 4.38.

Volume No.	**1**	**2**	**3**	**4**	**5**	**6**	**7**	
GP Sq Exp	100	100	100	100	100	100	100	
GP Mat 5	100	100	100	100	100	100	100	
GP Mat 3	100	100	100	100	100	100	100	
GP Exp	91	97	98	98	99	100	99	
Volume No.	**8**	**9**	**10**	**11**	**12**	**13**	**14**	**Mean**
GP Sq Exp	100	100	100	100	100	100	100	100
GP Mat 5	100	100	100	100	100	100	100	100
GP Mat 3	100	100	100	100	100	100	100	100
GP Exp	98	100	95	100	98	92	88	96.64

Table 4.9 – Number of estimates which are within 1σ of the true volume using a sample size of 320 over 100 different combinations of samples.

A summary of the results for all the methods in the 320 sample case can be seen in Table 4.10

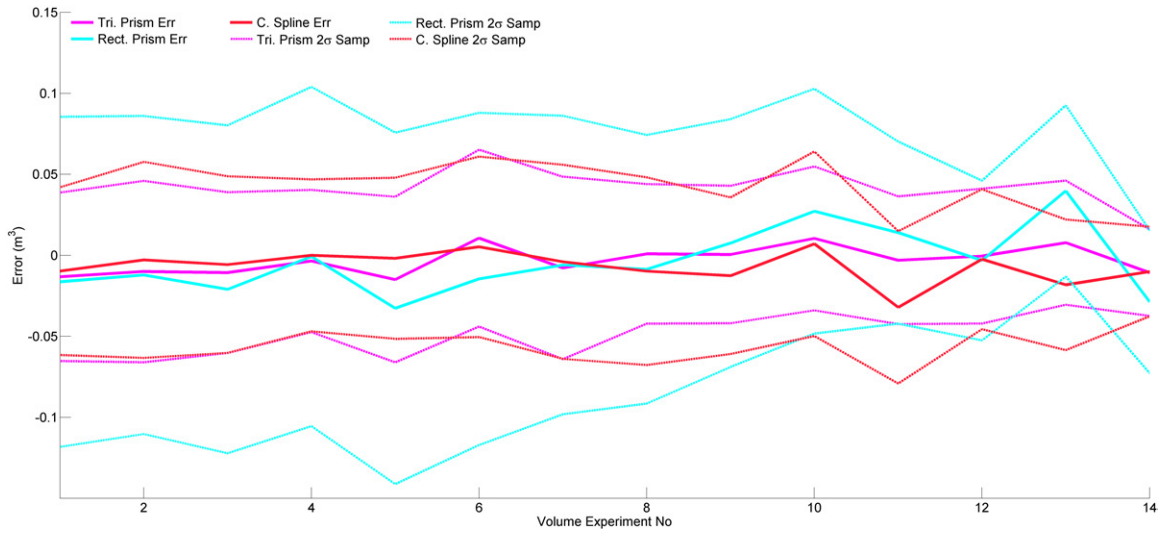

(a) State-of-the-art methods

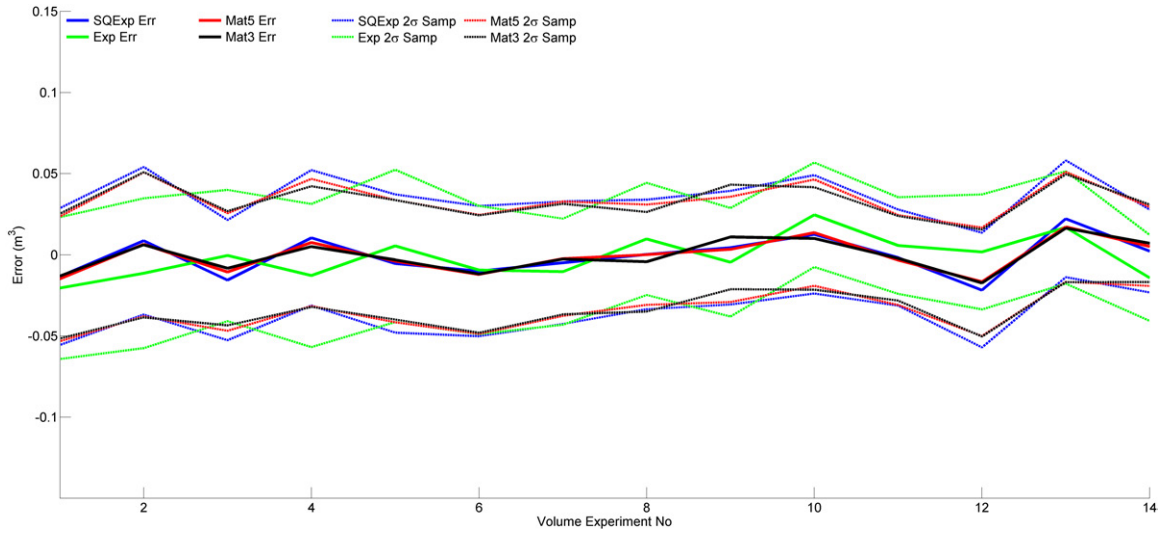

(b) Gaussian process method

Figure 4.36 – Mean volume error and 2σ distribution of mean volume error over the fifteen different volumes in the large scale experiment using **320** samples.

4.7.3 1152 Sample Scenario

The results of the 1152 sample volume scenarios can be seen in Figures 4.39 - 4.41. The relative performance of all the methods follows a similar trend as the 1024 sample case in the small scale volume experiments. Each of the methods in terms of accuracy have converged to very similar levels (see Table 4.12). The exception in this case is

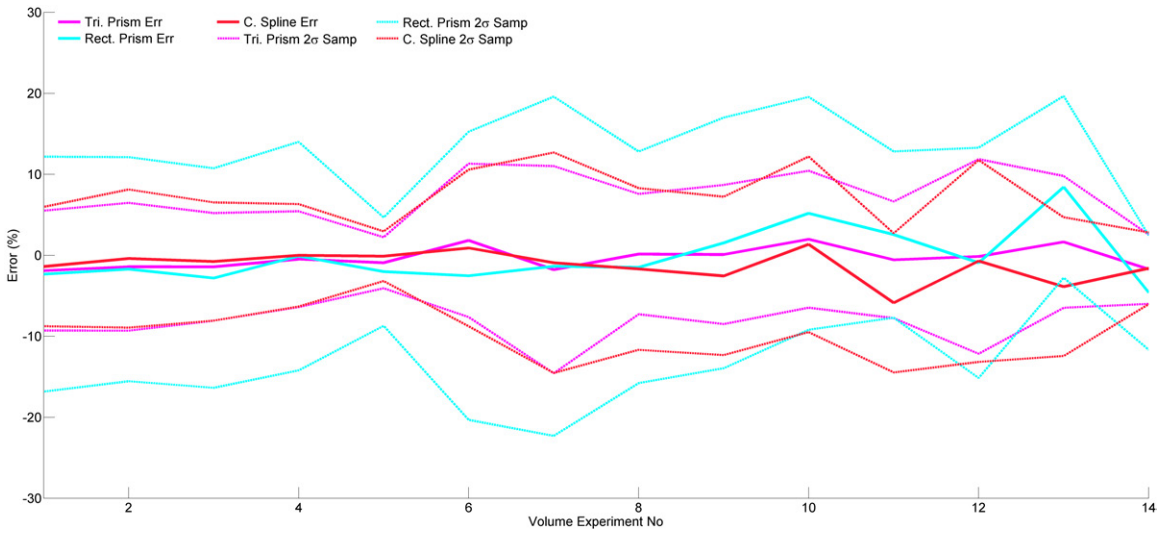

(a) State-of-the-art methods

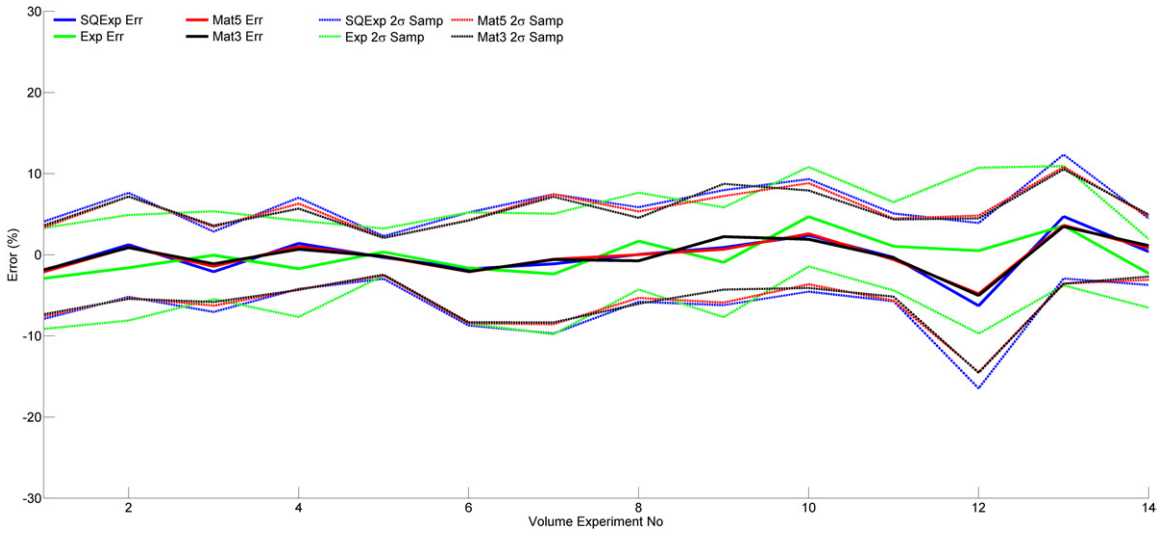

(b) Gaussian process method

Figure 4.37 – This figure shows a normalised error of the values in Figure 4.36 with respect to the true volume using **320** samples.

the cubic spline method which maintains a slight negative bias compared to the other methods. The accuracy and precision of the Gaussian process methods still provide an improvement over the other state-of-the-art methods. The absolute difference between methods is very slim when using this amount of samples however.

One of the interesting features when using the higher sample count can be seen in Figure 4.41, when compared to the 96 sample case (Figure 4.35) and the 320

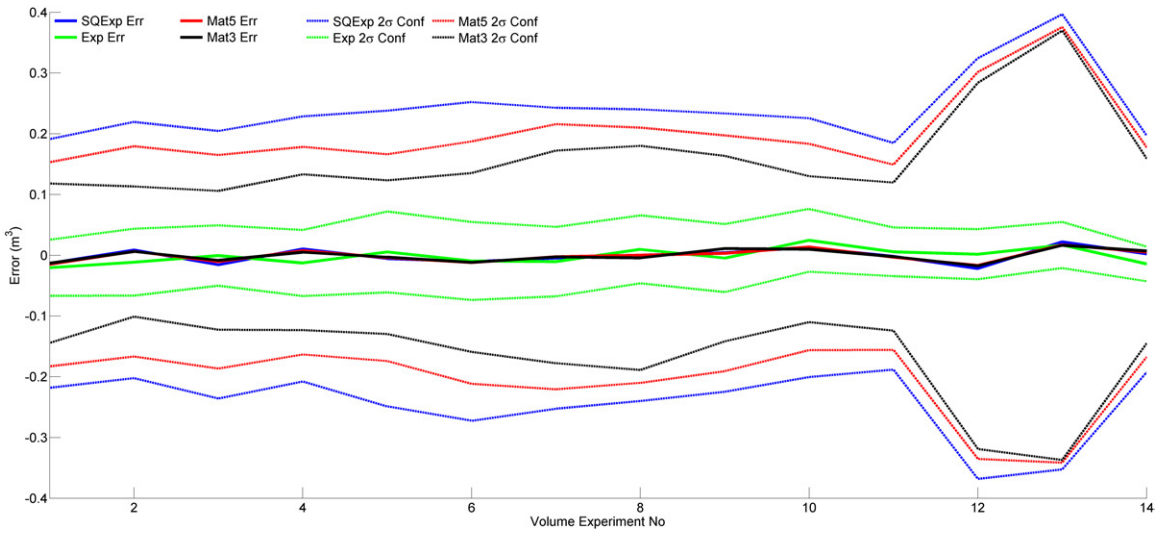

Figure 4.38 – Mean volume error of Gaussian process methods with mean 2σ uncertainty estimated of the volume estimate in the **320** sample large scale experiment.

Method	Normalised Mean Error	Normalised 2σ Sampling Error	1σ Consistency (GP methods only)
Triangular Prism	-0.33 %	7.81 %	-
Rectangular Grid	-0.16 %	13.45 %	-
Cubic Spline	-1.26 %	8.61 %	-
GP Sq Exp.	- 0.2%	6.31 %	100 %
GP Matern $\frac{5}{2}$	- 0.16%	5.89 %	100 %
GP Matern $\frac{3}{2}$	- 0.12 %	5.77 %	100 %
GP Exp.	- 0.12%	6.24 %	96.14 %

Table 4.10 – Summary of all methods over 320 Samples and all fifteen volumes

sample case (Figure 4.38). The mean uncertainty estimated by each of the covariance functions follow more consistent patterns, albeit offset proportionally, when compared to the other sample sizes.

A similar effect was noted in the 1024 sample case in the small scale experiments. More training points allow for a more consistent estimates of the hyper-parameters while learning, while also allowing for each of the covariance functions to better learn the hyper-parameters.

One common trait in each of the Gaussian process methods is the increase in un-

certainty predicted by each of the methods as the stockpile volume bin approaches empty (the bin is considered empty in Volume Experiment No. 15). One reason for this can be seen in Figure 4.32. The raw scan data also includes some slight portions of material which has compacted and stuck onto the Besa (concrete) block wall. These sharp near vertical surface changes are not handled well in general by smooth covariance functions like the squared exponential (the sharp change results in increasing the uncertainty across the whole surface).

Volume No.	**1**	**2**	**3**	**4**	**5**	**6**	**7**	
GP Sq Exp	100	100	100	100	100	100	100	
GP Mat 5	100	100	100	100	100	100	100	
GP Mat 3	100	100	100	100	100	100	100	
GP Exp	93	83	95	98	98	96	85	
Volume No.	**8**	**9**	**10**	**11**	**12**	**13**	**14**	**Mean**
GP Sq Exp	100	100	100	100	100	100	100	100
GP Mat 5	100	100	100	100	100	100	100	100
GP Mat 3	100	100	100	100	100	100	100	100
GP Exp	100	100	99	90	100	100	100	95.50

Table 4.11 – Number of estimates which are within 1σ of the true volume using a sample size of 1152 over 100 different combinations of samples.

Method	**Normalised Mean Error**	**Normalised 2σ Sampling Error**	**1σ Consistency (GP methods only)**
Triangular Prism	-0.087 %	2.21 %	-
Rectangular Grid	-0.12 %	3.97 %	-
Cubic Spline	-1.08 %	2.77 %	-
GP Sq Exp.	0.011%	2.01 %	100 %
GP Matern $\frac{5}{2}$	- 0.0011%	1.86 %	100 %
GP Matern $\frac{3}{2}$	- 0.0066 %	1.80 %	100 %
GP Exp.	- 0.026%	1.87 %	95.50 %

Table 4.12 – Summary of all methods over 1152 Samples and all fifteen volumes.

A summary of the results for all the methods in the 1152 sample case can be seen in Table 4.12

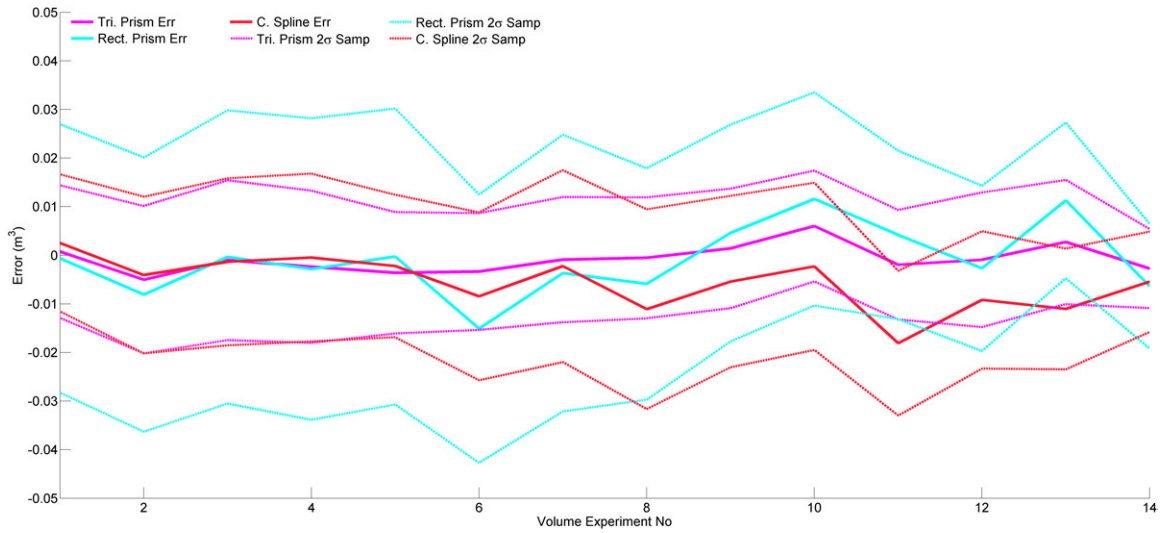

(a) State-of-the-art methods

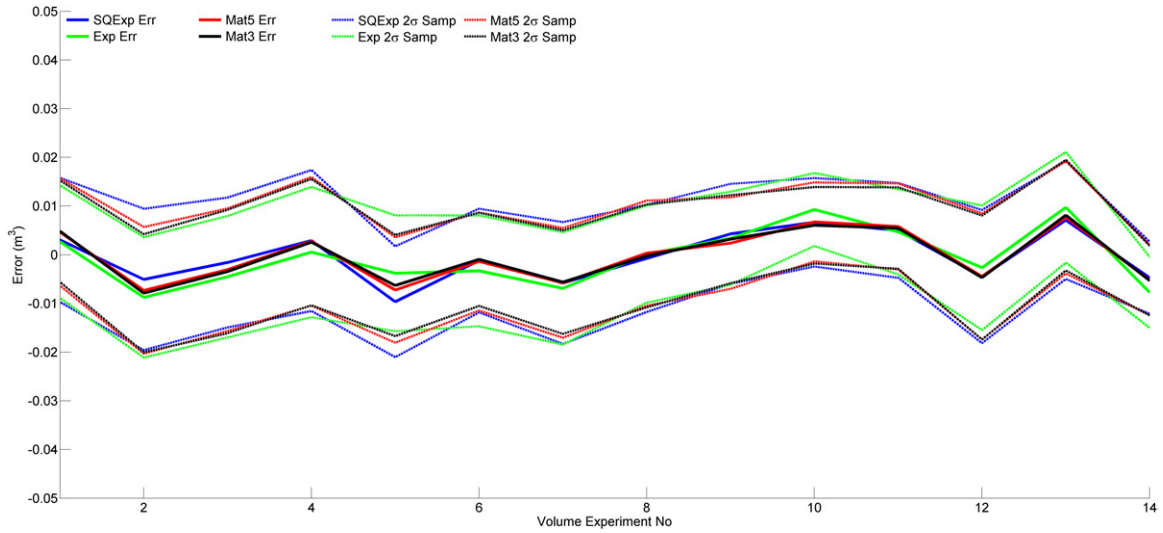

(b) Gaussian process method

Figure 4.39 – Mean volume error and 2σ distribution of mean volume error over the fifteen different volumes in the large scale experiment using **1152** samples.

4.8 Discussion

4.8.1 Accuracy

All of the methods are compared to a control method which uses Delaunay triangulation and triangular prisms using all available data from the sensor to estimate the

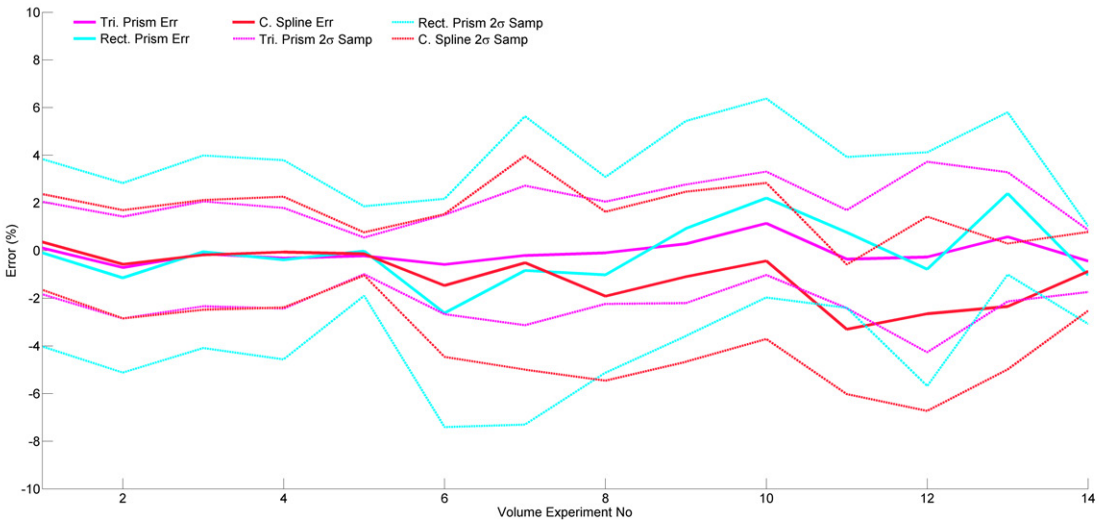

(a) State-of-the-art methods

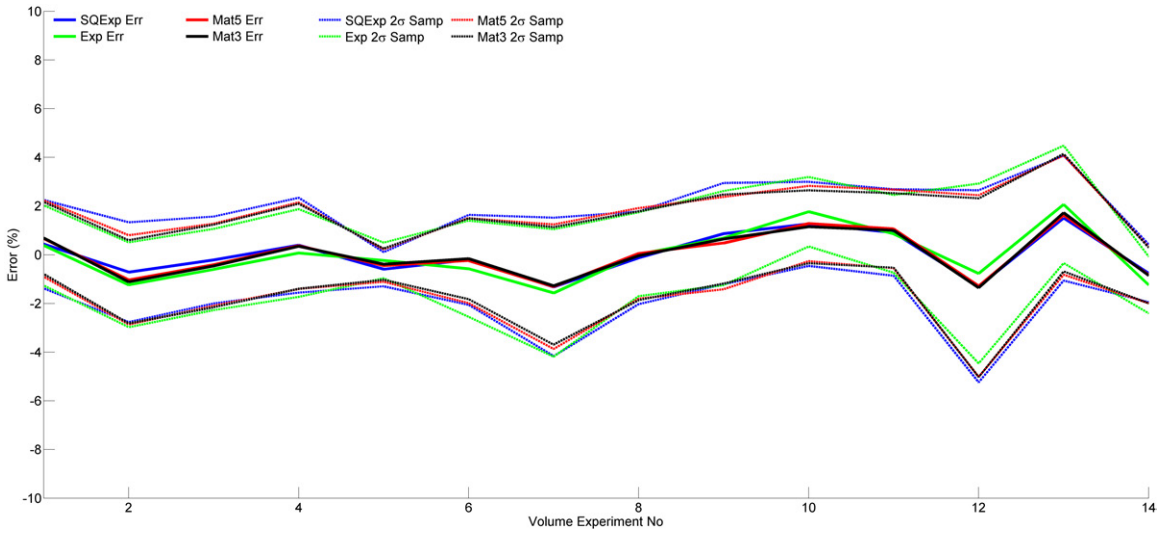

(b) Gaussian process method

Figure 4.40 – This figure shows a normalised error of the values in Figure 4.39 with respect to the true volume using **1152** samples.

volume. The volume calculated in the small scale experiment is the difference between the volume of the ground surface and the surface with an additional amount of material added as a stockpile. In the large scale experiment, the volume was calculated as the difference before and after each grade block excavator load.

In Tables 4.2 and 4.8 the results using 64 and 96 samples are summarised respectively. In these scenarios, the Gaussian process methods and the rectangular grid methods

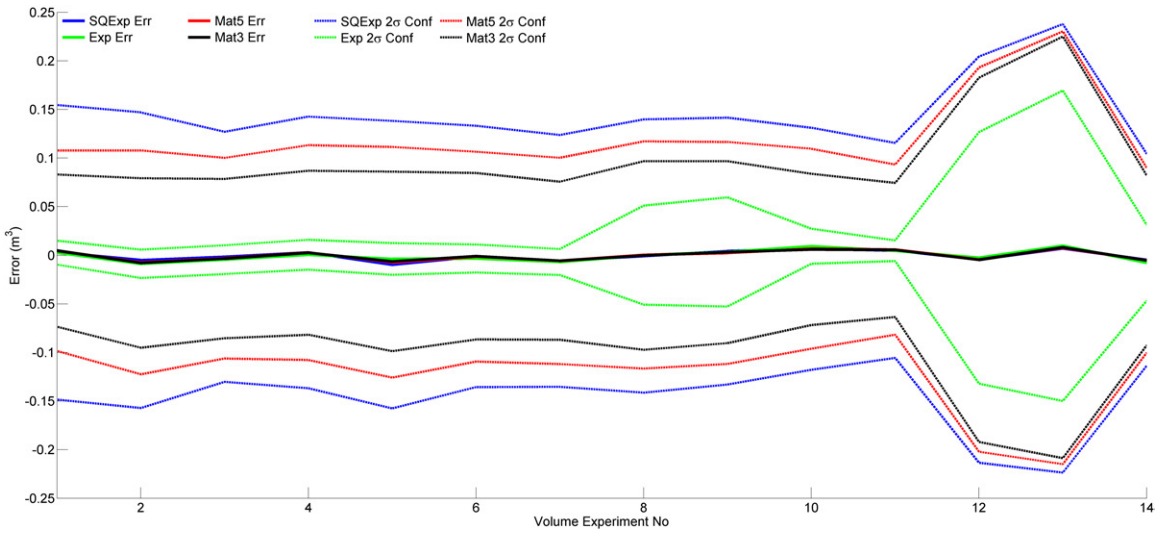

Figure 4.41 – Mean volume error of Gaussian process methods with mean 2σ uncertainty estimated of the volume estimate in the **1152** sample large scale experiment.

are the most accurate.

Tables 4.4, 4.6, 4.10 and 4.12 provide a summary of the results from the 256, 1024, 320 and 1156 sample scenarios respectively. In these scenarios, there is a trend for all of the volume estimation methods to become more accurate and converge to closer absolute levels of accuracy ($< 1\%$). This suggests that further increasing the amount of sample points will lead to only very minor differences between each method in terms of accuracy.

4.8.2 Precision

In both the small and large scale experiments the rectangular grid method is the least precise over all of the tested scenarios. The Gaussian process methods are more precise than any of the state-of-the-art methods. The triangular prism and cubic spline volume estimation methods are less precise compared to the Gaussian processes methods over all of the scenarios (these two methods are more precise however than the rectangular grid method). All of the methods become more precise as the number of samples increase.

One of the aims of developing the Gaussian process method as described in Section

4.2 was to have a method which would be able to deal with sparse data sets effectively as well as work over a variety of surface formations. In both the small and large scale experiments, the Gaussian process methods have the best performance, in terms of accuracy and precision, over all of the test scenarios.

4.8.3 Estimation of Uncertainty with the Gaussian Process Method

One of the requirements in the development of the Gaussian process method was to find a method which would be able to encapsulate the uncertainty in a volume estimate from a 2.5D surface scan.

The results from both experiments show how the choice of covariance function does have a significant impact on the uncertainty estimated.

In the small scale experiment, the uncertainty estimated by the squared exponential and Matern series of covariance functions perform better at lower levels of sparseness compared to the exponential covariance function. From the large scale experiments, the exponential covariance function was found to be considerably more accurate at encapsulating the uncertainty.

The estimated uncertainty over the test scenarios was on average 'conservative'. From Table 4.5, it was shown that given a high saturation of sample points of the surface, the choice of covariance function has a minimal impact. The estimated uncertainty in this scenario was also the closest to the true value.

One area in which this method could be improved in future work would be in the development of a covariance function which could better encapsulate the uncertainty over sparse data sets.

4.8.4 Computational Complexity

Given the previous results, the Gaussian process method appears to have a clear advantage over the other methods. The Gaussian process method does however have

one significant negative aspect when compared to the other estimation methods.

The computational requirements of the Gaussian process methods are substantially higher than the other state-of-the-art methods. The matrix inversion $[K(X,X)+\sigma_n^2 I]^{-1}$ has a computational cost of $O(N^3)$ [91]. As a reference, an iterative Delaunay triangulation implementation has a worst case cost of $O(N^2)$ [67]. Cubic spline construction is well known to be of complexity $O(N)$ with evaluation of the cubic spline at $O(log(N))$ [73].

On top of this evaluation cost, the process of learning when using the Gaussian process method increases the cost as well. This is important to consider when attempting to perform volume estimation in real-time. A common solution to the learning problem for real-time implementation is to take a data set representing on average the data to be evaluated in the field. The hyper-parameters are then learnt off-line using this data set and used as the parameters in the evaluation of the data as it arrives in real-time. This reduces the computational requirements. However, this solution will ultimately be less precise and accurate than learning the set of hyper-parameters online for each individual data set.

4.9 Summary

This chapter has provided a probabilistic method for estimating a 2.5D volume using Gaussian processes. The theory behind Gaussian process regression and learning was introduced as well as a description of several covariance functions which were experimentally compared.

The Gaussian process method developed was also compared to several state-of-the-art methods. This included Delaunay triangulation with triangular prisms, rectangular prisms with height averaging as well as cubic spline interpolation with Simpson's rule used for integration to determine volume. The comparison was performed over experiments of two separate scales. A small controlled experiment where a more definitive ground truth can be obtained. A larger more realistic mining scenario is

then used to test each of the methods. The ground truth was calculated using all of the raw data provided by the Riegl VZ-1000 survey laser and using Delaunay triangulation and triangular prisms to determine the volume. The experiments comprised of three different resolutions to compare how each method performs with varying sparseness of the sample data set.

The results show that the Gaussian process methods on average are more accurate and precise under both of the experiment conditions than the current state-of-the-art methods. The uncertainty estimated by the Gaussian process methods was, on average, of a conservative nature. The choice of covariance function was found to play a factor in the accuracy of the uncertainty estimation.

The representation of bulk material properties as probabilistic is vital in integrating this information into the estimation and tracking system developed in this thesis. The Gaussian process method with its intrinsic capability of estimating the uncertainty of the volume estimated provides a method which is capable of performing on a wide range of surface formations. The current state-of-the-art methods were unable to provide this functionality.

Future work in this area could include decreasing the computational requirements of the Gaussian process methods. This would allow for greater use in a real-time environment. The performance of this method could also be improved by the development of a covariance function which is better able to encapsulate the uncertainty over the 2.5D surface.

Chapter 5

Modelling Intensive Material Properties

5.1 Introduction

One of the main goals of the research work in this thesis (as stated in Section 2.3.4) is to "Provide a probabilistic inventory of all available stock". This goal involves keeping an estimate of material properties that are vital in mine operations. Chapter 3 discusses a method for estimating and tracking extensive material properties within an ASKF framework. This chapter describes a method for including intensive material properties. Some examples of intensive properties include chemical composition (e.g. Iron%, Silica%, Alumina%), fragmentation and bulk density.

It would be highly valuable to include intensive property states in an integrated tracking and estimation system. The ability to have a probabilistic estimate of ore grade in a haul truck, for example, would allow an autonomous control system to ensure the haul truck is always directed to the correct stockpile. The ability to have an estimate of the uncertainty of chemical properties in stockpiles would allow for more confidence in ensuring that blending stockpiles are within the correct tolerance levels for the product being produced. This information could be used in a mine

planning system to be able to plan more effectively which grade blocks to excavate in order to meet the correct grades on these stockpiles.

One of the other benefits is the ability to incorporate additional information about the chemical properties of the material and then be able to reconcile this in real-time to the point of excavation. This information could be used to update an underlying geological model. This would have significant benefits for a mine planning system seeking to find the optimal mine plan given the available information. One of the drawbacks of reconciliation as it is done at the moment is the considerable delay which occurs between excavation and reconciliation data becoming available.

As discussed in Section 2.3.3, there have been considerable advances in remote sensing (e.g. hyper-spectral cameras) which makes it more feasible to observe intensive material properties at different stages in the mining process. As with extensive material properties, the ability to consistently fuse information together from a variety of information sources of varying levels of uncertainty is important. This chapter provides a method for probabilistic estimation and fusion of intensive material properties along a process chain using the lumped mass representation. A method for reconciling this information back to the point of excavation is also presented.

5.2 Problem Formulation

5.2.1 Representation

One of the requirements when using a ASKF approach to tracking and estimation is the assumption that all states can be adequately represented by a Gaussian distribution. The performance of the filter, in regard to estimation accuracy and statistical consistency, will be a function of the degree in which the system models, observations and state properties can be approximated as Gaussian distributions.

This assumption becomes especially problematic when combining lumped masses with intensive material properties. Take for example the hypothetical scenario in Figure 5.1. In this scenario each lumped mass has two states, mass and Fe%.

Figure 5.1 – When combining the intensive properties from the two lumped masses pictured, the resultant distribution is non-Gaussian.

When the material in the excavator is combined with the material in the haul truck, a uniform blending of the two lumps is assumed (where each particle of material within both lumps is assumed to be of equal size and the amount of particles is proportional to the mass). When randomly selecting a particle within this combined blended lumped mass, the probability of selecting a particle belonging from either of the initial two lumped masses prior to blending will be proportional to the mass of each of the initial lumps. Assuming that the estimate of an intensive property (e.g. Iron content Fe%) was represented as a Gaussian for each of the initial lumped masses, the probability of selecting a particle with a particular intensive property will be weighted by the chance of drawing that particle from each of the initial lumps and the corresponding representation of the intensive property in the initial lumped mass. Further reading on the estimation of blended bulk material, particular for stockpiles

in mining, can be found in prior work in this area [104].

When combining the lumped mass in the excavator bucket with the lumped mass in the haul truck from Figure 5.1, the underlying Bayesian distribution (Figure 5.2) of the Fe% (Iron) is poorly approximated by a Gaussian distribution, this can be noted by the lack of common probability density.

The model shown in Figure 5.2 is a Gaussian Mixture Model [103] of the form:

$$p(x) = \sum_{m=1}^{M} w_m \, p\left(x \mid N\left(\mu_m; \sigma_m\right)\right), \; where \; \sum w_i = 1 \tag{5.1}$$

where $p\left(x \mid N\left(\mu_m; \sigma_m\right)\right)$ are the Gaussian distributions of the intensive properties of the two lumped masses prior to combining. The weighting of each respective gaussian (w_m) is calculated using the mean mass of each lump prior to combining as a fraction of the total combined mass of both lumped masses. The parameters used are shown in Figure 5.1.

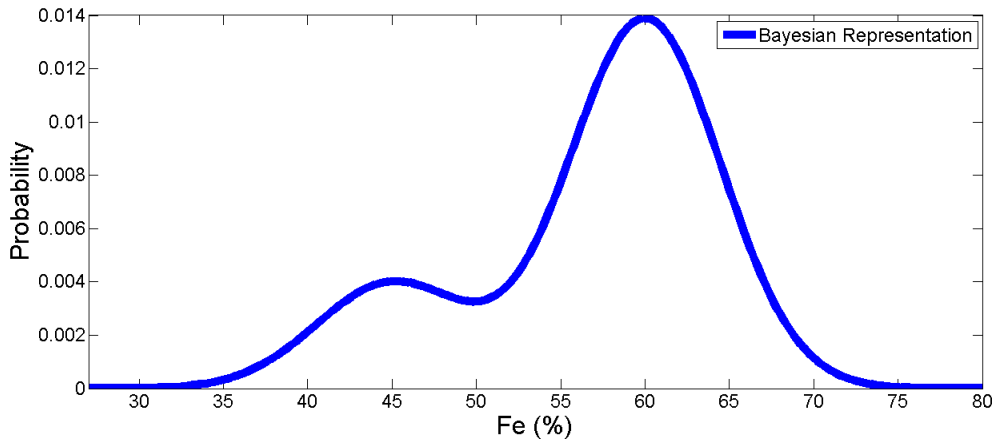

Figure 5.2 – The resultant distribution when combining the intensive lumped mass properties in the scenario shown in Figure 5.1.

As was discussed in the 'Introduction to Open Pit Mining' (Section 2.2), and specifically the section on 'Mine Visualisation' (Section 2.2.3), the scenario in Figure 5.1 is not likely to be common place for each grade block. Each grade block is typically grouped together with material of consistent chemical composition. However,

in circumstances where this not the case (such as blended grade blocks, see Section 2.2.3) the accuracy and consistency will be negatively impacted through the use of a Gaussian representation. As an illustration of a more ideal scenario for a Gaussian representation, take the same scenario as shown in Figure 5.1. However, instead of the excavator lumped mass having 45% Fe it has 62% Fe. When combining the two lumped masses the underlying probabilistic representation can be seen in Figure 5.3. From this distribution, it can be seen that a Gaussian approximation of this combined probabilistic distribution of the two lumped masses is more reasonable.

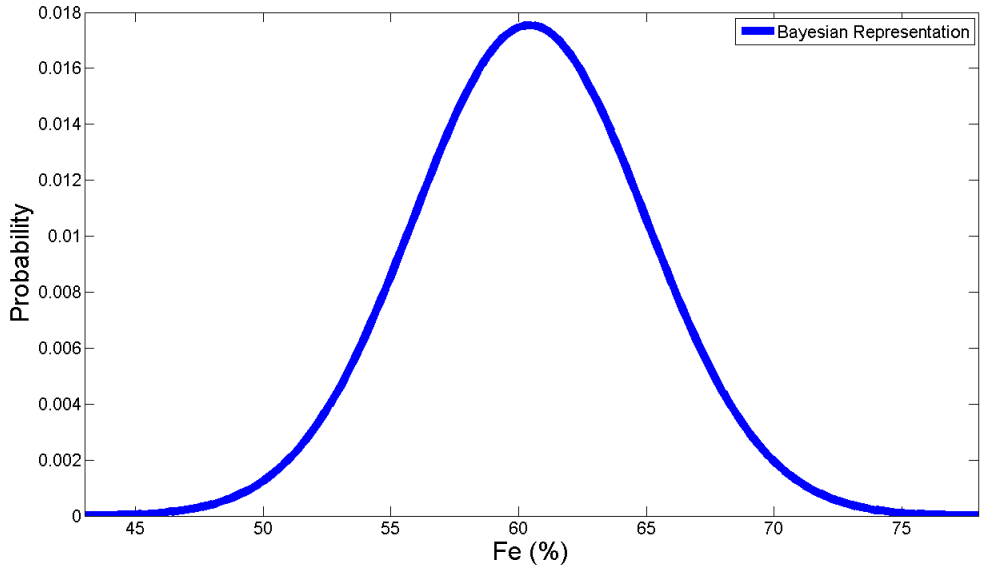

Figure 5.3 – This is the resultant distribution when the values of Fe in the excavator lumped mass in Figure 5.1 is changed to 62%.

Using a Gaussian representation is not the ideal choice, especially when considering the excavation of blended grade blocks as well as combining lumped masses into blended stockpiles where chemical compositions are likely to vary considerably. The choice to use this representation in this thesis is one of pragmatism. The development of a more rich representation is a complex process due to the inherent dependencies between extensive-intensive properties as well as between intensive properties (this is discussed further in Section 5.2.2). The Gaussian representation allows for a simplistic method of including intensive properties in the estimation process which maintains

a consistent approach to representation as the extensive properties. Improving the modelling of intensive properties to account for the physical constraints of the material properties (using a log-normal distribution) is discussed further in Section 6.3.1 as future work to extend upon the representation discussed in this Chapter.

5.2.2 The Issue of State Dependencies

One of the main research problems involved in including intensive material properties is accounting for the dependence on the extensive material properties when defining a lumped mass with an intensive material property.

This dependency can be seen in the prior discussion on the representation of the intensive material properties. In the scenario shown in Figure 5.1 the Fe % probability is weighted by the amount of material present originally in each lumped mass. The resultant probability distribution (Figure 5.2) when the two lumped masses are combined is based on the assumption that when the two lumped masses are combined the material is perfectly mixed.

One open-ended problem is how to consistently model the intensive properties taking into account the state dependency with the extensive properties. The following section discusses several different ways of approaching this problem within a Gaussian representation framework. It also discusses an additional problem of dependencies between intensive states.

A Percentage Based Approach

One approach is to model the intensive properties as a percentage of the estimated material present. This is what is shown in Figure 5.1. One of the difficulties in this approach is how to incorporate this into the constrained ASKF approach. The extensive properties can be modeled as linear combinations of each other. This is not possible when using a percentage approach with intensive properties as they are by their nature not linearly additive.

One possible approach is to assume that extensive and intensive properties are independent of each other. This approach would make it possible to remove intensive properties from the ASKF containing the extensive properties and run as a parallel filter if desired.

The assumption that extensive and intensive properties are independent however, has several disadvantages. The first is that, given there is no spatial, when fusing new information at a particular location there is no autonomous method using the standard LKF equations (Section 3.3) to update the spatially related states (as defined by the covariances between extensive properties) with this new information.

A Combined Extensive-Intensive Approach

A different approach is to account for the state dependency between the extensive and intensive properties in the ASKF by using a different representation of both the extensive and intensive properties. Instead of representing the intensive properties as a percentage of the extensive properties the intensive and extensive properties are combined into a single value. As an example, take again the scenario shown in Figure 5.1. Instead of representing the material in the haul truck lumped mass as two states 'mass' and 'Fe', these two values can be combined into a single value. Therefore the state is estimated as $84t$ of Fe. This is a combination representing the dependency between extensive and intensive properties (140t and 60% Fe). The uncertainty would then be estimated as a combination based on these two properties 'mass' and 'Fe'.

This method has several advantages over the percentage based approach. It enables many of the benefits of the extensive approach such as linearly additive states and a consistent method for maintaining spatial relationships. Thus when fusing additional information, this method would allow for the information to autonomously flow onto correlated lumped masses.

There are however several prominent research issues which must be overcome before this approach can be made viable.

One issue is that observational sensors in the mining domain do not observe in this combined extensive-intensive state. Sensors estimate either the extensive property (e.g. mass, volume) or the intensive property (e.g. chemical composition %) over a region. These observations can not be directly applied on their own to this new combined extensive-intensive state in an ASKF framework. The estimated mean and uncertainty approximated of the combined extensive-intensive state is an amalgamation of both the intensive and extensive properties. To apply one of these observations would require a method for incorporating the mean and uncertainty of either the intensive and extensive property (depending on which form the original observation takes) to derive the combined state.

The Problem of Dependencies between Intensive States

One of the other major issues when dealing with intensive properties is the dependencies between intensive states. One prime example of this is the dependencies between chemical properties.

Using an iron ore example, the chemical properties Fe, SiO_2. AlO_3 and P will be have strong dependencies driven by complex geological factors and processes. It is a non-trivial task to develop a method for modelling the relationship between these properties within an ASKF framework.

Another problem is the natural constraints imposed by specific intensive properties.

In the percentage based approach described a constraint would need to be enforced to ensure that intensive material properties of the same class sum to 100%. In this case, an example of a class of intensive properties would be chemical composition.

In the combined extensive-intensive approach a similar problem arises. Using the example of chemical composition class again, the total masses of each combined property should sum to the actual total mass at that particular location.

The development of this constraint is not within the scope of this thesis.

Discussion

The two discussed approaches using a Gaussian representation both have positive and negative qualities. The percentage based approach can be used alongside the extensive modelling method described in Chapter 3 without altering the performance or characteristics of the extensive modelling system. Therefore the benefits provided by the extensive property system described in Chapter 3 are maintained.

The combined extensive-intensive approach would take into account the dependent nature of extensive and material properties. This is beneficial in that it removes the need for approximations when combining lumped mass intensive properties. The main difficulty in this approach is that there are much more complex interactions between the state variables which need to be modeled than the percentage based approach. Modelling these interactions within a ASKF framework would be a non-trivial research problem.

This thesis uses the percentage based approach as the method for representing the intensive properties of the material at each location in the ASKF. The combined extensive-intensive solution has many attractive qualities, however solving the research problems involved in implementing this approach is beyond the scope of this thesis. Furthermore, for simplicity, the intensive properties are assumed to be independent for the work within this thesis.

5.2.3 Approximating the Sum of Gaussian Distributions

The approach to estimating intensive properties in this thesis is one by which the intensive property will be represented by a single Gaussian. The Gaussian representation uses a percentage based approach in which it is assumed the intensive state to be estimated is independent of other intensive property states as well as independent of extensive properties.

As described in the previous sections, this approach has several drawbacks. Notably, the inability to correctly model the underlying chemical distribution when combining

lumped masses together with different chemical compositions. The approximation will be less ideal the more the chemical compositions differ. This is slightly negated by the fact that in a large amount of cases where lumped masses are combined together they will be of similar chemical composition.

Given that this is the approach taken, a method for approximating the sum of two Gaussian distributions as a single Gaussian distribution is needed. This section will numerically compare several methods for achieving this with respect to optimising for the least amount of information loss.

Covariance Union

There are several methods for approximating a sum of Gaussians into a single Gaussian estimate. One approach is to use the 'Covariance Union' method [18].

This is a method which is commonly used in Multiple Hypothesis Tracking (MHT). In MHT, it is common problem that when the number of hypothesis keep increasing. This results in the calculations becoming computationally intractable. The covariance union is a technique aimed at consolidating several hypothesis into a single consistent hypothesis. This reduces the computational complexity making the estimation process computationally tractable.

Figure 5.4 gives an example of a covariance union approximation. The graph on the left shows a set of possible hypothesis which are to be approximated by a single Gaussian distribution. The graph on the right shows a single approximation produced by the covariance union method. As can be seen from Figure 5.4 the distribution estimated by the covariance union ensures that all the uncertainty in all original hypothesis is accounted for.

The problem with this approach, when applied to the problem of combining lumped mass intrinsic properties, is that it does take into account the state dependency between the extensive and intensive properties. Figure 5.5 shows an example of the distribution approximated using the data shown in Figure 5.1. The approximated distribution is not a good representation of the underlying true distribution.

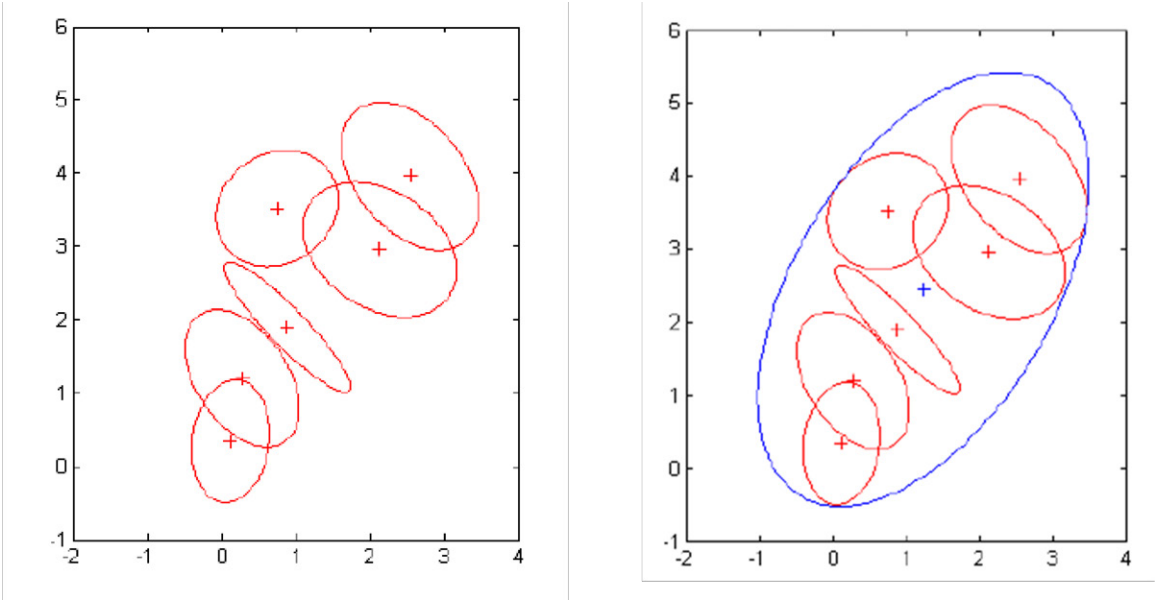

Figure 5.4 – An example of the covariance union method being applied over a set of hypothesis. This method ensures that the distribution estimated encapsulates all the uncertainty of the input hypothesis.

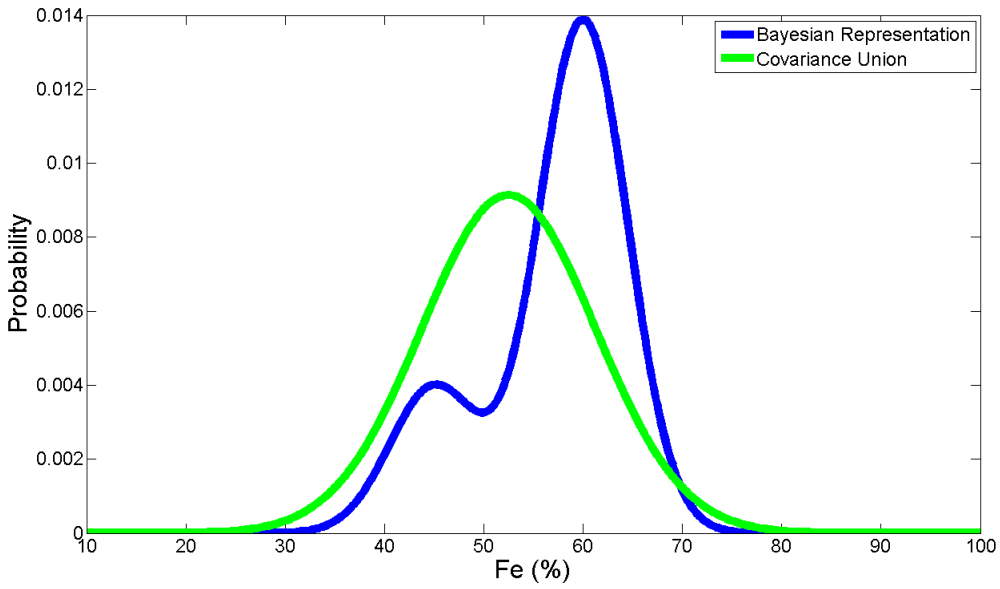

Figure 5.5 – The covariance union method being applied to the data from the scenario shown in Figure 5.1. The non-weighted mean intensive property estimate is located in the middle of the two lumped mass intensive mean values. This is problematic as it does not take into account the mass of each lumped mass.

One way of accounting for this using the covariance union method is to weight the mean value approximation based on the mass. The result from this can be seen in Figure 5.6. This method makes the approximation more conservative (larger spread). It does however appear to encapsulate the underlying distribution more adequately in this scenario.

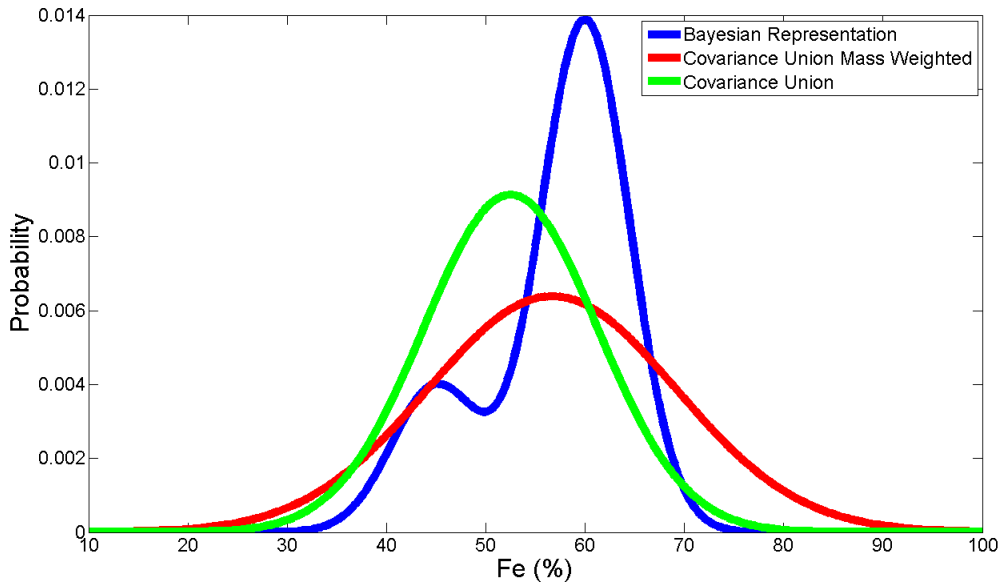

Figure 5.6 – The covariance union method being applied the data from the scenario shown in Figure 5.1, the mean estimated mass includes a weighting method for the mean.

Figure 5.4 shows the scenario in which the covariance union method is ideal for. In a bulk material scenario, where intensive material properties are being combined only two distributions will be involved. In MHT ensuring that the final approximation contains all possible hypothesis from the original inputs is important, this makes a conservative approach attractive. This level of conservatism could potentially be reduced in a bulk material tracking scenario.

The Mathematical Averaging (MA) Method

Another method of approximating the sum of Gaussian distributions is to take a weighted average of the two Gaussian distributions. The mean of the joint distribution

x_J can be calculated as the following:

$$x_J = p_1 x_1 + p_2 x_2 \tag{5.2}$$

where p_1 and p_2 represent the weights applied to each of the means of the intensive properties x_1 and x_2.

p_1 and p_2 can be given by

$$p_1 = \frac{M_1}{M_1 + M_2} \tag{5.3}$$

and

$$p_2 = \frac{M_2}{M_1 + M_2} \tag{5.4}$$

where M_1 and M_2 are the mass values of the first and second lumped masses which are being combined together.

The variance on the averaged distribution can be calculated as the second moment subtracted by the square of the first moment. The first moment is given by Equation 5.2, the second moment is given by the following:

$$x_J^{(2)} = p_1(x_1^2 + \sigma_1^2) + p_2(x_2^2 + \sigma_2^2) \tag{5.5}$$

where σ_1^2 and σ_2^2 represent the variances on the intensive properties x_1 and x_2, respectively.

The variance of the averaged distribution (σ_J^2) therefore can be calculated as

$$\sigma_J^2 = x_J^{(2)} - x_J^2 = p_1(x_1^2 + \sigma_1^2) + p_2(x_2^2 + \sigma_2^2) - (p_1 x_1 + p_2 x_2)^2 \tag{5.6}$$

A summary of the results is presented in in Equations 5.7 and 5.8. These equations

include substituting the values for p_1 and p_2 and factorisation in the mean (x_J) and variance (σ_J^2) equations.

$$x_J = \left(\frac{M_1}{M_1 + M_2} x_1\right) + \left(\frac{M_2}{M_1 + M_2} x_2\right) \tag{5.7}$$

$$\sigma_J^2 = \frac{M_1\sigma_1^2 + M_2\sigma_2^2}{M_1 + M_2} + \left(\frac{x_1 - x_2}{M_1 + M_2}\right)^2 M_1 M_2 \tag{5.8}$$

Representing Equation 5.8 as shown aids in understanding how the variance is calculated. The first term represents a weighted combination of the two previous lumped mass variances on the intensive properties. The second term represents the additional variance required to compensate for the difference in mean values between the two intensive lumped mass properties.

The result of applying this method to the scenario shown in Figure 5.1 can be seen in Figure 5.7. The covariance union methods are included as a comparison.

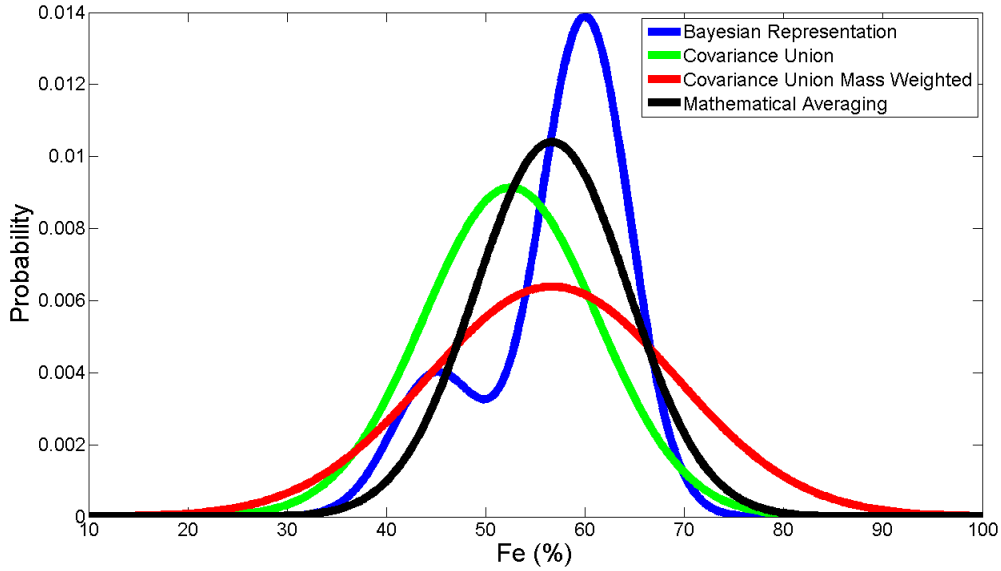

Figure 5.7 – An example showing the mathematical averaging method along with the covariance unions methods to approximate the combined intensive property from the scenario shown in Figure 5.1.

From Figure 5.7 it can be seen that this method provides a less conservative estimate than the covariance union methods.

5.3 Comparison between Approximation Methods

To compare the different methods more formally there are several different methods and metrics which can be used. The aim is to compare each of the approximation methods against the true distribution to see which method best approximates this distribution. It is difficult to compare the performance of each of the approximation methods using graphical methods (Q-Q plots, Histograms, Gaussian plots etc) over a wide range of scenarios given the vast range of values the different input values can take. This problem can be addressed by using a numerical metric as the method for comparison.

One way of numerically evaluating how good the approximation is, is to compare the Cumulative Density Function (CDF) of the true and approximated distributions. Ideally, the two CDF curves should be as close as possible. One metric for summarising the estimation performance is to calculate the max difference in the CDFs between the true and approximated distributions. A smaller number in this metric would signify an approximation which is closer to the true distribution. Figure 5.8 provides a graphical example of how this metric is calculated.

By using this metric as indicative of approximation performance, each of the approximations can be tested over a wide range of scenarios.

5.3.1 The Example Scenario

One of the recurring examples in this chapter is the scenario in Figure 5.1. Figure 5.9 shows the CDF of each of the different approximation methods as well as the true distribution. The method for comparing distributions is shown in Figure 5.8. The results of applying this to the CDFs shown in Figure 5.9 can be seen in Table 5.1.

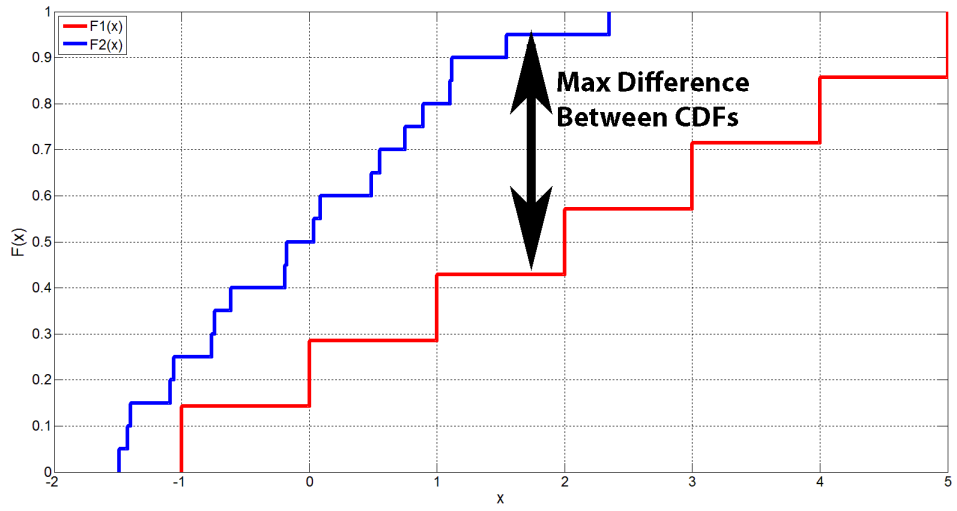

Figure 5.8 – A visual representation of the CDF max error metric.

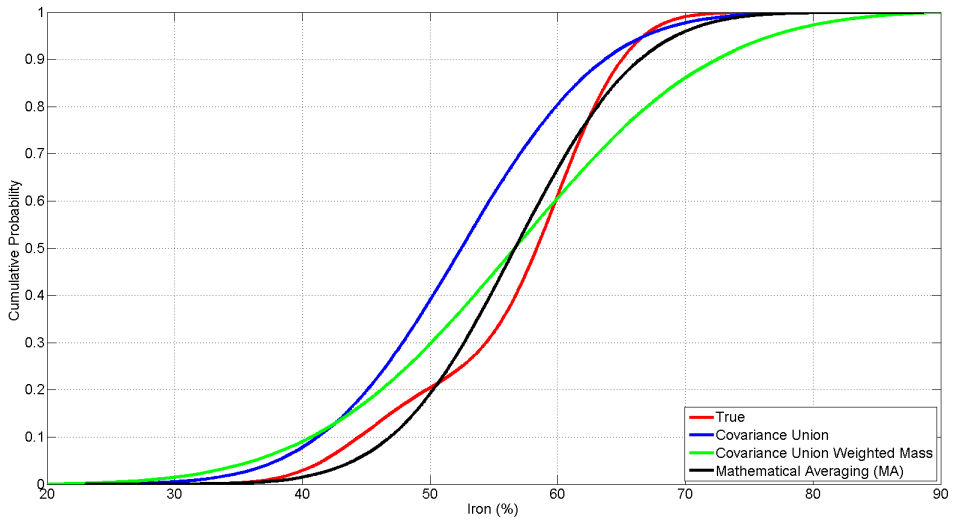

Figure 5.9 – A comparison of CDFs of the different approximation methods using the data from the example scenario shown in Figure 5.1. It is evident from this graph that the MA method (black line) has the smallest CDF error (the true distribution is the red line) compared to the covariance union methods.

As can be seen in Table 5.1 the MA method provides the smallest max difference in CDF compared to the true CDF. The 'Covariance Union' method weighted by mass, produces slightly worse results. The standard covariance union method provides the least accurate approximation using this metric.

Approximation Method	Max CDF Error
Covariance Union	29.18 %
Covariance Union Mass Weighted	15.74 %
Mathematical Averaging (MA)	10.16 %

Table 5.1 – Max CDF difference between approximation methods and the true distribution using the properties from the example scenario shown in Figure 5.1

Figure 5.10 shows the CDF values when the scenario is changed to have closer Iron % values in each of the lumped masses. This is using the same values as shown to generate the distribution in Figure 5.3. This Figure shows that the MA and weighted covariance union method are very close at approximating the true distribution in this scenario.

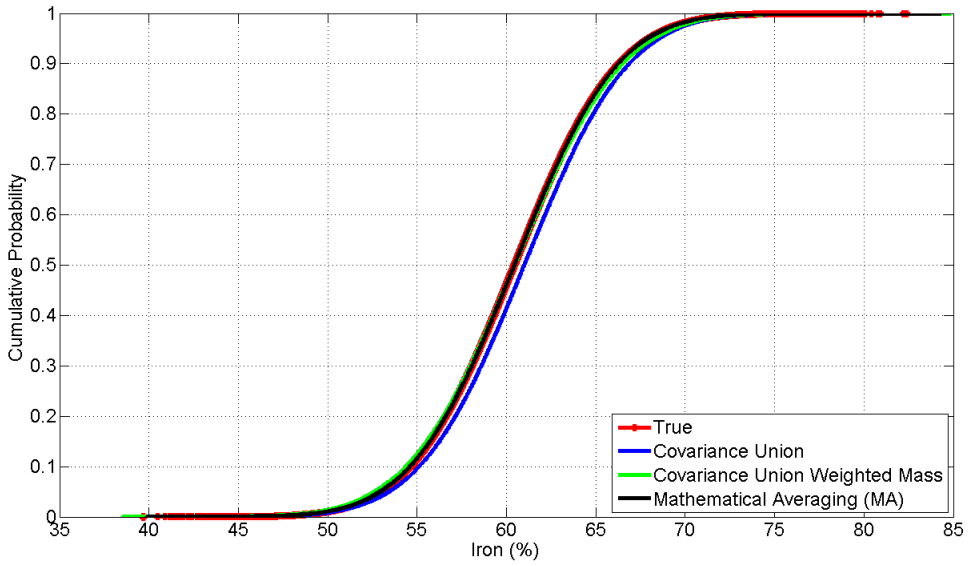

Figure 5.10 – A comparison of CDFs of the different approximation methods using the data from the example scenario shown in Figure 5.3. In this instance, there is only small visual differences between all of the methods.

Table 5.2 gives perspective on the quality of probability density approximation. When the mean values of the intensive properties being combined are close together, the standard covariance union method provides an estimate which is least representative according to the metric used.

Approximation Method	Max CDF Error
Covariance Union	5.04 %
Covariance Union Mass Weighted	1.02 %
Mathematical Averaging (MA)	0.15 %

Table 5.2 – Max CDF difference between approximation methods and the true distribution using the properties from the example scenario shown in Figure 5.1

5.3.2 A Wide Range of Scenarios

It is difficult to ascertain which method is overall the better approximation method based on one or two scenarios alone. The three approximation methods were tested over a set of scenarios which could possibly occur in an open pit mining scenario. The set of scenarios tested is summarised in Table 5.3. Overall, this includes testing 57344 different combinations of input properties.

Property	Range	Interval
Excavator Bucket Mean Iron	10 % - 80 %	10 %
Haul Truck Mean Iron	10% - 80 %	10 %
Excavator Bucket Iron Variance	10 % - 40 %	10 %
Haul Truck Iron Variance	10 % - 40 %	10 %
Excavator Bucket Mass	30 t - 60 t	10 t
Haul Truck Mass	30 t - 300 t	20 t

Table 5.3 – A summary of the scenarios in which each of the approximation methods was tested using the max CDF different statistic

Figure 5.11 displays histograms of the 'Max CDF error' over the range of scenarios for each of the approximation methods. It is evident from these histograms that the MA method, on average, has the smallest error. The results are summarised in Table 5.4, which shows the average accuracy of each approach using the max CDF error metric.

5.3.3 Discussion

Choosing which approximation method to use must take into consideration the trade offs of using that particular method. The standard covariance union method is an

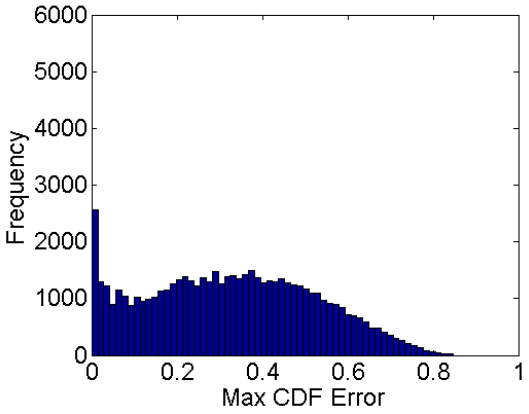

(a) Covariance union histogram of max CDF error

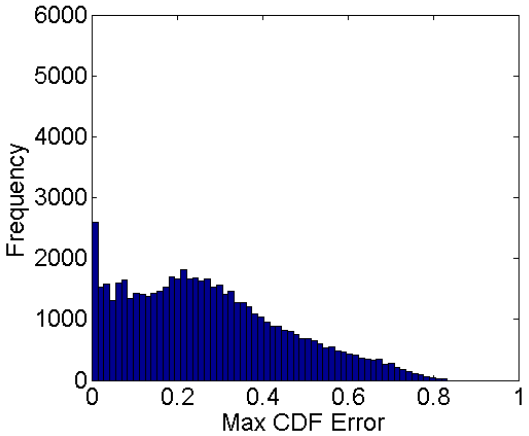

(b) Weighted mass covariance union histogram of max CDF error

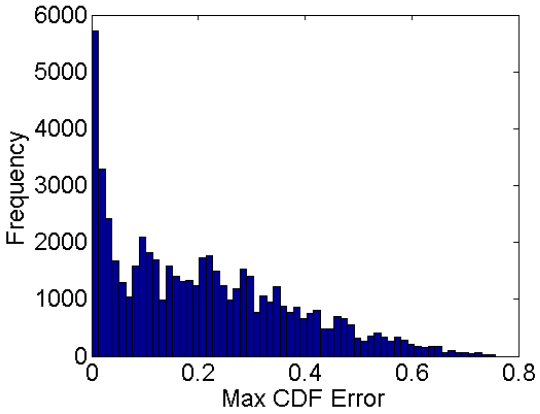

(c) Mathematical averaging histogram of max CDF error

Figure 5.11 – A comparison in the max CDF error between the different approximation methods over a wide range of scenarios, the mathematical averaging method provides the has on average the smallest residual error.

Approximation Method	Mean Max CDF Error
Covariance Union	32.75 %
Covariance Union Mass Weighted	27.29 %
Mathematical Averaging (MA)	20.91 %

Table 5.4 – The mean 'Max CDF Error' over the wide range of scenarios described in Table 5.3 using the different approximation methods

exception, as shown it is clearly a poor choice, when measured by max CDF error, compared to the other two options. The MA method, is superior at approximating the probability density comparatively to the mass weighted covariance union method over the test scenarios. The weighted covariance union method, by its nature, is a conservative approach which can be beneficial in ensuring that the solution accounts for the worst case scenarios more effectively.

The true distribution used for comparison is derived by assuming that the mass of each lumped mass is the most likely value. In simulation, this can be discounted by assuming the mass is a known quantity, therefore has no corresponding uncertainty. This will unlikely be the case however in an open pit mine. One improvement which could be made to the approximation process would be to develop a method for including the variance on the mass of each combined lumped mass. This is is a similar problem to that discussed between the percentage based approach and a combined intensive-extensive approach.

The method used in the experiments to test the inclusion of intensive properties in the ASKF is the MA approach. The uncertainty estimated by the MA method provides is closest to the true distribution. This should increase the chance that the estimate of intensive properties is statistically consistent in the ASKF framework. This hypothesis is tested in the experiments in this chapter.

5.4 Including Percentage Based Intensive Properties in the Constrained ASKF

Including intensive properties is a relatively straightforward process given that each intensive property is considered independent of all other states in the constrained ASKF. When a new lumped mass is initialised into the system the process for initialising the intensive property is the same as that of the extensive property with the exception that no spatial correlation is made to the prior lumped mass from which the new lumped mass was formed.

The method for combining lumped masses however does deviate from the extensive property method. Each time two lumped masses are combined, Equations 5.7 and 5.8 are used to derive an approximation of both the mean and variance of the combined lumped masses intensive properties. These values are then set in the state vector and covariance matrix for the lumped mass which remains. The prior values are overwritten.

The intensive lumped mass properties can be removed from the constrained ASKF when necessary in the same way as extensive properties (see Section 3.5.3).

5.5 Experiment

5.5.1 Method

Creating an experiment to test the modelling of intensive properties creates several additional problems than experiments with extensive properties only. In general, extensive sensors (e.g. scales, measuring cylinders) are cheaper then intensive sensors (e.g. hyper-spectral cameras). Managing the material in the experiment is also difficult, given that when material is combined and mixed together it is difficult to obtain the ground truth of the intensive properties as a percentage present at that particular location. Once material is mixed, especially on a large scale, it is difficult to

return the material to its original state. This makes it difficult to repeat experiments on a large scale.

Several of these problems can be overcome by using a small scale experiment. In this thesis, the intensive properties are simulated by using two sets of coloured stones (green and blue). These coloured stones can be imagined as a proxy for chemical properties (e.g. Fe % and Si %). The stones are the same dimension size for height. The diameter varies slightly from one stone to another. The ground truth is measured by comparing the ratio of mass between green stone and blue stones. Given the small scale of the experiment, it is easy to filter the rocks by colour. The colours of the stones are observed during the experiment using a web cam (Logitech C-120, a basic low-end web camera). The ratio of green to blue as distinguished by the camera is the observed estimate of the intensive properties.

The process chain which the intensive property experiment follows is the same as which occurs in the prior experiments for the extensive properties (see Chapter 3). The coloured stones are moved from the grade block by an excavator, the material is then moved from the excavator to a haul truck. Once the haul truck receives three loads of material the truck is unloaded to a final stockpile. The observations of the intensive properties are included at the excavator and haul truck stages. A set of scales (the same as used in the small scale experiment in Chapter 3) is used as an observation at the excavator and haul truck stages to observe the extensive property mass. A small amount of white gaussian noise is added to this observation.

In this experiment, the material is controlled such that no losses occur. The lumped masses in the system are limited to the following states:

- Grade Block
- Excavator Bucket
- Haul Truck
- Stockpile

Each lumped mass tracks the following extensive and intensive properties:

- Mass
- Green %
- Blue %

This experiment aims to show that a consistent estimate of intensive material properties can be achieved using the percentage based approach in the ASKF framework while using the MA to combine intensive properties together.

5.5.2 Observing Intensive Properties in the Small Scale Experiment

In this experiment there is assumed to be two separate types of ore present in the current grade block. These are represented by different coloured stones. The web camera takes pictures of the stones at the different lumped mass locations. Figure 5.12 shows an example of the output from the web cam. This simple system of colour modelling is aimed at being broadly representative of measuring chemical properties using hyper-spectral camera.

Figure 5.12a shows the output of the web cam on the excavator bucket, this includes colour saturation. This is done to make differentiation between stones easier. A black mat is used to help remove background noise. A series of image processing techniques are used in order to improve the classification of blue and green stones. An explanation of the image processing which occurs is described below:

Camera Colour Saturation: This filtering is done inside the Logitech camera drivers. Effectively what is done is that pixels with dominant red, green or blue colour attributes are further emphasised by enhancing the dominant colour value. Pixels with no dominant colour attributes tend towards a 0 (black) value. In the intensive experiment this is used to further distinguish between the two different

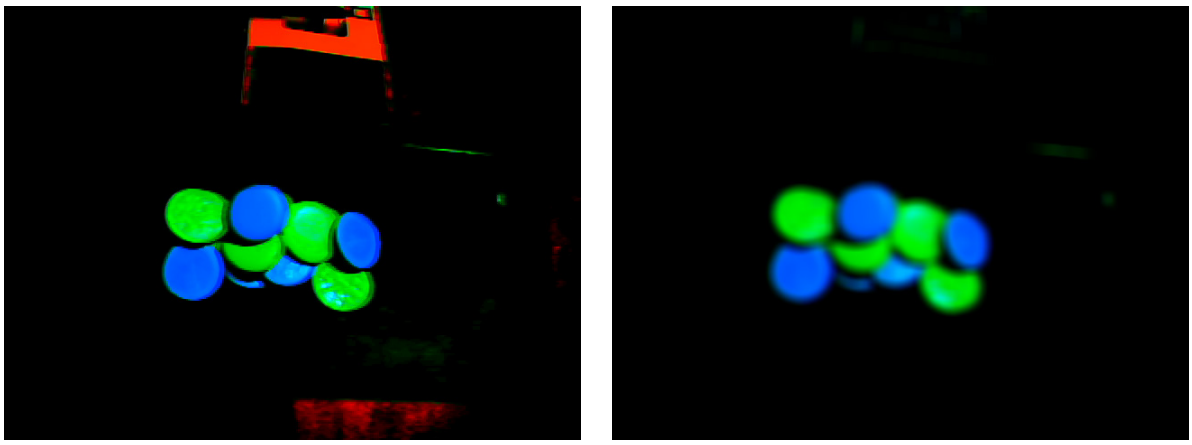

(a) Web cam image with colour saturation. **(b)** Web cam image after applying image filters.

Figure 5.12 – The base image has multiple image filtering techniques applied in order to ensure an accurate and consistent estimate of the coloured stones.

types of stones.

Median Filter: A median filter primarily removes outlying points in a localised neighbourhood. In a MxN neighbourhood, the value for each pixel located in that area is replaced by the median value of the pixels located within the MxN neighbourhood. This is done to remove some random white noise present in the image.

Gaussian Blur: A Gaussian blur is done to remove some of the induced colour distortion from lighting in the experiment. This enables a more accurate colour threshold to be used in order to determine whether a stone is green or blue.

Colour Identification: This is done by a simple pixel check of each pixel in the captured image. A comparison is made in the blue and green values of each pixel, the higher value is assumed to be the actual colour of the pixel and is stored. This process is aided by thresholding the background noise initially, as well as using the camera colour saturation techniques.

The result of applying these image processing techniques can be seen in Figure 5.12b.

Figure 5.13 shows the result of the observation system using a simple example of one blue stone and one green stone. The image on the far right is the result after all filtering and identification has been completed and displays its estimate of what are blue stones and what are green from the captured image.

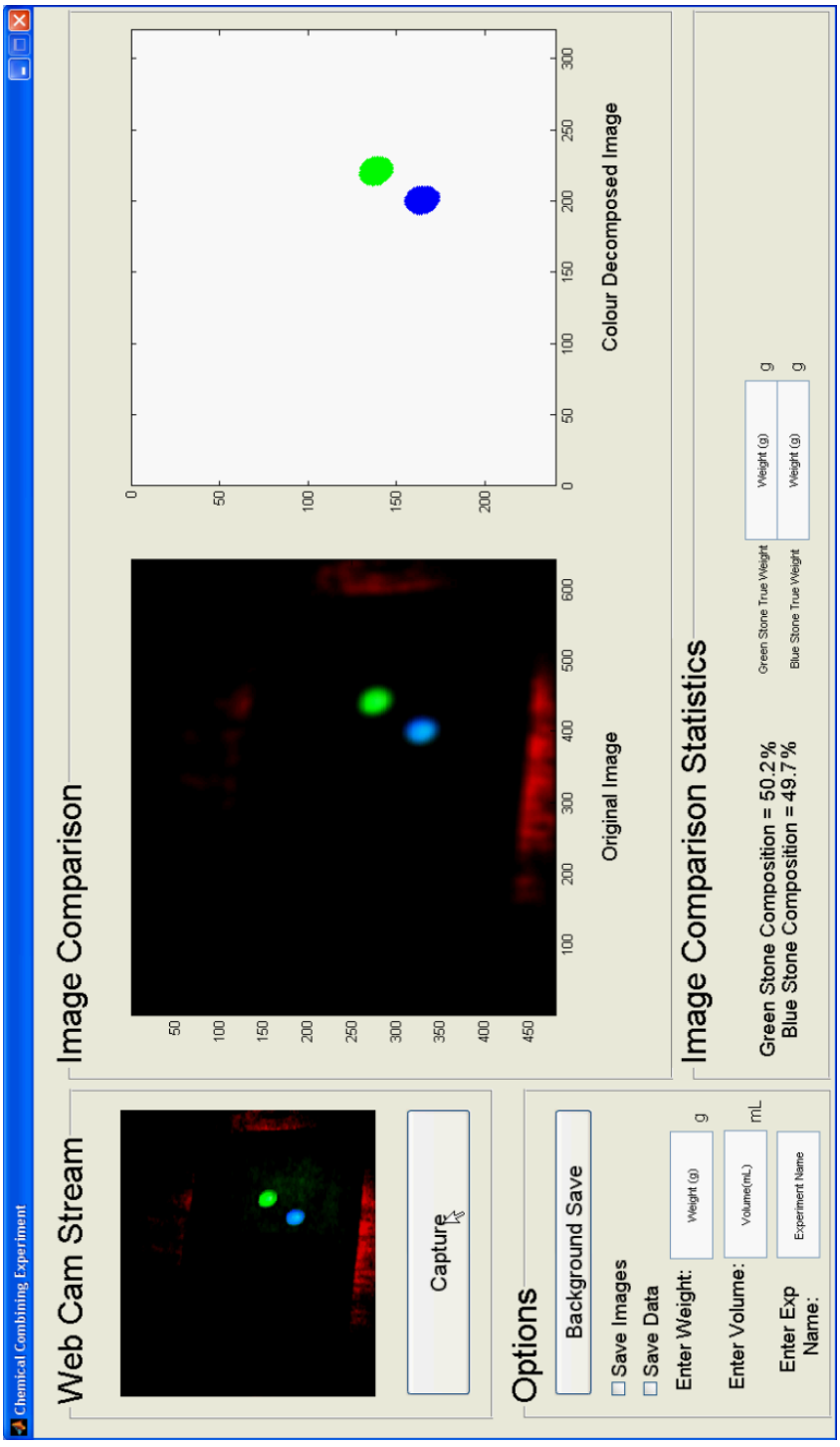

Figure 5.13 – The interface used to observe the ratio of coloured stones in the intensive experiment. The image titled 'original image' is a view of the coloured stones once the image processing techniques have been applied. The image title 'Colour Decomposed Image' contains the results of classifying the stones as either blue or green.

The ratio of blue to green is calculated and is displayed at the bottom of Figure 5.13. In this case the results displayed are 50.2% Blue to 49.7% Green (the results are rounded down for display purposes, the stored results combine to 100%).

During the experiment the stones were allowed to overlap each other. This was intended to represent a more realistic sensor system likely to be available for an autonomous mine such as face scanning using hyper-spectral cameras where only the surface of the lumped mass is likely to be available to ascertain the chemical properties. An example of this overlapping can be seen in figure 5.12.

5.5.3 Results

Figures 5.14 and 5.15 show the residual and 2σ confidence boundaries of the mass at the excavator and haul truck lumped mass locations. This result is included for completeness, validation of extensive properties is discussed in greater depth in Chapter 3.

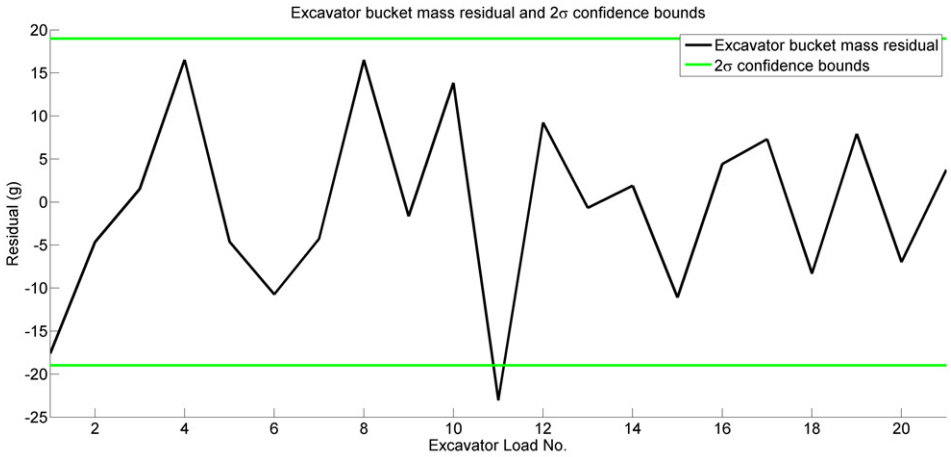

Figure 5.14 – A comparison between the ground truth estimates of **mass** and the system estimates of mass at the **excavator bucket** lumped mass location. The residual values should ideally be Gaussian distributed with a mean error of 0 and be consistent with the 2σ confidence boundaries estimated from the ASKF system.

Figures 5.16 and 5.17 show the residual and 2σ confidence bounds of the blue property at the excavator and haul truck lumped mass locations. In this graph, it should be

Figure 5.15 – A comparison between the ground truth estimates of **mass** and the system estimates of mass at the **haul truck** lumped mass location. The residual values should ideally be Gaussian distributed with a mean error of 0 and be consistent with the 2σ confidence boundaries estimated from the ASKF system.

expected that 20 out of 21 residual values should lie within the 2σ confidence bounds. As can be seen, all 21 of the values lie within the 2σ bounds. This could be partially attributed to the small sample size. From the graph, the residual values do not have any inherent negative or positive bias, the residual values are also reasonably spread over the 2σ confidence bounds. This suggests that the estimated mean and uncertainty are reasonable. A summary of the results for the blue property can be seen in Table 5.5.

Lumped Mass Location	**Mean Residual**	**Mean 2σ**	**Number of Units**
Excavator Bucket	0.8 %	12.5 %	21
Haul Truck	-0.4 %	5.6 %	7
Stockpile	-0.3 %	18.2 %	1

Table 5.5 – A summary of the estimates of the blue property in the intensive experiment

The residual and 2σ confidence boundary graphs for the green property at the excavator and haul truck lumped masses are seen in Figures 5.18 and 5.19. The results for the green property is a perfect mirror of the results for the blue property at these lumped mass locations (Figures 5.16 and 5.17).

This mirror effect creates an appearance that the system constrains the percentage

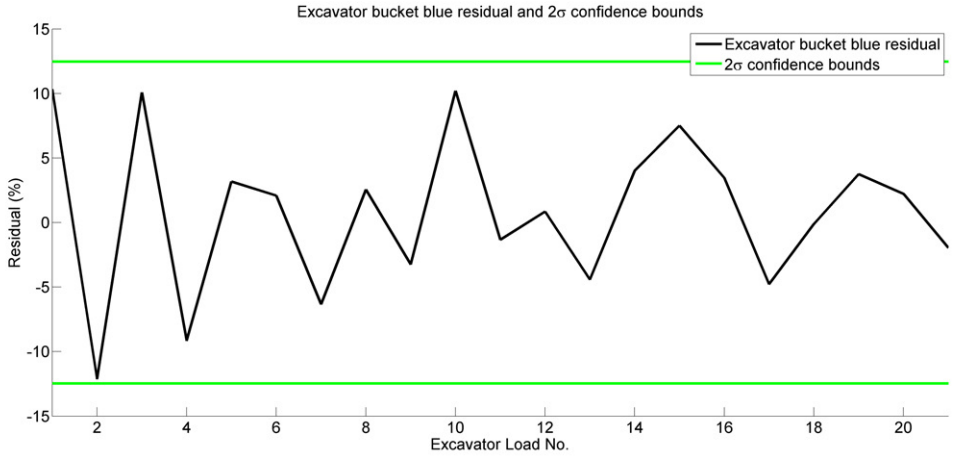

Figure 5.16 – A comparison between the ground truth estimates of the intensive blue property and the system estimates of the **blue** property at the **excavator bucket** lumped mass location.

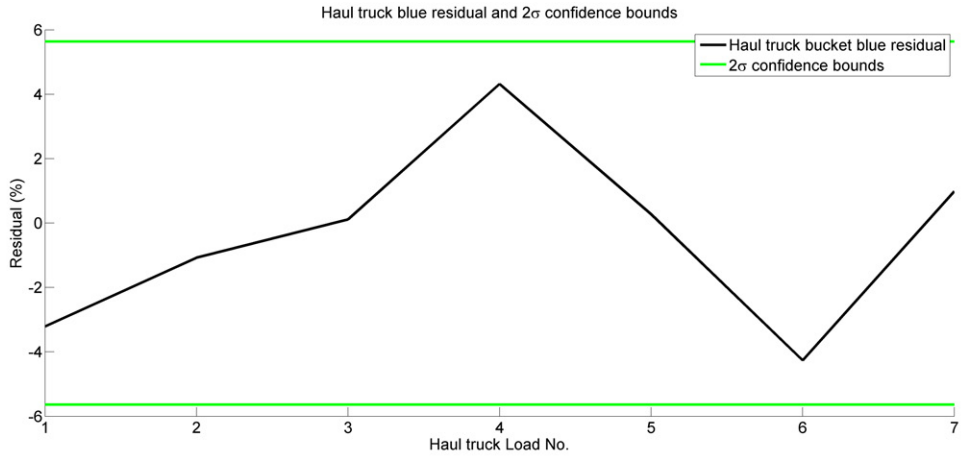

Figure 5.17 – A comparison between the ground truth estimates of the intensive blue property and the system estimates of the **blue** property at the **haul truck** lumped mass location.

of intensive properties of the same class to equal 100 %, this is not the case. This is the result of the specific modelling parameters used in this experiment. The predicted blue and green states in the excavator bucket location are initialised with the same variance. The mean estimates of both properties, on initialisation, sum to 100 %. When fusing information from the camera sensor, the observation noise on each

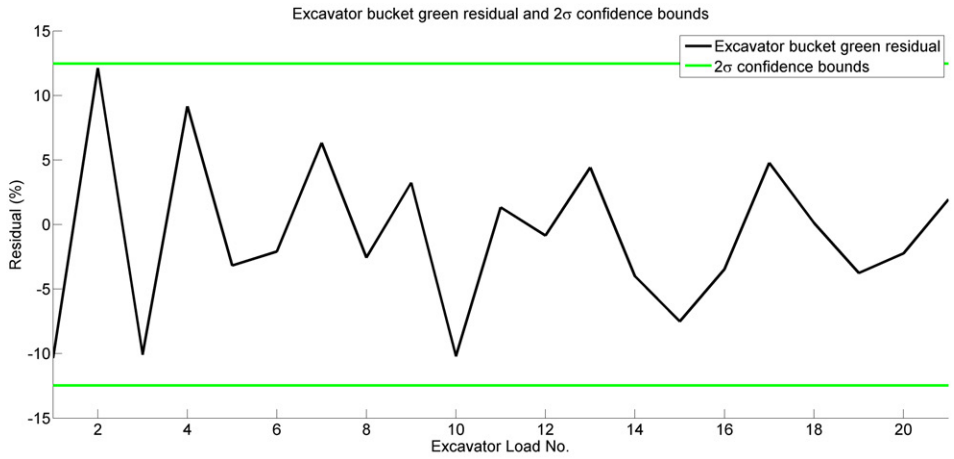

Figure 5.18 – A comparison between the ground truth estimates of the intensive **green** property and the system estimates of the green property at the **excavator bucket** lumped mass location.

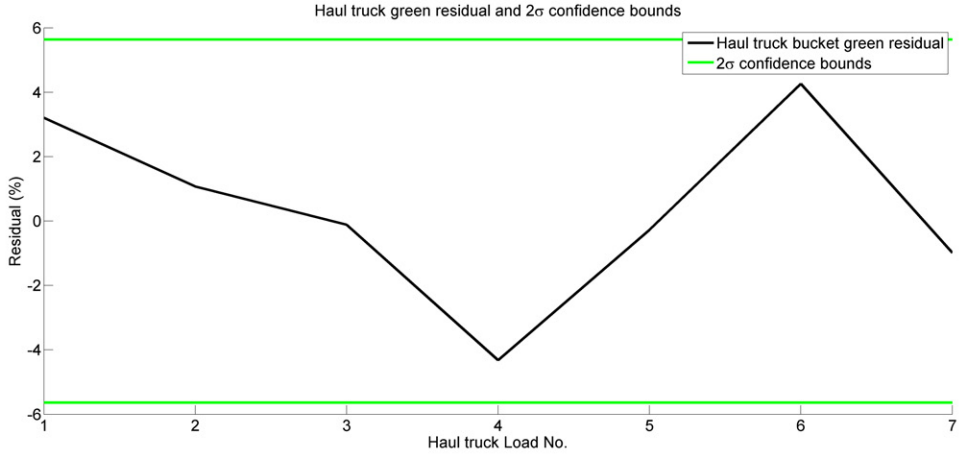

Figure 5.19 – A comparison between the ground truth estimates of the intensive **green** property and the system estimates of the green property at the **haul truck** lumped mass location.

property is equivalent. The summation of both of the observational means of the properties also is 100 %. Each of the intensive properties is also observed an equal amount of time. These are the reasons for the mirrored results.

5.5.4 Summary

The results from the intensive experiment are limited. They do suggest however, that it is possible to achieve consistent estimates of the intensive properties of the material at the different lumped mass locations using the experimental method.

5.6 Reconciliation Using the Constrained ASKF with the Percentage Based Approach and MA Approximation

5.6.1 Introduction

This section aims to fulfill the research goal of "Reconciliation with geological model" described in Section 2.3.4.

The process of reconciling extensive properties using the constrained ASKF is intrinsic to the chosen modelling method discussed in Chapter 3. For extensive properties no additional methods need to be employed in order for the reconciliation process to occur.

One way of implementing reconciliation of the intensive properties is to take advantage of the spatial relationships developed in the modelling of the extensive properties. The process for achieving this is developed in this section.

There are several areas which need to be considered when reconciling intensive properties using the lumped mass representation. One of the problems is determining the reconciliation resolution and its application. Reconciliation resolution can be thought of as a limit describing how far new information about intensive lumped mass properties 'correlate back' to update spatially correlated lumped masses. This problem is a result of the current lumped mass formulation, in which material which is physically grouped together is measured as a single lumped mass. The reconciliation resolution

increases proportionally to the size of the lumped mass. For example, an excavator bucket estimate is the average of the properties around the point of excavation, a haul truck lumped mass is an average over the cumulative areas from which its excavator buckets were sourced. This continues through the mining process. The different resolutions of data are likely to be useful to different applications and at different timescales. As an example, when updating a geological model, the smallest resolution of reconciliation data is likely to be much more useful. These observations could be used to more effectively identify ore boundaries within a grade block. The requirements for this would be an ability to determine the location of where the material was excavated from in the grade block. The intensive properties would also need to be observed in the excavator bucket.

In the lumped mass representation, the grade block extensive and intensive properties are represented as a single mean and variance. Using the reconciled data from the grade block lumped mass to update a geological model is likely to be less useful. There are areas in which this reconciled data can still be useful for applications such as geological modelling. For example, when a grade block has been excavated completely. The average of the intensive properties can be compared to the expected average of the intensive properties. If the reconciled data is inconsistent with the expected data it would suggest the geological modelling can be improved. In an autonomous mine, this could trigger increased sensing of the areas around the excavated grade block to improve the geological model.

The previous reconciliation resolution problem is a function of the averaging effect when combining lumped masses from different sources. A blended stockpile can be used as an example to illustrate this averaging effect. In this example, material combined at the blended stockpile is from two sources. One source exceeds the product specification while the other source is below specification. The goal of the blended stockpile is to average these two sources such that the material in the stockpile is within product specification.

This blended stockpile in this thesis is described using a single lumped mass. Using the spatial correlations between the blended stockpile and any of the source locations

to reconcile the intensive properties the results would be inconsistent with the true intensive properties at each source location. The reconciled values would be either above or below the actual true values. The decision to use reconciled data needs to take into consideration this averaging effect, particularly for applications such as geological model validation described prior.

An example of how this reconciled data can be used can be shown through using the example of a blended stockpile constructed from two grade blocks again. Once both of the grade blocks are empty, the reconciled values for each grade block can be combined and compared to the expected result from the combining the two grade blocks. An inconsistent result would suggest that there could be a problem in the geological modelling around each of those two grade blocks. This could again be used to instigate additional measures to improve the modelling.

This section describes a generic method for reconciling intensive properties in the ASKF. This method is applied to the previous experimental results.

5.6.2 Reconciliation Algorithm Derivation

The reconciliation algorithm uses the correlations between the extensive properties in the ASKF to determine the weighting of correlated material at other lumped mass locations.

The following is an example of a state vector (x_k) and covariance matrix (P_k) of a hypothetical system filled with M_n mass states.

$$x_k = \begin{bmatrix} M_1 \\ M_2 \\ \vdots \\ M_n \end{bmatrix}, P_k = \begin{bmatrix} \rho_{11} & \rho_{12} & \cdots & \rho_{1n} \\ \rho_{21} & \rho_{22} & \cdots & \rho_{2n} \\ \vdots & \vdots & \ddots & \\ \rho_{n1} & \rho_{n2} & & \rho_{nn} \end{bmatrix} \tag{5.9}$$

The amount of correlated mass from a particular state M_a to a state M_b ($[M_a, M_b] \in x_k$) can be calculated by the following equation.

$$M_c = \alpha_{ab} \times M_a \tag{5.10}$$

where

$\alpha_{ab} = \frac{\rho_{ba}}{\rho_{aa}}$,

M_c is the total amount of correlated mass.

Recall in Equations 5.7 and 5.8 the equations for approximating the mean and variance when combining intensive properties from two lumped masses.

This approximation method can be applied iteratively to all correlated lumped masses to provide a reconciled estimate.

The algorithm for this iterations is as follows:

$$x_R = \frac{\alpha_{1R}M_1x_1 + \alpha_{2R}M_2x_2 + \cdots + \alpha_{nR}M_nx_n}{\alpha_{1R}M_1 + \alpha_{2R}M_2 + \cdots + \alpha_{nR}M_n} = \sum_{i=1}^{n} \frac{\alpha_{iR}M_ix_i}{\alpha_{iR}M_i} \tag{5.11}$$

$$\sigma_R^2 = \frac{\sum_{i=1}^{n} \alpha_{iR}M_i\sigma_i^2}{\sum_{i=1}^{n} \alpha_{iR}M_i} + \frac{\sum_{i<j,i,j=1}^{n} \alpha_{iR}M_i\alpha_{jR}M_j \left(x_i - x_j\right)^2}{\left(\sum_{i=1}^{n} \alpha_{iR}M_i\right)^2} \tag{5.12}$$

x_R defines an intensive property of the state which is to be reconciled, σ_R^2 provides the estimated variance of this state.

5.6.3 Example Results with Intensive Experiment

Equations 5.11 and 5.12 are applied to the previous intensive experiment results. The state reconciled is the 'Blue' property of the grade block lumped mass.

Table 5.6 provides a set of observations of the grade block prior to excavation. The mean and variance of these observations are used as the method for estimating the prior model.

The reconciliation algorithm is run with each of the 7 haul trucks in the experiment having a full load of material. This is before these loads are unloaded at the final

Observation No	**Blue** (%)	**Green** (%)
1	58	42
2	53.5	46.5
3	57.5	42.5
4	56.5	43.5
5	46.4	53.6
6	55.3	44.7
7	52.7	47.3
Mean	54.27	45.73
Ground Truth	50.64	49.36
2σ	7.3	7.3

Table 5.6 – A set of observations on the blue and green intensive properties of the grade block lumped mass in the intensive experiment. The same set of samples is used for each observation. This mean and variance of these observations is used as the estimate of the blue and green intensive properties in the grade block.

Value	**Mean (%)**	2σ (%)
Prior Estimate	54.27	7.3
Reconciled Estimate	51.17	18.29
Ground Truth	50.64	-

Table 5.7 – A comparison between reconciled estimate, prior estimate and ground truth using the intensive property reconciliation algorithm. The reconciled estimate provides a result which is consistent within 2σ of the ground truth. The mean value estimate is improved compared to the prior estimate.

stockpile. A comparison of the reconciliation data, prior model and ground truth can be seen in Table 5.7. The results of the blue property are shown, the green property results mirror the blue results.

As can be seen, the reconciled estimate provides a mean estimate which is consistent within 2σ of the ground truth. This reconciled estimate could be fused with the prior model to form a better estimate of intensive properties removed from the grade block. This fusion would require a method to account for the dependence between the reconciled estimate and the prior estimate.

5.7 Summary

The core contributions of this thesis have concentrated on the development of an integrated stochastic estimation and tracking system for bulk material properties over a process chain which is based on a open pit mining operation.

The experiments in this chapter, although limited, have shown that it is possible to probabilistically estimate the intensive properties of the material at different lumped locations consistently over a specific controlled process. It was also shown that the intensive properties can also be reconciled using the spatial correlations developed through the modelling of the extensive properties in the ASKF.

The work in this chapter would benefit from future work involving additional experimentation over longer timescales with larger scale equipment (similar to the larger scale experimentation performed with the extensive properties in Chapter 3).

One of the goals of this thesis is to contribute towards the development of an end-to-end system for estimation of material properties in a preserved correlated process chain. This thesis is particularly focused on open pit mining and in an autonomous environment. There are many additional system dynamics which need to be taken into consideration when taking into account the end-to-end system. Examples of these additional complex dynamics were discussed in Section 5.6 in the introduction to reconciling intensive properties (blended stockpiles).

Chapter 6 describes how the contributions made in this thesis can be used together in a complete integrated system. It gives examples of how this can be specifically applied to open pit mining. Furthermore, it also discusses possible avenues of research to deal with the additional complexities in developing an end-to-end estimation system.

Chapter 6

An Integrated System

6.1 Introduction

A core contribution of this thesis is the development of a practically designed, integrated stochastic tracking and estimation system for bulk material properties in open pit mining. This chapter describes possible ways in which the contributions made in Chapters 3, 4 and 5 can be combined into a single system for use on an open pit mine site.

Prior to implementation, there are many practical challenges which need to be overcome. An example of some of these challenges which will be addressed in this chapter are:

- Determining appropriate models for initialisation of 'lumped mass' properties.
- Modelling of losses in the system at different locations.
- Creating a method for enacting system models when the corresponding action occurs in reality (e.g. when to perform the appropriate filter and modelling actions for combining lumped masses or initialising a new lumped mass which has been excavated.

- Modelling of information sources to be fused into the ASKF representation.

This chapter also presents some of the wider research problems required to fulfill the vision of having an end-to-end integrated tracking and estimation system, as well as possible ways in which the current system could be improved. Some of the areas discussed are:

- Inadequacies in representing lumped mass properties and information sources as Gaussian distributions.
- Including process plant operations.
- Refining the method and representation of material when complex mass transfer processes are involved (e.g. ROM blended stockpiles).
- Improving the value of the information provided by the system model to other mining systems.

6.2 An Integrated System

6.2.1 A Summary of the Developed System

The research outcomes in this thesis are categorised into three chapters. Chapter 3 describes a tracking and estimation system for extensive material properties. As part of Chapter 3 a representation, referred to as the lumped mass model, is used to segment the estimation and tracking problem into smaller more manageable components. A method for maintaining spatial correlations between each of the lumped masses extensive properties using a constrained ASKF is developed. This enables information from observational sources to be fused consistently amongst spatially correlated lumped masses. This method allows for conservation of mass in the system and enables real-time reconciliation of extensive properties.

Chapter 4 describes a method for volume estimation which can be integrated into the system described in Chapter 3. One common element in each of the contributions in this thesis is the representation of data as probabilistic. Chapter 4 provides a method for generating a probabilistic estimate of the bulk volume given a set of 2.5D cartesian data points (x,y,z) representing a surface. This method was found, when the data is sparse, to provide a more accurate and precise estimate of the bulk volume compared to state-of-the-art deterministic methods. This has several benefits in a mining environment. Firstly, the method is able to utilise data from lower quality sensors which collect sparser data sets compared with high quality surveying equipment which is currently used (e.g Riegl LMS-Z620 A.2.2). This could enable robust, inexpensive sensors, such cameras or laser systems, to attached to mining equipment (e.g haul trucks, excavators) to provide volume estimates at different locations. Another benefit is that the volume estimation method can be easily integrated into the ASKF framework. This is shown in the large scale experiment in Section 3.6.3.

The contributions in Chapters 3 and 4 provide both a method for representing, estimating and fusing extensive properties in a probabilistic manner. The lumped mass representation does not have a requirement for all properties of the material to be estimated in order for it to be used in operations. If desired, a system based on the work in Chapter 3 could be made to track extensive properties through a process chain on a mine site. The bulk volume estimation method in Chapter 4 can be used as an information source at different locations along the process chain.

Chapter 5 describes a method for including intensive properties in the constrained ASKF representation. Chapter 5 also discusses some of the complexities in modelling intensive properties, specifically in dealing with the state dependency between the intensive properties and the extensive properties. A method for reconciling intensive properties back to a particular lumped mass location is also shown.

The work in all three chapters was designed to be operate together. Section 6.2.3 describes scenarios in which all these components can be used in an open pit mine site.

Section 6.2.2 describes some of the practical challenges in implementing the work

described in these chapters in order to operate in the example scenarios described in Section 6.2.3.

6.2.2 Possible Implementation Challenges

Determining Appropriate Models for Initialisation of Lumped Mass Properties

The initialisation and system models in the experiments in Chapters 3 and 5 were derived from the ground truth observations available. The ground truth values were collated, then averaged to find the mean estimate as well as the variance.

In a practical real-time application of this system, the ability to know the ground truth values is not available. Additionally, there is likely to be more variables which affect the initialisation models than in the controlled experiments performed in this thesis. One example is generating a model for the amount of mass of the material in the excavator bucket. During the experiments in this thesis, the loading process was controlled to be as uniform as possible (single operator, constant weather, three loads of equal size per truck). In an open pit mine the loading process is likely to be influenced by a range of additional factors such as varied weather conditions, different operators with varying skill levels, night/day shift variations as well as operators moderating the final excavator load to bring the haul truck to capacity.

One area for future work is to develop a method for modelling these processes on a mine site. One possible solution is to use a method such as Gaussian process regression (the method used for volume estimation in Chapter 4). The initialisation model could be learnt from training data consisting of the prior mass observations and a set of appropriate variables which are likely to influence the mass.

Modelling of Losses in the System at Different Locations

Loss modelling was discussed in Chapter 3. Mass losses were included in the small scale experiment. In the experiment it was possible to model the losses in the con-

strained ASKF consistently. Modelling losses on a mine site has several challenges. Firstly, it is often difficult to 'observe' losses, which makes it challenging to rely solely on using observations as the basis to initialise a new loss lumped mass. Attempting to model the losses, similar to modelling excavator loads, is likely to be dependent on a variety of factors. One example is haul trucks unloading at a crusher. The haul truck, as it unloads, may not deposit 100% of the material into the crusher. The amount of material lost is dependent on several factors such as material type, load size, operator skill, crusher type and entry conditions to the crusher.

As the 'lost' material at the crusher builds up to a level which inhibits the unloading efficiency, typically, a front end shovel (or similar equipment) is used to push this lost material into the crusher. With the lumped mass representation and using the models described in Chapter 3 on loss modelling, this process can be dealt with inside the ASKF framework presented in this thesis.

Interacting with Real World Events

One of the requirements in making the integrated tracking and estimation system possible is linking the process models with real world events. As an example, an excavator unloading its current load into a haul truck. There needs to be a method for linking this real-world unloading action with the process of combining the excavator lumped mass with the haul truck lumped mass.

This problem would be simpler in a mine where all equipment and processes are fully automated. A data interface between the equipment and estimation system would enable the equipment to inform the estimation system that it has performed a certain action (such as the excavator unloading into a haul truck). In a manned system, the process of informing the estimation system could be done through operator input. Alternatively, the equipment actuators and sensors could possibly be monitored. Certain configurations of actuator and sensor information could be interpreted autonomously and classified to specific actions. For example, a system which monitors haul truck tilt tray angle. This system could indicate when the angle reaches a cer-

tain level (e.g. through a hydraulic piston position sensor) which could be classified as the haul truck unloading. This information could then be communicated to the estimation and tracking system.

Another aspect of this interaction between lumped masses which needs to be taken into account is how to determine which lumped masses are interacting with each other. This requires the ability to define the lumped masses in a common reference frame. One possibility is to use GPS co-ordinates. When a process occurs the GPS data can be used to infer which lumped masses have interacted. This specific problem is discussed further in Section 6.2.3.

Modelling of Information Sources

In order to utilise information sources in the constrained ASKF framework the data must be represented by a Gaussian distribution. Chapter 4 described a method for estimating bulk volume which provides the final estimate in this format directly. Other observational sources for properties such as mass, chemical, fragmentation etc which may be desired to be estimated in the system are also required to have an appropriate sensor model designed such that the information is represented by a Gaussian distribution.

6.2.3 Possible Mining Scenarios

This section describes several different scenarios in which the work in this thesis could be applied to an open pit mine operation.

Thesis Example

The first example is a scenario which mimics the processes performed in the experiments in this thesis in Chapters 3 and 5. Figure 6.1 provides an overview of the scenario using the lumped mass representation.

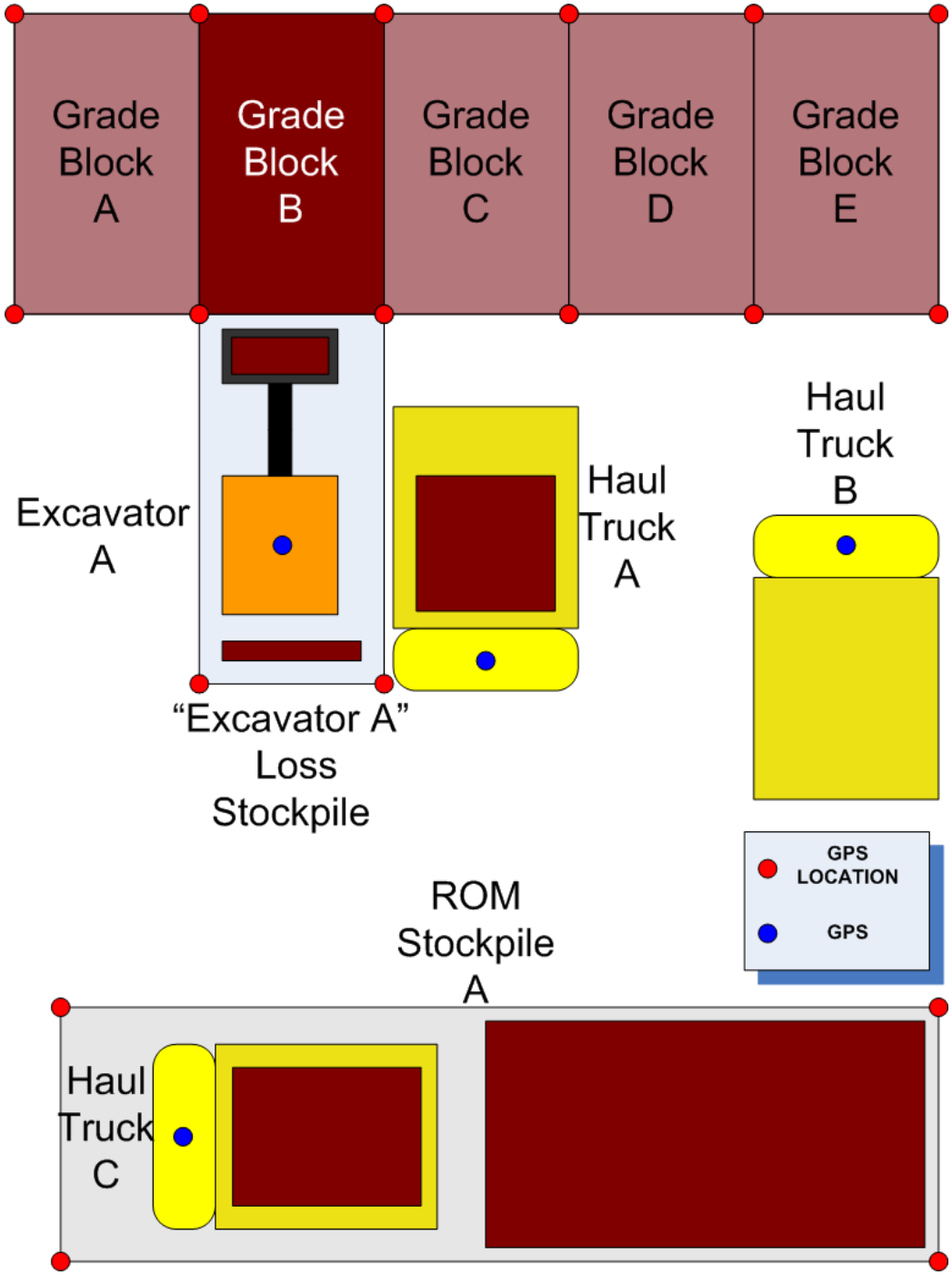

Figure 6.1 – An open pit mine scenario showing a hypothetical lumped mass representation. The scenario is an example of a mine site process which mimics the experiment processes used in this thesis.

In this example the ASKF at the instance shown in Figure 6.1 contains the following lumped masses:

- Grade Blocks A - E
- Excavator A
- Excavator A Loss Stockpile
- Haul Truck A
- Haul Truck C
- ROM Stockpile A

'Haul Truck B' is not estimated given that is does not contain any lumped mass. GPS co-ordinates (red dots) are used to identify the boundaries of the grade block and ROM stockpile lumped masses. The blue dots represent an active GPS system which would be able to update the boundaries of lumped masses in mobile equipment.

In this scenario Grade Blocks A - E could represent a series of grade blocks which have been part of a recent blast and now contain broken stocks. Grade Block B is tasked for excavation. The material is to be transferred to ROM Stockpile A. Excavator A Loss Stockpile represents material lost between the excavator and the haul truck, this lumped mass could be recombined with the Grade Block B lumped mass when a front end loader cleans up the grade block a the end of a shift.

In this example, the lumped mass properties (both extensive and intensive) at any location can be observed and the ASKF estimation system ensures that mass is conserved between Grade Block B and ROM Stockpile A. The reconciliation algorithm for intensive properties as described in Section 5.6 could be used to provide reconciled data in real-time on the intensive properties in lumped mass Grade Block B.

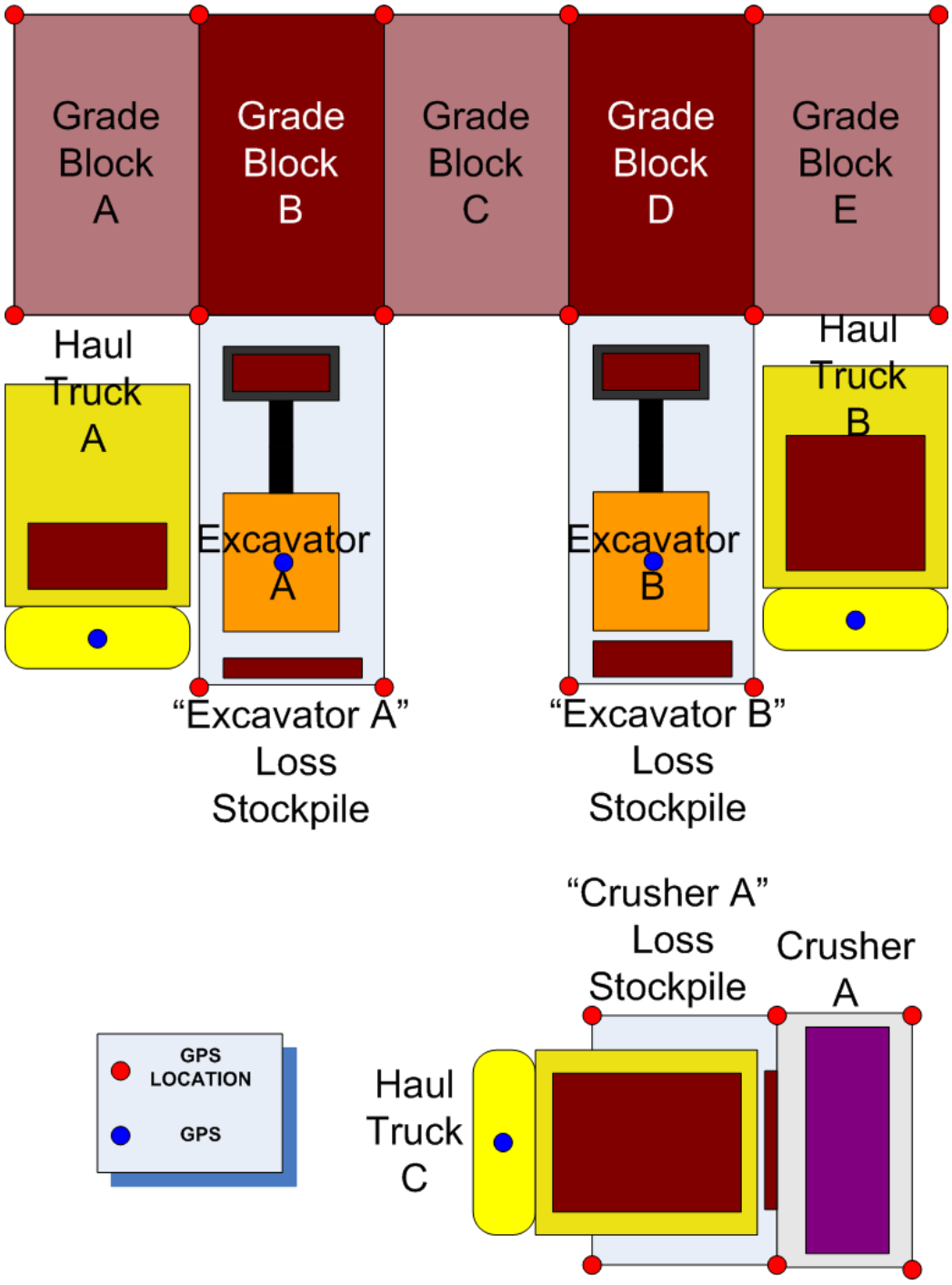

Figure 6.2 – This example open pit mine scenario involves multiple grade blocks transferred directly to a crusher. This example contains processes outside of the experiments developed in this thesis. The work in this thesis can be applied however to this scenario.

Multiple Sources Example with Crusher

The scenario in Figure 6.2 describes another scenario which the work in this thesis could be used to estimate the properties of the material.

The ASKF at the instance shown in Figure 6.2 contains the following lumped masses:

- Grade Blocks A - E
- Excavator A
- Excavator A Loss Stockpile
- Excavator B
- Excavator B Loss Stockpile
- Haul Truck A
- Haul Truck B
- Haul Truck C
- Crusher A
- Crusher A Loss Stockpile

This scenario is similar to the previous example. In this scenario however, two grade blocks (Grade Block B and Grade Block D) are tasked for excavation simultaneously. The haul trucks unload directly to the plant crusher (Crusher A). The 'Crusher A Loss Stockpile' lumped mass corresponds to material lost from the haul truck as it unloads at the crusher.

The method used in this thesis can be adapted for this scenario to provide an estimate of the total amount of material which has entered the crusher along with the intensive properties of this material. This can be achieved by treating Crusher A the same way as a stockpile lumped mass. The material from each successive haul truck lumped

mass is combined with the Crusher A lumped mass. In this scenario the reconciliation of intensive properties needs to take into account the averaging effect as described in Section 5.6.

If desired, the reconciliation data for each individual grade block could be conserved by treating the crusher as three separate lumped masses. Haul trucks from each grade block are combined into separate lumped masses at the crusher dependent on their source location. In this example there would be two lumped mass estimates for Crusher A. One would describe material properties unloaded at the crusher from Grade Block B, the other from Grade Block D. The third lumped mass would consist of the material from the Crusher A Loss Stockpile as it is pushed into Crusher A. This lumped mass would be correlated to both Grade Block B and D. It would be expected however that the amount of material in this lumped mass would be considerably smaller than the lumped masses specific to material unloaded from each of the grade blocks.

6.3 Developing an End-to-End Integrated System

6.3.1 Improving the Representation and Modelling of Properties

One of the assumptions when using the ASKF is that the process model and observational models can be represented as Gaussian distributions. This is a problem when considering the nature of the properties which are being tracked in the lumped masses. Take as an example the estimate of mass of a random lumped mass shown in Figure 6.3a. Mass can not be a negative number. Figure 6.3b highlights the areas in which the probability density is valid (green) and invalid (red).

A significant amount of material properties which would be estimated in mining have a positivity constraint. Some other examples include volume, chemical properties and density. Some intensive properties also have an additional constraint of being always $<= 100$ %.

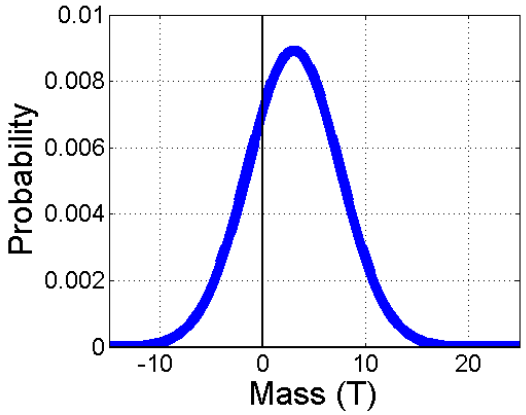

(a) An estimate of mass with a mean of 3 T and variance of 20 T

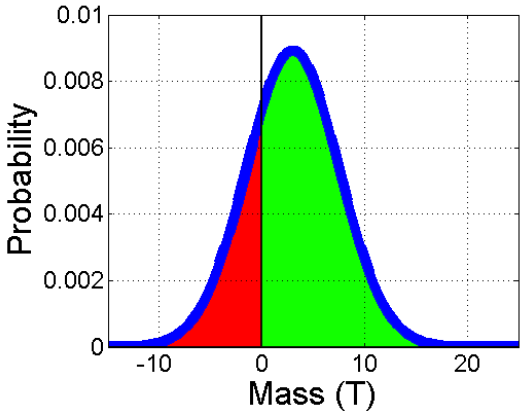

(b) Valid probability density is coloured green, invalid probability density is coloured red.

Figure 6.3 – The Gaussian assumption does not handle well the physical constraints of certain material properties. In this example, the Gaussian distribution assigns probability mass to negative values. The distribution is representing a mass estimate which can not take negative values.

This positivity constraint is problematic in cases where the mean estimate is close to zero and (or) the uncertainty associated with this mean estimate is high. In cases where the mean estimate is far away from zero, or the variance is small enough, the amount of invalid probability density would be negligible.

A similar problem occurs in meteorological predictions. One solution suggested by Cohn [29], when including properties with these positivity constraints, is to first estimate the properties as log-normal distributions. Then approximate the log-normal distributions as Gaussian distributions (for use in estimation techniques such as Kalman filters) using the mean and variance characteristics from the log-normal distribution.

An example of this process can be shown in Figure 6.4 which uses the same set of data from Figure 6.3. The log-normal distribution of the data is shown in Figure 6.4a. As can be seen, it is not possible for the log-normal distribution to allow negative values. Figure 6.4b shows the log-normal mean and variance properties used as values in a Gaussian approximation. The amount of negative probability mass has decreased from the original Gaussian distribution (seen in Figure 6.3).

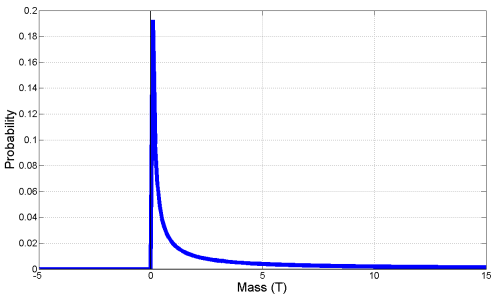

(a) Log normal probability distribution of the mass described in Figure 6.4

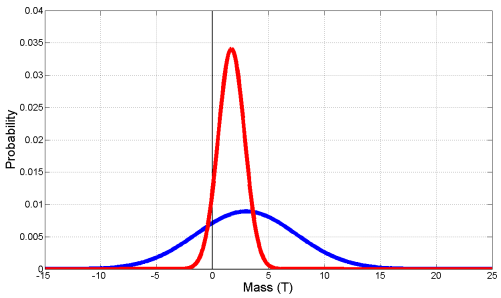

(b) Comparison between standard Gaussian (Blue) and Gaussian derived from log normal descriptive statistics(red)

Figure 6.4 – A method for accounting for the positivity constraint of material properties under a Gaussian assumption using a log-normal approximation.

The prior method describes one possible avenue where further work can be done in improving the representation and modelling of material properties in a system which requires a Gaussian assumption.

Another possible area of research is to consider reformulating the lumped mass representation away from the Gaussian based system used in this thesis. At present lumped masses are broadly classified as logically separated groupings of material. The material properties are then approximated using a single mean and variance. Using a continuous representation rather than a discrete formulation, especially for intensive material properties, has the potential to provide a much richer source of information. Maintaining a discrete lumped mass representation is also likely to be difficult when tracking the material flow through the process plant operations.

6.3.2 Including Process Plant Operations

The work in this thesis is limited in scope from point of excavation to point of entry into a plant process. The vision for this research work is to estimate the material probabilistically from excavation all the way to the final stockpiles used for transportation off site. This could possibly be extended even further to estimation through to centralised processing and transportation facilities of multiple mines.

The processes used to interact with lumped masses in the experiments in this thesis are all mass transfer processes. As discussed in the review of control theory (Section 2.4.3) there are many mine plant processes which are non-linear. This creates several interesting research questions.

- How do you model the change in material properties caused by the processing plant in a consistent probabilistic manner given the non-linearity of some of the processes?
- How do you reconcile these changes in properties to the point of excavation effectively?

One of the other research issues particular to material in the processing plant is the ability to track and estimate material as lumped masses. The nature of a processing plant means material is not transferred around as singular groupings of material but more as a continuous stream of ore. There is an issue of how to keep track and model the interactions between lumped masses as they are combined and separated with different rates of flow in the processing plant.

A continuous representation to solve this problem is difficult for several reasons. It requires a more complex model (both computationally and theoretically) to track intensive material properties from point of excavation. If a continuous model is used in the plant, but not outside the plant, how is transition handled between the two representations also requires additional research.

One other possible avenue for future work is using Finite Element Modelling (FEM) to dynamically model the interactions between the processing operations and the bulk material. Using FEM is traditionally a computationally expensive process, thus being able to develop a system which could function at a real-time level would be a valuable research contribution.

6.3.3 Refining the Methodology for Maintaining Spatial Correlations

One re-occurring issue which needed to be constantly accounted for in this thesis is the method for appropriately handling the spatial relationships in a manner which allows information to be shared appropriately between correlated lumps. The reconciliation that occurs, both for extensive and intensive properties, relies on the correlations developed between extensive properties in the constrained ASKF developed in this thesis.

One possible future area of research could be an approach which maintains the model of the original lumped mass representation when lumped masses are combined together. This is difficult when considering processes which physically mix material from lumped masses together (e.g. plant processes). Figure 6.5 shows an additional layer of lumped masses applied to the previous example shown in Figure 6.2. The aim of maintaining these additional smaller lumped masses is to be able to correlate to source locations at an improved resolution when fusing additional information.

This approach is a compromise between a continuous representation and the lumped mass representation described in this thesis.

6.4 Summary

This chapter has provided an overview of how the different contributions of this thesis can be combined to create an integrated tracking and estimation system on an open pit mine site.

Some of the implementation problems in order to transfer the work in this thesis from the lab to the field are presented. These include problems such as; model development for the mining processes, relating system model processes to real world events as well as developing the models for information sources to be fused into this system.

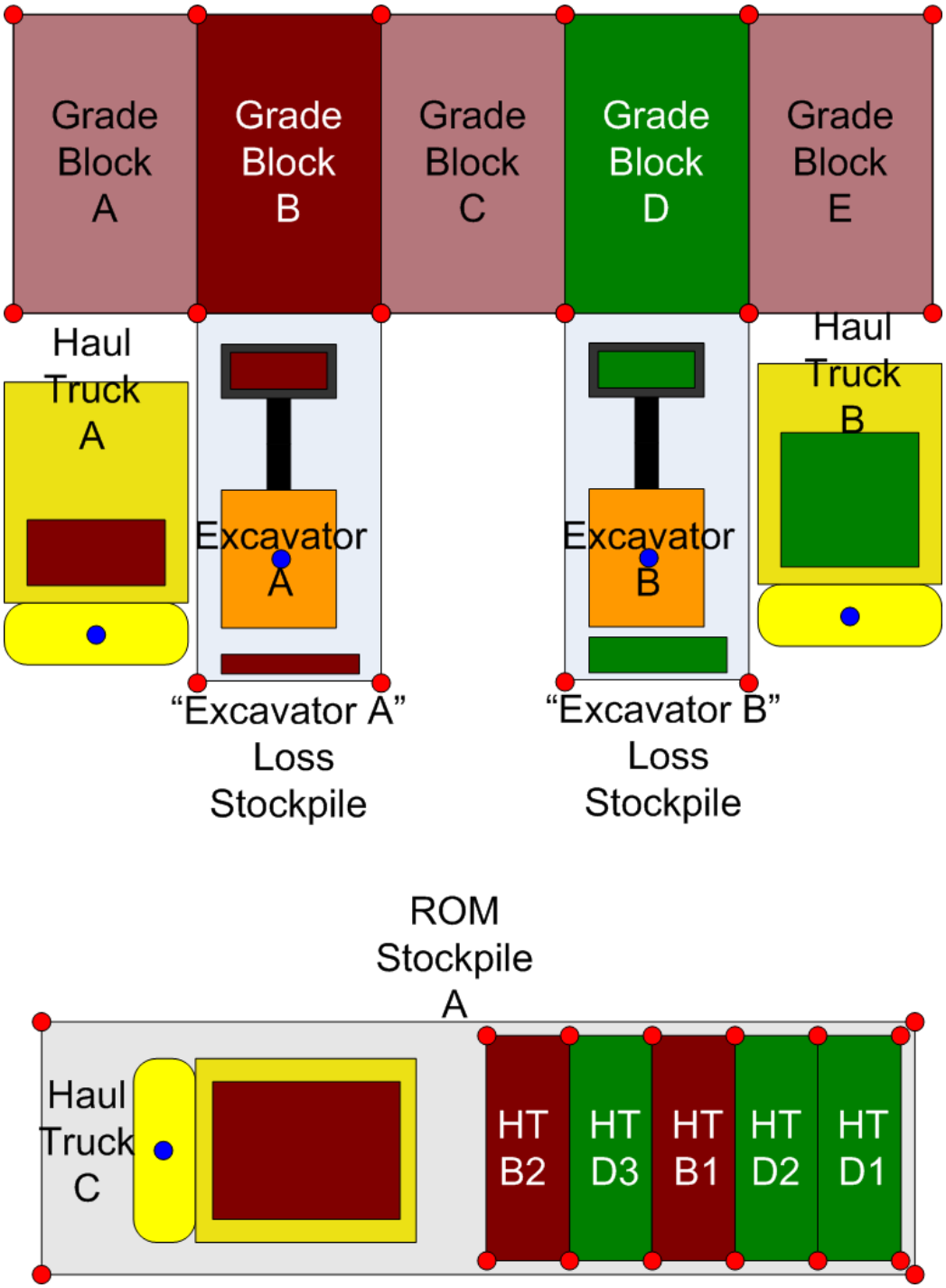

Figure 6.5 – By maintaining the original lumped mass representations in the ROM stockpile, observations of intensive properties could possibly be reconciled at a much smaller resolution then what is possible when using a single lumped mass representation.

Two generic scenarios were presented showing how the current representation could be used to estimate lumped mass properties given the prior implement. This included the scenario used for experiments in this thesis as well as an additional scenario which with some minor adjustments to the modelling process can estimate the total amount and averaged intensive properties of material entering a crusher.

The final section discussed several ways to build upon the contributions made in this thesis in regards to developing an end-to-end integrated tracking and estimation system. Some of the possible avenues for future research include developing an improved method for representing bulk material properties which does not require a Gaussian assumption. It also includes a discussion on extending the current method through process plant operations as well as possible methods for improving the spatial correlations between lumped masses in order to reconcile more useful information.

Chapter 7

Conclusion

The aim of this thesis was to develop a stochastic method for representing, estimating and fusing bulk material properties over a process chain.

This thesis presented a novel methodology to solving this problem with particular emphasis on providing a system which would operate on an autonomous open pit mine.

The basis for the modelling of extensive and intensive properties is the representation of physically separated groupings of bulk material as lumped masses.

A constrained ASKF is used for modelling the extensive and intensive bulk material properties within each lumped mass. A novel stochastic method for bulk volume estimation is used as an input to validate the proposed estimation system in the large scale experiments. The bulk volume estimation method has been shown through experimentation to provide an improvement in accuracy and precision under sparse data sets compared to state-of-the-art deterministic methods.

This chapter summarises the contributions made in this thesis.

7.1 Summary of Contributions

7.1.1 The Lumped Mass Model

The lumped mass model was developed as a means for reducing the complexity in the estimation problem to a more manageable size. This model represents groupings of logically separated bulk material as the basis for process modelling and estimation of material properties. This method represents individual extensive and intensive properties as Gaussian distributed, allowing for the utilisation computationally efficient methods for tracking and estimation. This contribution is discussed in Chapter 3.

7.1.2 Estimation of Extensive Properties

Chapter 3 introduces a method for stochastically modelling extensive lumped mass properties using an ASKF as the material moves through a process chain. This method has many useful properties, these include the following:

- The method allows for extensive lumped mass properties to be estimated consistently at each location in the process chain.
- The ability to add and remove lumped masses to the system at any point in time. This allows the system to evolve as lumped masses are moved, partitioned and combined throughout the process chain.
- Flexibility to model the unintended loss of material over a process chain.

These features are validated through small and large scale experiments.

7.1.3 A Constraint to Conserve Total Material in the System

The process chains that this thesis focuses on are closed systems. One of the characteristics of a closed system is that the total amount of material within the system

remains constant. A novel constraint for the ASKF is derived in Chapter 3 to ensure that spatial correlations between extensive material properties are maintained correctly. This guarantees conservation of material over the process chain. This constraint ensures that when fusing additional information about an extensive property of a lumped mass the information propagates appropriately to correlated lumped masses.

7.1.4 Probabilistic Bulk Volume Estimation

Chapter 4 introduced a novel method for estimating 2.5D bulk volumes to integrate into a stochastic material estimation system as described in Chapter 3. This method was used as an input in to the large scale experiments in Chapter 3 as an independent information source. This was an important information source used in validating the prior contributions in probabilistic extensive lumped mass property estimation.

Through experimentation it was found the Gaussian process method introduced in this thesis had the advantage over the comparative methods. The Gaussian process method provided greater accuracy and precision under sparse data sets while simultaneously providing an estimate of the uncertainty in the bulk volume estimate.

7.1.5 Estimation of Intensive Properties

Chapter 5 presented a method for including intensive lumped mass properties into a lumped mass based estimation system. This method includes a method for averaging intensive properties when combining two lumped masses together. The proposed 'Mathematical Averaging' method was tested during experimentation and was found to be consistent over the experimental data used. The overall effectiveness of the representation and modelling method for intensive properties was discussed within the context of the limitations of the assumptions used. These included that each intensive and extensive property states are mutually exclusive and can be adequately represented by a Gaussian distribution.

7.1.6 Reconciliation of Intensive Properties

An algorithm for reconciliation of intensive lumped mass properties was developed in Chapter 5. This algorithm is derived both from the spatial correlations between extensive lumped mass properties and the 'Mathematical Averaging' method for combing intensive lumped mass properties together. An example of applying this algorithm iteratively over a experimental data set is provided.

7.2 Future Work

Section 6.3 discussed possible areas in which the method in this thesis could be improved to be used as an end-to-end system on an open pit mine site. This section provides areas of future work specific to the contributions made in this thesis.

7.2.1 Accounting for the Bulk Factor in the Relationship between Mass, Volume and Density

One of the benefits of maintaining the spatial correlations between lumped mass extensive properties is the ability to use information sources more effectively in real-time by propagating the new information to correlated states.

The work in this thesis focussed primarily on estimating mass as the extensive property used to maintain the spatial relationships between lumped masses. Developing a system which accounts for bulk factor variations inside the ASKF framework would be useful. This allows for bulk volume estimates to be of more value.

7.2.2 Additional Experiments

Increasing the size and scope of the processes in the experiments in this thesis would allow for greater confidence that the system will be valid at a commercial mine scale.

An increased amount of samples data sets would allow for greater insight into the system dynamics and areas where the current representation may be inadequate.

7.2.3 Improved Sampling Methods for Bulk Volume Estimation

One of the difficulties in sampling from a data set is ensuring that the most valuable data is chosen. In surface estimation, these are points which give the most information about the structure of the surface. An approximately unform method as used in this thesis has the problem of assuming an equal weighting of data points over the sampling area. A method for increased sampling of data points around areas of complex features and comparatively reduced sampling over simple structural areas could allow for an improvement in the accuracy of not only the Gaussian process method but most of the comparative volume estimation methods used in this thesis.

7.2.4 Improving the Computational Efficiency of Gaussian Process Based Volume Estimation

As discussed in Section 4.8, the Gaussian process method for bulk volume estimation is considerably more computationally expensive then the comparative methods in this thesis. Developing methods for improving this method to be more efficient will be vital for enabling its use in real-time applications. One possible approach which is being actively researched in the community at the moment is increasing the sparsity in the covariance function to reduce the time required for the matrix inversion.

Another possible avenue for research is improving the method for deriving the bulk volume estimate from the gaussian process regression. Finding a closed form solution would significantly reduce the computational time required in numerically deriving a solution. It would also provide a more accurate and precise solution.

7.2.5 Development of a Combined Intensive-Extensive Representation of Lumped Material

Chapter 5 presented a discussion on the merits of different representations of lumped masses when intensive properties are incorporated. One suggested method is a combined intensive-extensive representation of the lumped mass. This is discussed in more detail in Section 5.2.2. Overcoming the research problems associated with implementing this method would be valuable to compare with the percentage based approach used in this Thesis. A combined intensive-extensive representation could simplify the combination of lumped masses and possibly enable a more accurate estimation of the material present.

7.2.6 Compare the Performance of the Stochastic Estimation and Tracking Method Developed with Current State of the Art on Mine Sites

A comparison of the method developed in this thesis with similar material tracking systems present on mine sites will provide useful information as to whether or not the developed method is practical to be used on a commercial mine site. It would also highlight any advantages or disadvantages the current representation and method has compared to current state of the art methods as well as present new areas for future research in the representation and method developed within this thesis.

Bibliography

[1] Australia wins rio tinto's mining automation effort. http://www.riotinto.com/media/18435_media_releases_6473.asp. July 2007.

[2] Tracelite, tracking timber supply chain management, chain of custody management, timber sustainability, rfid tags. http://corporate.helveta.com/products.html?pgid=95. January 2012.

[3] Autonomous haulage system - komatsu's pioneering technology deployed at rio tinto mine in australia. http://www.komatsu.com/ce/currenttopics/v09212/index.html. January 2012.

[4] Oretracker. http://www.oretracker.com/, January 2012.

[5] Cattleworks. http://www.cattleworks.com/. January 2012.

[6] Crt cropbase track & trace software. http://www.cropbase.com/. January 2012.

[7] Farm files crops. http://www.farmfiles.com/. January 2012.

[8] G. Agamennoni, J.I. Nieto, and E.M. Nebot. Robust inference of principal road paths for intelligent transportation systems. *Intelligent Transportation Systems, IEEE Transactions on*, 12(1):298 –308, march 2011. ISSN 1524-9050.

[9] H. Ahrens. The history of statistics. the measurement of uncertainty before 1900. *Biometrical Journal*, 30(5):631–632, 1988. ISSN 1521-4036.

[10] S. Alarie and M. Gamache. Overview of solution strategies used in truck dispatching systems for open pit mines. *International Journal of Surface Mining, Reclamation and Environment*, 16(1):59–76, 2002.

[11] S. M. Arulampalam, S. Maskell, N. Gordon, and T. Clapp. A tutorial on particle filters for online nonlinear/non-gaussian bayesian tracking. *IEEE Transactions on Signal Processing*, 50:174–188, 2002.

[12] Y. Bar-Shalom, X. R. Li, and T. Kirubarajan. *Estimation with Applications to Tracking and Navigation*. Wiley-Interscience, 1 edition, June 2001. ISBN 047141655X.

[13] G.S. Bastos, L.E. Souza, F.T. Ramos, and C.H.C. Ribeiro. A single-dependent agent approach for stochastic time-dependent truck dispatching in open-pit mining. In *Intelligent Transportation Systems (ITSC), 2011 14th International IEEE Conference on*, pages 1057 –1062, oct. 2011.

[14] Mr. Bayes and Mr. Price. An essay towards solving a problem in the doctrine of chances. by the late rev. mr. bayes, f. r. s. communicated by mr. price, in a letter to john canton, a. m. f. r. s. *Philosophical Transactions*, 53:370–418, 1763.

[15] D.P. Bertsekas and J.N. Tsitsiklis. *Introduction to probability*. Athena Scientific, 2002. ISBN 9781886529373.

[16] A. Bewley, R. Shekhar, S. Leonard, B. Upcroft, and P. Lever. Real-time volume estimation of a dragline payload. pages 1571 –1576, may 2011. ISSN 1050-4729.

[17] C. M. Bishop. *Pattern Recognition and Machine Learning (Information Science and Statistics)*. Springer-Verlag New York, Inc., Secaucus, NJ, USA, 2006. ISBN 0387310738.

[18] O. Bochardt, R. Calhoun, J.K. Uhlmann, and S.J. Julier. Generalized information representation and compression using covariance union. *9th International Conference on Information Fusion*, pages 1–7, 2006.

[19] A. Brewer, N. Sloan, and T. L. Landers. Intelligent tracking in manufacturing. *Journal of Intelligent Manufacturing*, 10:245–250, 1999. ISSN 0956-5515. 10.1023/A:1008995707211.

[20] G. Brooker, R. Henessy, and C. Lobsey. Millimetre wave radar for industrial applications. In *The 2nd International Conference on Wireless Broadband and Ultra Wideband Communications*, 2007.

[21] E. Brookner. *Tracking and Kalman Filtering Made Easy*. Wiley-Interscience, April 1998. ISBN 0471184071.

[22] Caterpillar. Caterpillar to develop autonomous system for blasthole drills. Press Release. http://australia.cat.com/cda/components/fullArticle?m=60164&x=7&id=1064002, September 2008.

[23] D. W. Chambers. Estimating pit excavation volume using unequal intervals. *Journal of Surveying Engineering*, 115(4):390–401, 1989.

[24] S.C. Chapra and R.P. Canale. *Numerical Methods for Engineers, 6th Edition*. McGraw-Hill Higher Education, 2009. ISBN 9780073401065.

[25] C. Chen and H. Lin. Estimating pit-excavation volume using cubic spline volume formula. *Journal of Surverying Engineering*, 117(2):51–66, May 1991.

[26] Z. Chen. Bayesian filtering: From kalman filters to particle filters, and beyond. Online. 2003.

[27] J.P. Chilès and P. Delfiner. *Geostatistics Modeling Spatial Uncertainty*. Wiley, 1999.

[28] I. Clark, S. Houlding, and M. Stoakes. Direct geostatistical estimation of irregular 3d volumes. In *Proceedings of the 22nd International Symposium on the Application of Computers and Operations Research in the Mineral Industry (APCOM)*, pages 515–528, September 1990.

[29] S.E. Cohn. Introduction to estimation theory. *Journal of the Meteorlogical Society of Japan*, 75:257–288, 1997.

[30] R. B. D'agostino, A. Belanger, and R. B. Jr. D'agostino. A suggestion for using powerful and informative tests of normality. *The American Statistician*, 44(4):316–321, 1990.

[31] S. D'Amours, M. Ronnqvist, and A. Weintraub. Using operational research for supply chain planning in the forest products industry. *INFOR: Information Systems and Operational Research*, 46(4):265–281, November 2008.

[32] P. Darling. *SME Mining Engineering Handbook (3rd Edition)*. Society for Mining, Metallurgy, and Exploration (SME), 2011.

[33] F. Daum. Nonlinear filters: beyond the kalman filter. *Aerospace and Electronic Systems Magazine, IEEE*, 20(8):57 –69, aug. 2005. ISSN 0885-8985.

[34] F. Daum and J. Huang. Curse of dimensionality and particle filters. *2003 IEEE Aerospace Conference Proceedings Cat No03TH8652*, 4:1979–1993, 2003.

[35] B.N. Delaunay. Sur la sphère vide. *Bulletin of Academy of Sciences of the USSR*, (6):793–800, 1934.

[36] G. Dissanayake, P. Newman, and S. Clark. A solution to the simulataneous localisation and map building problem. *IEE Transactions On Robotics and Automation*, 17:229, June 2001.

[37] C.H. Dowding and C.T. Aimone. Multiple blast-hole stresses and measured fragmentation. *Rock Mechanics and Rock Engineering*, 18:17–36, 1985. ISSN 0723-2632. 10.1007/BF01020413.

[38] E.S. Duff. Automated volume estimation of haul truck loads. In *Proceedings of the Australian Conference on Robotics and Automation*, pages 179–184. CSIRO, Melbourne, Australia, 2000.

[39] E.S. Duff, J.M. Roberts, and P.I. Corke. Automation of an underground mining vehicle using reactive navigation and opportunistic localization. 4:3775 – 3780 vol.3, oct. 2003.

[40] E.S. Duff, C. Caris, A. Bonchis, K. Taylor, C. Gunn, and M. Adcock. The development of a telerobotic rock breaker. *Field and Service Robotics*, pages 411–420, 2010.

[41] H.F. Durrant-Whyte. An autonomous guided vehicle for cargo handling applications. *The International Journal of Robotics Research*, 15(5):407–440, 1996.

[42] D.P. Dykstra, G. Kuru, and R. Nussbaum. Technologies for log tracking. *International Forestry Review*, 5(3):262–267, 2003.

[43] S.M. Easa. Smooth surface approximation for computing pit excavation volume. *Journal of Surveying Engineering*, 124(3):125–133, 1998.

[44] B. Gates. A robot in every home. *Scientific American*, 296:58–65, 2007.

[45] G.J. Giacaman, R.P. Medel, and J.A. Tabilo. Simulation of the material transporting and loading process in pedro de valdivia mine. *Winter Simulation Conference*, 1:1349–1355, 2002.

[46] P. Grabe and W.P. Johnstone. Comparison of polygonal and block model reserving techniques in gemcom, a case study on a thin reef deposit. http://www.gemcomsoftware.com/sites/default/files/whitepaper/GEMS_ComparisonofPoly 2011.

[47] M.S. Grewal and A.P. Andrews. *Kalman Filtering : Theory and Practice Using MATLAB*. Wiley-Interscience, 2 edition, January 2001. ISBN 0471392545.

[48] T. Hague, B. Southall, and N.D. Tillett. An autonomous crop treatment robot: Part ii. real time implementation. *The International Journal of Robotics Research*, 21(1):75–85, 2002.

[49] S. Haykin. *Kalman Filtering and Neural Networks*. Wiley-Interscience, October 2001. ISBN 0471369985.

[50] Y. Ho and R. Lee. A bayesian approach to problems in stochastic estimation and control. *Automatic Control, IEEE Transactions on*, 9(4):333 – 339, oct 1964. ISSN 0018-9286.

[51] D Hodouin, S.L. Jamsa-Jounela, M.T Carvalho, and L. Bergh. State of the art and challenges in mineral processing control. *Control Engineering Practice*, 9 (9):995 – 1005, 2001. ISSN 0967-0661. <ce:title>Review Papers on Automation in Mineral and Metal Processing</ce:title>.

[52] S. Houlding. Direct volume estimation - a geostatistcal technique for mine planning and grade control. *Computers & Geosciences*, 25:1113–1123, 1999.

[53] W. Jansen. *A Strategic Approach to Mine-Mill Reconciliation*. PhD thesis, Julius Kruttschnitt Mineral Research Centre, The University of Queensland, 2008.

[54] S Janssen and M.K. Ittersum. Assessing farm innovations and responses to policies: A review of bio-economic farm models. *Agricultural Systems*, 94(3): 622 – 636, 2007. ISSN 0308-521X.

[55] C. M Jarque and A. K. Bera. A test for normality of observations and regression residuals. *International Statistical Review*, 55:163–172, 1987.

[56] B. Johansson, J. Johansson, and L. Abrahamsson. Attractive workplaces in the mine of the future: 26 statements. *Int. J. Mining and Mineral Engineering*, 2(3):239–252, 2010.

[57] D.G. Johnson, M. Calleija, G.M. Brooker, and E. Nettleton. Terrain mapping at the cm level using a real-aperture mmw monopulse radar. In *Electromagnetics in Advanced Applications (ICEAA), 2011 International Conference on*, pages 432 –435, sept. 2011.

[58] R E Kalman. A new approach to linear filtering and prediction problems. *Journal Of Basic Engineering*, 82(Series D):35–45, 1960.

[59] R E Kalman and R S Bucy. New results in linear filtering and prediction theory. *Journal Of Basic Engineering*, 83(1):95–108, 1961.

[60] P. Keleher, D. Cameron, and M. Knijnikov. Improving fundamental stockpile management procedures. *Coal Operators Conference*, pages 422–428, 1998.

[61] B.A. Kennedy. *Surface Mining*. Society for Mining, Metallurgy, and Exploration, 1990. ISBN 9780873351027.

[62] P. K. Kitanidis. *Introduction to Geostatistics*. Cambridge University Press, 1997.

[63] J. Ko and D. Fox. Gp-bayesfilters: Bayesian filtering using gaussian process prediction and observation models. pages 3471 –3476, sept. 2008.

[64] A. N. Kolmogorov, W. L. Doyle, and I. Selin. *Interpolation and extrapolation of stationary random sequences*. RAND Corporation, Santa Monica, California, 1962.

[65] D. G Krige. *Lognormal-de Wijsian Geostatistics for Ore Evaluation*. South African Institure of Mining and Metallurgy Monograph Series, 1981.

[66] A.Y.T. Kudowor and G. Taylor. Triangulation based volume calculation. University of Newcastle. 1998.

[67] D. T. Lee and B. J. Schachter. Two algorithms for constructing a delaunay triangulation. *International Journal of Parallel Programming*, 9:219–242, 1980. ISSN 0885-7458. 10.1007/BF00977785.

[68] D. D. Lichti, S. J. Gordon, and M. P. Stewart. Ground-based laser scanners: Operation, systems and applications. *Geomatica*, 56:21–34, 2002.

[69] H. W. Lilliefors. On the kolmogorov-smirnov test for normality with mean and variance unknown. *Journal of the American Statistical Association*, 62: 399–402, 1967.

[70] W.E. Lorensen and H.E. Cline. Marching cubes: A high resolution 3d surface construction algorithm. *SIGGRAPH Comput. Graph.*, 21(4):163–169, August 1987. ISSN 0097-8930.

[71] S. Lowry, D.and Molloy and Y. Tan. The labour force outlook in the minerals resources sector 2005-2015. Technical report, National Institute of Labour Studies, Flinders University, Adelaide, Australia, May 2006.

[72] Acumine Pty Ltd. Acumine. http://www.acumine.com/index.php. January 2012.

[73] J. Malpica. Splines interpolation in high resolution satellite imagery. In George Bebis, Richard Boyle, Darko Koracin, and Bahram Parvin, editors, *Advances in Visual Computing*, volume 3804 of *Lecture Notes in Computer Science*, pages 562–570. Springer Berlin / Heidelberg, 2005. ISBN 978-3-540-30750-1.

[74] Maptek. Vulcan. Website. http://www.maptek.com/products/vulcan/index.html, January 2012.

[75] F. J. Jr. Massey. The kolmogorov-smirnov test for goodness of fit. *Journal of the American Statistical Association*, 46(253):68–78, 1951. ISSN 01621459.

[76] D. Massicotte, R.Z. Morawski, and A. Barwicz. Incorporation of a positivity constraint into a kalman-filter-based algorithm for correction of spectrometric data. *Instrumentation and Measurement, IEEE Transactions on*, 44(1):2 –7, feb 1995. ISSN 0018-9456.

[77] G. Matheron. Principles of geostatistics. *Economic Geology*, 58(8):1246–1266, 1963.

[78] P.S. Maybeck. *Stochastic Models, Estimation and Control*, volume 1. Academic Press, 1979.

[79] A. Melkumyan and R. Murphy. Spectral domain noise suppression in dual-sensor hyperspectral imagery using gaussian processes. In Kok Wong, B. Mendis, and Abdesselam Bouzerdoum, editors, *Neural Information Processing. Models and Applications*, volume 6444 of *Lecture Notes in Computer Science*, pages 684–691. Springer Berlin / Heidelberg, 2010. ISBN 978-3-642-17533-6. 10.1007/978-3-642-17534-3_84.

[80] A. Melkumyan and F.T. Ramos. A sparse covariance function for exact gaussian process inference in large datasets. In *Proceedings of the 21st international jont conference on Artifical intelligence*, IJCAI'09, pages 1936–1942, San Francisco, CA, USA, 2009. Morgan Kaufmann Publishers Inc.

[81] A. Melkumyan and F.T. Ramos. Multi-kernel gaussian processes. pages 1408–1413, 2011.

[82] Motion Metrics. Motion metrics website. www.motionmetrics.com.au. July 2010.

[83] Z. Min, L. Wenfeng, W. Zhongyun, L. Bin, and R. Xia. A rfid-based material tracking information system. In *Automation and Logistics, 2007 IEEE International Conference on*, pages 2922 –2926, aug. 2007.

[84] E. Mjolsness and D. DeCoste. Machine learning for science: State of the art and future prospects. *Science*, 293(5537):2051–2055, 2001.

[85] O. Mol and A.D.S. Gillies. Cut-off grade determination for mines producing direct-shipping iron ore. *Australasian Institute of Mining and Metallurgy*, (289):283–287, November/December 1984.

[86] S.T. Monteiro and R.J. Murphy. Calibrating probabilities for hyperspectral classification of rock types. pages 2800 –2803, july 2010. ISSN 2153-6996.

[87] M. Montemerlo, S. Thrun, D. Koller, and B. Wegbreit. Fastslam: A factored solution to the simultaneous localization and mapping problem. pages 593–598, 2002.

[88] C. Morley. Beyond reconciliation - a proactive approach to using mining data. In *Fifth Large Open Pit Mining Conference*, 2003.

[89] C. Morley and R Moller. Iron ore mine reconciliation - a case study from sishen iron ore mine, south africa. *Iron Ore Conference*, 1:311–318, 2005.

[90] E. Nebot, J. Guivant, and S. Worrall. Haul truck alignment monitoring and operator warning system. *Journal of Field Robotics*, 23(2):141–161, 2006. ISSN 1556-4967.

[91] D. Nguyen-Tuong, M. Seeger, and J. Peters. Model learning with local gaussian process regression. *Advanced Robotics*, 23(15):2015–2034, 2009.

[92] N.J. Nilsson. Introduction to machine learning: An early draft of a proposed textbook. http://robotics.stanford.edu/people/nilsson/mlbook.html. 1996.

[93] Jorge Nocedal and Stephen J. Wright. *Numerical Optimization*. Springer-Verlag New York, Inc., 2006.

[94] University of Sydney. Rio tinto centre for mine automation website. www.usyd.edu.au/cma. www.usyd.edu.au/cma, July 2009.

[95] M. Omid, M. Khokastehnazhand, and A. Tabatabaeefar. Estimating volume and mass of citrus fruits by image processing technique. *Journal of Food Engineering*, 100:315–321, 2010.

[96] E. S. Pearson. Note on tests for normality. *Biometrika*, 22:423–424, 1931.

[97] C. Plagemann, S. Mischke, S. Prentice, K. Kersting, N. Roy, and W. Burgard. Learning predictive terrain models for legged robot locomotion. In *Intelligent Robots and Systems, 2008. IROS 2008. IEEE/RSJ International Conference on*, pages 3545 –3552, sept. 2008.

[98] C.V. Rao, J.B. Rawlings, and J.H Lee. Constrain linear state estimation - a moving horizon approach. *Automatica*, 37:1619–1628, 2001.

[99] B.A. Rasco and G.E. Bledsoe. *Bioterrorism and Food Safety*, pages 571–600. John Wiley & Sons, Inc., 2008. ISBN 9780470439074.

[100] C.E. Rasmussen and C. Williams. *Gaussian Processes for Machine Learning*. the MIT Press, 2006.

[101] S. Reece and S. Roberts. An introduction to gaussian processes for the kalman filter expert. pages 1 –9, july 2010.

[102] J. M. Rendu. *An Introduction Geostatisical Methods of Mineral Evaluation*. South African Institure of Mining and Metallurgy Monograph Series, 1978.

[103] Douglas A. Reynolds, Thomas F. Quatieri, and Robert B. Dunn. Speaker verification using adapted gaussian mixture models. In *Digital Signal Processing*, page 2000. 2000.

[104] G.K. Robinson. How much would a blending stockpile reduce variation? *Chemometrics and Intelligent Laboratory Systems*, 74:121–133, 2004.

[105] S. Russell and P. Norvig. *Artificial Intelligence: A Modern Approach.* Prentice-Hall, Englewood Cliffs, NJ, 2nd edition edition, 2003.

[106] S. Sarata, N. Koyachi, T. Tubouchi, H. Osumi, M. Kurisu, and K. Sugawara. Development of autonomous system for loading operation by wheel loader. In *The 23rd International Symposium on Automation and Robotics in Construction*, pages 466–471, 2006.

[107] S. Scheding, G. Dissanayake, E.M. Nebot, and H. Durrant-Whyte. An experiment in autonomous navigation of an underground mining vehicle. *Robotics and Automation, IEEE Transactions on*, 15(1):85 –95, feb 1999. ISSN 1042-296X.

[108] S. Schneider, R. Murphy, and S. Monteiro. On the development of a hyperspectrali library for autonomous mining systems. In *Australiasian Conference on Robotics and Automation*, 2009.

[109] C. Sensogut and A.H. Ozdeniz. Statistical modelling of stockpile behaviour under different atmospheric conditions- western lignite corporation (wlc) case. *Fuel*, 84:1858–1863, 2005.

[110] A. Shavit and C. Gutfinger. *Thermodynamics: From Concepts to Applications, Second Edition.* Taylor & Francis, 2008. ISBN 9781420073683.

[111] D. Simon and T.L. Chia. Kalman filtering with state equality constraints. *IEEE Transactions on Aerospace and Electronic Systems*, 38:128–136, 2001.

[112] R. Smith, M. Self, and P. Cheeseman. A stochastic map for uncertain spatial relationships. In *Proceedings of the 4th international symposium on Robotics Research*, pages 467–474, Cambridge, MA, USA, 1988. MIT Press. ISBN 0-262-02272-9.

[113] R. Smith, M. Self, and P. Cheeseman. *Estimating uncertain spatial relationships in robotics*, pages 167–193. Springer-Verlag New York, Inc., New York, NY, USA, 1990. ISBN 0-387-97240-4.

[114] W. Smith. Undercutting sustainability. *Journal of Sustainable Forestry*, 19 (1-3):7–30, 2004.

[115] A. Swales. Geostatistical estimation of short-term changes in beach morphology and sand budget. *Journal of Coastal Research*, 18(2):338–351, 2002. ISSN 07490208.

[116] M. Thomas and V. Snowden. Improving reconciliation and grade control by statistical and geostatisical analysis. *Strategies for Grade Control*, 10:49–59, 1990.

[117] M. Thompson, G. Sylvia, and M. T. Morrissey. Seafood traceability in the united states: Current trends, system design, and potential applications. *Comprehensive Reviews in Food Science and Food Safety*, 4(1):1–7, 2005. ISSN 1541-4337.

[118] S. Thrun. Probabilistic algorithms in robotics. *AI Magazine*, 21(4):93–109, 2000.

[119] S. Thrun. Probabilistic robotics. *Commun. ACM*, 45:52–57, March 2002. ISSN 0001-0782.

[120] S. Thrun. Winning the darpa grand challenge. In Johannes Fürnkranz, Tobias Scheffer, and Myra Spiliopoulou, editors, *Machine Learning: ECML 2006*, volume 4212 of *Lecture Notes in Computer Science*, pages 4–4. Springer Berlin / Heidelberg, 2006. ISBN 978-3-540-45375-8. 10.1007/11871842_4.

[121] Transcale. Transcale website. www.transcale.com.au. July 2009.

[122] S. Vasudevan, F.T. Ramos, E. Nettleton, and H. Durrant-Whyte. Gaussian process modeling of large-scale terrain. *Journal of Field Robotics*, 26(10): 812–840, 2009. ISSN 1556-4967.

[123] S. Vasudevan, F.T. Ramos, E. Nettleton, and H. Durrant-Whyte. A mine on its own. *Robotics Automation Magazine, IEEE*, 17(2):63 –73, june 2010. ISSN 1070-9932.

[124] G. Welch and G. Bishop. An introduction to the kalman filter. *Design*, 7(1): 1–16, 2001.

[125] J.W. White and J.P. Olson. Computer-based dispatching in mines with concurrent operating objectives. *Mining Engineering*, 38:1045 – 1054, 1986. ISSN 00265187.

[126] N. Wiener. Extrapolation, interpolation, and smoothing of stationary time series: with engineering applications. *Journal of the American Statistical Association*, 47(258):319, 1949.

[127] M. Wortley, E. Nozawa, and K. J. Riihioja. Metso smarttag - the next generation and beyond. In *35TH APCOM Symposium*, pages 841–851, September 2011.

[128] M. Yanalak. Computing pit excavation volume. *Journal of Surveying Engineering*, 131(1):15–19, 2005.

[129] M. Yellishetty, P.G. Ranjith, and A. Tharumarajah. Iron ore and steel production trends and material flows in the world: Is this really sustainable? *Resources, Conservation and Recycling*, 54(12):1084 – 1094, 2010. ISSN 0921-3449.

[130] X. Zhang, J. Morris, and R. Reinhard Klette. Volume measurement using a laser scanner. The University of Auckland. 2005.

[131] H. Zhou, P. Hatherly, F.T. Ramos, and E. Nettleton. An adaptive data driven model for characterizing rock properties from drilling data. In *Robotics and Automation (ICRA), 2011 IEEE International Conference on*, pages 1909 –1915, may 2011.

Appendix A

Data sets & Data sheets

A.1 Large Scale Excavator Mass Data

Table A.1 – Excavator mass values from large scale experiment. All masses are in Kg.

1055	935	630	800	820	820	700	975	830	890	890
1000	535	700	680	855	785	785	705	780	730	980
1090	675	880	790	900	755	750	725	765	715	1010
1170	955	660	660	725	725	740	770	790	860	1050
1170	720	765	745	850	760	720	740	650	920	1005
940	755	760	600	585	705	645	570	640	920	975
940	635	565	770	655	705	670	525	675	1280	1035
760	460	755	775	675	900	820	800	825	1075	1000
1000	720	640	825	845	820	800	945	820	1095	870
660	655	630	760	790	715	870	755	870	1050	930
885	705	445	720	660	665	915	675	800	920	925
935										

A.2 Sensor Data sheets

A.2.1 Riegl VZ-1000

3D Terrestrial Laser Scanner with Online Waveform Processing

RIEGL VZ®-1000

very long range up to 1400 m
very high speed data acquisition
wide field-of-view, controllable while scanning
high-accuracy, high-precision ranging based on echo digitization and online waveform processing
multiple target capability
superior measurement capability in adverse atmospheric conditions
high-precision mounting pads for optional digital camera
integrated inclination sensors and laser plummet
integrated GPS receiver with antenna
various interfaces (LAN, WLAN, USB 2.0)
internal data storage capability

The V-Line® 3D Terrestrial Laser Scanner *RIEGL* VZ-1000 provides high speed, non-contact data acquisition using a narrow infrared laser beam and a fast scanning mechanism. High-accuracy laser ranging is based upon *RIEGL*'s unique echo digitization and online waveform processing, which allows achieving superior measurement capability even under adverse atmospheric conditions and the evaluation of multiple target echoes.

The line scanning mechanism is based upon a fast rotating multi-facet polygonal mirror, which provides fully linear, unidirectional and parallel scan lines. The *RIEGL* VZ-1000 is a very compact and lightweight surveying instrument, mountable in any orientation and even under limited space conditions.

Modes of Operation

stand-alone data acquisition without the need of a notebook, basic configuration and commanding via the built-in user interface
remote operation via RiSCAN PRO on a notebook, connected either via LAN interface or integrated WLAN
well-documented command interface for smooth integration into mobile laser scanning systems
Interfacing to Post Processing Software

User Interfaces

integrated Human-Machine Interface (HMI) for stand-alone operation without computer
high-resolution 3,5" TFT color display, 320 x 240 pixel, scratch resistant cover glass with anti-reflection coating and multi-lingual menu
water and dirt resistant key pad with large buttons for instrument control
loudspeaker for audible signaling of messages by voice

Topography & Mining
As-Built Surveying
Architecture & Facade Measurement
Archaeology & Cultural Heritage Documentation
City Modelling
Tunnel Surveying
Civil Engineering

visit our website
www.riegl.com

RIEGL®
LASER MEASUREMENT SYSTEMS

Terrestrial Laser Scanning

Preliminary Datasheet

System Configuration

Scanner Hardware *RIEGL* VZ-1000
allows high-speed, high resolution and accurate 3D measurements

Range up to 1400 m @ Laser Class 1
Repeatability 5 mm
Measurement rate up to 122 000 measurements/sec
Field of View up to 100° x 360°
LAN/WLAN data interface, easily allowing wireless data transmission
Operated by any standard PC or Notebook or cable less
Fully portable, rugged & robust

Software RiSCAN PRO
RIEGL software package for scanner operation and data processing

Data archiving using a well-documented tree structure in XML file format
Object VIEW / INSPECTOR for intelligent data viewing and feature extraction
Straightforward Global Registration
Interfacing to Post Processing Software

Digital Camera (optional)
provides high resolution calibrated color images

NIKON D700, NIKON D300(s)
- D700: 12.1 Megapixel, Nikon FX format
- D300(s): 12.3 Megapixel
- USB interface

Mounting device with digital camera can be easily fixed by means of two knurled head screws. Precise position and orientation is provided by three supporting points. Power supply and USB 2.0 interface is provided by the scanner directly.

The combination of the key components Scanner, Software and Camera results in

- Automatic generation of high resolution textured meshes
- Photorealistic 3D reconstruction
- Exact identification of details
- Online position and distance measurements
- Online setting of any virtual point of view

Global Scan Position Registration

Stand-alone Registration

integrated GPS receiver (L1)
integrated biaxial inclination sensors (tilt range ±10°, accuracy typ. ±0.008°)
RiSCAN PRO Processing and Multistation Adjustment Module (MSA)

Registration via control points

precise and fast fine scanning of retro-reflectors
RiSCAN PRO Processing

Totalstation-like-Registration

setup above well known point (integrated laser plummet)
integrated inclination sensors
precise fine scanning of well known remote target (reflector)
RiSCAN PRO Processing Backsighting function

Operating Elements and Connectors

WLAN antenna

Carrying handles

High-resolution color TFT display

Key pad for instrument control

Connectors for power supply and LAN interface 10/100 MBit/sec, power off/on button

Communication and Interfaces

LAN interface 10/100/1000 MBit/sec within rotating head
LAN interface 10/100 MBit/sec within base
integrated WLAN interface with rod antenna
USB 2.0 for external storage devices (USB flash drives, external HDD)
USB 2.0 for connecting the optional digital camera
connector for GPS antenna
two connectors for external power supply
connector for external GPS synchronization pulse (1PPS)

TOP VIEW

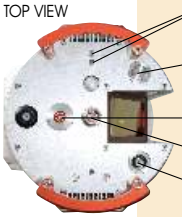

Mounting points (3x) and mounting threads inserts (2x) for digital camera

Connector for GPS antenna (optional)

USB and DC power connector for digital camera

Connector for GPS antenna

Connector for WLAN antenna

USB 2.0 slot for external memory devices

LAN 10/100/1000 MBit/sec, for rapid download of scan data

Scan Data Storage

- *internal 32 GByte flash memory (1 GByte reserved for the operating system)*
- *external storage devices (USB flash drives or external hard drives) via USB 2.0 interface*

Power Supply

Add-on rechargeable battery

optional add-on rechargeable battery pack (high power, high capacity NiMH cells)
compact disc design, short-circuit-proof and protected connection pins
rechargeable during standard scan operation via external power supply
integrated micro-controller based charging electronics
easily pluggable to base of the laser scanner by central locking screw
DC voltage source (11-32 V DC) sufficient for recharging

External power supply

Intelligent power supply management, up to three independent external power sources can be connected simultaneously for uninterrupted operation
Reliable under- and over voltage protection
Wide external voltage supply range 11-32 V DC
Power consumption typ. 82 W
LED indicators for power status

Technical Data 3D Scanner Hardware *RIEGL* VZ®-1000

Laser Product Classification	Class 1 Laser Product according to IEC60825-1:2007 The following clause applies for instruments delivered into the United States: Complies with 21 CFR 1040.10 and 1040.11 except for deviations pursuant to Laser Notice No. 50, dated June 24, 2007.
Physical Data	temperature range 0°C to +40°C (operation), -10°C to +50°C (storage) protection class IP64 (dust and splash-proof) weight approx. 9.8 kg

Range Performance[1]

Laser PRR (Peak) [2]	70 kHz	100 kHz	150 kHz	300 kHz
Effective Measurement Rate [2]	29 000 meas./sec.	42 000 meas./sec.	62 000 meas./sec.	122 000 meas./sec.
Max. Measurement Range [3] for natural targets ρ ≥ 90% for natural targets ρ ≥ 20%	 1400 m 700 m	 1200 m 600 m	 950 m[4] 500 m	 450 m[4] 350 m
Max. Number of Targets per Pulse	practically unlimited [5]			
Accuracy [6] [8]	8 mm			
Precision [7] [8]	5 mm			

Minimum Range	2.5 m
Laser Wavelength	near infrared
Beam Divergence [9]	0.3 mrad

1) with online waveform processing
2) rounded values, selectable by measurement program
3) Typical values for average conditions. Maximum range is specified for flat targets with size in excess of the laser beam diameter, perpendicular angle of incidence, and for atmospheric visibility of 23 km. In bright sunlight, the max. range is shorter than under an overcast sky.
4) limited by PRR
5) details on request
6) Accuracy is the degree of conformity of a measured quantity to its actual (true) value.
7) Precision, also called reproducibility or repeatability, is the degree to which further measurements show the same result.
8) One sigma @ 100 m range under *RIEGL* test conditions.
9) 0.3 mrad correspond to 30 mm increase of beamwidth per 100 m of range.

Scan Performance

	Vertical (Line) Scan	Horizontal (Frame) Scan
Scan Angle Range	total 100° (+60° / -40°)	max. 360°
Scanning Mechanism	rotating multi-facet mirror	rotating head
Scan Speed	3 lines/sec to 120 lines/sec	0°/sec to 60°/sec [10]
Angular Stepwidth Δ ϑ (vertical), Δ ϕ (horizontal)	0.0024° ≤ Δ ϑ ≤ 0.288° [11] between consecutive laser shots	0.0024° ≤ Δ ϕ ≤ 0.5° [11] between consecutive scan lines
Angle Measurement Resolution	better 0.0005° (1.8 arcsec)	better 0.0005° (1.8 arcsec)

Inclination Sensors	integrated, for vertical scanner setup position
GPS receiver	integrated, L1 antenna
Compass	integrated, for vertical scanner setup position
Internal Sync Timer	integrated real-time synchronized time stamping of scan data
Scan Sync (optional)	scanner rotation synchronization

10) frame scan can be disabled, providing 2D operation
11) selectable, minimum stepwidth increasing to 0.004° @ 70 kHz PRR

Max. Measurement Range

The following conditions are assumed:
Flat target larger than footprint of laser beam, perpendicular angle of incidence, average brightness

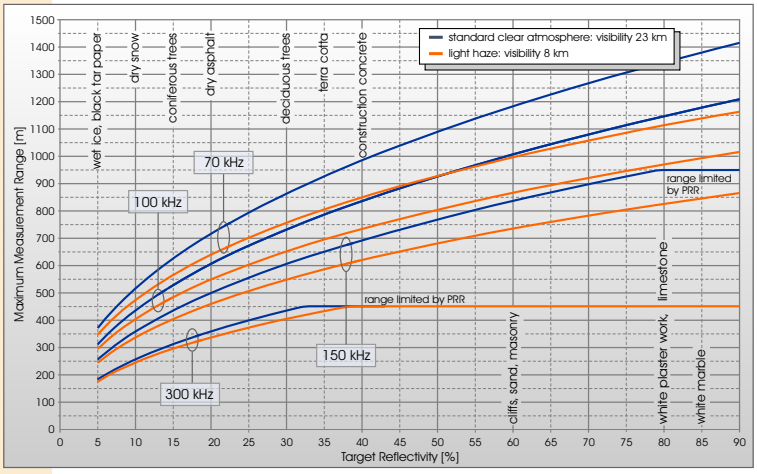

RIEGL®
LASER MEASUREMENT SYSTEMS

RIEGL Laser Measurement Systems GmbH, 3580 Horn, Austria
Tel.: +43-2982-4211, Fax: +43-2982-4210, E-mail: office@riegl.co.at
RIEGL USA Inc., Orlando, Florida 32819, USA
Tel.: +1-407-248-9927, Fax: +1-407-248-2636, E-mail: info@rieglusa.com
RIEGL Japan Ltd., Tokyo 1640013, Japan
Tel.: +81-3-3382-7340, Fax: +81-3-3382-5843, E-mail: info@riegl-japan.co.jp

www.riegl.com

A.2.2 Riegl LMS-Z620

Extra Long Range & High Accuracy 3D Terrestrial Laser Scanner System

LMS-Z620

The terrestrial laser scanner system *RIEGL* LMS-Z620 consists of a high performance long-range 3D scanner, the accompanying operating and processing software RiSCAN PRO, and a calibrated and accurately orientated and mounted high-resolution digital camera.

The system provides data which lends itself to automatic or semi-automatic processing of scan- and image data to generate products such as textured triangulated surfaces and high resolution panorama images as a basis for e.g., geotechnical analysis and mining assessment.

The *RIEGL* LMS-Z620 is a rugged and fully portable sensor especially designed for the rapid acquisition of high-quality three dimensional images even under highly demanding environmental conditions, providing a unique and unrivalled combination of a wide field-of-view, high maximum range, and fast data acquisition.

A standard Windows notebook and the bundled software package RiSCAN PRO enable the user to instantly acquire high-quality 3D data in the field and provide a variety of registration, post processing and export functions.

- ***Topography & Mining***
- ***Monitoring & Civil Engineering***
- ***Archaeology & Cultural Heritage Documentation***
- ***Architecture & Facade Measurement***

visit our webpage www.riegl.com

RIEGL
LASER MEASUREMENT SYSTEMS

Terrestrial Laser Scanning

System Key Performance Data

Scanner Hardware LMS-Z620
allows high-speed, high resolution and accurate 3D measurements

- *Ranges up to 2000 m @ Laser Class 1*
- *Repeatability up to 5 mm*
- *Measurement rates up to 11000 pts/sec*
- *Field of View up to 80° x 360°*
- *TCP/IP data interface, allowing easy wireless data transmission*
- *Operable with any standard PC or Notebook*
- *Fully portable, rugged & robust*

Software RiSCAN PRO
RIEGL software package for scanner operation and data processing

- *Data archiving using a well-documented tree structure in the XML file format*
- *Object VIEW / INSPECTOR for intelligent data viewing and feature extraction*
- *Straightforward Global Registration*
- *Interfacing to Post Processing Software*

Camera (optional)
provides high resolution calibrated color images

NIKON D700 / NIKON D300(s) / NIKON D200:

- *D300(s): 12.3 Megapixel*
- *D700: 12.1 Megapixel, Nikon FX format*
- *D200: 10.2 Megapixel*
- *USB interface*

The combination of the key components Scanner, Software and Camera results in

- Automatic generation of high resolution textured meshes
- Online position and distance measurements
- Photorealistic 3D reconstruction
- Online setting of any virtual point of view
- Exact identification of details

Principle of Scanner Operation & Dimensional Drawings

The range finder electronics of the 3D laser scanner *RIEGL* LMS-Z620 are optimized in order to meet the requirements of high speed scanning (high laser repetition rate, fast signal processing, and high speed data interface).

The vertical deflection ("line scan") of the laser beam is realized by a polygon with a number of reflective surfaces. For high scanning rates and/or a vertical scan angle of θ up to 80°, the polygonal mirror continuously rotates at an adjustable speed. For slow scanning rates and/or small scanning angles, it linearly oscillates up and down. The horizontal scan ("frame scan") is realized by rotating the complete optical head up to 360°.

Scandata: RANGE, ANGLE, SIGNAL AMPLITUDE, and optional TIMESTAMP are transmitted to a laptop via TCP/IP Ethernet Interface. Camera data is fed into the same laptop via USB/firewire interface.

The RiSCAN PRO software allows the operator to perform a large number of tasks including sensor configuration, data acquisition, data visualization, data manipulation, and data archiving. RiSCAN PRO runs on the platforms Windows XP Professional, Windows VISTA Professional, and Windows 7 Professional.

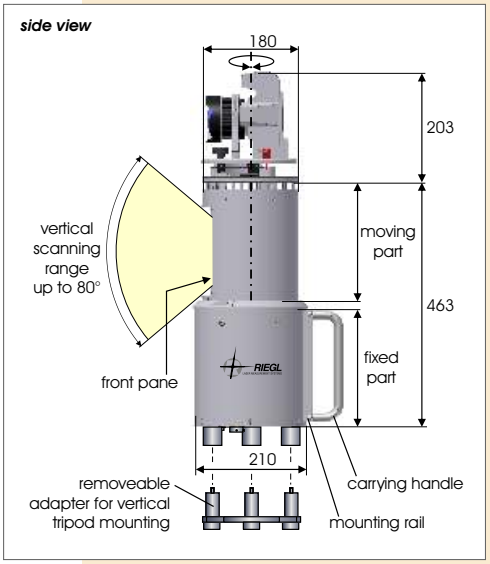

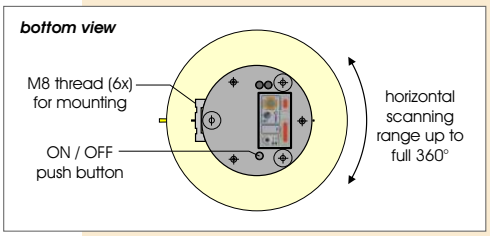

Maximum Measurement Range and Scan Pattern *RIEGL* LMS-Z620

The following conditions are assumed:
Flat target larger than footprint of laser beam, perpendicular angle of incidence, average brightness

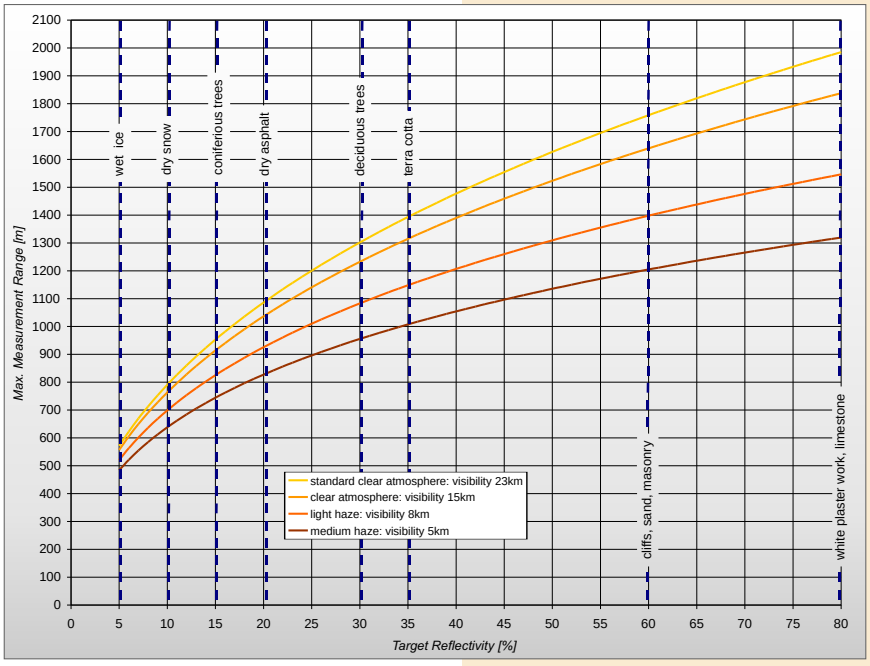

Technical Data 3D Scanner Hardware *RIEGL* LMS-Z620

Laser Product Classification	Class 1 Laser Product according to IEC60825-1:2007 The following clause applies for instruments delivered into the United States: Complies with 21 CFR 1040.10 and 1040.11 except for deviations pursuant to Laser Notice No. 50, dated July 26, 2001.

Rangefinder Performance[1]

Max. Measurement Range [2]	
for natural targets, ρ ≥ 80 %	up to 2000 m
for natural targets, ρ ≥ 10 %	up to 750 m
Minimum Range	2 m
Accuracy [3] [5]	10 mm
Repeatability [4] [5]	10 mm (single shot), 5 mm (averaged)
Measurement Rate	up to 11000 pts/sec @ low scanning rate (oscillating mirror) up to 8000 pts/sec @ high scanning rate (rotating mirror)
Laser Wavelength	near infrared
Beam Divergence [6]	0.15 mrad

1) First, Last, or Alternating Target Mode selectable.
2) Typical values under average conditions. Maximum range is specified for flat targets with size in excess of the laser beam diameter and near perpendicular incidence of the laser beam and atmospheric visibility in excess of 23 km. In bright sunlight the operational range is considerably shorter than under an overcast sky.
3) Accuracy is the degree of conformity of a measured quantity to its actual (true) value.
4) Precision, also called reproducibility or repeatability, is the degree to which further measurements show the same result.
5) One sigma @ 100 m range under *RIEGL* test conditions.
6) 0.15 mrad correspond to 15 mm increase of beamwidth per 100 m of range.

Scanner Performance

Vertical (Line) Scan	
Scan Angle Range	0° to 80°
Scanning Mechanism	rotating / oscillating mirror
Scan Speed	1 scan/sec to 20 scans/sec @ 80° scanning range
Angular Stepwidth $\Delta\vartheta$ [7] between consecutive laser shots	$0.004° \leq \Delta\vartheta \leq 0.2°$
Angle Measurement Resolution	0.002°
Horizontal (Frame) Scan	
Scan Angle Range	0° to 360°
Scanning Mechanism	rotating optical head
Scan Speed [8]	0.01°/sec to 15°/sec
Angular Stepwidth $\Delta\phi$ [7] between consecutive scan lines	$0.004° \leq \Delta\phi \leq 0.75°$
Angle Measurement Resolution	0.0025°
Inclination Sensors	integrated, for vertical scanner setup position (specifications to be found in separate datasheet)
Internal Sync Timer	option for real-time synchronized time stamping of scan data (specifications to be found in separate datasheet)

7) Selectable via Ethernet Interface or RS232.
8) Horizontal scan can be disabled, providing 2D-scanner operation.

General Technical Data

Interfaces: for configuration & data output	TCP/IP Ethernet, 10/100 MBit/sec
for configuration	RS 232, 19.2 kBd
for data output	ECP standard (enhanced capability port) parallel
Power Supply Input Voltage	12 - 28 V DC
Power Consumption	typ. 75 W max. 85 W
Current Consumption @ 12 V DC	typ. 6.25 A max. 7.1 A
@ 24 V DC	typ. 3.13 A max. 3.54 A
Main Dimensions	463 mm x 210 mm (length x diameter)
Weight	16 kg
Temperature Range	0°C to +40°C (operation), -10°C to +50°C (storage)
Protection Class	IP64, dust and splash-proof

RIEGL LASER MEASUREMENT SYSTEMS

RIEGL Laser Measurement Systems GmbH, A-3580 Horn, Austria
Tel.: +43-2982-4211, Fax: +43-2982-4210, E-mail: office@riegl.co.at
RIEGL USA Inc., Orlando, Florida 32819, USA
Tel.: +1-407-248-9927, Fax: +1-407-248-2636, E-mail: info@rieglusa.com
RIEGL Japan Ltd., Tokyo 1640013, Japan
Tel.: +81-3-3382-7340, Fax: +81-3-3382-5843, E-mail: info@riegl-japan.co.jp
www.riegl.com

A.2.3 CAS RW-10P

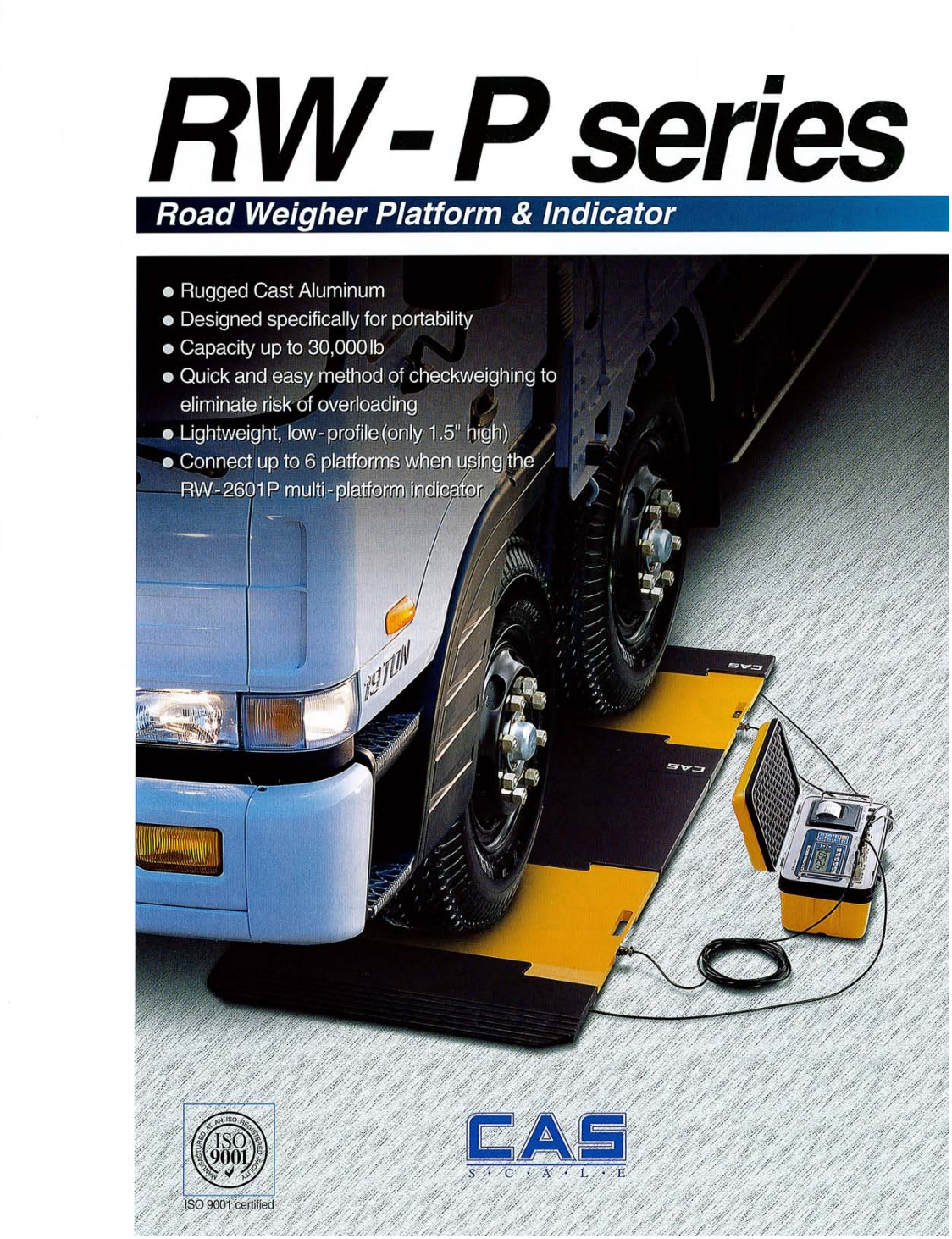

RW - P Road Weigher Platform & Indicator

Convenient vehicle weighing platform . . .

This rugged cast aluminum weighing plate is light enough to be portable yet large enough for any type of vehicle. The bright orange industrial paint is baked on to the aluminum alloy chassis. CAS platforms not only look tough, they're built tough ! With a variety of capacities & higher resolutions (1/2000 ~ 1/2500) the RW can be used in almost any application.
The RW can even accommodate for virtually any vehicle' s axle arrangement with the simple use of "Dummy Plates." These are simply solid rubber spacers of different sizes that can be placed between multiple platforms.

FEATURES

- High accuracy
- Portable
- By-Wheel Weight or Total Weight
- Water resistant
- Advanced Digital Filtering to minimize vibration
- Test for axle balance & overload conditions

Accessories : *Ramps & Cable*
Options : *Dummy Plates*

APPLICATIONS (RW-10P, RW-15P)

Multiple platforms can be connected to the indicator as well as various arrangements of dummy plates (see diagram.)

SPECIFICATIONS

Model		RW-01P	RW-02P	RW-05P	RW-10P	RW-15P
Max. Capacity	lb	2,000	4,000	10,000	20,000	30,000
	kg	1,000	2,000	5,000	10,000	15,000
Min. Division	lb	1	2	4	10	20
	kg	0.5	1	2	5	10
Accuracy		0.1%				
Size (inch/mm)	W	19.7"/500mm			35.4"/900mm	
	D	15.7"/400mm			19.7"/500mm	
	H	1.5"/39mm			1.5"/39mm	
Ramp		42lb/1.9kg			14lb/6.4kg	
Dummy plate					38lb/17.2kg	
Product weight		35lb/15.8kg			66lb/30.2kg	
Shipping weight		65lb/29.4kg			105lb/47.6kg	

RW-2601P Multi-Platform Indicator

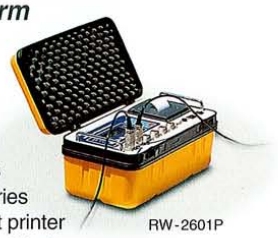
RW-2601P

FEATURES

- Built-in clock
- 1 Serial port : RS-232
- Built-in charger and batteries
- 10 "Vehicle number" memories
- High speed dot matrix receipt printer
- Connect to a PC or a Remote Display
- Connect up to 6 Platforms simultaneously
- Completely self-contained portable unit
- Large easy-to-read LCD display with back light
- Product Weight : 18.7lb/8.5kg

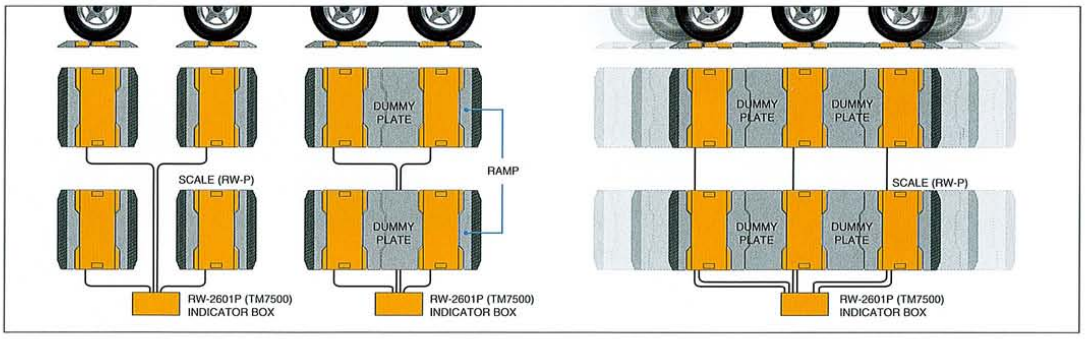

CAS USA Corporation

NJ OFFICE
99 Murray Hill Parkway
East Rutherford, NJ 07073
Tel : (201) 933-9002
Fax : (201) 933-9025
http://www.cas-usa.com

CA OFFICE
733 S. State College Blvd #98
Fullerton, CA 92831
Tel : (714) 870-1286
Fax : (714) 870-1167